Clinical applications of diffusion tensor magnetic resonance imaging in cardiovascular disease

Dr Arka Das MBChB, MRCP (UK)

Submitted in accordance with the requirements for the degree of

Doctor of Philosophy (PhD)

The University of Leeds

Multidisciplinary Cardiovascular Research Centre

Leeds Institute of Cardiovascular and Metabolic Medicine

(December/2021)

Intellectual Property and Publication Statements

The candidate confirms that the work is his own, except where work which has formed part of jointly authored publications has been included. The contribution of the candidate and the other authors to this work has been explicitly indicated below. The candidate confirms that appropriate credit has been given within the thesis where reference has been made to the work of others.

This copy has been supplied on the understanding that it is copyright material and that no quotation from the thesis may be published without proper acknowledgement.

Chapter 1

Publication:

A.Das, Plein S, Dall'Armellina E 'Role of CMR in Prognostic Stratification in Myocardial Infarction', published in Rev Esp Cardiol (Engl Ed). 2019 Feb;72(2):115-119

Authorship:

AD led the design, performed the literature search and drafted the manuscript. SP reviewed and revised the manuscript; whilst EDA contributed to the conception, offered intellectual input and approved the final version of manuscript.

Publication: Chowdhary A, Garg P, Das A, Nazir MS, Plein S. Cardiovascular magnetic resonance imaging: emerging techniques and applications. Heart. 2021 Jan 5;heartjnl-2019-315669. DOI: 10.1136/heartjnl-2019-315669

Authorship:

AC led the project design, AC, PG, MN and AD all performed the literature search and drafted the manuscript; whilst SP contributed to the conception, offered intellectual input and approved the final version of manuscript.

Chapter 4

Publication:

Das A, Kelly C., Teh I., Stoeck CT, Kozerke S, Chowdhary A, Brown LAE, Saunderson CED, Craven TP, Chew PG, Jex N, Swoboda PP, Levelt E, Greenwood JP, Schneider JE, Plein S and Dall'Armellina E. Acute Microstructural Changes after ST-Segment Elevation Myocardial Infarction Assessed with Diffusion Tensor Imaging. Radiology. 2021 Feb 9;203208. DOI: 10.1148/radiol.2021203208

Authorship:

AD led the project design, performed the literature search and drafted the manuscript. CK, IT, SP and JES reviewed and revised the manuscript; whilst EDA contributed to the conception, offered intellectual input and approved the final version of manuscript.

Chapter 5

Publication:

Das A, Kelly C, Teh I, Stoeck CT, Kozerke S, Plein S, Schneider JE, Dall'Armellina E. Depiction of intramyocardial iron in patients following ST-elevation myocardial infarction using diffusion tensor imaging. *Journal of Magnetic Resonance Imaging, 2022.*

Authorship:

AD led the project design, performed the literature search and drafted the manuscript. CK, IT, SP and JES reviewed and revised the manuscript; whilst EDA contributed to the conception, offered intellectual input and approved the final version of manuscript.

Chapter 6

Publication:

Das A, Kelly C, Teh I, Stoeck CT, Kozerke S, S, Sharrack N, Swoboda PP, Greenwood JP, Schneider JE, Plein S and Dall'Armellina E. Pathophysiology of LV remodelling

following ST-elevation myocardial infarction: a longitudinal cardiac diffusion tensor MRI study. *Journal of the American College of Cardiology: Cardiovascular Imaging, 2022.*

Authorship:

AD led the project design, performed the literature search and drafted the manuscript. CK, IT, SP and JES reviewed and revised the manuscript; whilst EDA contributed to the conception, offered intellectual input and approved the final version of manuscript.

Chapter 7

Publication:

Das A, Chowdhary A, Kelly C, Teh I, Stoeck CT, Kozerke S, Maxwell N, Craven TP, Jex NJ, Saunderson CED., Brown LAE, Ben-Arzi H, Sengupta A, Page SP, Swoboda PP, Greenwood JP, Schneider JE, Plein S and Dall'Armellina E. Insight Into Myocardial Microstructure of Athletes and Hypertrophic Cardiomyopathy Patients Using Diffusion Tensor Imaging. J Magn Reson Imaging. 2020; DOI: 10.1002/jmri.27257

Authorship:

AD and AC were joint first co-authors in this manuscript. AD and AC were jointly involved in the design of the project, literature search and drafting of the manuscript. CK, IT, SP and JES reviewed and revised the manuscript; whilst EDA contributed to the conception, offered intellectual input and approved the final version of manuscript.

The rights of Arka Das and Amrit Chowdhary to be identified as authors of this work has been asserted by her in accordance with the Copyright, Designs and Patents Act 1988.

Chapter 8

Publication:

Das A, Kelly C, Teh I, Nguyen C, Brown LAE, Chowdhary A, Jex N, Thirunavukarasu S, Sharrack N, Gorecka M, Swoboda PP, Greenwood JP, Kellman P, Moon JC, Davies RH, Lopes LR, Joy G, Plein S, Schneider JE, Dall'Armellina E. Phenotyping hypertrophic cardiomyopathy using cardiac diffusion MRI: the relationship between microvascular dysfunction and microstructural changes. *Under review at European Heart Journal: Cardiovascular Medicine, 2021.*

Authorship:

AD led the project design, performed the literature search and drafted the manuscript. CK, IT, SP and JES reviewed and revised the manuscript; whilst EDA contributed to the conception, offered intellectual input and approved the final version of manuscript.

The right of Arka Das to be identified as a named author of these publications has been asserted by her in accordance with the Copyright, Designs and Patents Act 1988.

Publications arising from this work

Papers

1. **A.Das,** Plein S, Dall'Armellina E.
   Role of CMR in Prognostic Stratification in Myocardial Infarction.
   Rev Esp Cardiol (Engl Ed). 2019 Feb;72(2):115-119

2. Chowdhary A, Garg P, **Das A**, Nazir MS, Plein S.
   Cardiovascular magnetic resonance imaging: emerging techniques and applications.
   Heart. 2021 Jan 5;heartjnl-2019-315669. DOI: 10.1136/heartjnl-2019-315669

3. **Das A,** Kelly C, Teh I, Stoeck CT, Kozerke S, Chowdhary A, Brown LAE, Saunderson CED, Craven TP, Chew PG, Jex N, Swoboda PP, Levelt E, Greenwood JP, Schneider JE, Plein S and Dall'Armellina E.
   Acute Microstructural Changes after ST-Segment Elevation Myocardial Infarction Assessed with Diffusion Tensor Imaging.
   Radiology. 2021 Feb 9;203208. DOI: 10.1148/radiol.2021203208

4. **Das A**,* Chowdhary A,* Kelly C, Teh I, Stoeck CT, Kozerke S, Maxwell N, Craven TP, Jex NJ, Saunderson CED., Brown LAE, Ben-Arzi H, Sengupta A, Page SP, Swoboda PP, Greenwood JP, Schneider JE, Plein S and Dall'Armellina E.
   Insight Into Myocardial Microstructure of Athletes and Hypertrophic Cardiomyopathy Patients Using Diffusion Tensor Imaging.
   J Magn Reson Imaging. 2020; DOI: 10.1002/jmri.27257
   * = Joint first author

5. **Das A,** Kelly C, Teh I, Nguyen C, Brown LAE, Chowdhary A, Jex N, Thirunavukarasu S, Sharrack N, Gorecka M, Swoboda PP, Greenwood JP,

Kellman P, Moon JC, Davies RH, Lopes LR, Joy G, Plein S, Schneider JE, Dall'Armellina E.

Phenotyping hypertrophic cardiomyopathy using cardiac diffusion MRI: the relationship between microvascular dysfunction and microstructural changes.

Eur Heart J Cardiovasc Imaging. 2021; doi: 10.1093/ehjci/jeab210

6. Das A, Kelly C, Teh I, Stoeck CT, Kozerke S, Plein S, Schneider JE, Dall'Armellina E

Depiction of intramyocardial iron in patients following ST-elevation myocardial infarction using diffusion tensor imaging

J Magn Reson Imaging, 2022

7. Das A, Kelly C, Teh I, Stoeck CT, Kozerke S, Sharrack N, M, Swoboda PP, Greenwood JP, Schneider JE, Plein S and Dall'Armellina E.

Pathophysiology of LV remodelling following ST-elevation myocardial infarction: a longitudinal cardiac diffusion tensor MRI study

JACC: Cardiovascular Imaging, 2022

Abstracts

1. **Das A**, Kelly C, The I, Stoeck CT, Kozerke S, Brown LAE, Saunderson CED, Chew PG, Swoboda PP, Levelt E, Greenwood JP, Plein S, Schneider JE, Dall'Armellina E. Diffusion tensor imaging in patients following acute myocardial infarction. Poster presentation at SCMR conference, Bellevue, Washington, USA, 2019.

2. **Das A**, Kelly C, The I, Stoeck CT, Kozerke S, Brown LAE, Saunderson CED, Craven TP, Chew PG, Swoboda PP, Levelt E, Greenwood JP, Plein S, Schneider JE, Dall'Armellina E. Longitudinal changes in diffusion tensor imaging parameters following acute ST-elevation myocardial infarction. Oral presentation at EuroCMR, Venice, Italy, 2019.

3. **Das A**, Ben-Arzi H, Kelly C, Teh I, Stoeck CT, Kozerke S, Brown LAE, Saunderson CED, Craven TP, Chowdhury A, Swoboda PP, Levelt E, Greenwood JP, Plein S, Schneider JE, Dall'Armellina E. Depiction of Microvascular Obstruction using Diffusion Tensor Imaging. Poster presentation at SCMR conference, Orlando Florida, February 2020.

4. **Das A**, Kelly C, Aldred M, Teh I, Stoeck CT, Kozerke S, Chowdhury A, Craven TP, Jex N, Ben-Arzi H, Thirunavukarasu S, Greenwood JP, Plein S, Schneider JE, Dall'Armellina E. The effect of microvascular obstruction on the myocardial microstructure – a Diffusion Tensor Imaging study. ePoster presentation at EACVI - Best of Imaging 2020 virtual conference.

5. **Das A**, Kelly C, Aldred M, Teh I, Stoeck CT, Kozerke S, Chowdhury A, Craven TP, Jex N, Ben-Arzi H, Thirunavukarasu S, Greenwood JP, Plein S, Schneider JE, Dall'Armellina E. Changes in diffusion tensor imaging markers from microvascular obstruction. ePoster presentation at SCMR Virtual Scientific Sessions 2021.

Acknowledgements

The work in this thesis would not have been possible without the contributions and dedicated support of many others. First and foremost, I would like to express my appreciation for my supervisors Dr Erica Dall'Armellina, Professor Sven Plein and Professor John Greenwood. Their leadership and academic guidance throughout my time at the University of Leeds has proved invaluable. In particular, I want to give a special thanks to Dr Dall'Armellina, as she has supported me virtually through every step of this journey. I thank her not only for providing me with this opportunity, but also for her passion, enthusiasm and expertise for clinical research, which has inspired and helped me overcome many barriers throughout my PhD.

This project would not have been possible without the contributions of physicists Professor Jürgen Schneider and Dr Irvin Teh. Their pioneering work and pre-clinical validation of cardiac diffusion imaging has paved the way for me to take the sequence forward into clinical validation on patients. I would like to give a special mention to my colleague and dear friend Dr Christopher Kelly, who engineered the post-processing software we now use for cardiac diffusion analysis. I have lost count of the hours we spent working together troubleshooting through various issues and I thank him for his guidance, patience and tireless support.

I am indebted to our dedicated and hard-working team of research nurses, including Eunice Ikongo, Melanie Spurr, Hannah Newman, Fiona Richards and Petra Bijsterveld for their diligent efforts in patient recruitment and administrative work, ensuring all the studies ran efficiently and that all our patients got home safely.

Clinically implementing and validating a novel imaging sequence is challenging; hence I was extremely fortunate to have had a talented group of radiographers working with me. They include Margaret, Lisa, Gavin, Julian, Faz and Sophie, as well as our clinical assistants Debbie and Claire who always made sure the department ran smoothly. I

thank them for their hard work, flexibility and for welcoming me into the CMR family. They are a credit to Leeds General Hospital.

I would like to thank my fellow colleagues: Dr Brown, Saunderson, Craven, Chew, Chowdhury, Jex, Thirunavukarasu, Sharrack and Gorecka for their support, comradery and making the department a fun place to work in.

I would next like to acknowledge my parents for their lifelong hard work which provided me access to good education, without which I would not be where I am today. They have inspired me to work harder and to always believe in myself. I also am grateful to my parents-in-law who have lovingly provided hours of childcare, which has enabled me to complete my write up. I thank my daughter Latika for bringing such joy into my life, which has helped me keep this all-consuming thesis in perspective. I thank my wife Maya for her unwavering kindness, love and patience during my long hours of work, which has given me the strength to deal with the most challenging times.

And finally, the greatest thanks go to the patients who invested their time to participate in these research projects, which helps to increase our understanding in this field and will hopefully lead to improvements in patient care. I would also like to thank the British Heart Foundation and Heart Research UK for funding various aspects of the project.

Table of contents

List of Figures

List of Tables

List of Equations

List of Abbreviations

ADC   Apparent Diffusion Coefficient

ANOVA   Analysis of variance

AUC   Area Under Curve

AMI   Acute Myocardial Infarction

CM   Myocytes with circumferential orientation

CMR   Cardiac Magnetic Resonance

CoV   Coefficient of Variation

CPEX   Cardio-pulmonary exercise

CSF   Cerebro-Spinal Fluid

DCM   Dilated Cardiomyopathy

DT-CMR   Diffusion Tensor Cardiac Magnetic Resonance

DW   Diffusion Weighted

DWI   Diffusion Weighted Imaging

ECV   Extracellular Volume

EPI   Echo Planar Imaging

FA   Fractional anisotropy

FOV   Field of View

FT   Feature Tracking

FWHM	Full width at half maximum
GLS	Global Longitudinal Function
G+/P-	Genotype positive phenotype negative
HCM	Hypertrophic Cardiomyopathy
HF	Heart Failure
ICD	Implantable Cardioverter Defibrillator
IMH	Intramyocardial Haemorrhage
LAD	Left Anterior Descending
LGE	Late gadolinium enhancement
LHM	Myocytes with left-handed orientation
LV	Left Ventricle
LVEF	Left Ventricular Ejection Fraction
LVOT	Left Ventricular Outflow Obstruction
LVH	Left Ventricular Hypertrophy
MACE	Major Adverse Cardiovascular Events
MD	Mean diffusivity
MI	Myocardial Infarction
MOLLI	Modified Look-Locker Inversion Recovery
MR	Mitral Regurgitation
MRI	Magnetic Resonance Imaging

MSI	Myocardial Salvage Index
MVO	Microvascular Obstruction
PCI	Percutaneous Coronary Intervention
PPCI	Primary percutaneous coronary intervention
PVP	Polyvinylpyrrolidone
RCT	Randomised Control Trials
RHM	Myocytes with right-handed orientation
ROI	Region of interest
RV	Right Ventricle
SAM	Systolic anterior motion
SCD	Sudden Cardiac Death
SD	Standard Deviation
SE	Spin echo
SNR	Signal-to-noise ratio
SPECT	Single-Photon Emission Computed Tomography
STEAM	Stimulated echo acquisition mode
STEMI	ST elevation myocardial infarction
TE	Echo Time
TE	Echo time
TR	Repetition time

Thesis Abstract

Diffusion tensor cardiac magnetic resonance (DT-CMR) is an emerging technique capable of characterising myocardial architecture in-vivo, something previously only possible in post-mortem studies. By measuring the velocity of diffusion of water molecules as it is impeded by cell membranes in the myocardium, DT-CMR can measure the mean diffusivity (MD) and fractional anisotropy (FA) - markers of magnitude and anisotropy of diffusion of water molecules. Based on the principle that water diffusion occurs preferentially along the long axis of cardiomyocytes, DT-CMR can infer upon the orientations of myocardial sheetlets by measuring the absolute secondary eigenvector angle (E2A), and the orientations of cardiomyocytes.

This offers the potential to elucidate many of the pathophysiological mechanisms of cardiovascular diseases that are currently not well understood, as well as providing diagnostic and prognostic biomarkers which can complement the techniques that are currently available. The overall aim for this thesis was to validate the technical and clinical applications for DT-CMR in cardiovascular diseases. Specifically, this thesis includes work on sequence development, post-processing refinements and clinical studies of patients following ST-elevation myocardial infarction (STEMI) and patients with hypertrophic cardiomyopathy (HCM).

Recent advancements in percutaneous coronary intervention have improved survival rates following STEMI, but despite optimal management, up to a third of STEMI survivors develop adverse left ventricular (LV) remodelling in the long-term. This is characterised by progressive cavity dilatation, impaired contractility and is associated with reduced survival. Adverse remodelling is difficult to predict and this maybe in part due to the incomplete understanding of the pathophysiological processes, particularly earlier in the disease pathway. By studying the acute and dynamic changes in microstructure post-injury, DT-CMR may help explain the ensuing maladaptive, mechanical changes in the myocardium.

The aims of chapters 3-4 were to examine how DT-CMR parameters are affected following STEMI, comparing infarcted myocardium with adjacent and remote areas. The aim of chapter 5 was to establish the predictive relevance of acute DT-CMR for adverse-remodelling at 12 months post-STEMI. Through our results, we demonstrate that patients are at significantly greater risk if their acutely infarcted myocardium exhibits reduced FA (signifying cardiomyocyte disarray) and reduced E2A (signifying the underlying myocardial sheetlets remain fixed in a hypo-angulated state during systole). These results demonstrate the potential clinical utility of DT-CMR for prognostic risk-stratification following STEMI.

These findings encouraged me to explore the behaviour of DT-CMR parameters in patients with HCM. This is another condition where the prognosis is diverse and difficult to predict, again partly owing to incomplete understanding about the underlying pathophysiological mechanisms particularly early on in the disease pathway. The aim of chapter 6 was to compare DT-CMR parameters between healthy volunteers, athletes and HCM patients. Our results demonstrated than HCM patients have globally higher MD (signifying diffusion is more unrestricted), reduced FA (signifying cardiomyocyte disarray) and higher E2A (signifying the myocardial sheetlets adopt a hyper-angular orientation during systole) than athletes and healthy volunteers. In chapter 8, the aim was to establish if these findings are evident beyond areas of macroscopic abnormalities. Our results demonstrate that in comparison with healthy volunteers, HCM patients – even in myocardial segment with normal wall thickness, normal perfusion and no scarring - have reduced FA, increased E2A and increased MD. These results shed light on the sequence of pathology and demonstrate the clinical utility of DT-CMR for early detection of phenotypic expression in HCM.

In conclusion, DT-CMR is safe, feasible and can provide quantitative information about the histological state of the myocardium, which can complement clinical and imaging risk factors and improve clinical decision making for managing a range of cardiovascular diseases.

Chapter 1: Introduction

Cardiac Magnetic Resonance (CMR) has emerged as a comprehensive imaging modality for patients with cardiovascular disease. Owing to its high spatial resolution, CMR imaging is considered the gold standard for assessing ventricular volumes, wall thickness, wall motion and systolic function. There are a variety of CMR techniques which allow for accurate and reproducible measurements of oedema and scarring by analysing the tissue composition of the myocardium. (1) Current techniques however cannot assess the organisation and integrity of the underlying microscopic components of the heart, such as cardiomyocytes and myocardial sheetlets. With the emergence of cardiac diffusion tensor cardiac magnetic resonance imaging (DT-CMR), this is now becoming possible, offering the potential for improving diagnostic accuracy and prognostic stratification in a wide range of cardiovascular conditions. In this chapter, I will begin by reviewing the current role of CMR in assessing patients following myocardial infarction (MI), in patients with hypertrophic cardiomyopathy (HCM), the currently available techniques and biomarkers and discuss their limitations. This will be followed by a separate introduction chapter focussing on the principles and fundamental concepts of DT-CMR.

1.1 Clinical utility of CMR following Myocardial Infarction

1.1.1 Myocardial Infarction: background of pathology

The heart receives its own blood supply from epicardial coronary arteries, which include the left anterior descending (LAD), the left circumflex artery and the right coronary artery. Acute MI, often referred to as a heart attack, results from a decrease or stoppage of blood flow to a portion of the heart, typically due to severe narrowing and/or plaque rupture with blood clots in one of the epicardial coronary arteries, which leads to cell death and permanent scarring of heart muscle in the affected territory. (2) In the acute stages, the necrotic tissue triggers an inflammatory response, resulting in

oedema. Over time, this oedema gradually resolves, and the necrotic tissue is replaced by collagenous connective tissue. The replacement fibrotic tissue lacks the mechanical apparatus needed for contraction during systole, hence the overall pump function of the heart is effectively impaired to some degree depending on the size and extent of infarction. (3) This sudden reduction of contractility in the left ventricle (LV) leads to an acute increase in loading conditions and triggers adaptive neurohormonal mechanisms. (4) Failure to normalise the increased wall stress results in progressive cavity dilatation and deterioration of contractility, a process known as adverse remodelling, which is associated with heart failure and reduction in survival. (5) The fibrotic scar is also a substrate for life-threatening arrhythmia such as ventricular tachycardia and ventricular fibrillation, which can lead to sudden death. (6)

Following MI, by restoring the patency of the culprit coronary artery, blood flow can be reinstated. In the modern era, 'reperfusion' is achieved via percutaneous coronary intervention (PCI), using techniques such as clot aspiration and the deployment of stents across the underlying diseased endothelium. Earlier reperfusion is thought to limit the damage and salvage more myocardium. While advances in PCI have substantially improved immediate outcomes following MI, heart failure (HF) and ventricular arrhythmias remain common and serious complications, leading to significant morbidity, mortality, and a reduced quality of life. The financial burden of heart failure (HF) on society is already considerable and will grow further with an ageing population.(6)

The dynamic tissue composition changes following ischaemia and reperfusion are summarised in the figure below (Figure 1.1).
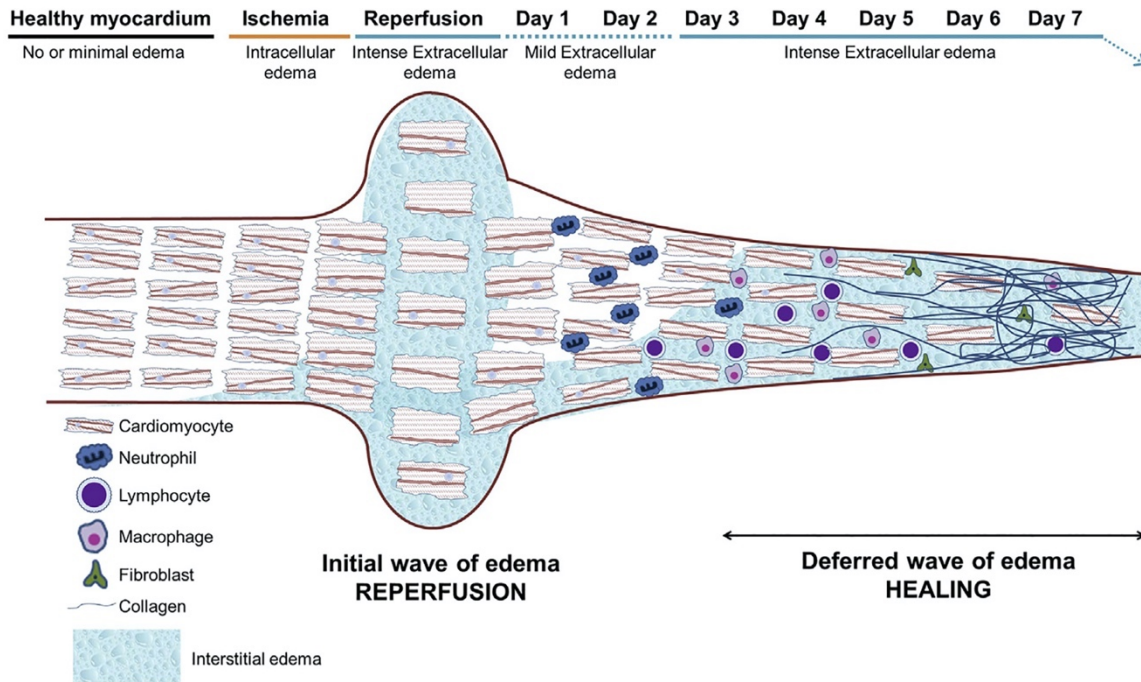
Figure 1.1: Dynamic changes in tissue composition following MI

A degree of intracellular oedema commences shortly following ischaemia. Reperfusion after prolonged ischemia is followed by extracellular oedema. Cardiac fibres become separated by this extracellular oedema, resulting there is a myocardial swelling, which can last for up to 24 hours. Neutrophils, macrophages, and other inflammatory cells infiltrate the post-ischaemic region and replace necrotic tissue with collagen and extracellular matrix over the following days. The healing process results in the so called "deferred wave of oedema," which can last for days to weeks depending on remodelling processes. Figure modified from original (7)

1.1.2 The role of CMR in patients following MI

In clinical practice, management decisions regarding heart failure and arrhythmia therapy following MI are usually based on surrogate biomarkers, such as left ventricular ejection fraction (LVEF). While LVEF can be measured via transthoracic echocardiography by the bedside, CMR can offer a more comprehensive assessment of LV function including the extent of myocardial damage. Using techniques such as late gadolinium enhancement (LGE) and parametric mapping, CMR can detect and measure areas of infarction, microvascular obstruction (MVO), haemorrhage and

oedema, which ultimately can help clinicians identify the patients most at risk of adverse outcomes. As a result, CMR is increasingly being used for detecting endpoints in clinical trials. (8)

1.1.3 CMR techniques and biomarkers for MI

1.1.3.1 Technique: Late gadolinium enhancement

When gadolinium-based contrast agents are injected into subjects, it distributes among extracellular space and is unable to enter intact cardiomyocytes. Over time, the contrast is washed out, however in scar tissue where there is more extracellular space, this washout takes relatively longer. T1 relaxation times (the time taken for 63% of proton spins to recover from longitudinal magnetisation) are relatively shortened where gadolinium is present, resulting in high signals. Hence areas of gadolinium-retention appear hyperenhanced/bright on T1-weighted imaging, and by detecting areas of LGE typically at around 10-15 minutes post injection, contrast-enhanced CMR can depict areas of myocardial fibrosis *in vivo*. This can be planimetered and the total amount of LGE can be expressed as a % of the total LV mass to derive the 'infarct size'.

LGE-derived biomarkers: Infarct Size

In a recent meta-analysis by Stone et al, (9) 2632 patients were pooled from 10 randomized primary PCI trials. They had undergone either CMR (n=1887) or single-photon emission computed topography (SPECT) (n=743) assessment for infarct size within 1-month post-MI. After multivariate analysis, infarct size was found to be a strong independent predictor of all-cause mortality and HF hospitalisation within 1 year (p value < 0.0001 for both). To date, this is the largest and most robust examination of the relationship between infarct size and prognosis after reperfusion.

LGE-derived biomarkers: detection of MVO

Despite restoring the patency of epicardial coronary circulation, a variety of mechanisms including distal embolization of thrombus/plaque, vasospasm and

reperfusion-associated injuries lead to the persistence of hypoperfusion of myocardial tissue in a considerable number of patients after PCI.(10) This phenomenon is referred to as MVO. With CMR, MVO is detected by the lack of gadolinium uptake within hyper-enhanced areas. Several studies have demonstrated a prognostic significance of the presence of MVO following AMI. Waha et al (10) recently pooled data from 1688 patients recruited to 7 randomised primary PCI trials who underwent CMR assessment within 7 days. In multivariable analyses adjusting for both MVO and infarct size, MVO remained significantly associated with all-cause mortality ($p<0.0001$). The absence of MVO meanwhile was an independent predictor of left ventricular recovery, reflected in improvements of LVEF over time.

Limitations of LGE following MI

In the chronic stages of MI when the initial wave of oedema has passed, the presence of LGE is suggestive of irreversible injury, but in acutely infarcted segments (especially in the first 72 hours), factors such as myocardial oedema and the effects of reperfusion therapy add complexity to infarct imaging, reducing the accuracy of LGE to predict 'final' infarct size and long-term remodelling. (11,12) Post-processing analysis of LGE also is signal intensity/threshold based and hence strictly dependent on the methodology and execution (i.e., image acquisition at the appropriate time delay post contrast injection to 'null' the myocardium) and post processing (i.e., choosing an appropriate reference 'region of interest' for the remote myocardium).

Therefore, calculation of infarct size is heavily influenced by the timing of scan following MI, the dose and type of contrast agent used, the timing of LGE image acquisition following contrast administration; as well as the method used for quantification. Bulluck et al. conducted a review of the CMR protocols used in 62 randomized control trials (RCTs) and found significant heterogeneity in the scanning protocols between the different trials.(11) Based on their findings, the authors made recommendations for more standardised future acute CMR scan protocols. (Table 1.1)

Category	Recommendations based from Bullock et al (11)
Optimal timing of acute scans	Because of excess oedema in the early phase, LGE analysis from CMR scans performed before 3 days following MI overestimates MI size. Meanwhile MVO and IMH size peaks by day 3 after MI before gradually reducing. Acute CMR scan should therefore be undertaken within 5±2 days post-MI.
Optimal timing of follow up scans	Pairing acute and follow-up scans allow the study of LV remodelling. Chronic MI size is relatively stable between 1 month and 1 year. Follow-up scans at 6 months is the most popular interval in clinical trials.
Timing of LGE acquisitions	Early acquisition (<8mins) of LGE images results in overestimation of MI size. Acquiring at 25 mins produces the most accurate estimation. As a compromise between scan times and accuracy, it is recommended to acquire LGE images between 10 and 15 mins.
Methods of quantifying infarct size	Manual contouring is time-consuming but remains the reference standard. Semi-automated models including 5-standard deviations (SD) and 'full width half method' techniques are more reproducible and timesaving but still require manual input. Thus far, the accuracy of semi-automated methods for infarct sizing has proved inferior to manual contouring. A more stringent 6-SD model may be more reliable and accurate but needs further development.

Table 1.1: Summary of recommendations for LGE assessment of MI patients

Even after following these recommendations, further limitations of LGE require highlighting. LGE assesses tissue dichotomously as either viable or nonviable across the transmural extent of myocardium but cannot measure the severity of tissue damage within the hyperenhanced area. Finally, LGE requires the administration of potentially nephrotoxic contrast agents and may be unsuitable in patients with advanced renal failure.

1.1.3.2 Technique: Parametric relaxometry mapping

Parametric relaxometry mapping is a quantitative technique that provides pixel-by-pixel representation of absolutely denominated numerical T1, T2 or T2* properties, expressed in units of time, typically in milliseconds. (13) The magnetic relaxation

properties of the myocardium can differ depending on the tissue composition. T2* relaxation times are shortened by magnetic field inhomogeneities induced by myocardial iron deposition, and hence can detect the presence of intramyocardial haemorrhage (IMH). (14) T1 and T2 relaxation times are affected by molecular motion, size and interactions. T2 relaxation times are longer in the presence of water, hence in the context of MI, T2 is increased in areas of oedema. Native myocardial T1 values have recently been validated in a large multicentre normal cohort study to have a tight normal range (15). T1 relaxation times become prolonged in areas of oedema and scar tissue. (14,16) T1 relaxation times can also be measured after injecting contrast agents; as T1 relaxation times become more shortened in areas of gadolinium-retention, post-contrast T1 relaxation times can be used to calculate the extracellular volume (ECV- expressed as %), using the following equation (Equation 1.1):

Myocardial ECV = $(1-\text{haematocrit}) \times (\Delta R1\text{myocardium}/\Delta R1\text{blood})$, were R = 1/ T1

Equation 1.1: Equation for calculating ECV

Unlike LGE, native T1 and ECV maps can provide absolute values per pixel, rather than relying on a thresholding process for identifying infarct tissue. This allows for measuring not only the infarct size, but also assess the severity of injury.

Mapping derived biomarkers: Detection of IMH

Severe microvascular injury causes a loss of endothelial integrity, leading to extravasation of blood into the myocardium, also known as IMH. This eventually leads to the deposition of iron in the myocardium, the persistence of which provides a source of prolonged inflammatory burden in the convalescent phase, promoting adverse LV remodelling. The breakdown products of haemoglobin alter the magnetic properties by shortening the T2* relaxation times. Hence T2* maps can depict and quantify the amount of IMH and persistent iron post-MI.

In an animal study by Cokic et al, higher iron content within infarcted canine hearts was associated with a significant prolongation of the QT and QTc interval, a phenomenon typically associated with ventricular arrhythmias. Observations from this

study suggest the extent of iron deposition could be a predictor of arrhythmias in humans. (6)

The predictive relevance for LV remodelling with IMH quantification by CMR was shown by Carberry et al in a prospective study of 203 AMI survivors following reperfusion. (17) They demonstrated that patients with IMH at 6 months had higher LVEDV and worse LVEF. In addition, there was a 4-fold increase in all-cause mortality, HF and a 3-fold increase in the likelihood of major adverse cardiovascular event (MACE).

Mapping derived biomarkers: Native T1 of infarct myocardium

Several studies have shown that higher T1 values within infarct myocardium is representative of more severe injury, is associated with reduced likelihood of functional segmental recovery (18,19) and increased likelihood of adverse LV remodelling. (20) This makes T1 mapping a useful tool for prognostication when assessing chronic infarct segments, but in the acute stages following MI, T1 maps cannot easily differentiate between infarcted and oedematous myocardium. Some authors have proposed cut-off values for differentiating between remote, oedematous and irreversibly damaged myocardium in the acute stages of MI, but this threshold will vary from scanner to scanner due to difference in magnetic field strengths and pulse sequence parameters. (19)

Mapping derived biomarkers: ECV of infarct myocardium

Increased ECV in the infarcted myocardium is indicative of more severe injury. Kidambi et al (21) performed acute (day 2) and convalescent (3 month) CMR scans in 99 patients following AMI, and demonstrated that higher acute infarct ECV was predictive of lower LV systolic function at 3 months.

Mapping derived biomarkers: Native T1 of remote myocardium

Structural changes in LV remodelling are not limited to the territory of the culprit artery, but also affect remote myocardium. In the weeks following AMI, the remodelling

process is predominantly driven by hypertrophy of the healthy remote myocardium for compensatory purposes. This phenomenon has been demonstrated previously in histological animal studies, but CMR allows a more comprehensive in vivo evaluation of such changes in humans with prognostic implications.

Carberry et al (22) performed CMR scans on 140 patients, on day 2 and 6 months post AMI. Using multivariate regression, they demonstrated LVEF was inversely associated with remote zone ECV alterations ($p<0.001$). In a more recent study, Reinstadler et al (23) performed non-contrast T1 mapping on 255 AMI patients following reperfusion. They were able to demonstrate that patients with increased remote zone native T1 had significantly higher MACE at 6 months. The inclusion of remote zone T1 alterations to more conventional risk factors such as LVEF and infarct size added incremental prognostic information.

Limitations of parametric mapping techniques

As mentioned above, both T1 and T2 relaxation times are prolonged in areas of oedema. So, while native T1 and ECV maps are useful tools for assessing the severity of injury in chronic infarct segments, both are affected by the presence of oedema which often ensues in the acute stages of MI. Hence it remains challenging to differentiate between infarcted and oedematous myocardium immediately post-MI. ECV mapping also requires the administration of potentially nephrotoxic contrast agents.

1.1.3.3 Technique: CMR Feature tracking

Advanced imaging of global and regional myocardial deformation, also referred to as CMR feature tracking, holds promise. The underlying principle is based on recognising and tracking patterns or features in one cine-image over several frames to provide an estimation of tissue displacement, not just in the radial plane, but also in the longitudinal and circumferential plane. Therefore, CMR feature tracking provides a marker of regional and global function beyond LVEF.

Feature tracking biomarker: Global longitudinal strain (GLS)

Recent evidence suggests global longitudinal impairment provides independent and incremental prognostic information for the prediction of all-cause mortality as shown by Eitel et al in 1,235 patients within the first 10 days following AMI.(24) Over a 12-month follow up period, GLS impairment in particular was found to be independently associated with MACE, even after adjustments for established CMR markers of poor prognosis such as LVEF and MVO. The value of GLS in predicting MACE post-MI may relate to the subendocardial location of the longitudinal fibers, the area most affected by AMI.(25) When combined with LVEF and infarct size, GLS assessments provided incremental prognostic value.

Limitations of CMR feature tracking

In CMR feature tracking, it remains challenging to distinguish features within the compact myocardium of the LV, presumably due to the relatively large dimensions of voxels and the relative homogeneity of water content and tissue properties. CMR feature tracking also predominantly focuses on in-plane motion and is unable to account for through-plane motion.(26) In general, this is a relatively novel technique, and warrants further validation in multi-centre studies.

1.1.4 Conclusions

CMR has emerged as a robust imaging technique for tissue characterisation and prognostic stratification following MI. LGE remains the reference standard for detecting infarcted myocardium and MVO, and recent advancements in parametric mapping allow for the detection of oedema, haemorrhage, and diffuse interstitial changes in remote myocardium. The various different tissue characteristics and relevant sequences described above are summarised in Figure 1.2.
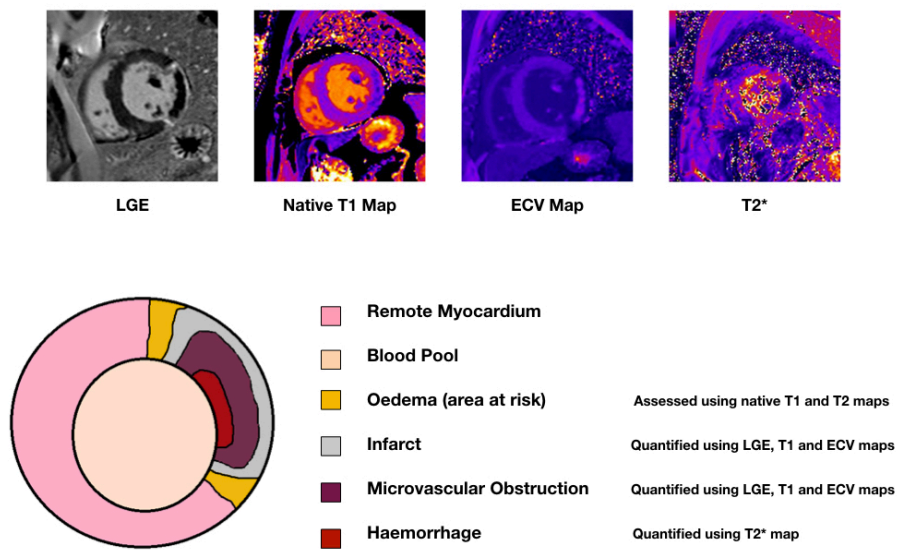
Figure 1.2: CMR tissue characterisation techniques

Representative parametric maps in a patient following an acute MI in the left circumflex territory. Tissue characteristics of the various regions shown above can be characterised using T1, T2, ECV and T2* maps as indicated.

In a recent expert panel consensus paper, based on currently available literature, the authors make designed a hierarchy of CMR biomarkers for use in future CMR-related clinical studies of MI patients, as shown in Figure 1.3.
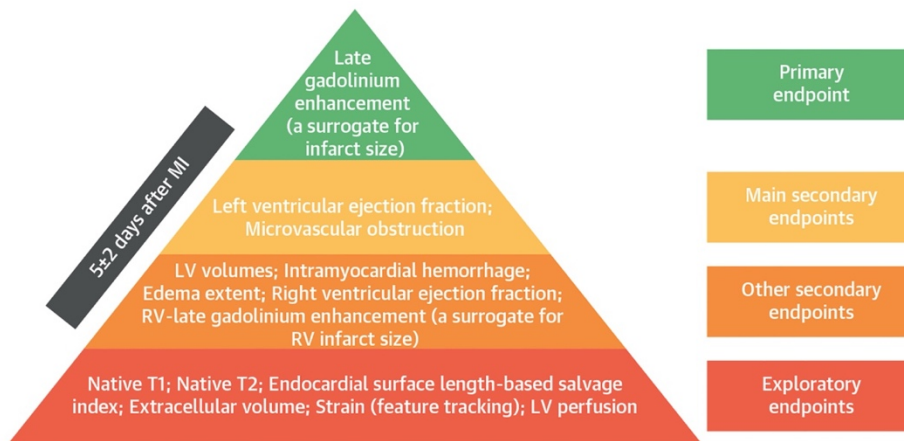
Figure 1.3: Hierarchy of recommended CMR endpoints in future clinical studies

Infarct size derived using LGE can predict mortality and incidence of heart failure and is recommended as the primary endpoint in CMR-related clinical trials of MI patients. LVEF and MVO have consistent links with MACE and therefore are listed as main secondary endpoints. Other secondary endpoints including IMH, and extent of oedema have association with MACE but do not persist after adjusting for either CMR variables. Exploratory endpoints include techniques with only anecdotal evidence of associations with MACE. Figure modified from original. (7)

It is worth noting most if not all the sequences mentioned in this chapter are affected by the presence of oedema by some degree; hence it remains challenging to depict areas which are irreversibly injured in the acute stages following MI. None of the sequences offer information about the underlying microstructure of the myocardium following ischaemic injury.

1.2 Clinical utility of CMR in hypertrophic cardiomyopathy

1.2.1 Hypertrophic cardiomyopathy: background of pathology

Hypertrophic cardiomyopathy is the most common inherited cardiomyopathy, characterised by unexplained increase in the LV wall thickness in a non-dilated chamber that is not solely explained by abnormal loading conditions. (27) The vast majority of HCM patients remain asymptomatic with normal life expectancy, however a small sub-group of patients have a substantially increased risk of developing adverse disease complications such as sudden cardiac death (SCD), progressive heart failure and stroke. This heterogeneous pattern of phenotypic expression makes HCM a challenging condition to diagnose and manage.

1.2.1.1 Histopathology

In 1958, Dr Teare, a pathologist working in St George's Hospital in London, performed histological assessment of 8 HCM patients, and noted the muscle bundles in the ventricular septum to have 'bizarre' and 'disorganised' arrangements. Advancements made in histological techniques have allowed pathologists to characterise microscopic features of HCM in greater detail, which now include the following:

- Myocyte hypertrophy at a cellular level with abundant eosinophilic cytoplasm and box shaped nuclei. Individual myocytes show myofibrillar disorganisation and fragmentation and irregular side-to-side connections between myocytes. (28)
- Disarray of myocardial architecture (myofibrillar disarray), with bundles of cardiomyocytes arranged at perpendicular and oblique angles to each other. (Figure 1.4) (28)
- Intramural coronary arteries exhibit smaller cross-sectional luminal area. (29)
- Type IV collagen forms thickened patches around myocytes (interstitial fibrosis), between disorganised myofibrillar matrices (plexiform fibrosis), around intramural arterioles (peri-vascular fibrosis) as well as in coarse scar tissue (replacement fibrosis). (30)
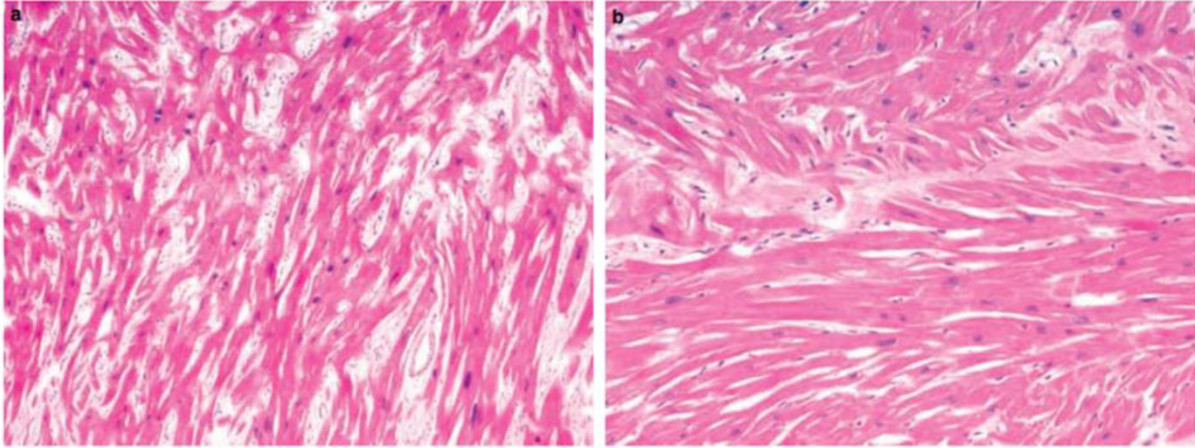
Figure 1.4: Histology of myocyte disarray

HCM patients have hypertrophied and misshapen myocytes arranged at perpendicular and oblique angles around foci of interstitial collagen in pinwheel (left) or herringbone patterns (right). (31)

Limitations of histological studies

The invasive nature of endomyocardial biopsies makes the technique unsuitable for routine use in asymptomatic patients, so the vast majority of biopsies are sampled from explanted end-stage HCM hearts. The lack of a suitable animal model, and the difficulty in obtaining tissue samples from patients in the earlier stages of the disease creates a gap in knowledge regarding the early microstructural changes that occur in HCM. (32)

1.2.1.2 Genetics

With the advent of contemporary genetic testing and imaging, the prevalence of HCM is thought to be 1 in 200. (33) Genetic mutations encoding for the sarcomeric proteins which form the contractile apparatus of cardiomyocytes have been identified as a cause; with cardiac β-myosin (MYH7) and cardiac myosin binding protein-C (MYBPC3) being the two most common mutant genes, although over 1,400 mutations in more than 13 different genes have been identified. (34) These mutations are transmitted in an autosomal dominant pattern, with each offspring having a 50%

chance of being affected. Most patients develop evidence of disease in early adulthood, however the penetrance of phenotypic expression can vary substantially depending on the affected genes, resulting in delayed phenotypic expression in mid-life and beyond. (35)

Genetic testing can identify mutations in 50-60% of HCM patients with phenotypic evidence of disease; the genetic basis for the remaining patients remains uncertain. However, once a mutation is identified in an index HCM patient (also termed as 'proband'), family members can be screened for the same mutation in order to identify relatives at-risk of developing the condition. Relatives who are found to have the mutation in the absence of LV hypertrophy are termed genotype positive/phenotype negative (G+/P-). There is a high likelihood that this group will develop phenotypic evidence later in life, hence interval imaging for surveillance is recommended. However, the precise relationship between mutations and phenotype remains unclear; disease expression can vary even amongst first-degree family members with the same mutation. This could be due to the incomplete understanding about factors such as how modifier genes and the environment can contribute to phenotypic expression. Hence at present, identification of specific mutations cannot independently predict risk of adverse disease related events such as SCD.

1.2.2 The role of CMR in patients with HCM

CMR has now emerged as an important imaging modality for the diagnosis and prognostic stratification of HCM. CMR provides 3D tomographic imaging of high spatial and temporal resolution in any plane without the need for ionising radiation. Functional cine-imaging sequences such as balanced steady-state-free-precession imaging create sharp contrast between myocardium and blood pool. This creates clear delineation of endo- and epicardial borders, which allow precise measurements of wall thickness and LV mass. Acquisition of short-axis stacks covering the full LV with no interslice gap allows for the detection of focal hypertrophy. Unlike echocardiography, CMR is not hampered by poor image quality in relation to patients' body habitus, or pulmonary parenchyma, or inaccurate wall thickness measurements from short-axis

obliquity. CMR can also assess tissue characterisation through sequences such as LGE and parametric mapping, which can help identify patients at higher risk of adverse outcomes. (36)

1.2.2.1 CMR for Diagnosis of HCM

In adults, HCM is defined by a wall thickness of ≥15 mm in one or more LV myocardial segment that is not explained solely by loading conditions. First-degree relatives of HCM patients with unexplained wall thickness of ≥13 mm also meet the diagnostic criteria. (27) Traditionally, two-dimensional echocardiography has been the primary imaging modality for the diagnosis and surveillance of HCM, however CMR can help overcome a number of limitations of echocardiography.

When echocardiographic images are of suboptimal quality, CMR has a distinct advantage of defining LV wall thickness with superior resolution imaging. CMR can also detect the presence and extent of focal hypertrophy in regions what are difficult to visualise with echocardiography, such as the anterior free wall, posterior septum and apex. These observations support the growing use of CMR in screening of family members. (37)

1.2.2.2 Phenotypic characterisation using CMR

Patterns of ventricular hypertrophy

The most common location for LVH in HCM patients is the basal anterior septum with the contiguous anterior free wall, followed by the inferoseptum at the mid-LV level. The majority of patients have diffuse hypertrophy involving more than 50% of the LV, however a minority exhibit only focal hypertrophy. Although septal predominance is more common, through CMR observations there is a growing appreciation of cases where hypertrophy isolated to the LV lateral wall and apex. (38) Wall hypertrophy exceeding 30mm is thought to increase risk of sudden death.

A subgroup of HCM patients have thin-walled apical aneurysms, usually associated with mid-ventricular hypertrophy. Given the known limitations of echocardiography in

visualising the LV apex, this group was historically under-diagnosed prior to the introduction of CMR imaging. With contrast-enhanced CMR imaging, it is now appreciated that these apical aneurysms are primarily composed of fibrotic tissue and thus present an important substrate for the generation of malignant ventricular arrhythmias. (39) Therefore the presence of apical aneurysms helps identify patients at high risk of SCD and is factored into decision making regarding ICD implantation for primary prevention. (27)

Accurate characterisation of RV morphology is difficult with echocardiography because of known limitations, however through CMR, it is now recognised that up to a third of HCM patients also have right ventricular hypertrophy, defined as wall thickness >8mm. This most commonly occurs at the anterior or inferior interventricular junction points, however the prognostic significance of RVH in HCM still remains uncertain. CMR can also help identify prominent RV muscle structures such as the crista supraventricularis – a structure located adjacent to the basal LV septal wall which often mistakenly included in measurements of LV wall thickness, resulting in overestimation of maximal wall thickness. CMR allows accurate delineation of the epicardial walls, which allows the reporter to identify and exclude the RV crista muscles from their measurements.

Outflow obstruction

Depending on the location, LVH can obstruct the left ventricular outflow obstruction (LVOT), effectively causing sub-aortic stenosis. This mechanical obstruction impairs the ability of the heart to increase the stroke volume when required, for instance during exercise, leading to symptoms such as shortness of breath, chest pain and syncope. As a consequence of this obstruction, high velocity jets in the LVOT can drag the anterior mitral valve leaflet (AMVL) into the LVOT via venturi effect, a phenomenon known as systolic anterior motion (SAM). This not only worsens the LVOT obstruction itself, but also prevents the mitral valves from closing during systole and leads to a posteriorly directed jet of mitral regurgitation (MR), which further reduces the effective stroke volume. Invasive treatment in the form of alcohol septal ablation and surgical

septal myomectomy are recommended for symptomatic patients with provoked LVOT gradients greater than 50mmHg. (27)

In CMR, phase velocity flow-mapping sequences can be performed to obtain peak velocities of blood flow through the LVOT, as well as quantify the amount of mitral regurgitation, however it is not clear how well CMR-derived velocities correspond with doppler echocardiography, and CMR measurements can only be made in resting conditions rather than on provocation (during exercise for instance). Hence current management decisions continue to rely predominantly on pressure gradients derived from doppler echocardiography. Should the patient require invasive therapy in the form of surgery or alcohol ablation, CMR can still be helpful in pre-procedural planning by revealing the pattern and distribution of wall thickness, as well as identifying additional morphologic abnormalities of the mitral valve apparatus which may also require repair. (32)

Anomalies of mitral valve apparatus

The growing use of CMR has helped identify a range of anomalies of the mitral valve apparatus in HCM patients, which include:

- Elongated mitral valve leaflets (anterior >30mm, posterior > 17mm) (40)
- Anterior displacement of the mitral valve (40)
- Increase in number and size of papillary muscles (41)
- Anterior displacement of papillary muscles which increases the likelihood of SAM and LVOT (41)

These morphological abnormalities can occur independent of LV thickness, and is thought to represent primary phenotypic expressions of the disease. (32)

Diastolic dysfunction

Radial contraction and LVEF is typically preserved or increased in the majority of HCM patients (27), however LV hypertrophy results in chamber stiffness, which impairs ventricular relaxation in diastole. Mechanisms for this include: increased systolic

contraction load caused by LVOT obstruction, non-uniformity of ventricular contraction and relaxation, and delayed inactivation caused by abnormal intracellular calcium reuptake. (42) HCM patients can develop heart failure symptoms despite having preserved LVEF due to diastolic dysfunction. Doppler echocardiography remains the preferred method of assessing the diastolic function through the study of LV blood in-flow patterns, although CMR can still be useful for obtaining accurate measurements of left atrial dimensions, which is known to enlarge in diastolic function and is an independent predictor of adverse outcomes in HCM. (27)

Microvascular disease (MVD)

HCM patients can have myocardial ischemia in the absence of epicardial coronary artery stenosis. Exact mechanisms are not fully clear but are thought to be composite effects of intramural small-vessel abnormalities, myocardial bridging, abnormal myocellular architecture, massive hypertrophy and impaired coronary flow reserve. In addition to the above mechanisms, impaired LV relaxation and increased intra-cavity left ventricular end-diastolic pressure can compress the coronary microcirculation and further restrict coronary blood supply. (42) (Figure 1.5)
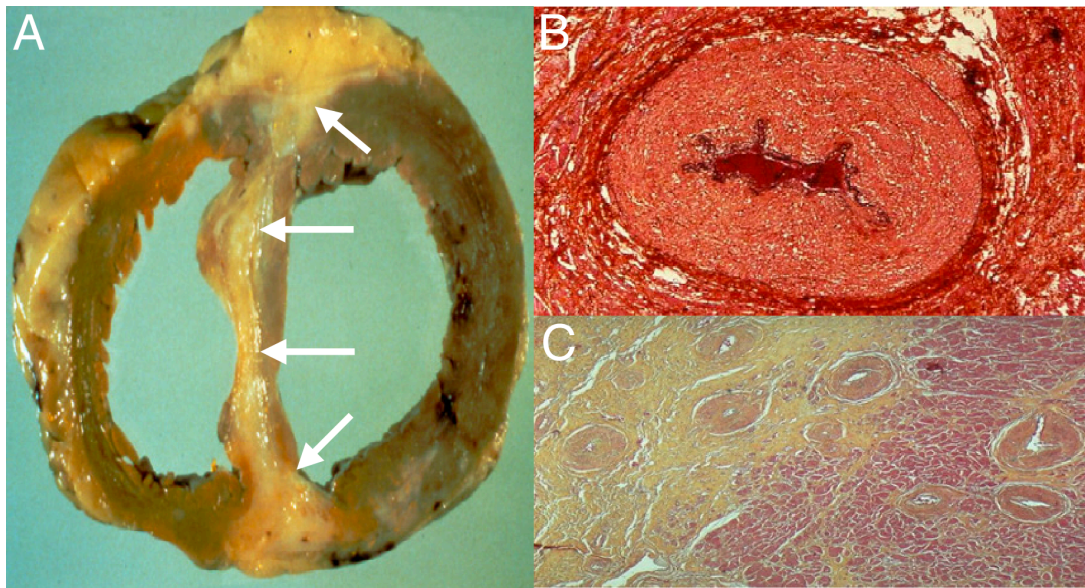
Figure 1.5: Small vessel disease in HCM

Panel A shows the explanted heart of a patient with end-stage HCM. Large areas of scarring are highlighted with the white arrows. Panel B shows an abnormal intramural coronary arteriole with intimal and medial thickening, resulting in a small luminal area. Panel C shows the presence of these abnormal arterioles with and around areas of scarring. (43)

Repeated bouts of microvascular ischaemia over a period of time are thought to lead to myocardial ischaemia-mediate myocyte death, which is subsequently replaced with scar tissue – i.e., replacement fibrosis.

Myocardial fibrosis and systolic dysfunction

Myocardial fibrosis has been extensively documented in HCM. Galati et al histologically analysed 30 hearts explanted from end-stage HCM patients and quantified the extent, type, and distribution of fibrosis. All hearts had massive amounts of myocardial fibrosis, ranging from 23% to 56%, with an average amount of 37%, mostly present in the mid-wall (Figure 1.6). (44)
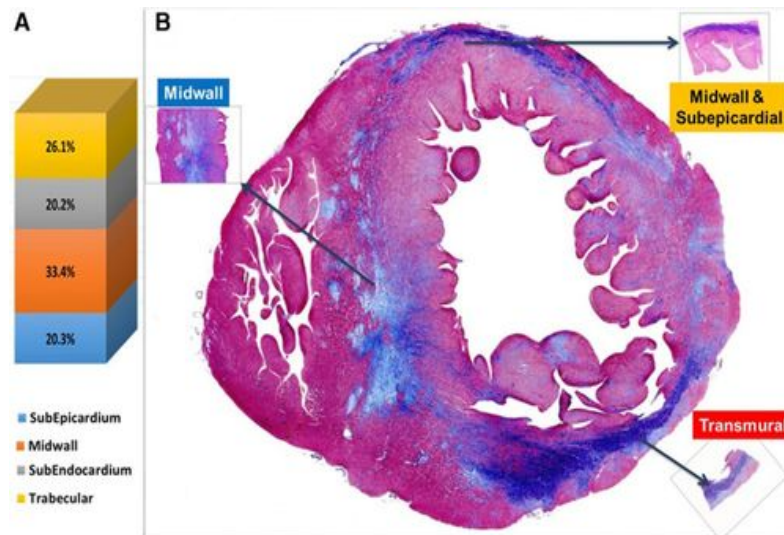
Figure 1.6: Distribution of fibrosis in HCM

From the cumulative analysis of 30 end-stage HCM specimens, fibrosis was most prevalent in the mid-wall, as shown in panel A. Example of heterogeneous fibrosis distribution into myocardial layers are shown in panel B. (44)

1.2.2.3 CMR for family screening

As described previously, cine-imaging CMR sequences can visualise the entire LV cavity and hence detect focal areas of hypertrophy in segments not easily visualised with echocardiography. In addition, CMR can help detect various morphological abnormalities present in G+/P- relatives (in the absence of LVH) including the following:

- Myocardial crypts: These are narrow, deep, blood-filled invaginations within the LV myocardium and are usually located in the basal posterior septum and LV free wall
- Elongated mitral valve leaflets
- Evidence of MVD on perfusion imaging (discussed in section 1.2.3.3)
- Evidence of diffuse fibrosis on T1/ECV maps (discussed in section 1.2.3.2)

These observations support a growing role of CMR in earlier diagnosis of HCM relatives and can prompt close surveillance to detect disease progression.

1.2.2.4 The role of CMR in differential diagnosis of LVH

While HCM accounts for the majority of cases of unexplained LVH in adults, a number of non-sarcomeric disease can result in LVH, mimicking HCM in the process. CMR can be helpful for the identification or exclusion of some of these conditions.

Athlete's Heart

LVH can result from a secondary physiologically adaptive response to intense athletic training sustained over long periods of time, however in clinical practice this can be challenging to distinguish from the pathological LVH in HCM. This is particularly relevant because HCM is one of the commonest causes of sudden unexpected cardiac death among young athletes, so underdiagnosis can expose the athletes to an unduly increased risk of SCD. Meanwhile a false-positive diagnosis of HCM can cause premature discontinuation of a professional sporting career.

While the pattern of LVH in athlete's heart is mostly concentric, the same pattern has been seen in HCM patients.(42) So while a focal asymmetrical pattern of hypertrophy points to a diagnosis of HCM, a concentric pattern of LVH does not exclude HCM. Athletes with LVH are thus advised to undergo a period of systemic deconditioning. A resultant regression of wall thickness more than 2mm supports the diagnosis of athlete's heart, while hypertrophy which remains unchanged supports the diagnosis of HCM. (45) Owing to its high spatial resolution, CMR is well suited for accurate monitoring of wall thickness and LV mass, however the process is still time-consuming and disruptive to the athletes' careers.

The presence of LGE was historically thought of as a good discriminator, adding weight to the diagnosis of HCM. (32) However more recent studies have found that LGE can also be detected in athletes, usually in a non-ischaemic pattern and typically located at the interventricular junctions. A diffuse pattern of LGE has not been demonstrated in athlete's hearts, and still points to alternative diagnosis. (46)

CMR parametric mapping sequences such as T1 and ECV mapping have provided further insights into the underlying mechanisms of LVH in athletes. Swoboda et al

demonstrated athletes with LVH to have significantly lower ECV than HCM patients. (Figure 1.7) The authors postulate that the increase in LV mass in athletes is mediated by cellular hypertrophy, whereas in HCM patients it is driven by cellular disarray and expansion in extracellular matrix. (47)
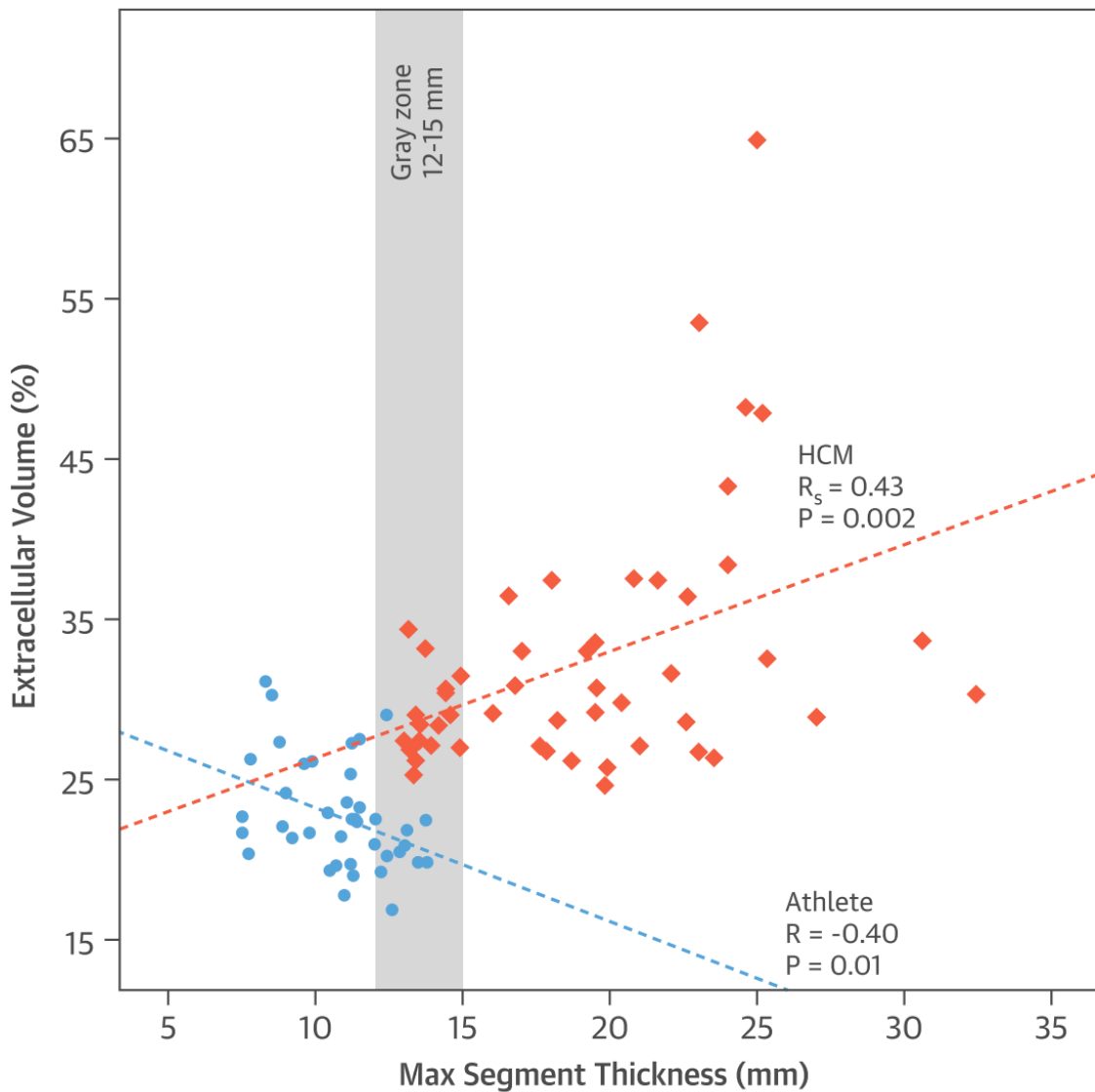
Figure 1.7: Relationship between segmental thickness and ECV

Scatter plot showing maximal segmental thickness and corresponding ECV for HCM patients (orange) and athletes (blue). The grey zone highlights the intermediate zone of 12-15mm which creates diagnostic ambiguity for clinicians. (47)

Given the invasive nature of endomyocardial biopsies, histological analysis of athletes hearts is lacking, presenting another gap in knowledge about the underlying microstructural changes that occur in this cohort, which could potentially help differentiate them from HCM patients.

Hypertensive cardiomyopathy

Exposure to long-standing pressure overload from systemic can invariably result in adaptive LVH, a process known as hypertensive cardiomyopathy. While the pattern of LVH is mainly concentric, subgroups of HCM patients can also have concentric LVH, so differentiating the two conditions can be challenging. CMR can help identify more non-contiguous patterns of hypertrophy (hypertrophied segments separated by non-hypertrophied segments) as well as abnormalities with the mitral valve apparatus, both of which would favour the diagnosis of HCM over hypertensive cardiomyopathy. Another diagnostic strategy is to implement anti-hypertensive medications and monitor LV wall thickness over time; a regression in wall thickness would favour the diagnosis of hypertensive cardiomyopathy, and CMR is yet again well suited to provide accurate serial measurements of wall thickness. (32)

Infiltrative and metabolic cardiomyopathies

Infiltrative cardiomyopathies such as cardiac amyloidosis and metabolic storage diseases (including Fabry's disease) can all result in LVH and non-specific fibrosis.

Fabry's disease is an X-linked lysosomal storage disorder in which mutations in the α-galactosidase A gene leads to cellular accumulation of glycosphingolipids in various organs including the heart. Concentric LVH and inferolateral mid-myocardial scar are the most common manifestations of Fabry's disease, but the pattern can vary and even mimic certain subtypes of HCM. (48)

Amyloidosis is a systemic, infiltrative disorder caused by plasma cell dyscrasia, which results in the deposition of abnormal protein light chains in various tissues. Myocardial amyloid deposition leads to cell death and replacement fibrosis, which results in a number of characteristic features on CMR imaging, including impairment in

longitudinal contraction, pericardial effusion, early 'nulling' of the myocardium following contrast administration and atrial enhancement with LGE.

These conditions generally tend to result in concentric LVH, but as discussed before, that does not exclude HCM per say. The development of parametric mapping sequences such as native T1 and ECV has however proved useful in differential diagnosis. This is discussed in more detail below in section 1.2.3.2.

1.2.3 CMR techniques for assessing HCM

1.2.3.1 LGE for characterising fibrosis

LGE is the reference standard for detecting myocardial fibrosis *in vivo* in HCM patients. In keeping with findings from histological studies, (44) the pattern of LGE can vary in HCM but generally follow a non-coronary distribution. LGE is typically diffuse and patchy, predominantly affecting the midwall, most commonly (but not exclusively confined to) the hypertrophied segments. (32) (Figure 1.8)
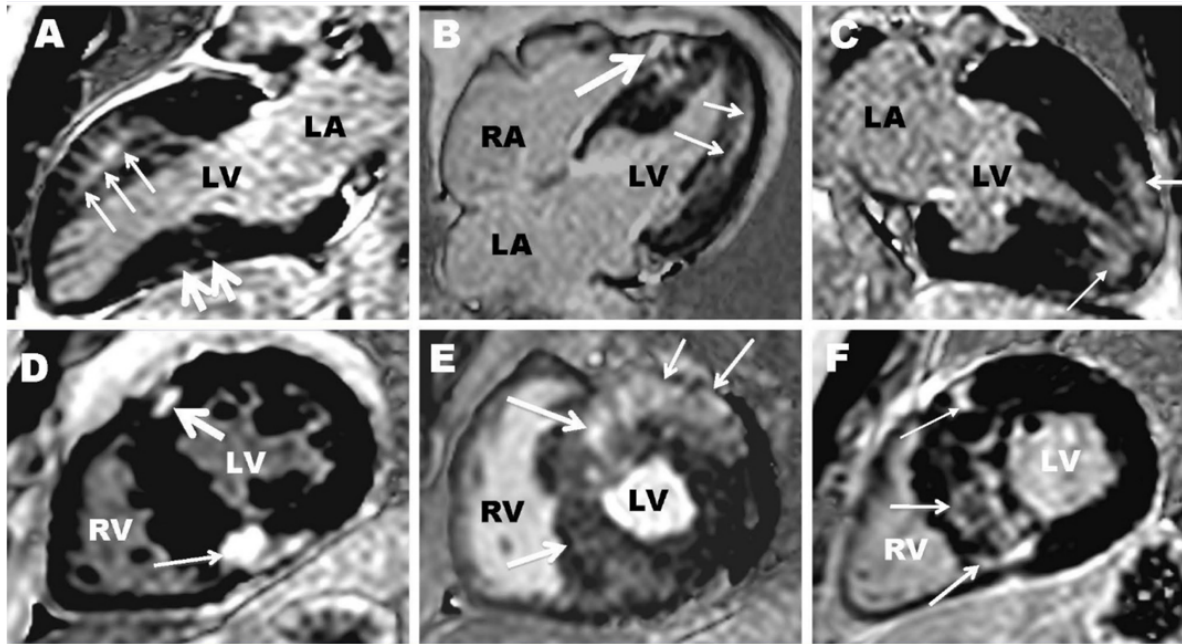
Figure 1.8: Patterns of LGE in HCM

In this figure, 6 difference patterns of LGE in HCM patients are shown. Panel A shows extensive transmural LGE in the anterior wall (small arrows) with a smaller focus in the inferior wall, panel B shows mid-myocardial LGE in the lateral wall with diffuse LGE in the ventricular septum, panel C shows LGE confined the LV apex, panel D shows focal scarring of the insertion point between the LV and the RV, panel E shows transmural LGE involving the ventricular septum and anterior wall, while panel F shows transmural LGE located mainly in the septal walls. (32)

Various studies have shown that the extent of LGE is inversely associated with LV systolic function; HCM patients with LVEF<50% (i.e. end-stage disease) have significantly higher LGE than HCM patients with hyperdynamic LV function. (49,50) However the extent of LGE in HCM patients with low-normal LVEF (50-65%) can vary significantly and overlap with those with impaired function. Hence some HCM patients with low-normal LVEF remain at risk of adverse LV remodelling and heart failure, thus the extent of LGE alone is unable to identify patients at risk of disease progression. (32)

The presence of LGE is also thought to be an arrhythmogenic substrate and a risk factor for SCD. Results from a number of cross-sectional studies have established a strong association between LGE and arrhythmia on 24-hour ambulatory monitoring, with LGE increasing the risk of ventricular tachycardia by as much as 7 times. However a direct link between the presence of LGE and SCD has proved elusive. Conflicting results from various prospective studies have only demonstrated a weak association between LGE and SCD, therefore while current HCM risk stratification models take LGE into account, recommendation for primary prevention implantable cardioverter-defibrillators (ICD) are not based solely on the presence of LGE.

Limitations of LGE

As mentioned previously, despite an abundance of literature, LGE alone cannot predict disease progression and SCD in HCM. The reason for this may in part lie with limitations of contrast-enhanced CMR sequences. In ischaemic heart disease, gadolinium contrast accumulates in areas of increased extra-cellular space, namely in areas of scarring where replacement fibrosis has occurred. In HCM, as mentioned in above in chapter 1.2.1.1, diffuse collagen formation around myocytes (interstitial fibrosis), between disorganised myofibrillar matrices (plexiform fibrosis), around intramural arterioles (peri-vascular fibrosis) can all cause an increase in ECV and provide an opportunity for gadolinium accumulation that may not reflect true replacement fibrosis. Disorganised myocyte architecture also results in expanded areas of myocardial matrix where gadolinium could aggregate. Current LGE sequences cannot reliably distinguish interstitial from replacement fibrosis, or an expanded matrix compartment created by myocyte disarray.

The quantification of LGE also relies on sampling a remote region of interest (ROI) containing normal nulled myocardium, which subsequently highlights LGE pixels that have greyscale signal intensities several SD (typically 5 or 6 SD) higher, or which have peak intensity of scarred myocardium (i.e full width at half maximum {FWHM}). These algorithms are readily applicable in ischaemic heart disease where pathology is highly regional, however in HCM, a large proportion of the LV can contain abnormal

myocardial substrate (interstitial fibrosis, replacement fibrosis and myocyte disarray), hence reliable sampling of a truly remote myocardium can be highly challenging.

In addition to this, technical issues with image acquisition need to be considered. The quality of contrast-enhanced images can be heavily affected by the selection of poor inversion times and motion artefacts, making it difficult to distinguish diffuse fibrosis from 'background noise'. (32) Hence it has thus far proved challenging to establish a threshold amount of LGE which can identify HCM patients at risk of disease progression and SCD.

1.2.3.2 Parametric mapping for detecting diffuse fibrosis

As discussed in chapter 1.1.3.2, recent developments in parametric mapping sequences can help address such limitations with LGE. Unlike LGE, native T1 and ECV maps can detect both focal and diffuse pathology without the need for sampling remote ROIs. In HCM, as healthy myocardium is replaced by fibrotic tissue, native T1 relaxation times and ECV increases, and a number of studies have shown that both T1 and ECV can be raised even in the absence of wall hypertrophy, contractile dysfunction and LGE, hence parametric mapping could play a role in early detection of HCM. (51,52)

Parametric mapping can also help differentiate HCM from some infiltrative cardiomyopathies. In Fabry's disease, the increased fat content from the accumulation of glycosphingolipids shortens native T1 relaxation times of affected myocardium, while the diffuse fibrosis that ensues in HCM and amyloidosis results in prolonged native T1 times. Hence low myocardial native T1 values strongly point to the diagnosis of Fabry's disease.

Systemic amyloidosis meanwhile is characterised by extensive diffuse fibrosis with marked expansion in ECV, and recent studies have shown cardiac amyloidosis patients to have significantly higher ECV than any other cardiomyopathies, which can be useful in differentiating the condition from HCM. (53)

Limitations of parametric mapping

Parametric mapping sequences can help overcome certain limitations of LGE, as they do not require the sampling of remote myocardium. However native T1 and ECV mapping is still not widely used in clinical practice, as further validation is required. Pulse sequence parameters can vary from centre-to-centre; hence a normal reference range is required for each scanner; actual values cannot be compared across centres or even scanners. Also, while parametric mapping may incrementally improve the sensitivity of CMR studies for detecting diffuse fibrosis, they do not infer upon the underlying microstructural changes that occur in the disease. This makes it challenging to differentiate between phenocopies of HCM remains, such as hypertensive cardiomyopathy or athlete's heart.

1.2.3.3 Quantitative perfusion for detecting microvascular dysfunction

Microvascular dysfunction (MVD) in HCM was first assessed using nuclear medicine techniques, which demonstrated perfusion impairment to correlate with hypertrophy and poor outcomes. (54) CMR perfusion sequences can measure myocardial blood flow both at rest, and during hyperaemia following the administration of a vasodilator agent such as adenosine. CMR perfusion studies of HCM patients have also demonstrated an inverse relationship between perfusion, hypertrophy and fibrosis. (43,55,56) Recent studies have used quantitative perfusion sequences to demonstrate that perfusion during vasodilator stress is impaired even in segments with normal wall thickness and no LGE, suggesting that MVD maybe an early phenotypic expression in HCM patients. (57) This supports previous prospective studies which have shown that HCM patients can remain asymptomatic with severe MVD for several years prior to deterioration. (58)

Limitations of quantitative perfusion

Quantitative perfusion is a growing field in the world of CMR, and as of yet there are no widely available vendor-supported in-line systems for mean blood flow (MBF) quantification. It requires the administration of potentially nephrotoxic contrast agents

which may be unsuitable in patients with advanced renal failure. Vasodilator agents such as adenosine also have undesirable, albeit short-lived side effects which include dyspnoea, dizziness, and chest pain, hence is not popular with patients, especially those with established cardiovascular disease. (59) Like T1 and ECV mapping, pulse sequence parameters can vary from centre-to-centre; hence a normal reference range is required for each scanner; actual values cannot be compared across centres or even scanners.

1.2.4 Conclusion

CMR has emerged as an excellent tool for the diagnosis and long-term monitoring of HCM patients. Advancements in parametric and perfusion sequences have shed light on various pathophysiological mechanisms such as diffuse fibrosis and MVD, which may precede LVH and scarring, however it remains challenging to detect the microstructural changes that occur, particularly earlier on in the disease pathway. It also remains challenging to exclude HCM from phenocopies such as hypertensive cardiomyopathy and athlete's heart.

Chapter 2: Diffusion tensor cardiac magnetic resonance (DT-CMR)

Diffusion weighted imaging (DWI) is an advanced MR technique which can probe into the microscopic architecture of organs. By examining the three-dimensional process by which water molecules diffuse within organic tissue and is impeded by cell membranes, DWI allows us to calculate the orientations of micro-organic structures. The technique was first described in 1965 by Stejskal and Tanner; and has been widely in use for brain and musculoskeletal imaging for several decades. Thanks to recent advancements in ultrafast imaging sequences and motion compensation algorithms such as ECG and respiratory tracking, it has now become feasible to perform DWI on moving organs such as the heart, a technique known as diffusion tensor cardiac magnetic resonance (DT-CMR). While there is already an abundance of CMR techniques that can quantify myocardial oedema, scarring and the consequent impairment in contractility in cardiovascular disease, the unique feature of DT-CMR is its ability to assess the organisation and integrity of microstructural components, something previously only possible in post-mortem studies. In this chapter, the underlying principles and mechanisms behind DT-CMR acquisition are explored.

2.1 Brownian Motion

Figure 2.1: Portrait of Scottish botanist Robert Brown

Diffusion describes the random motion of particles within a medium; a process that was first discovered by the botanist Robert Brown in 1827 (Figure 2.1), when he was observing the random movements of pollen grains immersed in water under a microscope.

Almost 80 years later, this theory (Brownian motion) was further expanded upon by theoretical physicist Albert Einstein, who added that the displacement of molecules was related to time and the diffusion coefficient, which takes into account the size of the molecule, the viscosity and the temperature of the medium that it is suspended in. (60) DT-CMR is a study of the random displacement of water molecules within the myocardium, which is used to examine and describe the characteristics of underlying microstructural components.

2.2 Diffusion weighted imaging acquisition

Conventional MR sequences like the T2-weighted echo planar sequence are made sensitive to molecular diffusion by the application of two strong magnetic field gradient pulses that are equal in magnitude and symmetrically centred around a 180°

refocussing radiofrequency pulse. The first 'diffusion winding' gradient pulse causes molecules to acquire phase shifts; the second 'diffusion unwinding' gradient pulse applied in the opposite direction cancels the gained shifts by rephasing non-moving stationary spins. Protons that have diffused in the time gap between the two gradient pulses will acquire an effective phase shift, as their motion will limit rephasing by the second gradient pulse. The higher the resultant spin dephasing, the more MR signal is lost, resulting in darker voxels. The greater the degree of diffusion along the line of the gradient, the greater signal loss and the darker the image. (61)

Diffusion Gradients are characterised by the *b* value – named after the medical doctor and physicist Dennis LeBihan. The *b* value is defined by the Stejskal-Tanner equation (Equation 2.1):

$$b = \gamma^2 G^2 \delta^2 \, (\Delta - \delta/3)$$

Equation 2.1: Stejskal-Tanner equation

γ is the gyromagnetic ratio, G, δ, Δ correspond to the amplitude, duration and interval of the diffusion gradient respectively. The b value (measured in s/mm^2) assimilates these physical factors into a single parameter. (62)

The greater the *b* value, the more sensitive the image is to diffusion but at the cost of lower signal-to-noise (SNR) ratio. Larger *b* values are achieved by increasing the amplitude and duration of the gradient, and by expanding the time interval between the paired gradient pulses (Figure 2.2).
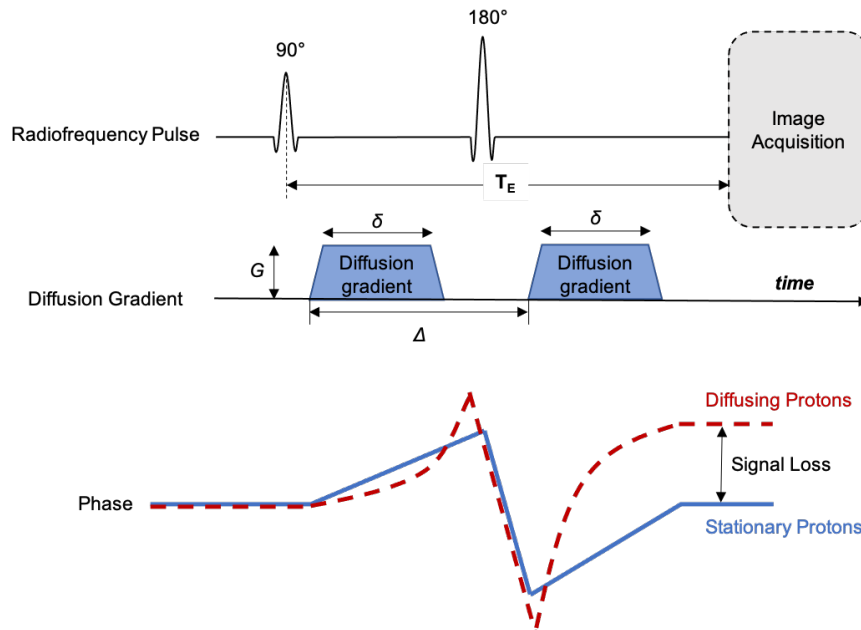
Figure 2.2: Stejskal-Tanner pulsed gradient echo diffusion sequence

Diffusion gradients are applied on both sides of the 180° radiofrequency pulse. T_E = echo time; G is the amplitude of the diffusion gradients, δ is their duration and Δ is the delay time between them. (63)

In order to quantify the magnitude of diffusion, baseline 'reference' images with a *b* value close to 0 (b_{ref}) are first acquired, followed by acquisition of images with greater *b* values (b_{main}). Since the diffusion gradients are added to a T2-weighted sequence, the measured MR signal is essentially the T2-signal intensity decreased by the amount of MR signal loss, which is determined by the diffusion coefficient and strength of applied diffusion gradient.

In brain DWI, the optimal b_{main} value is 900-1000 mm/s^2, but owing to the significantly shorter transverse relaxation time in the myocardium (~40ms in the myocardium at 3T compared to ~80ms in the brain), most *in vivo* cardiac studies have used b_{main} values between 300-500 s/mm^2, combined with a b_{ref} of 50-150 s/mm^2. (64–70)

Acquisitions in each direction and at each *b* value are repeated to increase SNR, and a final average of the signal is measured. This technique is called 'signal averaging'. Tensor estimation accuracy again improves with greater amount of signal averaging,

but this also lengthens scan times, and increases the risk of registration of artefacts between averages. In brain DWI, 8 signal averages from each directions are deemed optimal. (71)

The resulting signal intensity for each voxel is subsequently mapped as a 2-dimensional image, essentially creating a DWI map. However, diffusion is a three-dimensional (3D) phenomenon. The surrounding microstructural architecture and local physiological factors both impact on the direction, magnitude and 'shape' of diffusion. In the brain, water molecules are free to diffuse in all directions in the cerebrospinal fluid for instance; but in white matter tracts, diffusion predominantly occurs along the direction parallel to the long axis of the tracts and is limited in the direction perpendicular to the tracts by the semi-permeable cell membranes. By applying diffusion encoding gradients along different axes, it is possible to measure the directionality of diffusion by the calculation of diffusion tensors.

2.3 The Diffusion Tensor

In mathematics, a tensor is defined as a geometric object that maps geometric vectors and scalars in a multilinear fashion. The diffusion tensor is therefore a geometric map of the three-dimensional (3D) shape of diffusion (Figure 2.3).(72)
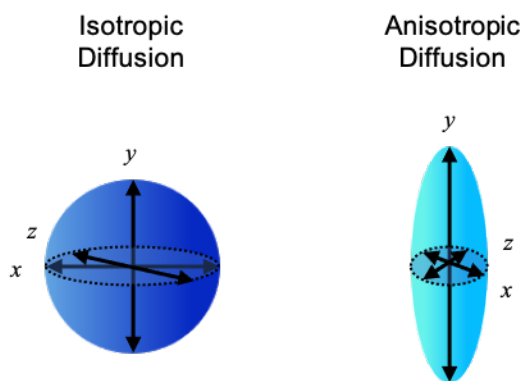
Figure 2.3: The diffusion tensor

When water molecules are free to diffuse in any given direction, the motion of water molecules are isotropic (random and equal in all directions), which can be represented in 3D as a sphere

using diffusion tensors. In biological tissue such as the myocardium, semi-permeable cell membranes restrict diffusion at a cellular level in certain directions, thus diffusion is more anisotropic and the 3D shape of diffusion is more ellipsoid.

The diffusion tensor is a 3x3 symmetric matrix, measuring the rate of diffusion in each combination of three orthogonal, mutually perpendicular directions, namely x, y and z (Figure 2.4). This creates 9 directions in total (D_{xx}, D_{xy}, D_{xz}, D_{yx}, D_{yy}, D_{yz}, D_{zx}, D_{zy} and D_{zz}), although diffusion along *xy* direction is the same as *yx* direction, i.e $D_{xy} = D_{yx}$. Similarly, $D_{xz} = D_{zx}$ and $D_{yz} = D_{yz}$. So in reality, the matrix provides measurements in 6 distinct directions. Hence conventional DT-CMR requires the acquisition of diffusion-weighted images in a minimum of 6 different directions, as well as one non-diffusion weighted image. (61)

$$\mathcal{D} = \begin{bmatrix} D_{xx} & D_{xy} & D_{xz} \\ D_{yx} & D_{yy} & D_{yz} \\ D_{zx} & D_{zy} & D_{zz} \end{bmatrix}$$

Figure 2.4: The diffusion tensor matrix

The diffusion tensor is a 3x3 symmetrical matrix which measures the displacement in three dimensions, with 6 different elements.

Once the diffusion tensors are calculated, they are described using 3 eigenvalues (λ) and 3 eigenvectors (ε). Eigenvalues describe the magnitude of diffusion, representing the squared distance diffused by molecules over a given time in a given plane. Eigenvectors meanwhile incorporate the direction as well as the distance and together, they form the eigensystem (Figure 2.5).
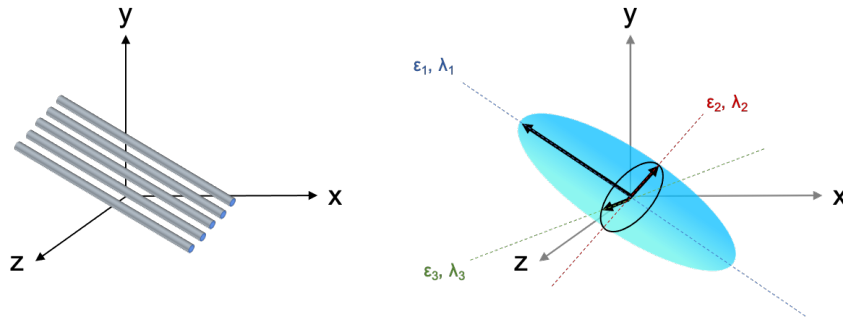
Figure 2.5: The eigensystem

The 3D shape of diffusion of myofibrils (left) is described by an ellipsoid tensor (right) using 3 orientations (eigenvectors ε_1, ε_2 and ε_3) with corresponding lengths (eigenvalues λ_1, λ_2 and λ_3).

The primary eigenvalue λ_1 is the longest, representing the direction of fastest diffusion, the secondary eigenvalue λ_2 is intermediate while λ_3 is the shortest, representing the direction of slowest diffusion.

2.4 Diffusion Tensor Parameters

Once the diffusion tensors have been calculated, they are used to derive various parameters, which can be plotted for each voxel of an image to create maps.

2.4.1 Mean Diffusivity (MD)

Mean diffusivity (mm^2/s), also known as the apparent diffusion coefficient, is the average of the tensor's eigenvalues, as shown below (Equation 2.2):

MD = $(\lambda 1 + \lambda 2 + \lambda 3) / 3$

Equation 2.2: Calculation of mean diffusivity

MD represents the overall magnitude of diffusion in a given voxel. MD can be affected by both water content and the presence (or absence) of semi-permeable structures such as cell membranes. Areas with fast diffusion will have high MD and appear hyperintense on MD maps, while areas with restricted diffusion will have lower MD values and appear hypointense. (61)

2.4.2 Fractional Anisotropy (FA)

Fractional anisotropy (FA) is the ratio of the anisotropic component of the diffusion tensor to the whole diffusion tensor (i.e. the difference between the tensor's ellipsoid shape from that of a perfect sphere) and serves as a scalar that quantifies the shape of diffusion. (61) FA is calculated for each voxel using the following equation (73) (Equation 2.3):
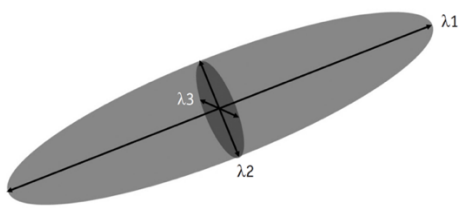
$$FA = \sqrt{\frac{1}{2}} \; \frac{\sqrt{(\lambda_1 - \lambda_2)^2 + (\lambda_2 - \lambda_3)^2 + (\lambda_3 - \lambda_1)^2}}{\sqrt{\lambda_1^2 + \lambda_2^2 + \lambda_3^2}}$$

Equation 2.3: Calculation of fractional anisotropy using eigenvectors λ1, λ2 and λ3

FA values range from zero to one; with zero representing maximal isotropic diffusion as in a perfect sphere; whilst one representing maximal anisotropic diffusion as represented by a long ellipsoid shape (Figure 2.6).
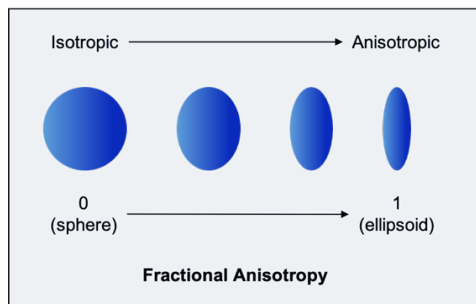
Figure 2.6: Fractional Anisotropy

An FA value of 0 represents complete isotropic diffusion i.e a perfect sphere, while an FA value of 1 represents diffusion in just one single linear direction.

Both MD and FA are derived from eigenvalues only and are rotationally invariant, however the tensor eigenvectors can provide additional information about the orientations of underlying microstructures.

2.4.3 Helix Angle

As described before, the primary eigenvector (ε_1) represents the direction of fastest diffusion. In the myocardium this corresponds with the long axis of cardiomyocytes, and hence delineates their orientation. (64) In DT-CMR, the helix angle (HA) describes the angle between ε_1 and the short axis (circumferential) plane. In DT-CMR imaging of healthy subjects, the HA transmurally evolves from left-handed helix (LHM) at the subepicardium; to circumferential arrangement in the mid-wall (CM), to right-handed helix (RHM) at the subendocardium; (74–77) which corresponds with the classic counter clockwise rotation of cardiomyocytes that was originally described by Pettigrew in 1866 (Figure 2.7). (78) Voxel-wise HA values can be plotted to create HA maps as shown in (Figure 2.10C).
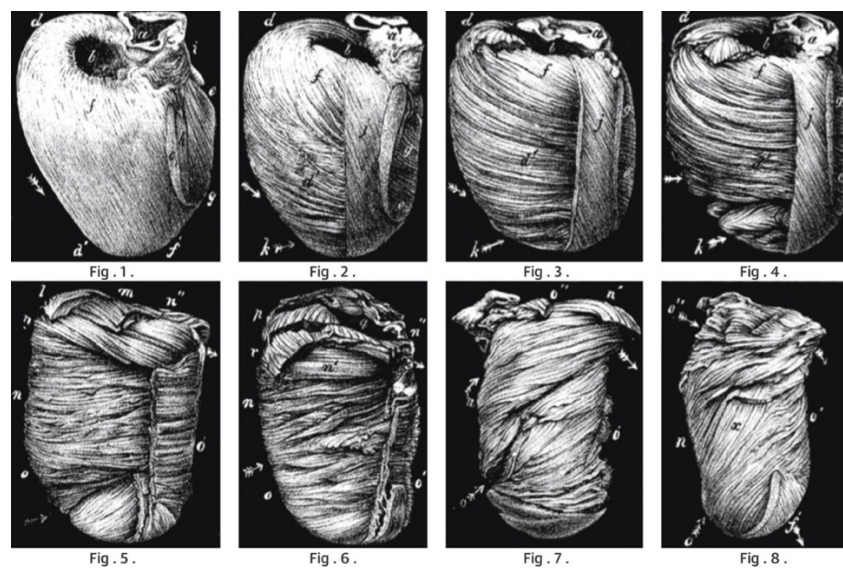
Figure 2.7: Dissection planes demonstrating the helical arrangement of LV fibers

In healthy myocardium, the helix angle progresses transmurally from myocytes with left-handed orientation (LHM) at the subepicardium, progressing through to myocytes with

circumferential orientation (CM) in the mesocardium, to myocytes with right-handed orientation (RHM) at the subendocardium. (78)

2.4.4 Tractography

By increasing the number of directions in which diffusion encoding gradients are applied, direction of diffusion can be measured from more angles. This enhances tensor estimation accuracy but lengthens scan times. In DWI of the brain, by calculating the direction of primary eigenvectors, it is possible to delineate the course and trajectories of white matter tracts; a process known as tractography. (61) Because neuronal axons are highly anisotropic (linear), diffusion in most directions will be close to zero, so it is necessary to measure diffusion in as many as 256 directions. Myocytes in comparison are more isotropic, and conventionally 6 directions are deemed sufficient. A few studies have attempted tractography using DT-CMR to depict areas of MI in a variety of species including humans *in-vivo* (Figure 2.8), (79) but the relatively long scan times needed to cover the entire LV in 10 directions makes this technique unfeasible for routine use in clinical patients.
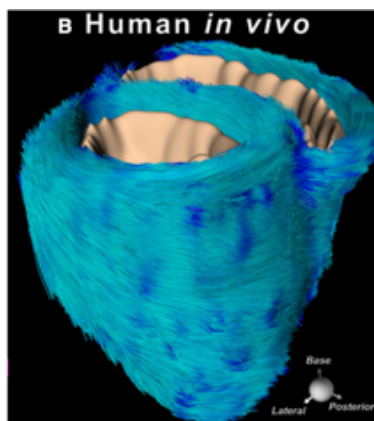
Figure 2.8: Tractography of fibers in the human heart

Image from Mekkaoui et al. (79)

2.4.5 Secondary Eigenvector Angle

Cardiomyocytes aggregate together to form laminar secondary structures known as 'sheetlets'. Each sheetlet is typically 5-10 cardiomyocytes thick. In healthy myocardium, the laminar sheetlets reorientate from a low angle in diastole, to a high angle in systole (Figure 2.9). It is the reorientation of sheetlets throughout the cardiac cycle that is thought to be the principal mechanism driving LV wall thickening during systole, which generates the force to pump blood out into the systemic circulation. In DT-CMR, the angle of the secondary eigenvector (ε_2) – also referred to as the absolute E2A – reflects the orientation of these myocardial sheetlets. Absolute E2A values can also be plotted on a voxel-wise map, as demonstrated in Figure 2.10D.
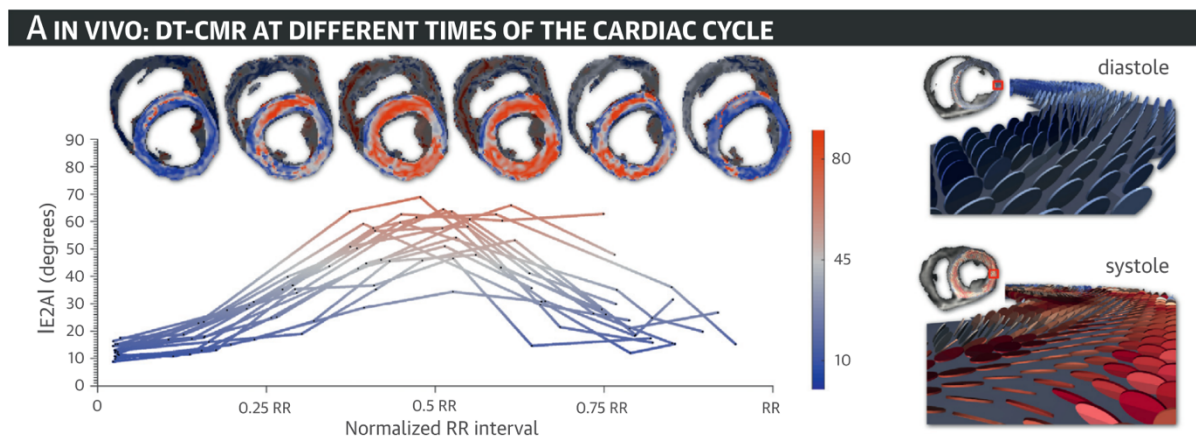
Figure 2.9: Sheetlet dynamics

In-vivo secondary eigenvector angle (E2A) maps are displayed at multiple time points across the cardiac cycle. The E2A swivels from a low angle (blue) in diastole to a high angle (red) in systole. (69)
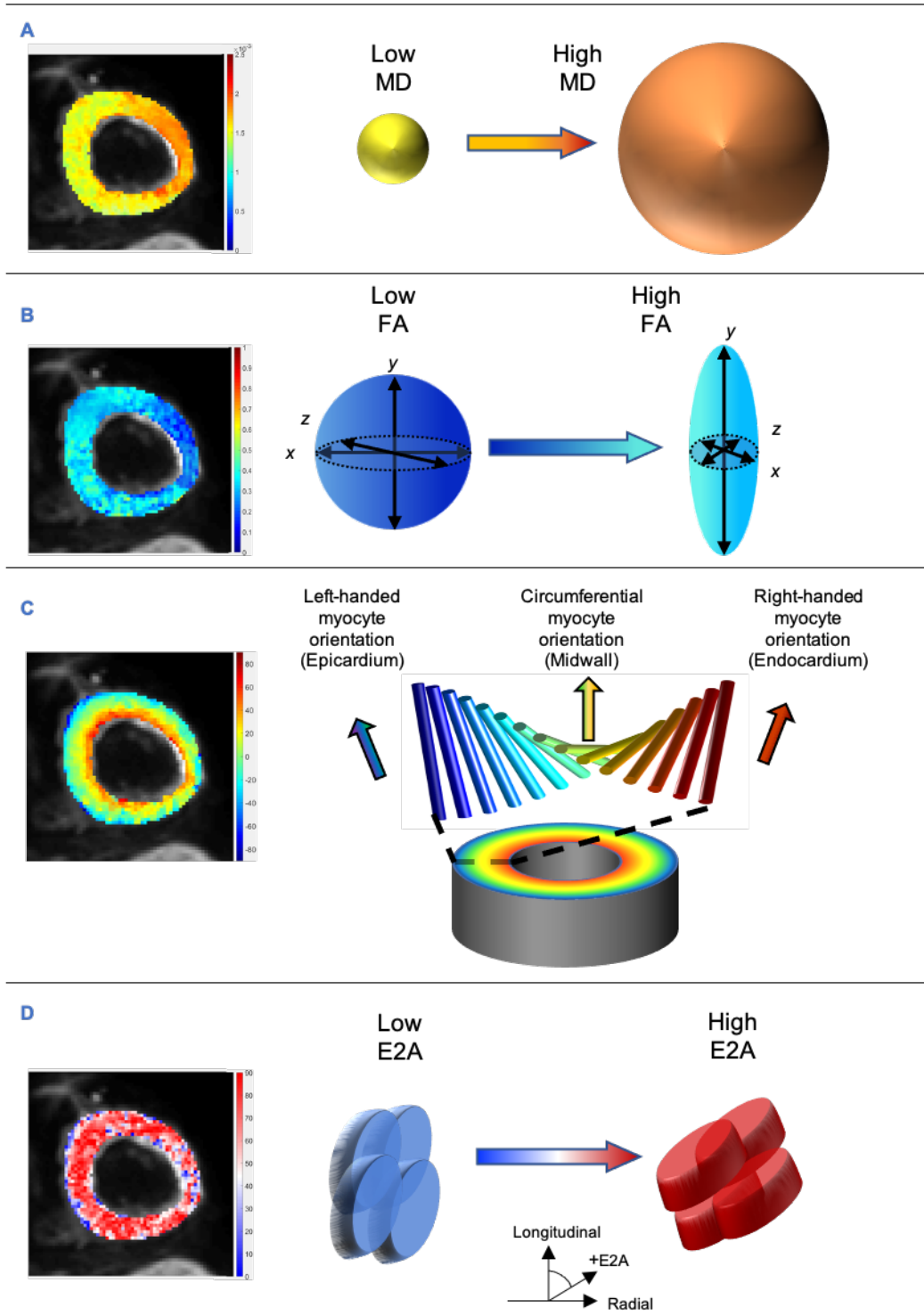
Figure 2.10: Schematic diagrams of diffusion tensor imaging parameters

In healthy myocardium, cell membranes offer physiological barriers to diffusion of water molecules and restrict diffusion to primarily the long-axis, i.e y-axis of the myocytes. As cell

membranes are destroyed, the magnitude of diffusion, i.e mean diffusivity (MD) increases (panel A), and the anisotropy of diffusion, i.e fractional anisotropy (FA) decreases (panel B). Helix angle (HA) maps provide voxel-wise representation of the average myocyte orientation (panel C). Histological studies have demonstrated subendocardial myocytes to have right-handed orientation (RHM), midwall to have circumferential orientation (CM) and subepicardial myocytes to have left-handed orientation (LHM). These orientation changes are quantified by the HA measure which ranges from -90° to 90° transmurally. Previous authors have measured the proportions of HA voxels that belong to three categories of orientation – LHM (-90° ≤HA< -30°), CM (-30° ≤HA≤ 30°) and RHM (30° <HA≤ 90°). Secondary eigenvector angle (E2A) maps provide voxel-wise representation of the angle of laminar sheetlets in mid-systole (panel D).

2.5 Development of in vivo DT-CMR

In neuroradiology, DWI is widely used on patients for the diagnosis of acute cerebrovascular infarction. *In vivo* DT-CMR however introduces considerable challenges with regards to bulk motion during the cardiac cycle as well as myocardial strain during diffusion encoding. Additionally, the transverse relaxation time in the myocardium is significantly shorter than in the brain (~40ms in the myocardium at 3T compared to ~80ms in the brain), which significantly limits the echo time that can be used. Finally, the B_0 inhomogeneities within the thorax can result in more susceptibility-related artefacts in echo planar imaging.

In order for *in vivo* methods to detect the microscopic movements of water molecules, they need to account for the macroscopic cardiac and respiratory motion during acquisition. ECG-gating ensures that acquisitions are made at identical points in the cardiac cycle, mitigating cardiac motion. Meanwhile manual breath-holding, synchronised breathing and navigator tracking have also been incorporated. (64,66) To date, there are two *in vivo* DT-CMR sequences in use:

- Stimulated echo acquisition mode (STEAM)
- Spin Echo (SE)

2.5.1 Stimulated echo acquisition mode (STEAM)

In STEAM, following the initial 90° radiofrequency (RF) pulse is followed by two separate 90° RF pulses. (Figure 2.11) Diffusion encoding gradients are applied at identical trigger times in two consecutive cardiac cycles enabling the measurement of diffusion that has taken place over this time period. The advantage of this approach is the relative ease at which they can be performed using standard clinical CMR systems without the need for high-performance gradient hardware. The relatively long diffusion time allows for the use of smaller diffusion gradients which are less sensitive to cardiac motion and T_2-decay. However, there is an assumption that the spatial trajectories of the tissue points are identical for consecutive heart beats, therefore in order to avoid severe signal loss, this approach is heavily reliant on patient breath-holding in order to suppress respiratory motion induced displacements. The position of the heart in two consecutive heart beats is allowed to vary within narrow limits, which means examination times can be very long and considerable patient cooperation is required. In addition, there is an intrinsic weighting of the diffusion signal due to myocardial strain. This issue is resolved by acquiring the data at the so called 'sweet spots', which are specific time points in the cardiac cycle when the cardiac configuration approximates its temporal mean. However, this limits imaging to two pre-defined time points in the cardiac cycle which do not coincide with systole or diastole. (80)
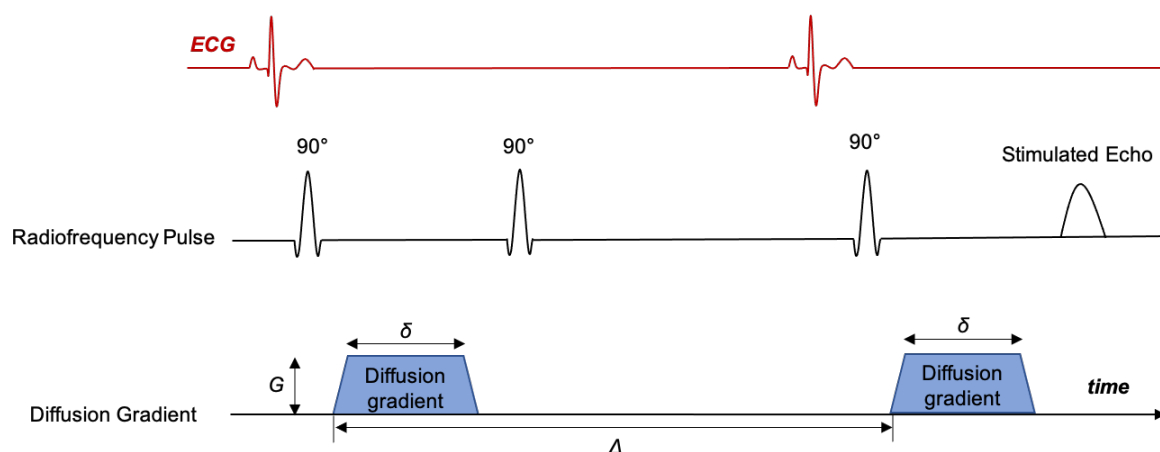
Figure 2.11: Stimulated Echo Acquisition Mode (STEAM) sequence

2.5.2 Diffusion-weighted single-shot spin echo imaging (SE)

In the single-shot spin echo (SE) sequence, the Stejskal-Tanner diffusion sequence (Figure 2.2) is used with echo planar imaging (EPI) readout. (63) In contrast to the STEAM approach, SE sequences encode diffusion during a single cardiac cycle because with EPI, individual MR slices can be acquired in a shorter time frame of 50-100ms, thus minimising the effect of patient motion. The fast acquisition also makes the incorporation of respiratory navigation more feasible, thus negating the need for long breath-holds.

This faster acquisition introduces additional challenges however, specifically the requirement of stronger diffusion gradients and longer echo times (TE), making the sequence more susceptible to cardiac motion and T_2-decay. Second-order motion-compensated SE has been proposed to limit this effect, where the diffusion gradients are compensated for velocity and acceleration. (81) Recent studies comparing the two sequences have shown that SE DT-CMR produced helix angles with reduced deviation from the linear transmural model, and ultimately acquired images with higher SNR than STEAM DT-CMR (Figure 2.12). (80)
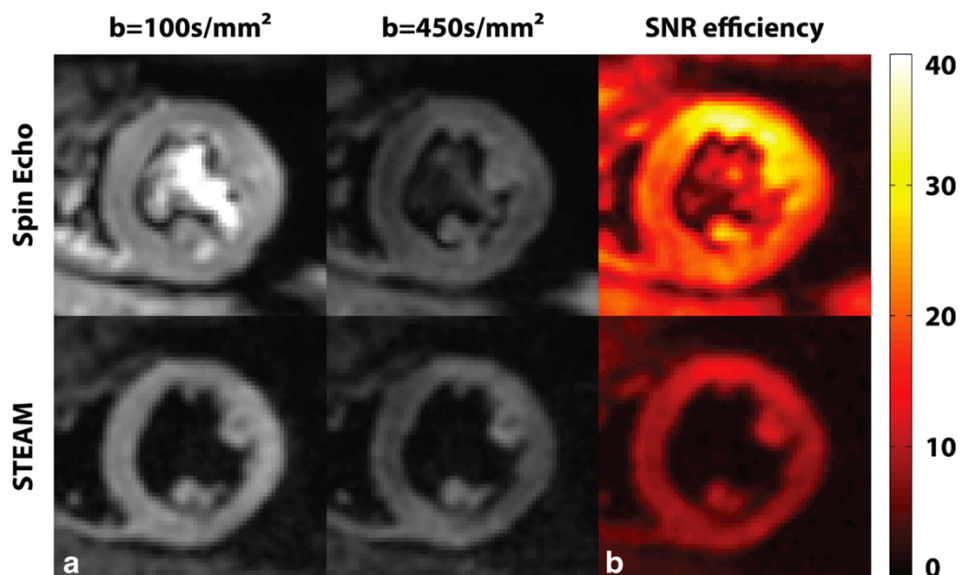
FIG. 3. In vivo data. **a:** Example dataset acquired at b = 100 s/mm^2 and 450 s/mm^2. **b:** Corresponding SNR efficiency maps for b = 450 s/mm^2.

Figure 2.12: Comparison of image quality between two DT-CMR techniques

2.5.3 Relevant DT-CMR studies to date

Various authors have used DT-CMR to assess pathology in animal and human studies. Table 2.1 provides a summary of findings from various studies that are relevant to this thesis.

Study	Subjects	Sequence	Summary of findings
Pathology: Myocardial Infarction			
Scollan et al, Am J Physiol, 1998 (82)	Rabbits (n=2) ex-vivo	Spin Echo	One of the first ex-vivo studies to directly compare and show excellent agreement between histology and DT-CMR derived orientations of cardiomyocytes and laminar fibers.
Chen et al, AJP Heart, 2003 (83)	Rats (n=15) ex-vivo	Spin Echo	At 4 weeks following MI, MD was increased and FA was decreased in infarct regions compared to remote. Following histological corroboration, the reduced FA was attributable to cardiomyocyte disarray.
Nguyen et al, JCMR, 2014 (84)	Pigs (n=11) ex-vivo	Spin Echo	At 8 weeks following MI, MD was increased in areas of infarction compared to remote. Scar borders detected using MD maps were in excellent agreement with LGE. The authors attribute the increased MD to be reflective of more unrestricted diffusion in fibrotic areas due to the lack of diffusion-restrictive structures such as cell membranes.
Wang et al, KJR, 2016 (85)	Monkeys (n=6) ex-vivo	Spin Echo	Serial imaging was performed at 1 hour and 84 days post-MI. Histological corroboration suggested the acute increase in MD and reduction in FA in infarct areas were due to the presence of oedema and spherical inflammatory cells. Serial increase in MD was attributed to expansion in ECV, while serial reduction in FA were shown to reflect increased cardiomyocyte disarray.
Wu et al, Circulation Cardiovascular Imaging, 2009 (65)	Humans (n=17) in-vivo	STEAM	One of the first in-vivo study of MI patients comprising of serial imaging at 1- and 6-months post-infarction. In an attempt to monitor and quantify changes in helix angle maps, the authors classified voxels into one LHM, CM and RHM according to their orientation. RHM was reduced in areas of infarction and the authors attributed this to represent the loss of organisation amongst subendocardial myocytes. Furthermore preservation of RHM was associated with improvement in regional contractility at 6 months.

Moulin et al, Radiology, 2020 (86)	Humans (n=34) in-vivo	Spin Echo	At 5 days following MI, MD was increased in areas corresponding to oedema. MD maps provided superior contrast between remote and oedematous areas than T1 and T2 maps.
Pathology: Hypertrophic Cardiomyopathy			
Nielles-Vallespin et al, JMRI, 2017 (69)	Humans (n=51) in-vivo	STEAM	DT-CMR was used to compare healthy volunteers (controls), HCM and dilated cardiomyopathy (DCM) with a focus on E2A. Compared with controls, HCM patients had increased E2A during systole which remained high in diastole, suggesting their myocardial sheetlets adopt hyper-angulated orientations during systole, which remain fixed in diastole. Meanwhile DCM patients have low E2A in systole, signifying their sheetlets are unable to reach the usual systolic configuration angle during systole.
Ariga et al, JACC, 2019 (68)	Humans (n=50) in-vivo	STEAM	HCM patients had reduced FA. Building on histological validation work by Abdullah et al as shown below, (87) the authors attribute this reduced FA to be concomitant of cardiomyocyte disarray and collagen infiltration. Reduced FA was shown to be associated with ventricular arrhythmia.
Pathology: Dilated Cardiomyopathy			
Abdullah et al, NMR Biomed, 2014 (87)	Humans (n=19) ex-vivo	Spin Echo	DT-CMR study with histological validation of excised specimens of end-stage DCM patients demonstrated that FA correlates with collagen deposition and cardiomyocyte disarray.

Table 2.1: Summary of relevant DT-CMR studies to date

2.6 Limitations of DT-CMR

- Low spatial resolution – because of low SNR, large voxels are required to generate adequate signal.
- Long scan times, as at-least 8 acquisitions are required in each direction for each *b* value (signal averaging) in order to increase SNR.
- The requirement for regular R-R intervals makes DT-CMR virtually impossible in patients with arrhythmia.
- Inhomogeneities in the magnetic field (e.g from the presence of iron) can interfere with diffusion encoding gradients, which results in lower SNR.
- STEAM DT-CMR requires consistent breath-holding as the heart needs to be in the exact same position for the second diffusion gradient. STEAM DT-CMR images also need to be accounted for strain, which adds an extra step to the post-processing stage.
- Acquisition of apical slices is challenging. Due to its conical geometry, the LV tapers towards the apex, hence apical slices are more prone to partial voluming effects. It's close proximity to adjacent structures such as the diaphragm and stomach also makes it susceptible to artefacts from unsuppressed fat, signal loss and suboptimal signal-to-noise ratio.
- Exact pulse sequence settings can vary between centres, which can impact on DT-CMR measurements, hence exact values may vary between scanners and cannot be directly compared.

2.7 Conclusion

DT-CMR is a relatively novel sequence which is unique in its ability to characterise myocardial architecture in-vivo. It is therefore well suited for detecting early and irreversible changes in the myocardium, however scan times are considerably longer than more standardised parameters, and while it has been validated with histology in pre-clinical studies, there are only a handful of studies of patients to date, raising the need for further clinical validation.

2.8 Study aims and hypothesis

Chapter 4: Longitudinal changes in DT-CMR over 3 months following STEMI

Given the capabilities of DT-CMR in characterising myocardial microstructure in-vivo, the aim of this study was to perform serial DT-CMR imaging on STEMI patients to infer upon the microstructural differences between infarcted and remote myocardium, and how acute changes in infarct regions relate with LV function recovery. I hypothesised that DT-CMR derived biomarkers of more severe injury in infarcted myocardium would correlate with lower LVEF at 3 months post-MI.

Chapter 5: Detection of IMH using DT-CMR

From the results of chapter 4, I observed the unusual behaviour of parameters MD and FA with areas of MVO, and based on available literature, I hypothesised that this paradoxical reduction in MD, and paradoxical increase in FA may be explained by the presence of iron within the myocardium and its paramagnetic susceptibility effects. The aim of this stud was therefore to assess the sensitivity of DT-CMR in depicting areas of IMH, using T2* mapping as the reference standard.

Chapter 6: DT-CMR predictors of adverse LV remodelling

Building on findings from chapters 4 and 5, this study aimed to measure serial changes in DT-CMR parameters over 3 scans spanning 12 months in patients following STEMI, and how they associate with long-term adverse LV remodelling. I hypothesised that markers of severe injury in the acute scan derived using DT-CMR can be predictive of adverse LV remodelling.

Chapter 7: DT-CMR study of controls, athletes and HCM

Having elucidated the behaviour of DT-CMR parameters in the STEMI population, I aimed to explore the clinical application of DT-CMR in HCM, where diffuse changes in the microstructure may precede macroscopic changes such as wall hypertrophy and scarring. In this chapter, we used DT-CMR to infer upon microstructural differences

between healthy controls, athletes and HCM patients. I hypothesised there would be significant differences in DT-CMR parameters between the 3 cohorts.

Chapter 8: Phenotyping HCM patients using DT-CMR

Building on findings from chapter 7, the purpose of this chapter was to examine the associations between myocardial perfusion and DTCMR parameters in HCM patients to understand the sequence of pathophysiology and the interrelation between vascular function and underlying myocardial microstructure. I hypothesised that there would be significant differences in DT-CMR parameters between healthy controls and even the 'normal' segments of HCM patients, where there is no evidence of perfusion defect, wall hypertrophy or scarring.

Chapter 3: Methods

I will begin this chapter by going through the steps taken to validate DT-CMR acquisition and analysis at our centre. This will be followed by a description of the methods used in the subsequent studies on patients.

3.1 DT-CMR sequence validation

In this thesis, we acquire DT-CMR on 2 separate scanners. The Philips 3.0T scanner was used for the following studies:

Chapter 4: Longitudinal changes in DT-CMR over 3 months following STEMI

Chapter 5: Detection of IMH using DT-CMR

Chapter 6: DT-CMR predictors of adverse LV remodelling

Chapter 7: DT-CMR study of controls, athletes and HCM

In chapter 8, we aimed to examine the associations between DT-CMR and perfusion biomarkers. As quantitative perfusion imaging was not available on the Phillips 3.0T scanner, a Siemens 3.0T was used instead.

As mentioned previously in chapter 2.6, the DT-CMR sequence parameters can vary between centres, which can impact on DT-CMR measurements, hence readings may differ from scanner to scanner. In order to ensure scanner accuracy and reproducibility, we undertook independent validation studies for both the Phillips and Siemens 3.0T scanners prior to clinical applications on patients.

3.1.1 Phantom validation

3.1.1.1 Phillips 3.0T scanner

The DT-CMR sequence used on the Philips 3.0T scanner is described in detail below in section 3.3.1.2 This sequence was originally developed and provided to us by Prof

Kozerke et al, who performed phantom validation tests at Zurich University, Switzerland. (80,81) In order to test the sequence stability and reproducibility on our scanner, we measured intra-subject reproducibility, as described below in section 3.1.2.

3.1.1.2 Siemens 3.0T scanner

The DT-CMR sequence used on the Siemens 3.0T scanner is described in detail below in section 3.3.2.3. The sequence was originally developed and provided to us by Dr Nguyen et al at Harvard University, USA. (88) In order to measure the accuracy with which this sequence can measure MD and FA on our Siemens 3.0T scanner, we acquired DT-CMR on 7 phantoms comprising of water with increasing concentrations of polyvinylpyrrolidone (PVP), ranging from 0 to 20%, as shown in Figure 3.1. The phantoms were chilled in ice water and imaged at 0°C. DT-CMR scans (as outlined in section 3.3.2.3) were triggered with simulated ECG at 60 bpm. This scan was repeated another 3 times under the same conditions on different days over the next 30 days. (89)
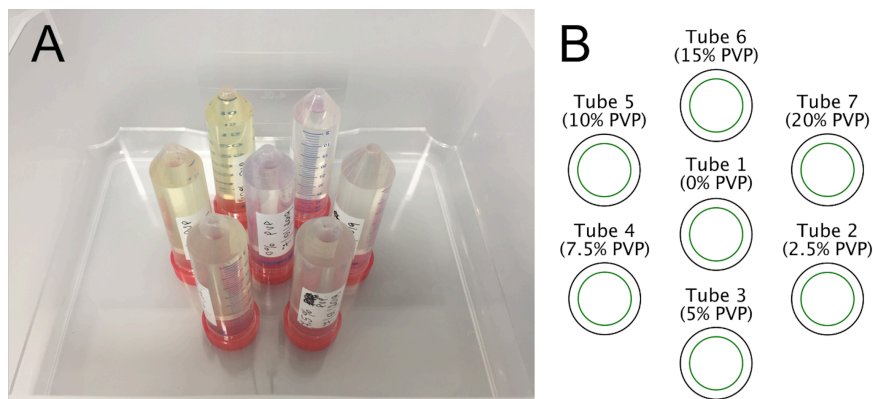
Figure 3.1: Phantom Validation

Phantoms comprising of 7 tubes (Panel A) filled with 0 to 20% of polyvinylpyrrolidone (PVP) as shown in panel B.

The measured MD and FA of the 7 tubes are shown in Table 3.1 and Figure 3.2. The average MD of 0% PVP (i.e H20, $0.133 \times 10^{-3} mm^2/s$) was in good agreement with

reference diffusivity for H20 (1.113×10^{-3}mm^2/s) and decreased with increasing concentrations of PVP as expected. (90) Results across the 4 scans were also consistent for each phantom, with an overall standard deviation of 0.0138×10^{-3}mm^2/s. As mentioned in section 2.4.2, FA quantifies the shape of diffusion, however this can vary significantly even in pure water, and at present, it is challenging to create phantoms with reference FA values. Hence unlike MD, the FA values across the 7 tubes do not show any clear pattern and have higher standard deviations between tests. For this reason, phantoms for eigenvector-related parameters such as E2A and HA are not currently available, and to test the reproducibility of these parameters, we performed repeat scans on healthy volunteers.

Phantom Tube	Mean Diffusivity ($\times 10^{-3}$mm^2/s)					
	Scan 1	Scan 2	Scan 3	Scan 4	Mean	SD
1 (H20)	0.135	0.144	0.123	0.130	0.133	0.009
2 (2.5% PVP)	1.065	1.065	0.997	1.022	1.037	0.034
3 (5% PVP)	0.972	0.969	0.945	0.962	0.962	0.012
4 (7.5% PVP)	0.903	0.906	0.905	0.899	0.903	0.003
5 (10% PVP)	0.844	0.841	0.842	0.843	0.842	0.001
6 (15% PVP)	0.721	0.741	0.690	0.710	0.715	0.021
7 (20% PVP)	0.623	0.622	0.587	0.609	0.610	0.017
	Fractional Anisotropy					
1 (H20)	0.0267	0.0208	0.0305	0.0333	0.028	0.005
2 (2.5% PVP)	0.0183	0.0229	0.0373	0.0443	0.031	0.012
3 (5% PVP)	0.0172	0.0209	0.0204	0.0274	0.021	0.004
4 (7.5% PVP)	0.0235	0.019	0.0439	0.0482	0.034	0.015
5 (10% PVP)	0.0638	0.0425	0.0392	0.0383	0.046	0.012
6 (15% PVP)	0.0335	0.0364	0.0212	0.0240	0.029	0.007
7 (20% PVP)	0.0292	0.0288	0.0385	0.0410	0.0341	0.006

Table 3.1: Results from phantom validation studies

A

B
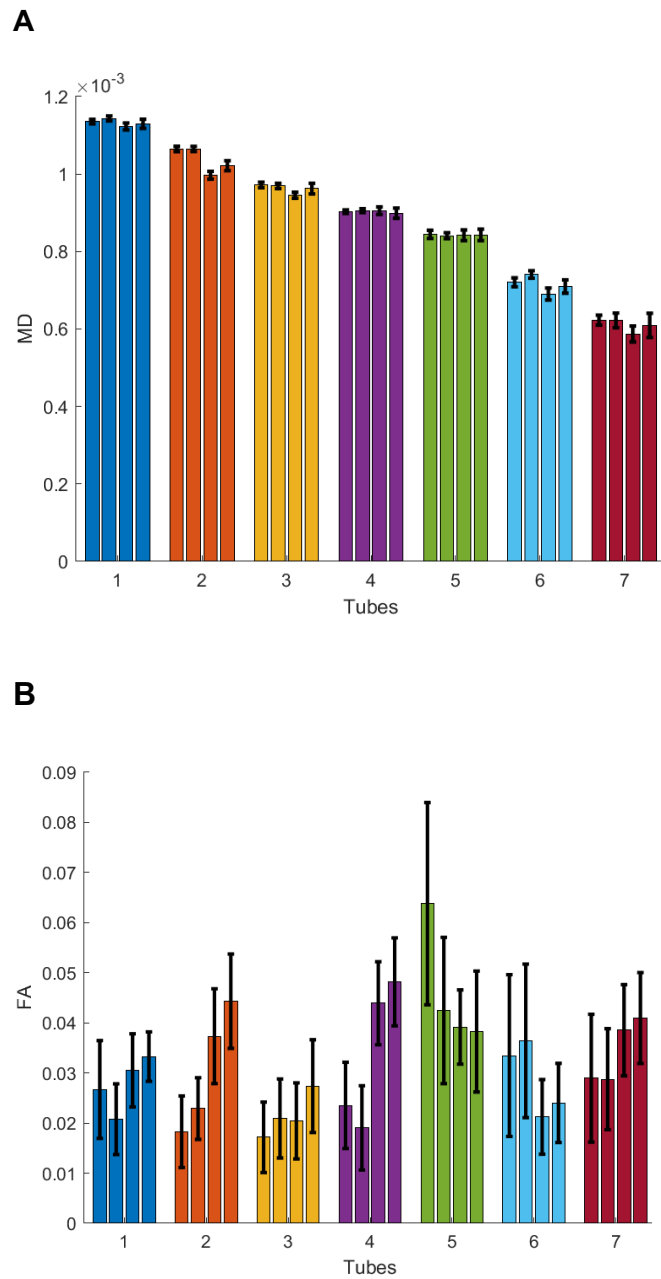
Figure 3.2: MD and FA from repeated acquisitions of PVP phantoms

MD (Panel A) and FA (Panel B) from repeat acquisitions of phantoms comprising of 7 tubes filled various concentrations of polyvinylpyrrolidone (PVP), showing excellent reproducibility of MD.

3.1.2 Intra-subject reproducibility

In order to assess the intra-subject reproducibility of in-vivo DT-CMR acquisition on the Phillips 3.0T scanner, we performed repeat scans on 5 healthy controls. Detailed sequence parameters (section 3.3.1.2), post-processing (section 3.4.2) and statistical methods (section 3.5) used in this section are described later in this chapter. To ensure consistent slice positioning, scans were acquired back-to-back in the same session. The global results including MD, FA, E2A and HA proportions were compared (Table 3.2).

	Bias	Limits of agreement		Coefficient of variation (%)
		Lower	Upper	
MD ($\times 10^{-3} mm^2/s$)	-0.02	-0.13	0.10	2.68
FA	-0.02	-0.09	0.05	6.82
E2A (°)	0.87	-7.97	9.71	6.92
HA proportions				
RHM (%)	<0.01	-0.06	0.06	6.92
CM (%)	<0.01	-0.14	0.15	5.99
LHM (%)	-0.01	-0.10	0.08	19.70

Table 3.2: Intra-subject reproducibility results

Intrasubject reproducibility results are shown for the 5 healthy controls who underwent repeat DT-CMR acquisitions.

MD was found to be the most reproducible parameter with a coefficient of variation (CoV) of 2.68, closely followed by FA, E2A, proportions of RHM and CM. Manually defining the epicardial borders proved challenging on the reconstructed diffusion weighted images. This likely explains the increased CoV noted with LHM measurements. Hence caution must be taken when drawing any conclusion from LHM

measurements. Bland-Altman plots for intrasubject reproducibility are shown in Figure 3.3.
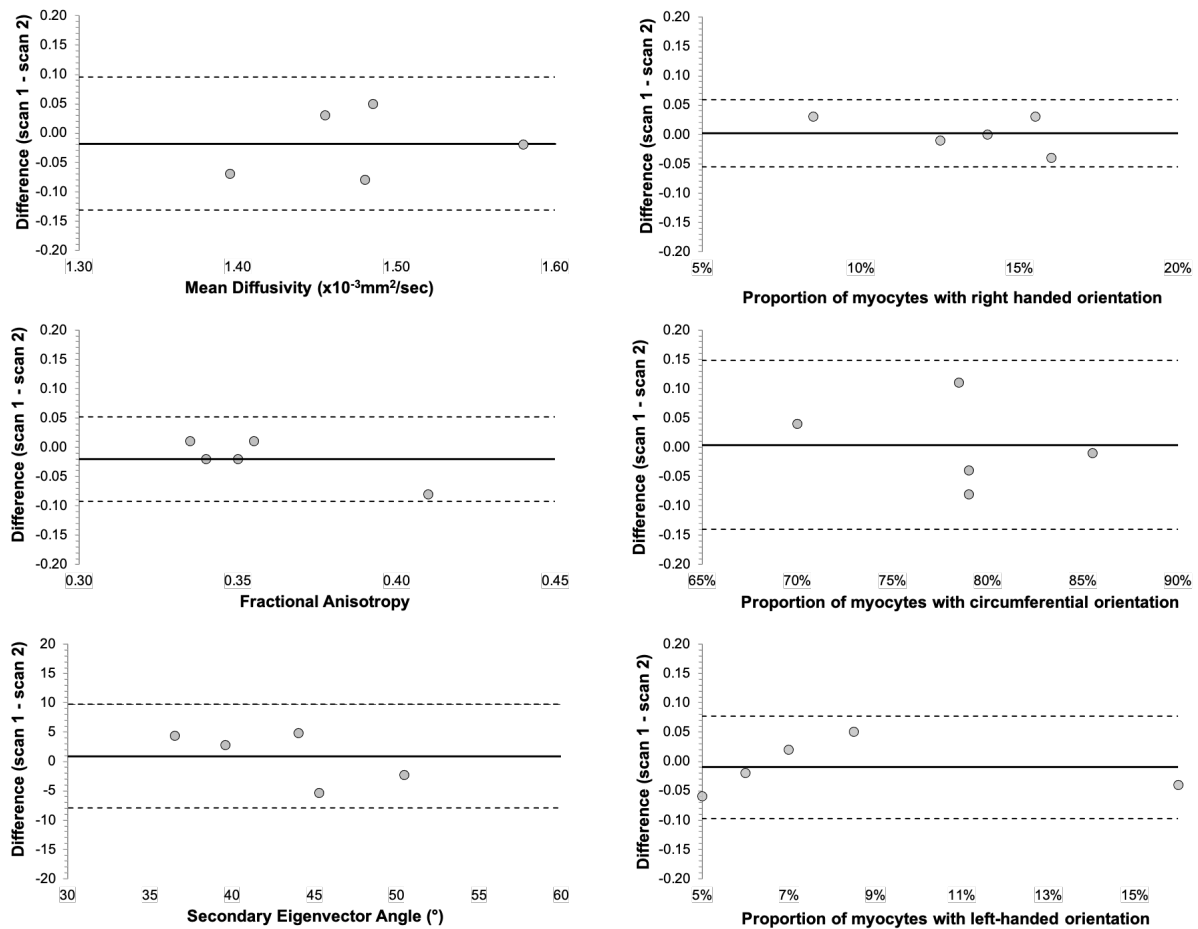
Figure 3.3: Bland-Altman plots for intra-subject reproducibility

Bland-Altman plots for repeat measurements in 5 healthy controls, showing the difference between scan 1 and scan 2 for different DT-CMR parameters. The central (thick) line represents the bias and the dashed lines represent the 95% limits of agreement.

3.1.3 Comparison with published data

SE DT-CMR is not currently standardised due to variance in magnetic field strengths, b-values, trigger delay in the cardiac cycle, different motion compensation schemes, voxel size and post-processing techniques between different centres, therefore inter-centre reproducibility of healthy controls is lacking. After assessing intra-subject

reproducibility, we performed DR-CMR acquisition on 20 healthy controls on the Phillips 3.0T scanner, 10 volunteers on the Siemens 3.0T scanner and compared our results with previously published values in healthy controls by Von Deuster et al (80), who used a similar sequence to ours on a well-matched group of healthy controls (Table 3.3). Overall, we report similar MD and FA in our controls; the small differences observed could be attributed do differences in magnetic field strengths and minor differences in sequence parameters. At time of sequence validation, there were no published E2A, or helix angle proportions on healthy controls derived from SE-DT-CMR available for direct comparison. The difference in E2A between our Philips and Siemens 3.0T scanners are most likely due to the difference in trigger delay.

	Phillips 3.0T (Das et al, JMRI 2020)	Siemens 3.0T (Das et al, EHJ CVI, 2021)	Von Deuster et al (MRM 2016)
Demographics			
Number of subjects	20	10	7
Age	27 ± 8	27 ± 9	28 ± 6
Sex (Male %)	35%	40%	29%
Weight (kg)	67 ± 5	70 ± 11	64 ± 6
Scan parameters			
Magnet field strength	3T	3T	1.5T
DT-CMR sequence	2nd order motion compensation spin echo	2nd order motion compensation spin echo	2nd order motion compensation spin echo
Spatial resolution (mm^3)	2.3×2.3×8	2.3×2.3×8	2.5x2.5x8
TE (ms)	89	77	70
TR	3 beats	3 beats	3 beats
Trigger delay	60% of systole	30% of systole	65% of systole
Parameters (Global)			
MD (x10^{-3}mm^2/s)	1.49 ± 0.03	1.47 ± 0.08	1.43 ± 0.06
FA	0.35 ± 0.02	0.34 ± 0.03	0.38 ± 0.02
E2A (°)	49 ± 12	38 ± 12	Not published
Helix Angle proportions			
RHM (%)	0.14 ± 0.03	0.17 ± 0.06	
CM (%)	0.78 ± 0.06	0.71 ± 0.17	Not published
LHM (%)	0.09 ± 0.05	0.12 ± 0.14	

Table 3.3: Comparison of previously published DT-CMR values in healthy controls

Results from DT-CMR acquisition on 20 healthy controls (91) *are reported and compared with previously published data by Von Deuster et al (80).*

3.1.4 Interobserver reproducibility

As well as validating the sequence on the 2 scanners, we also assessed the reliability of our DT-CMR data analysis methods. The post-processing pathway (described in detail in section 3.4.2) was developed by Dr Kelly using in-house developed MATLAB software. In order to measure interobserver reproducibility, DT-CMR was performed on 30 STEMI at 3 months following their index presentation, using the Phillips 3.0T scanner. Images were analysed by 2 separate operators who were blinded to clinical data (me – 2 years of CMR experience and CK – 3 years of CMR experience). Initial analysis showed a bias in E2A and HA analysis due to difference between operators in the manual contouring of endocardium and epicardium on diffusion weighted images. To aid this process, manual contouring was repeated alongside cine images (which are of higher resolution than diffusion images) to ensure more precise depiction of endocardium and epicardium, as shown in Figure 3.4. This considerably improved interobserver reproducibility, and subsequent results are shown in the Bland-Altman plots for MD (Figure 3.5A), FA (Figure 3.5B), E2A (Figure 3.5C) and HA (Figure 3.5D & Figure 3.5E).
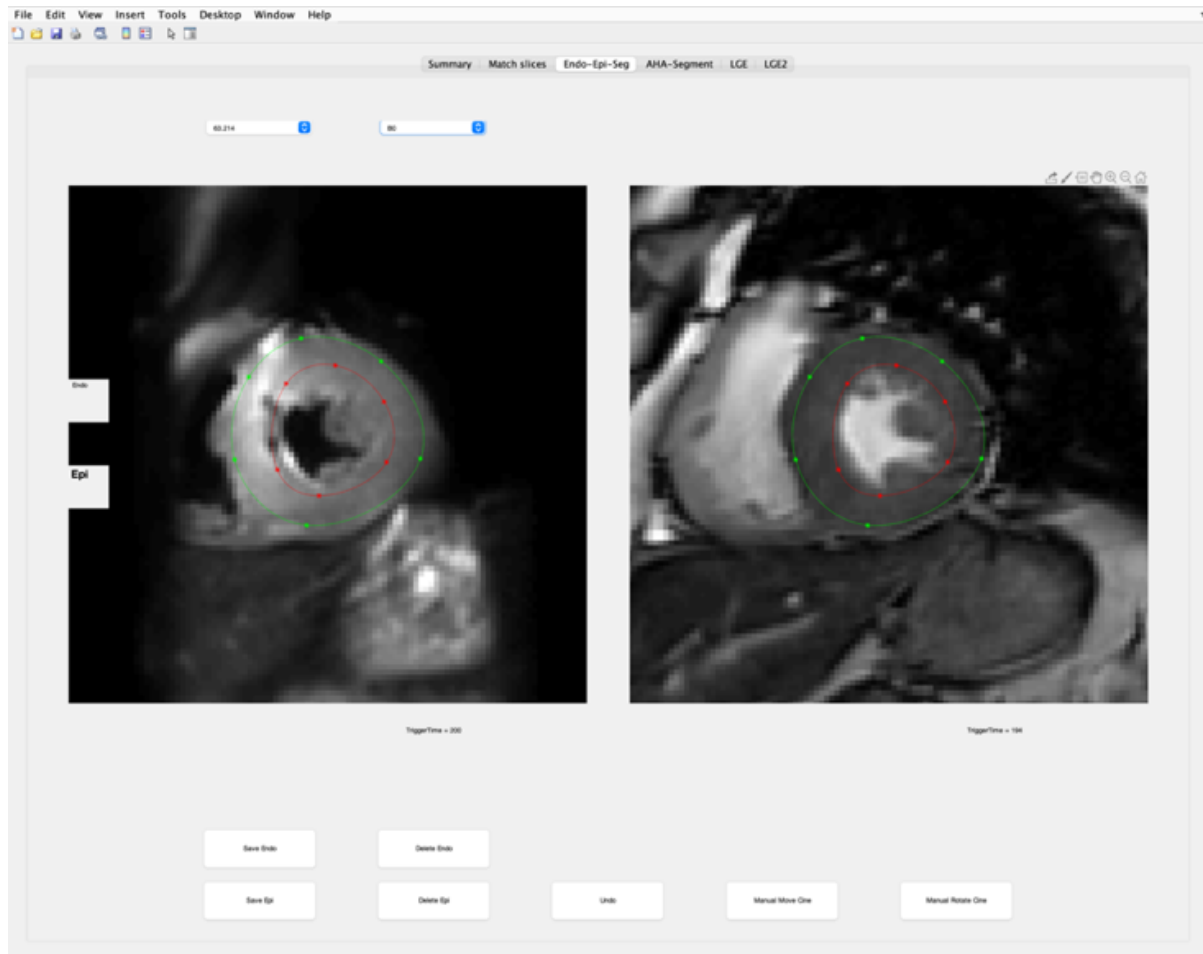
Figure 3.4: Manual contouring of DT-CMR maps

This figure shows a typical example of myocardial contouring of a basal LV slice on MATLAB software. Contours are manually drawn on the reconstructed non-diffusion weighted images (left). In order to improve interobserver reproducibility, a cine image (right) at a similar trigger delay is used a visual guide for endocardial and epicardial borders.

A

		Bias	Limits of agreement	
			Upper	Lower
Infarct		<0.01	0.12	-0.11
Remote		<0.01	0.08	-0.08

B

		Bias	Limits of agreement	
			Upper	Lower
Infarct		-0.02	0.030	-0.063
Remote		<0.01	0.054	-0.051

C

		Bias	Limits of agreement	
			Upper	Lower
Infarct		0.58	5.480	-4.325
Remote		0.69	4.760	-3.391

D

		Bias	Limits of agreement	
			Upper	Lower
RHM		<0.01	0.054	-0.005
CM		<-0.01	0.080	-0.016
LHM		<-0.01	0.071	-0.014

E

		Bias	Limits of agreement	
			Upper	Lower
RHM		-0.01	0.08	-0.01
CM		0.03	0.10	-0.01
LHM		-0.02	0.07	-0.02

Figure 3.5: Bland-Altman plots of interobserver variability

*Bland-Altman plots displaying agreement between interobserver variability for MD (**panel A**), FA (**panel B**), E2A (**panel C**) and proportions of RHM, CM and LHM on helix angle maps, encompassing remote (**panel D**) and infarct segments (**panel E**). The dashed lines represent the 95% limits of agreement.*

Through these validation tests, we have demonstrated the stability of our DT-CMR acquisition and analysis methods. I will now move on to describing the methods used for the clinic studies that follow this methods chapter.

3.2 Subject Recruitment

3.2.1 Myocardial infarction patients

Patients following their 'first-event' STEMI were prospectively recruited from the coronary care unit of Leeds General Hospital, Leeds, UK, for the following studies:

Chapter 3: DT-CMR sequence validation (interobserver reproducibility)

Chapter 4: Longitudinal changes in DT-CMR over 3 months following STEMI

Chapter 5: Detection of IMH using DT-CMR

Chapter 6: DT-CMR predictors of adverse LV remodelling

Inclusion criteria:

a) MI as defined by current international guidelines (17)
b) revascularisation via percutaneous coronary intervention (PCI) within 12 hours after onset of symptoms

Exclusion criteria:

a) contraindications to CMR
b) previous revascularisation procedure (coronary artery bypass grafts or PCI)
c) known cardiomyopathy
d) severe valvular heart disease

    e) atrial fibrillation

    f) haemodynamic instability lasting longer than 24 hours following PCI

3.2.2 Healthy volunteers

Healthy volunteers (controls) were enrolled from amongst students, staff and alumni of the local University for the following studies:

Chapter 3: DT-CMR sequence validation

Chapter 7: DT-CMR study of controls, athletes and HCM

Chapter 8: Phenotyping HCM using DT-CMR

Inclusion criteria:

    a) Asymptomatic
    b) No existing medical conditions
    c) Not taking any regular medication
    d) Normal physical examination
    e) Normal 12-lead ECG

Exclusion criteria:

    a) Any contraindications to CMR scanning (Impaired renal function with eGFR <30 ml/min/m^2, metal implants, pacemakers, claustrophobia, previous head or eye surgery)
    b) History to suspect pregnancy, a positive pregnancy test or breastfeeding

3.2.3 Athletes

Athletes were used in the following study:

Chapter 7: DT-CMR study of controls, athletes and HCM

Athletes were contacted through advertisement at local competitive cycling clubs and were included if they had performed cycling based exercise for over 6 hours/week, with no history of cardiovascular disease. Basic demographic information was gathered using a questionnaire, which included the frequency and duration of cycling per week as well as the number of years they had been training. Athletes had a cardio-pulmonary exercise (CPEX) test, after abstaining from intense physical exercise for 24 hours. Exclusion criteria was the same as for controls.

3.2.4 Hypertrophic cardiomyopathy patients

Patients with HCM were recruited from referrals to the clinical MRI service for the following studies:

Chapter 7: DT-CMR study of controls, athletes and HCM

Chapter 8: Phenotyping HCM using DT-CMR

The diagnosis of HCM was made independently by clinicians in keeping with current guidelines and based upon imaging including MRI, ECG, exercise testing, family history and genetic testing if possible.(92)

Inclusion criteria:

a) Left ventricular wall thickness (LVWT) of ≥15mm in at least one myocardial segment on CMR or echo

Exclusion criteria included the following:

a) Contraindications to CMR
b) Significant valve disease
c) Systemic hypertension

An overview of the study designs for each chapter are shown below in Figure 3.6.
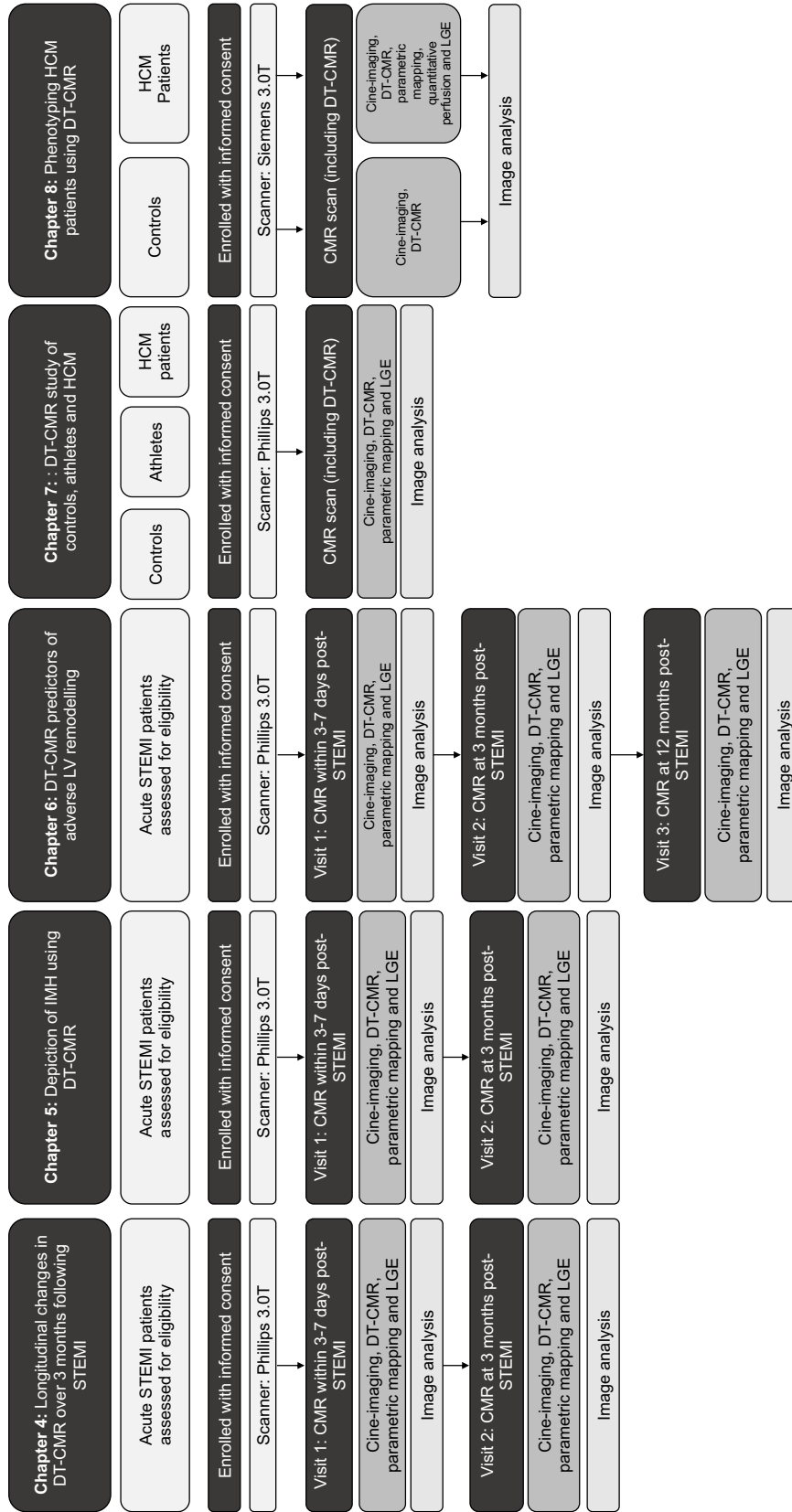
Figure 3.6: Study designs for the different studies

3.2.5 Ethical approval

All participants in this thesis provided written informed consent. All the study protocols in this thesis were approved by the institutional research ethics committee and complied with the Declaration of Helsinki (chapters 4-6: NIHR 33963, REC 17/YH/0062, chapters 7: 18/YH/0168, chapter 8: NIRH 39787, REC 18/YH/0372).

3.3 Image Acquisition

3.3.1 CMR sequence parameters (Phillips 3.0T)

All CMR examinations in chapters 4-7 were performed using a **3.0 Tesla Philips Achieva TX system** (Philips, Best, The Netherlands) equipped with a 32-channel cardiac phased array receiver coil, MultiTransmit technology and high-performance gradients with Gmax = 80mT/m and slew rate = 100 mT/m/ms. Study protocol and sequence parameters for this scanner were as follows:

3.3.1.1 Cine imaging

Cine imaging were acquired using a balanced steady-state free precession (bSSFP) pulse sequence (TE 1.3ms, repetition time (TR) 2.6ms, flip angle 40°, spatial resolution 1.6×2.0×10mm, typical temporal resolution 25ms). Images obtained included a LV volume contiguous short axis stack as well as two, three and four chamber views. (21)

3.3.1.2 DT-CMR sequence

DT-CMR data were acquired using ECG-gated second-order motion-compensated single-shot spin echo EPI sequence with asymmetric bipolar diffusion waveforms (93) and respiratory navigator tracking. Acquisition parameters were: (TE/TR = 89ms/3RR intervals, Flip angle = 90°, field of view (FOV) = 238 x 238mm, Matrix Size = 108 x 105, acquired in-plane resolution = 2.20x2.27, slice gap = 8mm, reconstructed voxel size = 1.7 x 1.7 x 8 mm, 3 repetitions, SENSE acceleration = 1.8). Each DT-CMR dataset constituted 18 non-collinear diffusion-weighted acquisitions with b-values of 100 s/mm^2 (3 diffusion weighted {DW} directions, 12 repetitions), 200 s/mm^2 (3 DW

directions, 12 repetitions), and 500 s/mm^2 (12 DW directions, 12 repetitions). Cine data were used to define the time from R peak to maximum systole. Trigger delay was set individually for each patient to coincide with 60% peak systole and the centre of k-space was approximately at 85% of peak systole. (80,93)

Three ventricular short-axis slices (base, mid and apical) were acquired: the mid ventricular slice was defined as the first slice from the mitral annulus to contain papillary muscles, the basal and apical slices was acquired as either the next or the second contiguous slice from the mid depending on the LV length to ensure consistent slice positioning between different scans.

Addressing common DT-CMR Artefacts

Ghosting artefacts can usually be addressed by changing the FOV. Typically starting with the FOV box perpendicular to the chest wall, repeat acquisitions with gradual incremental changes to the angle of the FOV box would eventually get rid of ghosting artefacts. Grainy images are typically a result of incorrect trigger delay. When encountering this artefact, decreasing the trigger delay to 25% or even 20% of peak systole would typically result in cleaner images. Other artefacts which include unsuppressed fat, signal loss and suboptimal signal-to-noise ratio are harder to address, and if they persist despite adjusting FOV and trigger delay, the affected segments will require exclusion from analysis. Examples of artefacts and segment rejection are discussed later in this chapter (section 3.4.2).

3.3.1.3 Native T1 mapping

3 short-axis slices matching the DT-CMR slice locations were acquired using a modified look-locker inversion recovery (MOLLI) sequence (5/3/0 acquisition, slice thickness 8mm, TE 2.1ms, TR 0.82ms, flip angle 20°, spatial resolution 0.91x0.91x8mm, SENSE 2 acceleration, cardiac delay time 777ms). (21)

3.3.1.4 T2 mapping

3 short-axis slices matching the DT-CMR slice locations were acquired using a dark-blood T2w fast spin echo short tau inversion-recovery (STIR) sequence (8mm thickness, TE 90 ms, TR 2 R-R intervals, flip angle 90°, spatial resolution 0.91×0.91×8mm) (94) and constant level appearance (CLEAR) homogeneity correction. (95)

3.3.1.5 T2* Mapping

3 short-axis slices matching the DT-CMR slice locations were acquired using a gradient echo sequence (TE 1.18 ms, TR 17 ms, flip angle 20°, spatial resolution 1.8x1.8x8mm). (96)

3.3.1.6 LGE

Following parametric mapping, a bolus of gadolinium contrast - 0.15mmol/kg gadobutrol (Gadovist, Bayer, Berlin, Germany) was administered intravenously. TI scout (Look-locker sequence, single mid-ventricular slice) was obtained to determine the optimal inversion time (TI) to null the myocardium. Late gadolinium imaging was performed 10-15 minutes after administration of contrast. 3 short-axis slices matching the DT-CMR slice locations were acquired using an inversion recovery-prepared T1-weighted gradient echo sequence (8mm thickness, inversion time according to Look-Locker scout, TR 3.7 ms, TE 2.0 ms, flip angle 25°, spatial resolution 0.91×0.91×8mm). (21)

3.3.1.7 Post-contrast T1

3 short-axis slices matching the DT-CMR slice locations were acquired 15 minutes after the administration of contrast, using a MOLLI sequence (4/3/2 acquisition, TE 2.1ms, TR 0.82 ms, flip angle 35°, spatial resolution 0.91×0.91×8mm, SENSE 2 acceleration, cardiac delay time 728ms). (21)

3.3.2 CMR sequence parameters (Siemens 3.0T)

All CMR examinations in chapter 8 were performed using a **Prisma 3.0T MRI scanner (Siemens Healthineers, Erlangen, Germany)**. Study protocol and sequence parameters for this scanner were as follows:

3.3.2.1 Cine Imaging

Cine imaging were acquired using a balanced bSSFP pulse sequence (TE 1.4ms, TR 38ms, flip angle 42°, spatial resolution 1.9×1.9×8mm). Images obtained included a LV volume contiguous short axis stack as well as two, three and four chamber views. (97)

3.3.2.2 Native T1 mapping

T1 mapping using a MOdified Look Locker Inversion recovery (MOLLI) sequence (native 5(3)3 acquisition, slice thickness 8mm, TE 1.1ms, TR 736 ms, flip angle 20°, spatial resolution 1.5x1.5x8mm).

3.3.2.3 DT-CMR

DT-CMR data were acquired using ECG-gated second-order motion-compensated single-shot spin echo EPI sequence with respiratory navigator tracking. (88,98) Acquisition parameters were: (TE/TR 77ms/3R-R intervals, Flip angle = 90°, FOV 320×121 mm^2, matrix size 138×52, in-plane resolution 2.3×2.3mm^2, 8mm slice thickness, 8mm inter-slice gap, partial Fourier = 7/8. Scout (diffusion weighted data were acquired with diffusion-weighting applied in three orthogonal directions to ensure data quality. Each full data set comprised b-values of 100 s/mm^2 (3 DW directions, 12 repetitions), and 450 s/mm^2 (30 DW directions, 6 repetitions). Based on cine data, trigger delay was defined as approximately 30% of peak systole. (88) The same methods were used to address common artefacts as the Phillips 3.0T scanner, as described above in section 3.3.1.2.

3.3.2.4 Perfusion imaging

Perfusion imaging was acquired using free-breathing, motion-corrected automated in-line perfusion mapping. (99) Adenosine was infused at a rate of 140 µg/kg/min and increased up to a maximum of 210 µg/kg/min according to haemodynamic and symptomatic response (blood pressure and heart rate were recorded during adenosine infusion). An intravenous bolus of 0.05mmol/kg gadobutrol (Gadovist, Leverkusen, Germany) was administered at 5ml/s followed by a 20ml saline flush using an automated injection pump (Medrad MRXperion Injection System, Bayer). Inadequate heart rate response was defined as <10 rise in beats-per-minute in keeping with Society of Cardiovascular Magnetic Resonance (SCMR) guidelines. (100) A minimum of ten-minute interval was kept between stress and rest perfusion acquisitions to ensure equilibration of gadolinium kinetics and that all haemodynamic effects of adenosine had resolved. (8mm slice thickness, TE 1ms, TR 146ms, flip angle 14°, spatial resolution 1.9x1.9x8mm). (97)

3.3.2.5 LGE

TI scout (Look-locker sequence, single mid-ventricular slice) was obtained to determine the optimal inversion time (TI) to null the myocardium. Motion corrected LGE imaging was performed 10-15 minutes after administration of contrast. 3 short-axis slices matching the DT-CMR slice locations were acquired an inversion recovery-prepared T1-weighted gradient echo sequence (8mm thickness, inversion time according to Look-Locker scout, TR 904 ms, TE 1.2 ms, flip angle 50°, spatial resolution 1.6×1.6×8mm). (97)

3.3.2.6 Post-contrast T1

3 short-axis slices matching the DT-CMR slice locations were acquired 15 minutes after the administration of contrast, using a MOLLI sequence (4/3/2 acquisition, TE 1.1ms, TR 736 ms, flip angle 20°, spatial resolution 1.5×1.5×8mm).

3.4 Image analysis

The post-processing pathway was the same for scans acquired using Phillips 3.0T and Siemens 3.0T scanners. The methodology for the analysis of the various sequences is discussed in the following section.

3.4.1 CMR post processing

Cardiac magnetic resonance analysis was performed quantitatively offline by a single operator (AD) who was blinded to long-term outcomes. Cine, mapping and LGE data were analysed using cvi42 software (Circle Cardiovascular Imaging Inc, Calgary, Canada).

3.4.1.1 Cine data

LV subendocardial and subepicardial borders were defined by manual planimetry excluding papillary muscles at end-systole and end-diastole. LV mass, end-diastolic volumes (EDV), end-systolic volumes (ESV) and LV ejection fraction (EF) were measured from short-axis cine images. For chapter 8, maximal wall thickness was measured using a machine learning algorithm as previously described. (101)

3.4.1.2 LGE analysis

LV short-axis stack of LGE images was first assessed visually for the presence of LGE, followed by quantification when LGE was present, as done in previous studies. (102) LGE was defined as areas of signal intensity ≥ 5 standard deviations from normal myocardium and was expressed both as a percentage of the segment, as well as the percentage of LV mass. MVO was defined as dark zones within an area of LGE at 15 mins. MVO was planimetered separately and expressed both as a percentage of the segment, as well as the percentage of LV mass.

3.4.1.3 Parametric mapping analysis

On both T1 and T2 maps, a 10% offset was applied to subendocardial and subepicardial borders to minimise partial volume effect. ECV was calculated using Equation 1.1 as shown in chapter 1, with haematocrit measured from blood tests on the day of the CMR scan. Using the basal, mid and apical slices, segmental T1, T2 and ECV values were calculated for each of the 16 segments of the American heart association (AHA) model. (103)

Segmental analysis however provides an average value across the segment, and in conditions like MI, values can significantly vary transmurally across the myocardium. To detect regional changes, for instance exclusively within areas of infarct myocardium, ROI analysis is recommended. (104) In this thesis, ROI analysis was used for regional analysis of patients following MI (chapters 4-6). ROIs were manually drawn on parametric maps in accordance to standards set by the European Association for Cardiovascular Imaging (104). As recommended, ROIs were drawn on greyscale images to avoid bias. Very small ROIs (<20 pixels) were avoided. ROIs were sampled away from endo- and epicardial borders to avoid the effects of partial voluming. For each patient, during their first scan, three ROIs were drawn corresponding to: infarct (positive for LGE), adjacent oedematous myocardium (negative LGE, raised native T1 [departmental threshold >1240ms]) and remote myocardium (opposite infarct). (Figure 3.7) These regions were used as a reference for ROI sampling for subsequent visits.
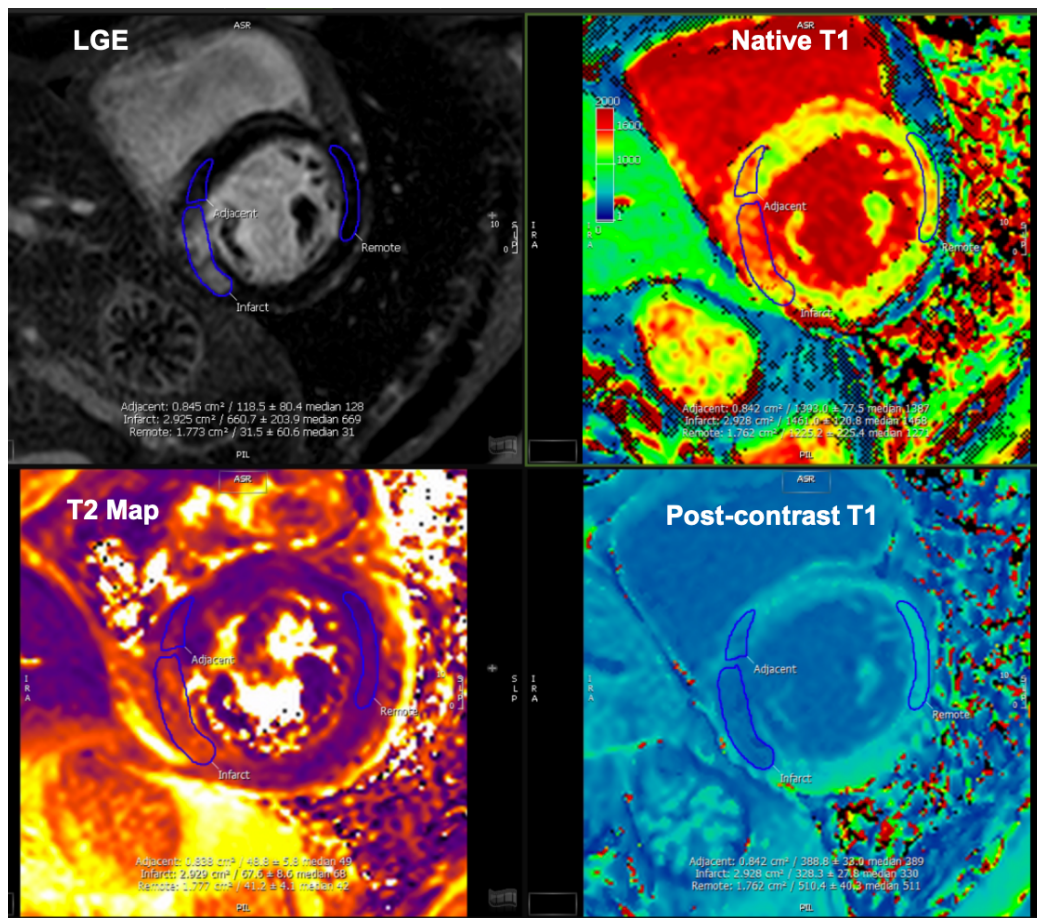
Figure 3.7: ROI analysis of parametric maps

Infarct and remote myocardium were identified on LGE images (top left) and copied across to parametric maps. Areas of oedema adjacent to infarct was identified on native T1 maps (relaxation time >1240ms {departmental threshold}) and copied across to other maps. Please note ROIs were originally drawn on a greyscale image to avoid bias; colour scales have been added to this figure for the reader's benefit.

On the T2* maps, an area of reduced signal intensity within infarcted myocardium, with a T2* value of <20ms was considered to confirm the presence of IMH. (105) If iron was detected on T2* mapping, the area was measured using manual planimetry. Averaged DW images, native T1 and T2 maps for the corresponding patient were subsequently analysed. On averaged DW images, the presence of an area of

hypointense signal in the same region constituted to a positive detection of iron, and the area of hypointense signal was measured using manual planimetry. On native T1 and T2 maps, a relative reduction in relaxation times within this area compared to surrounding infarct myocardium constituted to a positive detection of iron. (Figure 3.8)
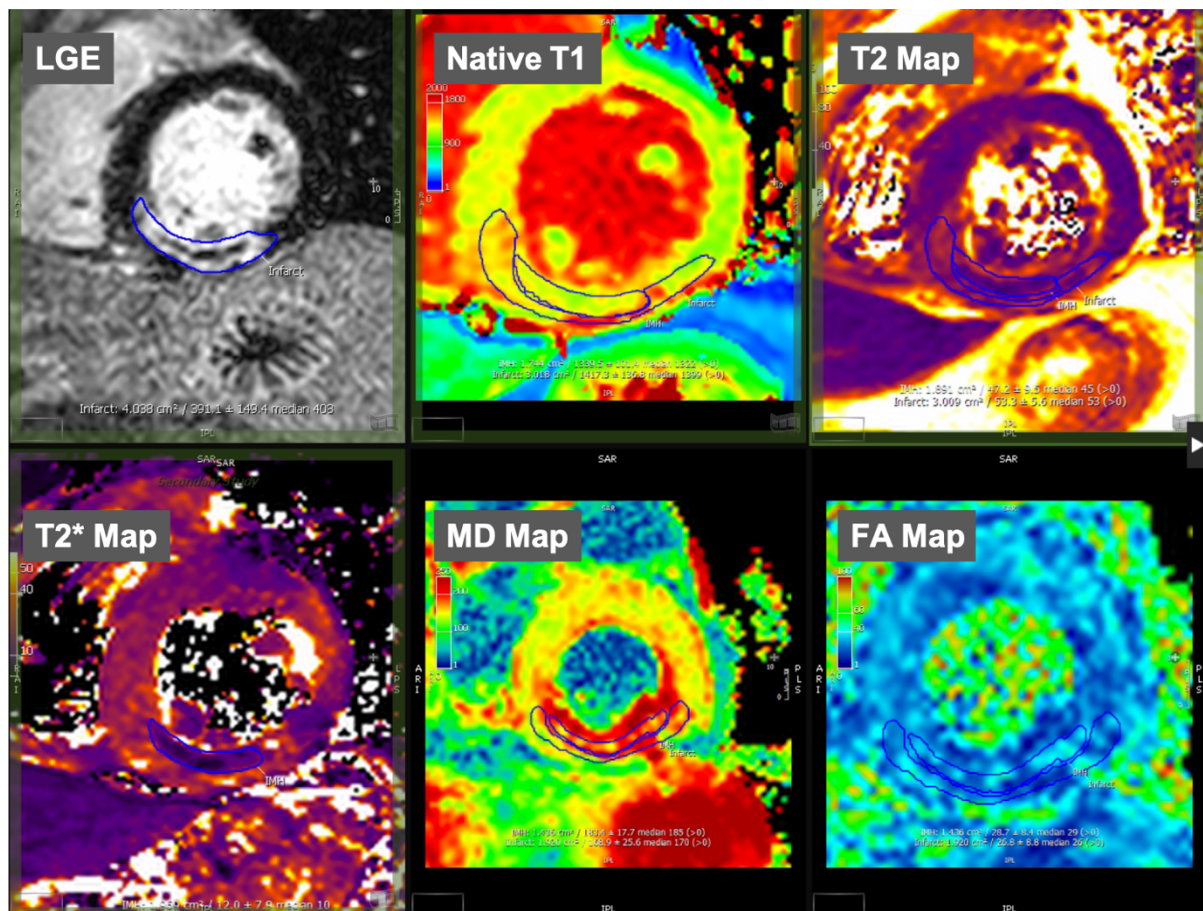
Figure 3.8: ROI analysis of IMH

For cases with IMH, infarct myocardium was identified on LGE and areas of IMH was identified on T2* maps. ROIs were drawn and copied across to parametric and DT-CMR maps. Infarct ROIs on parametric and DT-CMR maps were adjusted so they did not sample areas of IMH. Please note ROIs were originally drawn on a greyscale image to avoid bias; colour scales have been added to this figure for the reader's benefit.

3.4.1.4 Perfusion mapping

Perfusion mapping (in chapter 7) was performed and implemented on the scanner using the Gadgetron streaming software image reconstruction framework as previously described. (99) Global and segmental MBF were calculated inline from the perfusion maps (where each pixel encodes MBF in mL/g/min). Subendocardial and subepicardial borders were contoured automatically using a machine learning approach. Where the left ventricular outflow tract was included, or partial volume effect meant segments were too thin to contour, these segments were excluded from further analysis. Each segment was also further divided into subendocardial (inner 50%) and subepicardial (outer 50%) regions. Myocardial perfusion reserve (MPR) was calculated as stress MBF:rest MBF.

3.4.2 DT-CMR post processing

DT-CMR data registration and tensor calculation was performed using in-house developed MATLAB software (MathWorks, MA, USA) by an independent investigator (CK) who was blinded to clinical data.

3.4.2.1 DT-CMR tensor calculation

All diffusion images were co-registered via a mutual-information-based, multi-resolution, affine scheme using the elastix toolbox. Quality control was undertaken by visual assessment, with DW images corrupted by artefact or failed registration omitted from further processing. Based on the registered data, magnitude averaged images were generated according to diffusion direction and b-value; diffusion tensors were calculated using a linear least-squares approach. Tensor eigenvalues, MD, FA, HA and absolute E2A maps were calculated based on the tensors derived from DWI data acquired at diffusion gradients with b=100, 200 and 500 s/mm^2 images.

3.4.2.2 DT-CMR segmentation

DT-CMR segmentation was performed by an investigator (me) who was blinded to clinical data, using MATLAB software as described above. Myocardial contours were

manually drawn directly on the reconstructed non-diffusion weighted images for the basal, mid and apical slice (Figure 3.9). In order to separate myocardial tissue from blood pool and minimise the effects of partial voluming, a conservative approach was adopted, ensuring the borders were drawn within the myocardium.

These contours were subsequently copied across to MD, FA, HE and absolute E2A maps (Figure 3.9). Apical slices were excluded from analysis due to persistent artefacts from unsuppressed fat, signal loss and suboptimal signal-to-noise ratio. The basal and mid slice were divided into 6 equiangular segments based on the 16-segment AHA model for analysis, using the anterior insertion point as a reference. (103) MD, FA, E2A and HA averages were calculated for each segment. HA maps were described by classifying voxels to one of three groups: LHM (-90≤ HA<-30), CM (-30≤HA≤30) and RHM (30<HA≤90) and quantitative markers derived as the respective myocardial proportions of each type, as done in previous studies. (65)
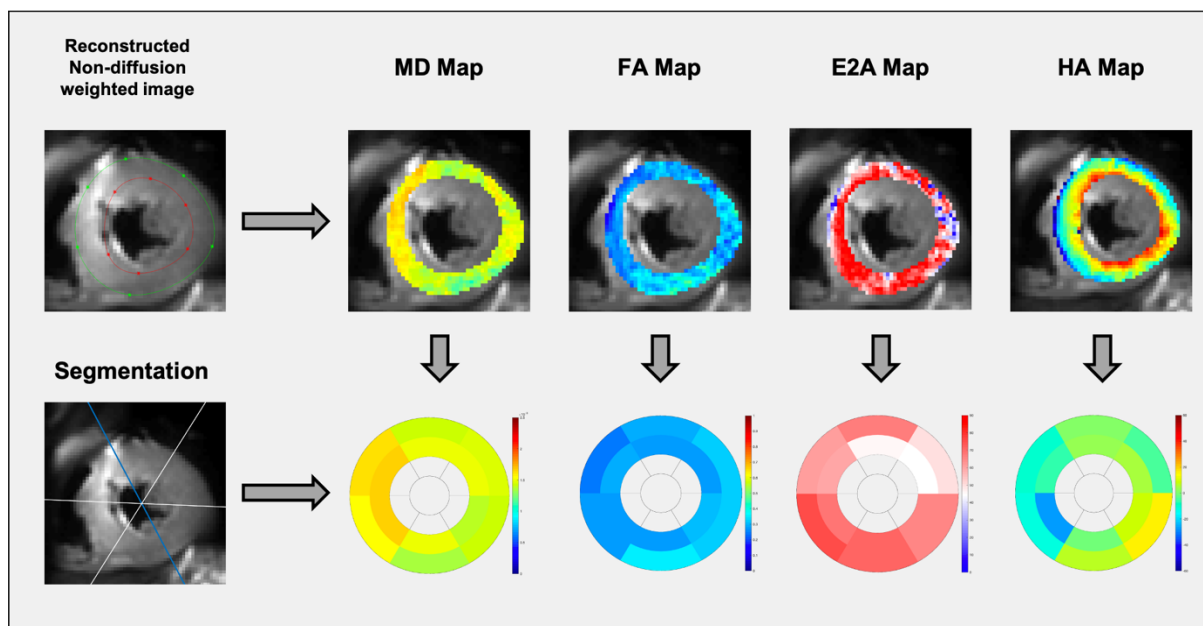
Figure 3.9: DT-CMR segmentation

Following manual contouring, basal and mid slice contours were copied across to different DT-CMR maps, which were segmented unto 6 equiangular segments using the anterior insertion point as a reference.

For chapter 8, in order to investigate possible explanations for the subendocardial pattern of MVD seen in HCM, each segment of MD and FA maps were further divided into subendocardial (inner 50%) and subepicardial (outer 50%) regions.

3.4.2.3 Rejection of artefacts

Following the creation of segmental polar plots, each segment was visually inspected. Segments with persistent artefacts were identified and excluded from analysis, as shown below. (Figure 3.10)

Figure 3.10: Artefact rejection

In both panels, despite adjusting the field-of-view, there is signal overlap from adjacent anatomical structures, most likely due to unsuppressed fat, impinging on the inferolateral wall. As a result, the affected segments were excluded from further analysis.

3.4.2.4 DT-CMR ROI analysis

ROIs were used for the analysis of MD and FA in patients following STEMI (chapters 4-6). In order to do this, MD and FA maps were re-imported into cvi-42 software and ROIs were sampled from infarct, adjacent, remote zones as well as areas of IMH as described above for parametric mapping analysis. Unlike MD and FA, E2A and HA

values varies transmurally across the myocardium in healthy subjects. Due to this expected spatial inhomogeneity, it is challenging to define the 'normal range' for a specific region within the myocardium, making ROI analysis unfeasible, hence segmental analysis was performed for E2A and HA maps.

3.5 Statistics

Statistical analyses were performed in IBM SPSS Statistics 21.0 (Armonk, New York). Normality was checked using the Shapiro-Wilk test. Continuous variables are reported as mean±SD. Parametric data were compared using Student's T-Test or analysis of variance (ANOVA), non-parametric data were compared using the Kruskal-Wallis test. For comparing results from initial and repeated measurements, paired t-tests and ANOVA with Bonferroni post-hoc comparisons were used. For sequence validation in chapter 3, interobserver variability was analysed using the Bland-Altman method and paired t-tests were used to determine the statistical significance to any difference. Pearson correlation analysis was used to calculate the correlation coefficients between independent continuous variables. Univariate and multivariate linear regression was used to assess the predictive capabilities of clinical and acute CMR biomarkers of long-term LVEF. Binary logistic regression models were used to assess the predictive capabilities of clinical and acute CMR biomarkers of long-term adverse remodelling. Statistical significance of the differences between ROC curves was assessed using the method of DeLong et al. (106) Comparison between categorical data were performed using χ^2 tests. All tests were assumed to be statistically significant when $p<0.05$. Detailed statistical methods used in specific chapters are outlined in the relevant chapters.

3.6 Conclusion

Having outlined the steps taken for sequence validation, and the methods used for the studies in this thesis, I will now move on to clinical applications of DT-CMR, beginning with looking at how the parameters are affected in patients following STEMI.

Chapter 4: Assessment of microstructural changes following ST-elevation myocardial infarction using diffusion tensor cardiac magnetic resonance imaging

Short title: Longitudinal changes in DT-CMR over 3 months following STEMI

4.1 Introduction

LV remodelling following MI is characterised by chamber dilatation and regional wall thinning. The disproportionate increase in myocyte length without the adaptive increase in myocyte cross-sectional area that is needed for force generation, leaves the long slender myocytes at a mechanical disadvantage to deal with the ensuing increasing wall stress and leads to worsening functional impairment over time. (107) In healthy myocardium, cardiomyocytes aggregate together to form laminar secondary structures known as 'sheetlets'. Reorientation of sheetlets throughout the cardiac cycle is thought to be the principal mechanism driving LV wall thickening during systole (69) however the impact of ischaemic injury on sheetlets have not been explored in detail. As described in chapter 1, there are numerous CMR sequences capable of depicting and quantifying myocardial oedema, scarring and the consequent impairment in contractility following ischaemic injury, however these techniques do not allow for the assessment of the organisation and integrity of microstructural components. With the emergence of DT-CMR however, this has now become possible. (108,109)

4.1.1 Hypothesis and aims

We therefore performed second-order motion-compensated spin echo DT-CMR on reperfused ST-elevation myocardial infarction (STEMI) patients in order to infer upon microstructural differences between infarcted and remote myocardium and assess how acute changes in infarct regions relate with LV function recovery. I hypothesised

that DT-CMR derived biomarkers of more severe injury in infarcted myocardium will correlate with lower LVEF at 3 months post-MI.

4.2 Methods

37 patients were prospectively recruited following their 'first-event' STEMI. See chapter 3 for full details regarding subject recruitment (chapter 3.2.1), image acquisition (chapter 3.3.1), image analysis (chapter 3.4) and basic statistical analysis (3.5).

Detailed statistics

Paired t-tests were used to compare initial (from acute scan) and repeated measurements (at 3 months) of DT-CMR and parametric parameters to detect the significance of longitudinal changes in tissue characteristics of remote, adjacent and infarct areas. ANOVA test was used to detect significant differences in CMR measurements between 3 sub-groups of patients (categorised according to LVEF outcome at 3 months). Pearson correlation analysis was used calculate correlation coefficients between the different acute CMR biomarkers (including DT-CMR parameters); between acute DT-CMR parameters and change in infarct size; and between DT-CMR parameters and LVEF at 3 months. Univariable analyses were performed to identify predictors of reduced LVEF at 3 months. Variables with a probability value <0.1 in the univariate analysis were included in a multivariable linear regression analysis.

Subgroup analysis

To investigate changes in DT-CMR parameters in patients with worsening LV function, three groups of patients were identified based on LVEF (in accordance with European Society of Cardiology Guidelines) (21) : group 1 with preserved LVEF% (>50%), group 2 with acutely impaired LVEF% (<50%) which recovered to normal limits (>50%) by 3 months, and group 3 with acutely impaired LVEF%, which remained impaired at 3 months (<50%).

4.3 Results

4.3.1 Baseline patient characteristics

The study flowchart is shown in Figure 4.1. Thirty patients (M:F = 21:9, aged 59 ± 10 years) completed acute (5 ± 2 days) and 3 month scans (104 ± 14 days). As described in Table 4.1, 56% presented with inferior STEMI. In acute scans, all patients showed evidence of oedema on T2 maps and infarction on LGE, with a mean infarct size of 10±8g. By the 3-month scan, the mean LVEF across the cohort improved from 48±7%, to 53±7% (p=0.006). (Table 4.2)
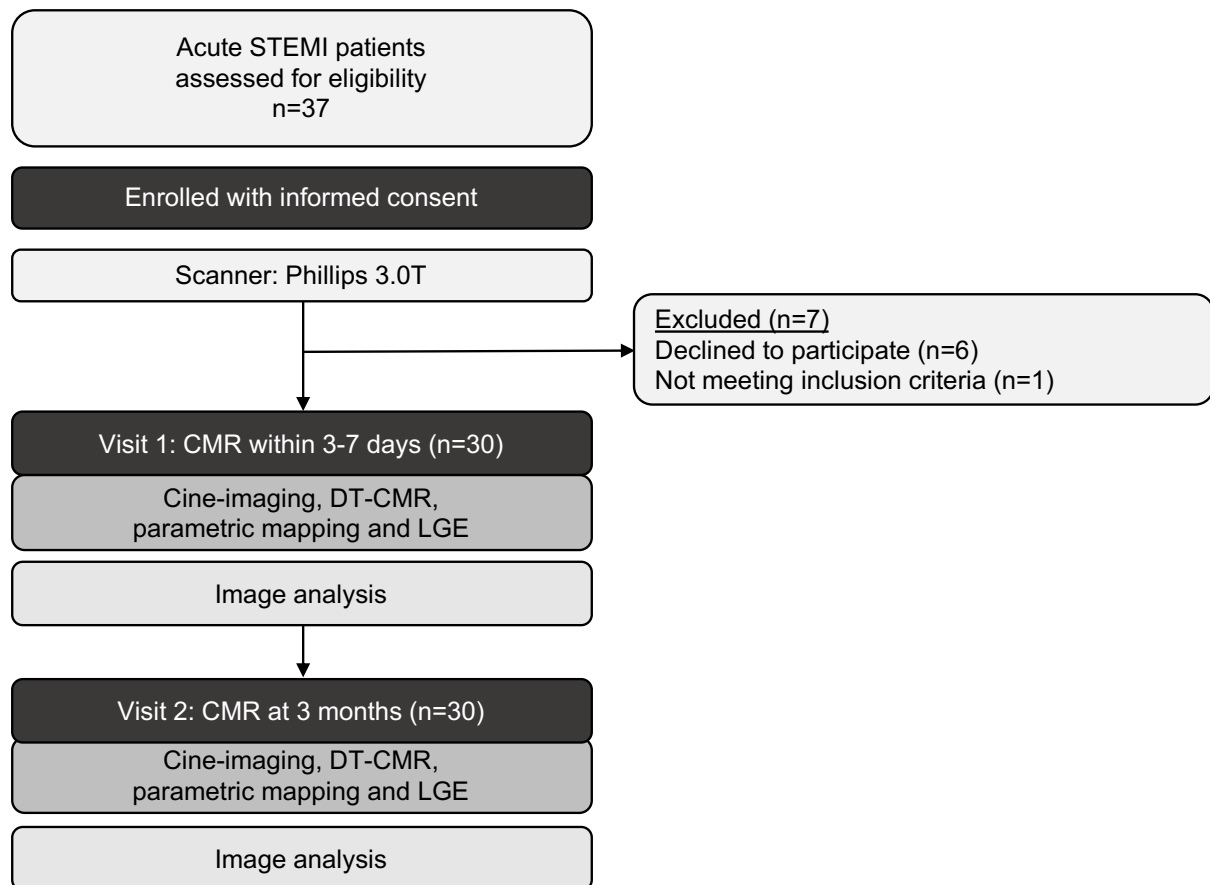
Figure 4.1: Flowchart of study enrolment

Table 4.1: Baseline characteristics of the study population

Patient Characteristics	All (n=30)
Age (years)	59 ± 10
Sex	21:9 (M:F)
Risk Factors (No)	
Smoker	11
Hypertension	4
Diabetes	2
Family History	9
Peripheral Vascular Disease	1
Presenting characteristics	
Culprit coronary artery [No (%)]	
Left Anterior Descending	10 (33)
Left Circumflex	3 (10)
Right Coronary	17 (56)
Infarcted segments	4 ± 2
Microvascular obstruction (number of patients)	13
Mean time from onset of symptoms to balloon (mins)	238 ± 172
Treatment [No (%)]	
Aspirin	30 (100)
Adenosine diphosphate receptor antagonist (Ticagrelor)	30 (100)
Angiotensin converting enzyme (ACE) inhibitor	30 (100)
Beta-blocker	28 (93)

Table 4.2: CMR Results

Global Values (mean ± SD)	Acute scan (n=30)		3 month scan (n = 30)
Interval to scan (days)	5 ± 2		104 ± 14
LVEF (%)	48 ± 7		53 ± 7
LVEDV (ml)	154 ± 31		154 ± 34
LVEDVi (ml/m2)	78 ± 15		78 ± 16
LVESV (ml)	75 ± 17		73 ± 24
LV Mass (g)	105 ± 25		99 ± 23
Mean LGE (% of LV)	21 ± 14		15 ± 9
Infarct Size (g)	10 ± 8		8 ± 6
MVO Positive (n)	13		0
MVO (g)	0.65 ± 1.18		n/a

Regional values	Remote	Adjacent	Infarct	ANOVA	Remote	Adjacent	Infarct	ANOVA
Native T1 (ms)	1194 ± 66	1295 ± 75	1478 ± 123	<0.001	1188 ± 42	1211 ± 62*	1398 ± 91*	<0.001
Extracellular Volume (%)	27 ± 3	32 ± 4	53 ± 9	<0.001	29 ± 6	29 ± 6	60 ± 16*	<0.001
T2 (ms)	50 ± 5	53 ± 6	68 ± 10	0.009	48 ± 4	49 ± 5*	55 ± 5*	0.007
Mean Diffusivity (x10⁻³ mm²/s)	1.48 ± 0.12	1.59 ± 0.10	1.69 ± 0.14	<0.001	1.45 ± 0.11	1.53 ± 0.13*	1.83 ± 0.21*	<0.001
FA	0.36 ± 0.02	0.33 ± 0.03	0.25 ± 0.03	<0.001	0.35 ± 0.03	0.33 ± 0.02	0.22 ± 0.03*	0.008
E2A (°)†	55 ± 9	52 ± 7	49 ± 10	0.008	44 ± 11	51 ± 8	46 ± 9	0.843
HA†								
RHM (%)	16 ± 6	20 ± 5	9 ± 5	<0.001	19 ± 6	20 ± 6	12 ± 7	0.343
CM (%)	78 ± 7	66 ± 11	80 ± 7	0.617	68 ± 9	69 ± 11	77 ± 11	0.786
LHM (%)	6 ± 5	14 ± 6	11 ± 9	0.112	13 ± 7.	11 ± 8	11 ± 8	0.784

Significant change from acute scan (p<0.05). † Measured using segmental analysis. LVEDVi = Left ventricular end-diastolic volume indexed for BSA, LVESV = Left ventricular end-systolic volume

4.3.2 Feasibility of DT-CMR acquisition

DT-CMR acquisition was successful in all patients with a mean acquisition time of 13±5 mins. Representative CMR maps (including DT-CMR) are shown in Figure 4.2. Apical DT-CMR slices were excluded from analysis due to persistent artefacts from unsuppressed fat, signal loss and suboptimal signal-to-noise ratio. Out of all basal and mid slices segments, 65/720 (9%) were excluded because of the mentioned image artefacts.

Figure 4.2: Representative Cardiac MRI and DT-CMR images

Panels A and **B** correspond to 2 separate patients.

Panel A: Short-axis images in a 61-year-old man 7 days post lateral STEMI and subsequent primary percutaneous coronary intervention (PPCI) to the obtuse marginal branch of the left circumflex artery. His acute LVEF was 40%. LGE images demonstrate a subendocardial scar in the basal anterolateral wall, (column 1) with high T1 values on T1 mapping (column 2). The corresponding areas on DT-CMR maps show high MD (column 3), low FA (column 4), high E2A (column 5) and HA (helix angle) with preservation of RHM (red and orange pixels, 30° < HA < 90°). This patient's LVEF improved to 52% at 3 months.

Panel B: Short-axis images in 61-year-old man 7 days post anteroseptal STEMI and subsequent PPCI to the LAD. His LVEF was 30% at this stage, his LGE images demonstrate transmural scar and MVO in the mid septal walls, with hyperintense signals on T1 mapping. The corresponding areas on DT-CMR maps show high MD and low FA. As demonstrated on the schematic diagram, within the infarct segments are areas of low MD and high FA likely in relation to MVO artefact. Meanwhile E2A maps show significantly low values, and the HA shows less RHM (reduced red and orange pixels) in the infarct segments in comparison with panel A. This patient's LVEF only improved to 33% at 3 months.

4.3.3 DT-CMR biomarkers post-acute ischemic injury

Acutely, MD and FA in remote myocardium matched previously reported values in healthy volunteers using SE-DT-CMR at 3T. (22) In keeping with previous literature, our results show MD to be increased in adjacent and infarct regions, with FA showing the opposite trend. (Table 4.2)

At the acute scan, 13 patients showed evidence of MVO on LGE imaging. MD and FA were significantly different in the core of the MVO compared to surrounding injured myocardium within the LGE positive areas (MD_{MVO}=1.49±0.1 x $10^{-3}mm^2/s$ vs MD_{LGE} = 1.75±0.19 x $10^{-3}mm^2/s$, $p<0.001$, mean FA_{MVO}=0.34±0.07 vs mean FA_{LGE}=0.25±0.03, $p <0.001$), as shown in Figure 4.3.
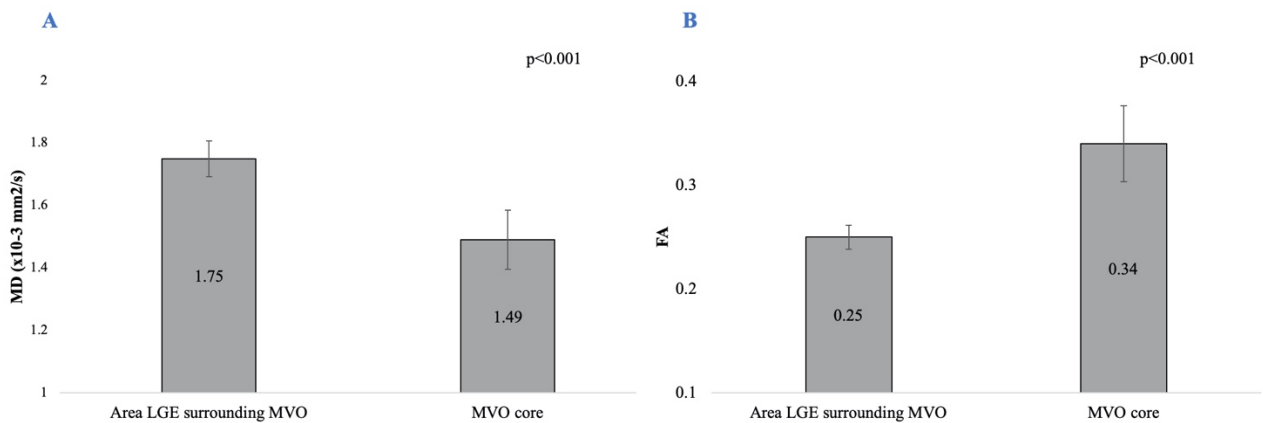
Figure 4.3: MD and FA values within MVO

MD (panel A) within the MVO regions are significantly lower than in the surrounding LGE-positive myocardium. Mean FA (panel B) shows the opposite trend.

Mean E2A values were lower in infarct segments in comparison to adjacent and remote ($E2A_{remote}$ = 55±9°, $E2A_{adjacent}$ = 52±7°, $E2A_{infarct}$ = 49±10°, ANOVA p=0.008) (Table 4.2). The HA range of infarct and remote segments during the acute scan is shown in Figure 4.4. Infarct segments had less RHM in comparison to adjacent and remote segments ($RHM_{infarct}$ = 9±5%, $RHM_{adjacent}$ = 20±5%, RHM_{remote} = 16±6%,

ANOVA $p<0.001$). Proportions of RHM in infarcted segments as depicted on HA maps correlated with corresponding segmental E2A (Figure 4.5). 13 patients showed evidence of MVO on LGE. Segmental E2A and RMH% were lower in infarct segments with MVO compared to infarct segments without MVO both in acute (E2A$_{MVO+ve}$=43±4° vs E2A$_{MVO-ve}$=50±6°, p=0.031; RHM%$_{MVO+ve}$=5±4% vs RHM%$_{MVO-ve}$=11±5%, $p<0.001$) and 3 month scans (E2A$_{MVO+ve}$=40±7° vs E2A$_{MVO-ve}$=48±9°, p=0.018; RHM%$_{MVO+ve}$=8±5% vs RHM%$_{MVO-ve}$=13±6%, p=0.008).
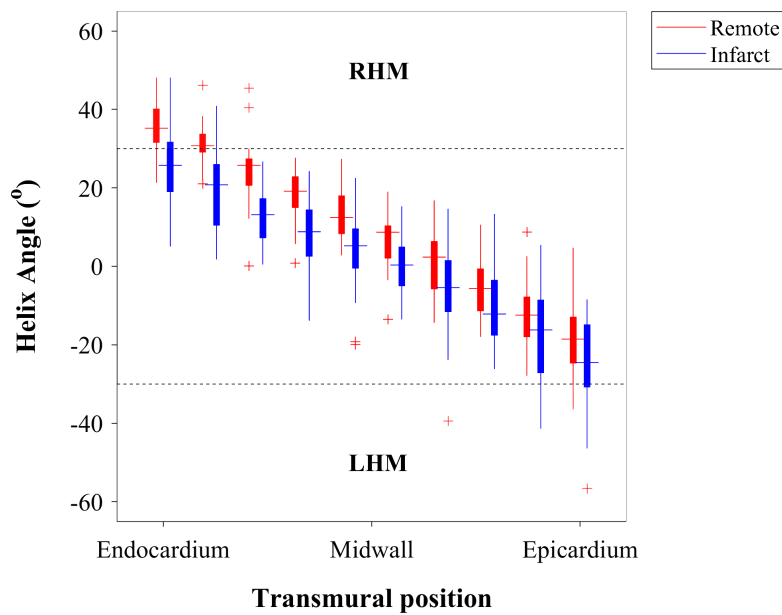
Figure 4.4: Transmural helix angle range across acute infarct and remote segments

Infarct segments had less RHM than remote, signifying reduced organisation among cardiomyocytes in the subendocardium.
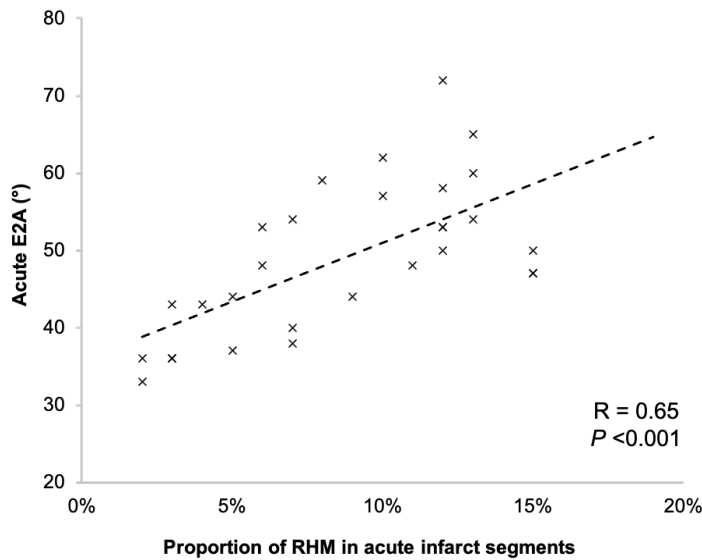
Figure 4.5: Associations between RHM and absolute E2A

Acute infarct segments with less RHM (corresponding to subendocardial cardiomyocytes) had lower E2A in corresponding segments. This signifies that infarct segments with less organisation among subendocardial cardiomyocytes had myocardial sheetlets that were more hypo-angulated during systole.

4.3.4 Longitudinal changes in DT-CMR biomarkers

In comparison to the acute scans, at 3 months, MD increased in infarct regions from 1.69 ± 0.14 to $1.83\pm0.16 \times 10^{-3} mm^2/s$) (Table 4.2). Conversely, FA decreased in the infarct regions from 0.25 ± 0.03 to 0.22 ± 0.03). MD and FA values in infarcted regions correlated with ECV at 3 months, (Figure 4.6) indicating that in the absence of oedema, both markers are sensitive to the expansion in ECV. There were no significant longitudinal changes in E2A or HA proportions, indicating that the microstructural changes they depict remain relatively fixed.
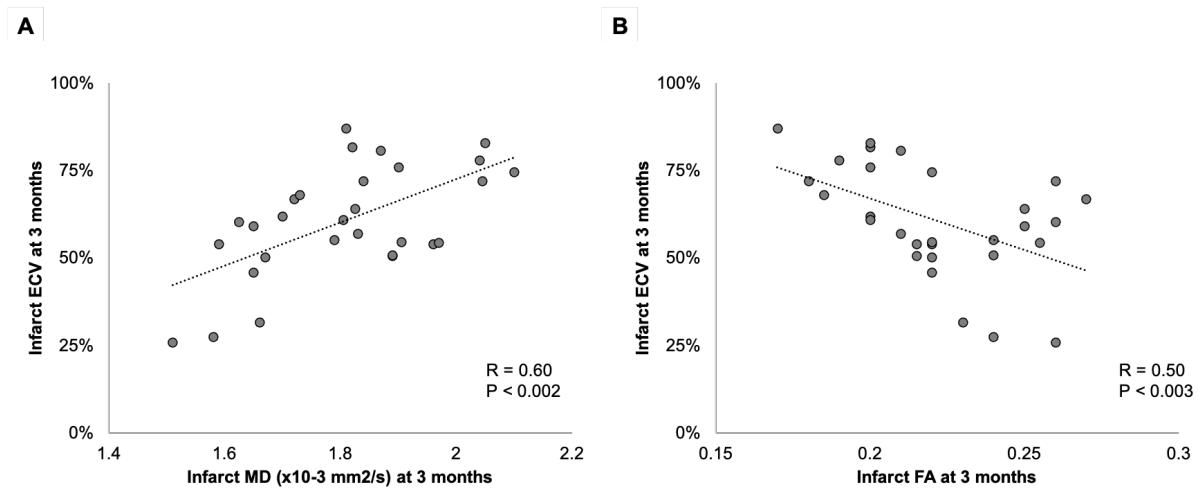
Figure 4.6 Correlation between MD, FA and ECV at 3 months.

In the 3-month scan, MD (Panel A) and FA (Panel B) both correlate with ECV values in corresponding infarct regions.

4.3.5 Acute DT-CMR markers of irreversible injury

Patients with lower acute FA in infarct regions experienced significantly less change in infarct size over time, whilst higher FA values were associated with significant reductions in final infarct size ($p<0.001$). (Figure 4.7A).

In order to understand the long-term implications of acute changes in DT-CMR parameters within infarct regions, we grouped patients based on LV recovery at 3 months (Table 4.3). In comparison with patients with preserved LVEF at 3 months (groups 1 and 2), patients with impaired LVEF at 3 months (group 3) had significantly lower FA, lower RHM (Figure 4.7B) and lower E2A in their infarct segments during the acute scan. Segmental RHM and E2A in acute infarct segments correlated with LVEF at 3 months (Figure 4.7C and D). At 3 months, group 3 patients retained significantly lower E2A and RHM% values in their infarct segments compared to infarct segments of patients in groups 1 and 2. (Table 4.3)

Univariate linear regression analysis (Table 4.4) identified several cardiac MRI-based infarct characteristics to be significantly associated with ejection fraction at 3 months. Among DT-CMR parameters, acute infarct FA, E2A and RHM all correlated with LVEF at 3 months (r = 0.68, r = 0.59 and r = 0.53 respectively). In multivariate linear regression analysis adjusting for factors including acute ejection fraction, infarct size and MVO, only infarct FA (standardised β 0.56, p=0.008) was independently associated with LVEF at 3 months.
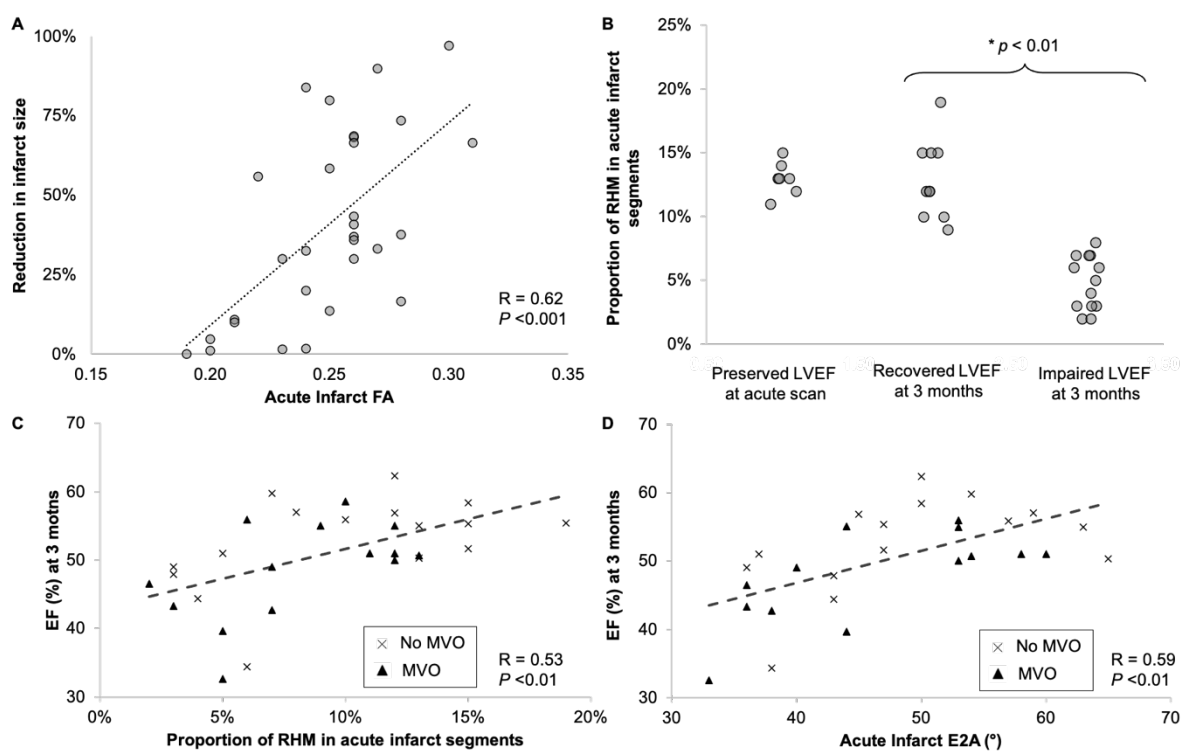
Figure 4.7: Correlation between acute DT-CMR markers, 3-month infarct size and 3-month LVEF

Patients with lower FA in the infarct regions had significantly less change in their infarct size between the acute and 3-month scans (panel A). Patients with impaired LVEF at 3 months had significantly lower proportions of RHM in their infarct segments in their acute scans (panel B). Lower proportions of RHM (Panel C) and segmental E2A (Panel D) in acute infarct segments correlated with lower LVEF% at 3 months.

Table 4.3: CMR characteristics of patients with different LVEF outcomes at 3 months

	Group 1 Preserved LVEF at acute scan	Group 2 Recovered LVEF at 3 months	Group 3 Impaired LVEF at 3 months	ANOVA *P* Value
(n)	7	10	13	
Acute Scan				
LVEDV (ml)	140 ± 22	149 ± 28	152 ± 34	0.653
LVEF (%)	53 ± 2	44 ± 3	41 ± 5	0.002
Infarct Size (g)	7 ± 6	11 ± 6	15 ± 9	<0.001
MVO (g)	0	0.12 ± 0.38	1.1 ± 1.5	0.012
Infarct T1 (ms)	1380 ± 136	1468 ± 101	1532 ± 84	0.049
Infarct ECV (%)	48 ± 7	54 ± 11	54 ± 5	0.034
Infarct MD ($\times 10^{-3}$ mm^2/s)	1.69 ± 0.05	1.66 ± 0.07	1.75 ± 0.1	0.022
Infarct FA	0.27 ± 0.03	0.26 ± 0.02	0.23 ± 0.03	0.004
Infarct E2A (°)	56 ± 9	52 ± 7	40 ± 5	0.005
Infarct RHM (%)	12 ± 2	11 ± 3	4 ± 2	<0.001
3 Month Scan				
LVEDV (mls)	135 ± 22	158 ± 34	171 ± 41	0.074
LVEF (%)	55 ± 4	56 ± 3	43 ± 5	<0.001
Infarct Size (g)	3.6 ± 6	6.4 ± 4	11.4 ± 7	<0.001
Infarct T1 (ms)	1363 ± 96	1395 ± 62	1442 ± 88	0.240
Infarct ECV (%)	58 ± 12	54 ± 19	64 ± 12	0.945
Infarct MD ($\times 10^{-3}$ mm^2/s)	1.78 ± 0.17	1.81 ± 0.12	1.88 ± 0.14	0.336
Infarct FA	0.23 ± 0.04	0.22 ± 0.03	0.21 ± 0.02	0.587
Infarct E2A (°)	48 ± 7	50 ± 6	39 ± 8	0.007
Infarct RHM (%)	15 ± 6	16 ± 6	5 ± 2	0.009

Table 4.4: Predictors of decreased EF: univariate and multivariate regression analysis

Cardiac MRI characteristics at acute scan	Ejection fraction at follow up			
	Univariate		Multivariate	
	r	P Value	β	P Value
LVEF (%)	0.49	0.006	-0.14	0.582
Infarct size (g)	-0.50	0.005	-0.18	0.464
MVO size (g)	-0.42	0.020	-0.07	0.698
Infarct T1 (ms)	-0.39	0.079	-	-
Infarct T2 (ms)	0.26	0.339	-	-
Infarct ECV (%)	-0.47	0.022	-0.18	0.334
Infarct MD ($\times 10^{-3}$ mm^2/s)	-0.05	0.411	-	-
Infarct FA	0.68	<0.001	0.56	0.008
Infarct E2A (°)	0.59	<0.001	0.18	0.391
Infarct RHM %	0.53	<0.001	0.23	0.284
Infarct CM %	0.20	0.294	-	-
Infarct LHM %	0.42	0.210	-	-

Variables are taken from the acute scan. Multivariable standardized regression coefficient (β) and p values are shown where the variable was included in the multivariable analysis.

4.4 Discussion

DT-CMR offers unique insights into in-vivo microstructural changes following STEMI. The main findings from this study are:

1) Myocardial sheetlets in acutely infarcted myocardium are unable to adopt their usual steep orientations in systole as suggested by low E2A values ($E2A_{remote}$=55±9°, $E2A_{infarct}$=49±10°, p<0.001)

2) The reduction of RHM on HA maps is likely reflective of a loss of organisation amongst subendocardial myocytes (RHM_{remote}=16±6%, $RHM_{infarct}$=9±5%, p<0.001). (110)

3) Meanwhile longitudinal changes in MD and FA suggest diffusion becomes more unrestricted and isotropic ($MD_{infarct}$=1.83±0.21x14^{-3}mm^2/s, $FA_{infarct}$=0.22±0.03), eigenvector related parameters like E2A and HA proportions do not change longitudinally, suggesting the axes of microstructural organisation remain relatively fixed post-injury

4) Acute FA (r = 0.68, p<0.001), E2A (r = 0.59, p<0.001) and RHM (r = 0.53, p<0.001) within infarct segments all correlate with LVEF at 3 months and following multivariate regression analysis, having lower FA values within acutely infarcted myocardium was independently predictive of poor LVEF% recovery (standardised β 0.57, p=0.008). These findings help elucidate the microstructural effects of acute MI and may provide novel acute biomarkers for risk stratification.

Congruent with the theory of the ischemic wave-front phenomenon (111), large circumferentially oriented collagen fibers deposit first in the damaged subendocardium.(110) Wu et al demonstrated significant reductions of RHM in infarct segments 26 days post MI.(65) Our results demonstrate this reduction can be detected in as early as 5 days, but this could be reflective of a combination of factors including: a) discontinuity in myocyte trajectory due to ischemic loss of subendocardial myocardium with deposition of collagen fibers more circumferentially oriented;(112) b) possible reorientation of cardiomyocytes due to the deforming effect of adjacent non-

infarcted myocardium in the longitudinal and radial directions.(110) Our results are corroborated by findings of concomitant reduced E2A in segments with reduced RHM, suggesting that disruption of the subendocardial myocyte organisation impacts on the ability of the myocardial sheetlets to adopt their usual steep orientations in systole.(69,110) This is particularly apparent in segments with MVO. Meanwhile, patients with higher RHM% and E2A values in their acute infarct segments had higher LVEF% at 3 months.

In a recent study, Moulin et al demonstrated the superior diagnostic ability of MD maps in depicting acute myocardial oedema compared with T1 and T2 maps, (86) indicating that interstitial oedema contributes substantially to the acute changes in MD following ischaemic injury. This however makes it highly challenging to ascertain how much irreversible injury has occurred from MD alone in the presence of oedema. FA values reflect the anisotropy of diffusion and studies have shown FA values to correlate negatively with histological measurements of collagen, a major component of fibrotic tissue.(87) In the early stages post-MI, reductions in FA within infarct segments could be representative of oedema and the accumulation of spherical inflammatory cells such as swollen myocytes and myofibroblasts; as shown in previous histology studies.(83,85) As the oedema settles over time and necrotic myocytes are replaced by collagen fibers, the further longitudinal reductions in FA in our results are likely reflective of the deposition of collagen and the disarray of fibers. (87,110) Longitudinal changes in MD and FA in our results correlate with the increase in ECV and highlight the dynamic nature of changes taking place within infarct zones. Despite this serial change over 3 months, patients with lower infarct FA values in the acute scan had significantly less change in infarct size over time and worse LV function at 3 months. Hence unlike MD, FA is potentially capable of detecting irreversible injury even in the acute stages in the presence of oedema.

It is worth noting that in patients with MVO, MD was noted to be lower, and FA was higher within the MVO core than surrounding infarcted myocardium. The exact mechanisms are not clear and requires further investigation but demonstrates a potential flaw in obtaining averaged global/segmental measurements of MD and FA.

Eigenvector-related biomarkers like HA and E2A did not demonstrate this paradoxical behaviour within MVO. E2A and RHM values also changed very little between the 2 scans, suggesting that changes to the axes of microstructural components can be detected in the acute stages of MI and remain relatively fixed. Hence maybe better suited for predicting LV remodelling. This presents a potential clinical utility of DT-CMR in the realms of acute imaging post MI; however, a more comprehensive understanding is still required regarding the effects of oedema, MVO and IMH on DT-CMR parameters.

4.4.1 Limitations

Recruiting patients following STEMI for complex acute and longitudinal imaging is challenging and the study sample size is therefore relatively small, but in keeping with similar studies. (65) Conclusions drawn from this study are based on correlations with published evidence and other cardiac MRI markers, whereas validation with histological specimens would be preferable. By allowing for non-contrast and free-breathing acquisitions, DT-CMR SE offers some practical benefits in the context of acute imaging post-STEMI; however, acquisition was limited to only 3 slices and technical developments are needed to allow full LV coverage in shorter scan times. Post-processing can be labour-intensive and clinical implementation requires further optimisation, particularly with tractography postprocessing for accurate definition of HA variation across the myocardium and scar borders.(79)

4.5 Conclusions

Through this study we demonstrate the unique capabilities of DT-CMR in assessing microstructural changes following STEMI. In summary, infarcted myocardium, depending on severity, typically has raised MD, low FA, low E2A and RHM compared to remote. Within areas of MVO however, a paradoxical decrease in MD and a paradoxical rise in FA (with respect to surrounding infarcted myocardium) was noted. The relevance of this is further investigated in more detail in the following chapter. HA and E2A maps were able to detect early changes to the axes of microstructural

components which remained fixed over time and correlated with LVEF at 3 months. Furthermore, low FA values in acutely infarcted myocardium was independently predictive of poor LVEF recovery. All three parameters therefore could be potential predictive biomarkers for adverse LV remodelling; however, further studies involving more subjects and longer follow up will be required to demonstrate this.

Chapter 5: Depiction of intramyocardial haemorrhage in patients following ST-elevation myocardial infarction using diffusion tensor cardiac magnetic resonance imaging

Short title: Depiction of IMH using DT-CMR

5.1 Introduction

Despite recent advancements in PPCI, up to 50% of patients have evidence of MVO following reperfusion, which is associated with worse prognosis. (113) Reperfusion of severely ischaemic myocardium can lead to intramyocardial haemorrhage within areas of MVO by extravasation of red blood cells through damaged endothelial walls. The paramagnetic properties and magnetic susceptibility effects of hemosiderin – a breakdown product of red blood cells – can shorten T2 and T2* relaxation times on cardiac magnetic resonance (CMR) imaging. (114) Therefore on T2-weighted (T2W) imaging, IMH is typically characterised as hypointense regions surrounded by oedema (bright signal). This has been corroborated with histology, (115) and regions with relaxation times less than 20ms on T2* maps indicate the presence of iron. (105) Acute IMH and the presence of residual iron in chronic infarct segments following STEMI are associated with increased risk of adverse LV remodelling and ventricular arrhythmia. (114,116) Diffusion weighted imaging (DWI) is intrinsically T2 weighted, thus the obtained images are also susceptible to the paramagnetic properties of methaemoglobin.

5.1.1 Hypothesis and aims

In DWI of the brain, previous studies have shown iron deposition to have a significant impact on regional MD and FA values; (117) so we hypothesized that DT-CMR could also depict areas of IMH and residual iron in the heart following STEMI.

5.2 Methods

Fifty patients were prospectively recruited following their 'first-event' STEMI. See chapter 3 for full details regarding subject recruitment, image acquisition, image analysis and statistical analysis.

5.3 Results

5.3.1 Baseline results from acute scan

The study flowchart is shown in Figure 5.1. Baseline characteristics are shown in Table 5.1. Fifty patients underwent the acute scan, in which the mean LVEF was $43\pm9\%$ and the mean infarct size was 15 ± 11g. The mean pain-to-balloon time was 246 ± 188 mins and 45/50 patients (90%) had thrombolysis in myocardial infarction (TIMI) flow of 0 on arrival. MD was significantly higher in infarct zones compared to remote (MD $_{remote}$ = 1.48 ± 0.07 x10^{-3}mm^2/s, MD $_{infarct}$ = 1.72 ± 0.14 x10^{-3}mm^2/s, p <0.001) and FA was significantly lower in infarct zones compared to remote (FA $_{remote}$ = 0.36 ± 0.04, FA $_{infarct}$ = 0.25 ± 0.04, p<0.001). Representative maps are shown in Figure 5.2.
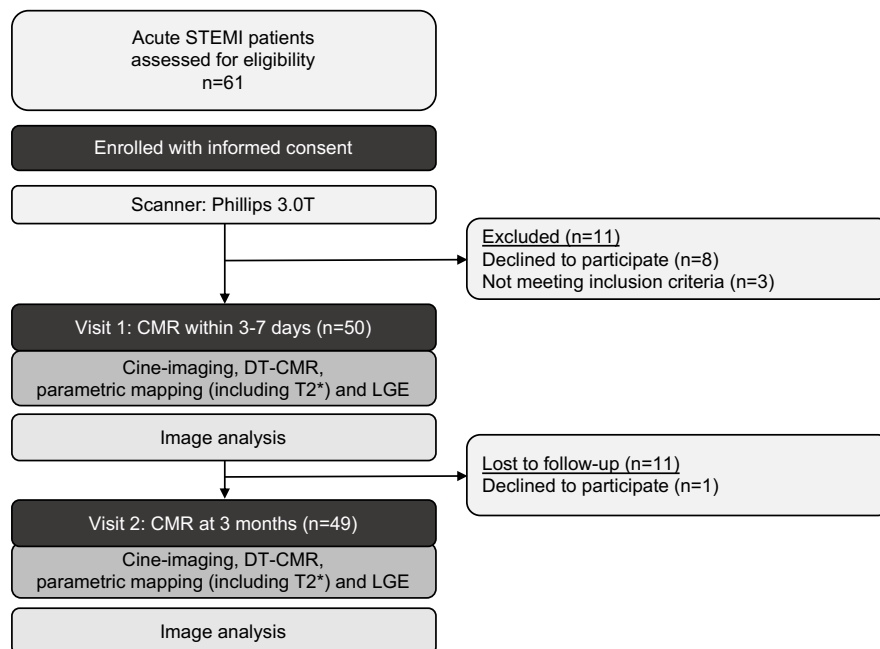
Figure 5.1: Flow chart of study enrolment

	MVO at acute scan (n=25)	No MVO at acute scan (n=25)	P value
Demographics			
Age	60 ± 11	60 ± 10	0.96
Male	22 (88)	18 (72)	0.94
BSA (m^2)	1.9 ± 0.2	2.0 ± 0.1	0.47
Current Smoker	6 (24)	9 (36)	0.90
Diabetes Mellitus	2 (8)	2 (8)	1.00
Hypertension	8 (32)	5 (20)	0.85
Family History	10 (40)	10 (44)	1.00
Infarct Characteristics			
Pain to balloon time (mins)	252 ± 169	240 ± 207	0.86
TIMI flow pre-PCI	0.0 ± 0.0	0.4 ± 0.9	0.03
TIMI flow post-PCI	2.9 ± 0.3	3.0 ± 0.0	0.16
Culprit Artery			
Left Anterior Descending Artery	12 (48)	6 (24)	0.57
Left Circumflex Artery	5 (20)	4 (16)	0.99
Right Coronary Artery	8 (32)	14 (68)	0.65
CMR Measurements			
LVEDV index (ml/m^2)			
Acute scan	83 ± 22	77 ± 17	0.17
3-month scan	92 ± 30 *	75 ± 14	0.03
LVEF (%)			
Acute scan	37 ± 8	48 ± 6	<0.001
3-month scan	42 ± 11 *	54 ± 5	<0.001
Infarct mass (g)			
Acute scan	21 ± 11	8 ± 6	<0.001
3-month scan	15 ± 10 *	5 ± 4	<0.001
MVO			
Mass at acute scan (g)	3.8 ± 4.9	-	-
Persistent at 3-month scan	0 (0) *	-	-
Size at 3-month scan (g)	-	-	-
T2* mapping			
Presence of IMH at acute scan	24 (96)	0 (0)	<0.001
T2* relaxation time within IMH at acute scan (ms)	11.7 ± 3.7	-	-
Area of IMH at acute scan (cm^2)	1.89 ± 0.96	-	-
Persistent at 3-month scan	22 (96) *	0 (0)	<0.001
Diffusion Tensor Imaging			
Acute Scan			
Remote MD (x10^{-3}mm^2/s)	1.50 ± 0.06	1.45 ± 0.08	0.03
Infarct MD (x10^{-3}mm^2/s)	1.75 ± 0.16	1.69 ± 0.11	0.09
Remote FA	0.35 ± 0.03	0.37 ± 0.04	0.11
Infarct FA	0.23 ± 0.03	0.26 ± 0.04	<0.01
Hypointense signal within infarct	25 (100)	0 (0)	<0.001
Area of hypointense signal (cm^2)	2.02 ± 1.0	-	-

MD within hypointense signal (x10^{-3}mm^2/s)	1.29 ± 0.20	-	-
FA within hypointense signal	0.40 ± 0.07	-	-
3 Month Scan			
Persistence of hypointense signal within infarct at 3 months	23 (100) *	-	-
Remote MD at 3 months	1.47 ± 0.08 *	1.46 ± 0.06	0.51
Remote FA at 3 months	0.34 ± 0.03 *	0.35 ± 0.03	0.60
Infarct MD at 3 months	1.86 ± 0.14 *	1.76 ± 0.13	0.02
Infarct FA at 3 months	0.22 ± 0.03 *	0.23 ± .04	0.23
Native T1 Mapping			
Acute Scan			
Remote T1 at acute scan (ms)	1232 ± 48	1178 ± 45	<0.001
Infarct T1 at acute scan (ms)	1486 ± 72	1476 ± 135	0.77
T1 within IMH at acute scan (ms)	1253 ± 143	-	-
Cases with reduced T1 within IMH (n, %)	8 (32%)	-	-
3 Month Scan			
Remote T1 at 3 months (ms)	1231 ± 41 *	1149 ± 101	<0.001
Infarct T1 at 3 months (ms)	1439 ± 72 *	1348 ± 89	<0.001
T1 within area of IMH at 3 months (ms)	1348 ± 194 *	-	-
Cases with reduced T1 within IMH (n, %)	0 (0%) *	-	-
T2 Mapping			
Acute Scan			
Remote T2 at acute scan (ms)	48 ± 7	50 ± 6	0.60
Infarct T2 at acute scan (ms)	57 ± 7	51 ± 6	0.11
T2 within IMH at acute scan (ms)	48 ± 12	-	-
Cases with reduced T2 within IMH (n, %)	16 (65%)	-	-
3 Month Scan			
Remote T2 at 3 months (ms)	49 ± 5 *	48 ± 5	0.44
Infarct T2 at 3 months (ms)	55 ± 6 *	48 ± 5	0.03
T2 within area of IMH at 3 months (ms)	53 ± 8 *	-	-
Cases with reduced T2 within IMH (n, %)	3 (13%) *	-	-

Table 5.1: Results from acute and 3-month scan

*Continuous variables are represented as mean ± SD and categorical variables are represented as n (%). * = Based on 23 patients that returned for 3-month scan. For comparison, segmental MD and FA values of healthy volunteers as previously published are as follows: MD: 1.47±0.08, FA: 0.38±0.03. (91) Departmental 3.0T scanner reference range for native T1 is 1190±50ms.*
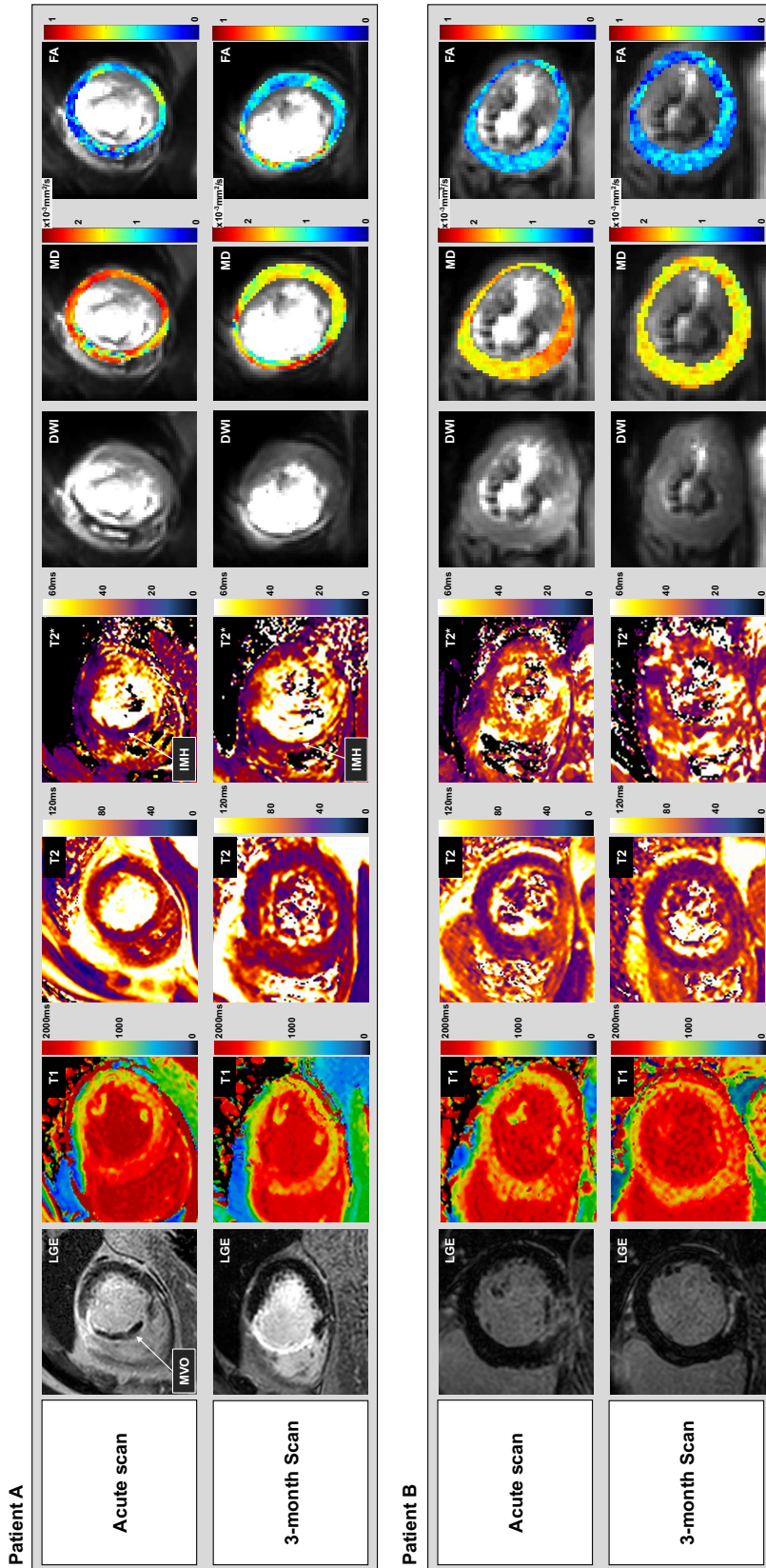
Figure 5.2: Representative maps of 2 separate subjects

Patient A:

Representative maps for a 63-year-old male who presented with anteroseptal STEMI and underwent PPCI to his left anterior descending artery. In his acute scan, LGE image demonstrates extensive transmural infarction of the mid septal wall with MVO. Native T1 and T2 relaxation times are increased in and around areas of infarction with a subtle area of hypointensity within the infarct. This hypointensity is considerably more visually evident on T2* and averaged DWI. T2* within this area is <20ms and is suggestive of the presence of iron from IMH. On MD mapping, values are relatively higher in and around infarction than remote, however within the areas of MVO, MD values are significantly lower. On FA maps, values show the opposite trend as MD. At the 3-month scan for the same patient, LGE shows transmural enhancement of the septal walls. Native T1 and T2 relaxation times remain increased in areas of infarction, suggesting there is on-going inflammation and oedema. There is no longer any visual evidence of MVO, nor any area of low relaxation times on native T1 and T2 maps within the infarct, however on the T2* and averaged DWI, an area of hypointense signal within the infarct is still notable, indicating the presence of residual iron. MD remains decreased, and FA remains increased within these areas of hypointense signal, however in the surrounding infarcted myocardium, MD remains increased, and FA remains decreased in comparison to remote myocardium.

Patient B:

Representative maps of a 67-year-old male who presented with inferior STEMI and PPCI to his right coronary artery. In his acute scan, LGE image demonstrates hyperenhancement of the mid inferior wall with no evidence of MVO. Native T1 and T2 maps demonstrate hyperintense signals in and around areas of infarction, however in comparison to patient A, there is no area of hypointense signal on native T1, T2, T2* maps or averaged DWI. At 3 months, in the area of infarction, native T1 remains increased, however T2 relaxation times have decreased, signifying the resolution of oedema. There is still no area of hypointense signal on T2* and averaged DWI. MD has decreased in and around the areas of infarction, while there has been no notable serial change in FA.

Twenty-five patients (50%) had evidence of MVO on LGE images. In this subgroup, on T2* mapping, 24 had evidence of IMH within their MVO (mean area 1.89 ± 0.96 cm^2, mean T2* relaxation time 11.7 ± 3.7ms). The one outstanding patient did have a hypointense region within the infarct on T2* mapping but the relaxation time of this area was 22ms, just over the range for IMH. On averaged DW images, all 25 MVO patients had an area of hypointense signal within their MVO which coalesced with the areas of IMH detected on T2* maps. The mean area of hypointense signal within infarct measured using averaged DW images (2.02 ± 1.0 cm^2) was non-significantly greater than that detected by T2* mapping (1.89 ± 0.96cm^2, p=0.69). In the remaining 25 patients with no MVO on LGE, none had evidence of IMH on T2* mapping, none had areas of hypointense signal within their infarcted myocardium on averaged DW images, and none had areas of reduced relaxation times within their infarcts on native T1, T2 maps.

5.3.2 Differences between patients with and without MVO and IMH on acute scan

In the acute scan, patients with MVO/IMH had tended to have higher MD in their infarct myocardium surrounding the MVO than patients without MVO although the difference was not statistically significant (1.75 ± 0.16 vs 1.69±0.11 x$10^{-3}$$mm^2$/s, p=0.09). Patients with MVO/IMH had significantly lower FA in their infarct regions surrounding MVO than in infarct segments of patients without MVO (0.23±0.03 vs 0.26±0.04, p<0.01). In the acute scan, there was no significant difference in native T1 and T2 in infarct segments between patients with and without MVO/IMH. (Table 5.1)

5.3.3 Regional DT-CMR changes within areas of IMH

As mentioned above, areas of IMH on T2* maps coalesced with hypointense regions on averaged DW images. MD was significantly reduced within these hypointense regions in comparison with surrounding infarcted myocardium (1.29±0.2 x$10^{-3}$$mm^2$/s vs 1.75±0.16 x$10^{-3}$$mm^2$/s, p<0.001), while FA was significantly increased within these

hypointense regions in comparison with surrounding infarcted myocardium (0.40±0.07 vs 0.23±0.03, p<0.001) as shown in Figure 5.3.
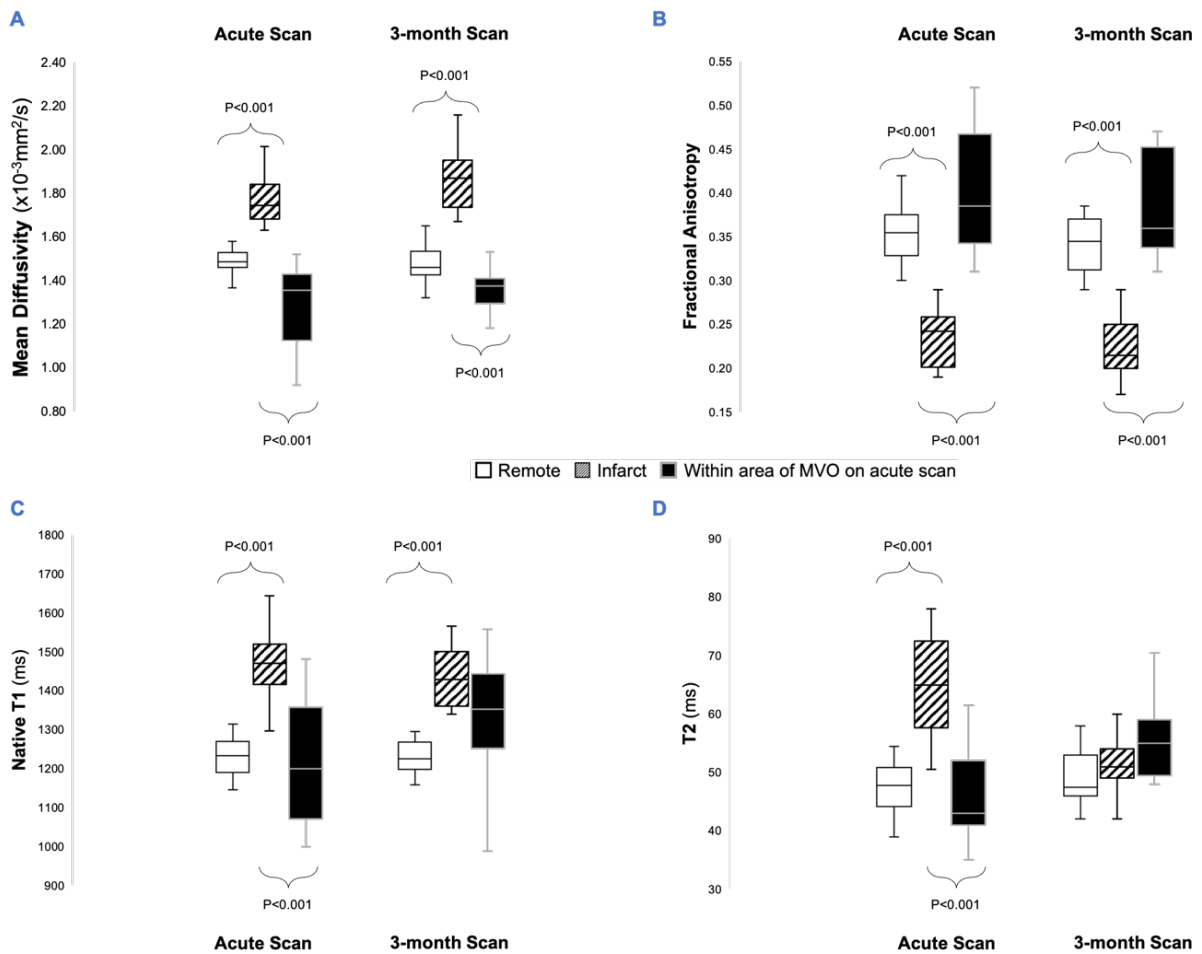
Figure 5.3: Regional variance MD, FA, native T1 and T2

In patients with MVO during the acute scan; MD, native T1 and T2 were all higher in the infarct myocardium than remote, but significantly lower within the area of MVO compared to surrounding myocardium. By 3-months, this phenomenon persists with MD despite the visual absence of MVO on LGE images. Meanwhile FA shows the opposite trend; FA within MVO was significantly higher than surrounding infarcted myocardium in the acute scan, and this phenomenon also persisted at 3 months. On native T1 and T2 maps at 3-months, there is no longer a significant difference in relaxation times between infarcted myocardium and areas where there had been MVO on the acute scan.

5.3.4 Results from 3-month scan

Forty-eight patients returned for their 3-months scan, at which point the mean LVEF had significantly improved to 48±10% (p<0.01), and the mean infarct size had significantly reduced to 10±10g (p<0.03) across the entire cohort. Out of the 25 patients with MVO/IMH on the acute scan, 23 returned for their 3-month scan. Whilst none of the patients had visual evidence of MVO on LGE images; on averaged DWI images, all 23 patients still had an area of hypointense signal within their infarct. T2* maps detected the presence of iron in 22 out of these 23 patients (96%) within these areas of hypointense signal. T2* had significantly increased between acute and 3-month scan within these areas ($T2^*_{acute}$ = 11.7±3.7ms, $T2^*_{3\text{-months}}$ = 15.2±3.8ms, p<0.01), but there were no significant serial changes in MD or FA values. (Figure 5.3)

5.3.5 Differences between patients with and without iron at 3-months

Patients with evidence of persistent iron on T2* maps had significantly higher MD, native T1 and T2 relaxation times in their infarct myocardium than patients without persistent iron (MD: 1.86±0.14 vs 1.76±0.13x10^{-3}mm^2/s, p=0.02, native T1: 1486±72ms vs 1348±89ms, p<0.001, T2: 55±6ms vs 48±5ms, p=0.03). In addition, patients with persistent iron also had significantly higher native T1 in their remote segments at 3 months than patients without persistent iron (1231±41ms vs 1140±101ms, p<0.001).

5.3.6 Comparison of sequences for the detection of iron

Using T2* mapping as the reference standard, the sensitivity and specificity of different sequences (native T1, T2 and DWI) for the detection of IMH were compared, the results are shown in Table 5.2. Across the 100 studies (50 acute and 48 follow-up scans), there was evidence of IMH in 48 cases on T2* mapping. Using the criteria defined in methods (chapter 3.4), DWI detected IMH in all 48 cases, and detected 2 false negatives. Meanwhile native T1 correctly detected IMH in 30 patients, and T2 in 33 patients.

	Sensitivity	Specificity
Acute scans (n=50)		
Native T1	40%	92%
T2	52%	92%
DWI	100%	96%
Chronic scans (n=48)		
Native T1	22%	91%
T2	17%	96%
DWI	100%	96%

Table 5.2: Diagnostic accuracy of various sequences for detecting IMH

Using T2* mapping as the reference standard, DWI had superior sensitivity and specificity for the detection of IMH both at the acute and chronic scan than native T1 and T2 mapping.

Patients with hypointense signals within their infarct on their averaged DW images during the acute scan experienced significantly greater increase in LVEDV by 3 months compared to patients without (19% vs 2%, $p < 0.001$). (Figure 5.4)
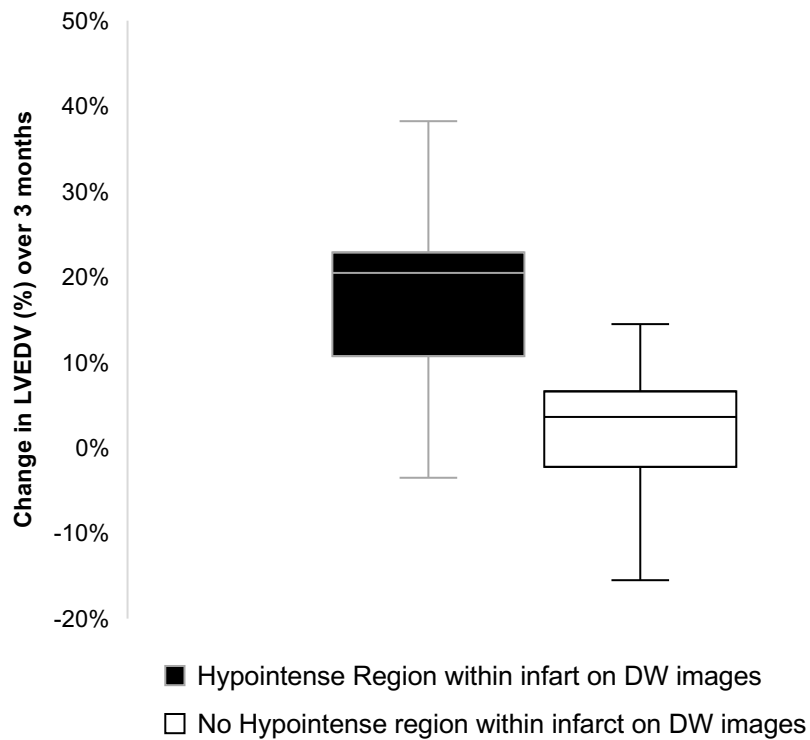
Figure 5.4: Change in LVEDV over 3-months

On averaged diffusion weighted images, patients who had an area of hypointense signal within their infarct experienced significantly greater increase in LVEDV over 3 months than patients who did not (19% vs 2%, p<0.001).

5.3.7 Effects of SNR on DT-CMR parameters

To assess the potential effects of SNR on the DT-CMR parameters, data in two example patients were further analysed by performing DT-CMR analysis, as described in chapter 3, based on subsets of data that include all 18 diffusion-weighting directions and b-values, and up to the first n repetitions, where $1 \leq n \leq 12$ and $n = 12$ was the full dataset described in Results. Figure 5.5 shows MD and FA in manually drawn ROIs in remote myocardium and MVO. The results show a positive bias in FA as the cumulative repetitions and hence SNR decreases, particularly at low n. At higher n, the bias in $FA_{n=6}$ relative to $FA_{n=12}$ averaged across both patients was +17% in remote myocardium and 8% in MVO. $MD_{n=6}$ relative to $MD_{n=12}$ was -2% and +2% in remote myocardium and MVO respectively. In both MD and FA, the heterogeneity across ROIs increased with lower n.

These results are consistent with previous reports describing SNR dependence in DT-CMR. (118–120) With further increases to SNR or cumulative repetitions beyond $n = 12$, further changes to MD and FA would be expected to decrease. We conclude that whilst SNR does influence DT-CMR measurements, this does not account for the +74% higher FA seen in MVO compared to infarct regions.
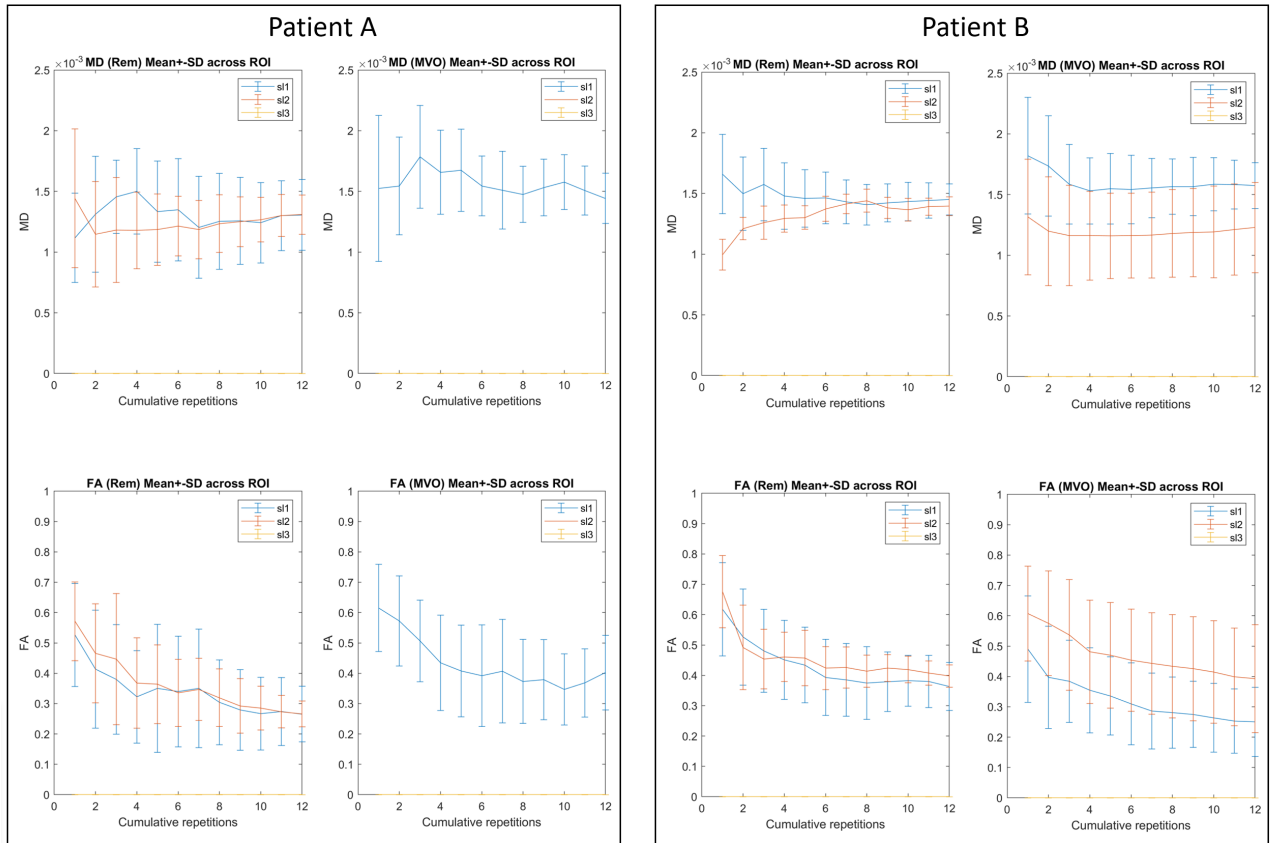
Figure 5.5: Effect of SNR on MD and FA

MD and FA reconstructed from subsets of data including the first 1 to 12 cumulative repetitions (mean SD ± across ROI). Data shown in two example patients, in slices where ROIs are available.

5.4 Discussion

In this prospective study, using T2* as the gold standard, we compare the capabilities of parametric mapping and DT-CMR at detecting IMH in patients at 1-week and 3-months post-STEMI. Our results demonstrate:

1) Averaged DW images to have excellent sensitivity (100%) and specificity (96%) for the detection of IMH on acute CMR, and residual iron at 3-months, with superior diagnostic accuracy than parametric mapping sequences
2) Persistence of iron at 3-months detected by DWI is associated with enlargement of EDV, as well as increased T1 relaxation times in remote segments

In the acute scans, all patients with evidence of IMH on T2* mapping had areas of hypointense signals within their infarct on averaged DW images. In the one subject with a 'false positive' detection of IMH on averaged DW images, T2* was only marginally outside the category for IMH, indicating that there may have been a degree of underlying haemorrhage, but there is no histology to validate this. By 3 months, all patients with acute MVO had lost the visual appearance of MVO on LGE, however on averaged DWI images, there remained areas of hypointense signal within the infarct of all these patients. T2* relaxation times were significantly decreased in these areas (<20ms) in most of these patients (96%), indicating the presence of residual iron. Therefore, our findings suggest that on averaged DW images, the presence of hypointense signal within chronic infarct segments is strongly suggestive of residual iron and is a marker of severe ischaemic injury in the past.

Previous authors have reported that the deposition of crystalised iron in the myocardium carries a pro-inflammatory burden, hence myocardial segments with IMH can remain inflamed for up to 6 months, which in itself is associated with adverse long-term adverse outcomes including LV remodelling. (17,20,116,121–123) In keeping with this, patients in our study with residual iron at 3-months also had significantly higher MD, native T1 and T2 relaxation times in their infarct regions than patients without residual iron, signifying on-going inflammation. These patients also experienced a significantly greater increase in their LVEDV over the 3 months than

patients without residual iron. Furthermore, they had significantly higher native T1 relaxation times in their remote segments. Carrick et al previously observed that LVs which went on to remodel following STEMI had significantly higher native T1 in their remote myocardium during their acute scans and attributed this to a combination of oedema and hypercellularity. The authors also reported patients with reperfusion injury had higher remote T1. (124) Our results corroborate this finding, both on acute and follow-up scans, but without histology, it is difficult to establish if this increased remote T1 is reflective of diffuse interstitial fibrosis, or adaptive hypercellularity from increased wall stress. Nonetheless, the ability to detect the presence of iron at both an acute and chronic stage following STEMI underlines a prognostically relevant, clinical utility of DT-CMR.

In keeping with findings from DWI of the brain, (117) our results also show a decrease in estimated MD and an increase in estimated FA in areas of haemorrhage and residual iron. The underlying mechanisms are thought to relate to the MR signal dephasing form magnetic inhomogeneities induced by local iron deposition. As a paramagnetic substance, hemosiderin causes variations in magnetic susceptibility on a microscopic scale, and this impacts the strength of the effective diffusion gradient. Areas of MVO and IMH will also contain blood with greater proportion of deoxyhaemoglobin, which (being more paramagnetic than oxyhaemoglobin) will also contribute to local MR signal dephasing through the blood oxygen level dependent (BOLD) effect mechanism. (125) Interactions between the local gradients induced by iron oxide particles and the applied diffusion-weighting gradients have the net effect of increasing the diffusion-weighted signal, and reducing the apparent diffusivity. (126) Furthermore, shorter T2 within the MVO reduces SNR and could result in an overestimation of the primary eigenvalue and an underestimation of tertiary eigenvalue due to eigenvalue repulsion. (118,127) This may contribute to an overestimation of FA but is unlikely to be the sole factor, as demonstrated by the SNR simulation experiments in this study.

This finding has important implications; the influence of local iron deposition on diffusion measurements must be taken into consideration in the interpretation of diffusion data. When undertaking global and segmental analysis, the presence of iron

can affect the overall average MD and FA. The use of ROI analysis approach can overcome this limitation, and we recommend this method for more accurate estimation of MD and FA in cases where iron maybe present. The regional effect of iron on other DT-CMR parameters such as helix angle and secondary eigenvectors remain unclear and requires further investigation.

In conventional CMR, spin echo sequences generally produce better image quality than gradient echo sequences. However, owing to the longer relaxation times required, gradient echo sequences are more sensitive to the presence of magnetic field inhomogeneities from iron, and hence are better suited for T2* mapping. In DT-CMR, the application of diffusion encoding gradients seemingly makes spin echo more susceptible to the paramagnetic properties of iron due to the reasons discussed above, hence when comparing with native T1 and T2 mapping, DT-CMR had better sensitivity and specificity for the detection of iron in our results. In order to compare the diagnostic accuracy of DT-CMR with T2* mapping, histological analysis would be required as the gold standard, which is not easily feasible in patients following STEMI but could be considered in animal studies. Given the excellent agreement between DT-CMR and T2* for detecting IMH, as demonstrated in these results, it would be reasonable for clinicians to rely on DT-CMR for IMH detection for the time-being; and unlike T2* imaging, DT-CMR provides an abundance of information about the myocardial microstructure, making it a more versatile sequence. (86,128)

5.4.1 Limitations

Conclusions drawn from this study are based on correlations with published evidence and other cardiac MRI markers, whereas validation with histological specimens would be preferable.

5.5 Conclusion

DT-CMR has already been shown to be capable of characterising acute changes in myocardial microstructure following STEMI. In this chapter, we highlight that on averaged diffusion weighted images, the presence of hypointense signal within infarcted myocardium is suggestive of intramyocardial iron. Compared with native T1

and T2 maps, averaged DW images provide superior contrast for the detection of intramyocardial iron, however DT-CMR parameters such as MD and FA are affected by the paramagnetic susceptibility effects of iron, hence caution is required in the interpretation of DT-CMR data in segments where iron may be present.

Chapter 6: Assessment of microstructural changes in long-term adverse remodelling following ST-elevation myocardial infarction

Short title: DT-CMR predictors of adverse LV remodelling

6.1 Background

Following myocardial infarction (MI), the sudden reduction of contractility in the left ventricle (LV) leads to an acute increase in loading conditions and triggers adaptive neurohormonal mechanisms. (4) Failure to normalise the increased wall stress results in progressive cavity dilatation and deterioration of contractility, a process known as adverse remodelling, which is associated with reduction in survival. (5) The exact mechanisms underpinning adverse remodelling is incompletely understood.

6.1.1 Hypothesis and aims

In chapter 2, reduced FA, E2A and RHM in acutely infarcted myocardium were all shown to correlate with lower LV ejection fraction (LVEF) at 3-months post-MI. (128) The link between remodelling and DT-CMR parameters has been hypothesized but not demonstrated yet. In this study, the aims were:

1. To measure serial changes in DT-CMR parameters over 3 scans spanning 12 months in patients following STEMI
2. To determine how acute DT-CMR parameters associate with long-term adverse LV remodelling. I hypothesised that markers of severe injury in the acute scan derived using DT-CMR can be predictive of adverse LV remodelling.

6.2 Methods

132 patients were prospectively recruited following their 'first-event' STEMI. See chapter 3 for full details regarding subject recruitment (chapter 3.2.1), image

acquisition (chapter 3.3.1), image analysis (chapter 3.4) and basic statistical analysis methods (3.5). Adverse remodelling was defined as an increase in LV end-diastolic volume indexed for body surface area (LVEDVi) >20% at 12-months from baseline. (124)

Detailed statistics

Paired t-tests were used to compare initial (from acute scan) and repeated measurements (at 3 and 12 months) of DT-CMR and parametric parameters to detect the significance of longitudinal changes in tissue characteristics of remote, adjacent and infarct areas. Pearson correlation analysis was used to calculate the correlation coefficients between CMR biomarkers (including DT-CMR and parametric mapping parameters) and outcomes at 12 months (which includes changes in LVEDVi and LVEF). Univariate analyses were performed to identify predictors of LVEF and change in LVEDVi over 12 months. Only variables with a probability value <0.1 in the univariate analysis were included in a multivariable linear regression analysis. Binary logistic regression models were used to identify associates of adverse remodelling at 12-months, and alongside DT-CMR parameters, only included the best CMR covariates (acute LVEF and infarct size) to reduce the number of analysable parameters with respect to our sample size and improve the statistical robustness of the model. Statistical significance of the differences between ROC curves was assessed using the method of DeLong et al. (106)

6.3 Results

6.3.1 Baseline patient characteristics

The study flowchart is shown in Figure 6.1. 100 patients (M:F 80:20, aged 59±10) completed acute (5±2 days) and 12 month scans (391±73 days). As described in

Table 6.1, 43% presented with anterior STEMI. In acute scans, all patients showed evidence of oedema on T2 maps and infarction on LGE, with a mean infarct size of 22±14% of LV mass. (Table 6.2) By the follow-up 12-month scan, the mean LVEDVi across the cohort had increased from 79±15 to 85±22 ml/m^2 (p=0.015), while the mean

LVEF had improved from 43±9% to 49±9% (p<0.001), as shown in Table 6.3. Representative images including parametric mapping are shown in Figure 6.2.
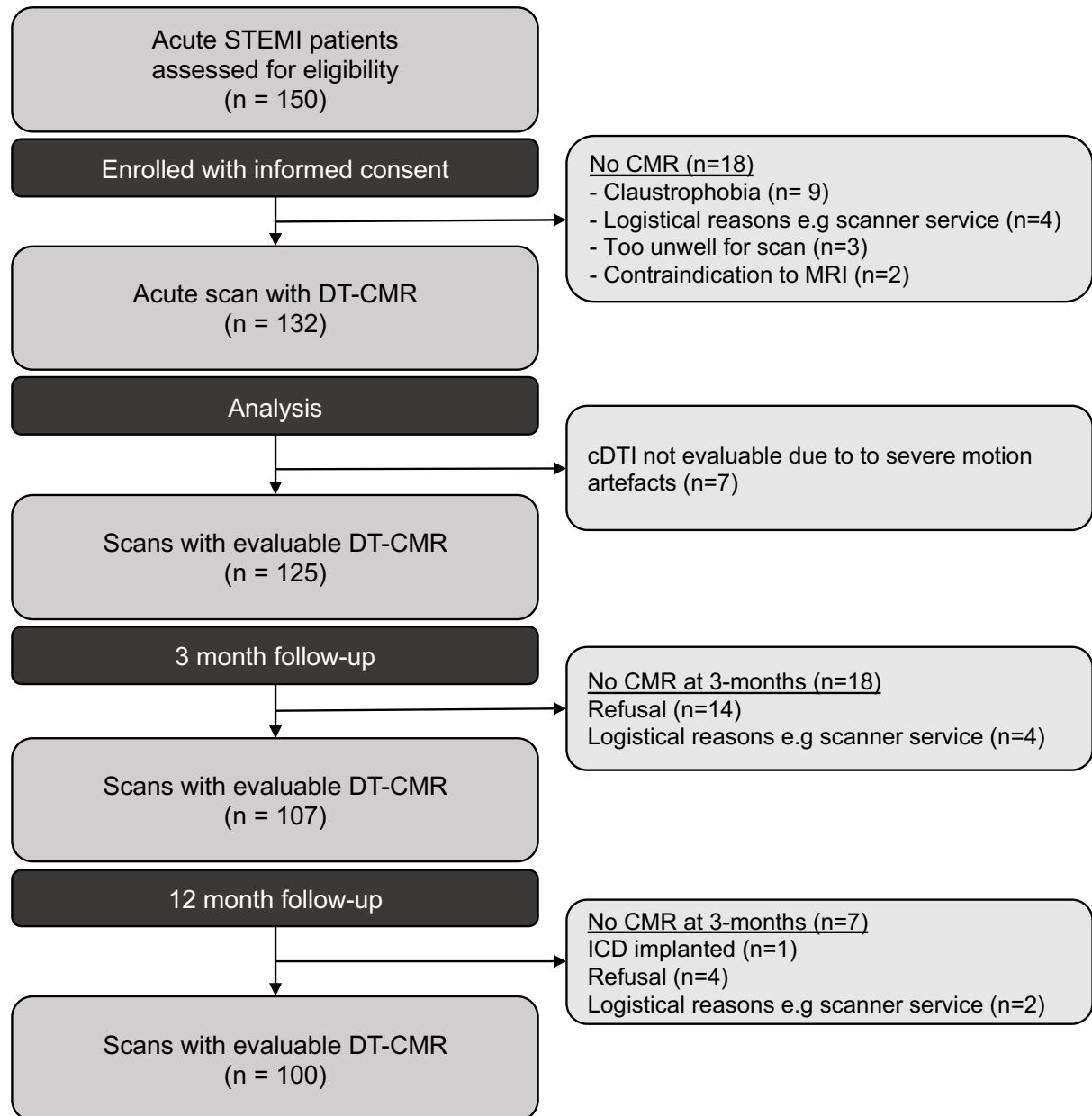
Figure 6.1: Flowchart of study enrolment

Baseline Demographics	All patients (n=100)	No remodelling (n=68)	Adverse remodelling (n=32)	P Value
Age (years)	59±10	59±10	60±11	0.72
Male	80 (80)	54 (79)	26 (81)	0.83
BSA (m^2)	1.94±0.17	1.93±0.18	1.95±0.17	0.67
Hypertension	25 (25)	17 (25)	8 (25)	1.00
Diabetes Mellitus	18 (18)	13 (19)	5 (16)	0.67
Current smoker	27 (27)	19 (27)	8 (25)	0.76
Heart Rate (beats/min)	77±14	76±13	79±14	0.88
Systolic blood pressure (mmHg)	133±53	132±48	135±44	0.76
Diastolic blood pressure (mmHg)	75±12	74±10	76±8	0.92
Presenting characteristics				
Pain to balloon time (mins)	245±170	265±202	213±94	0.25
Culprit Artery:				
Left main stem	0 (0)	0 (0)	0 (0)	1.00
Left anterior descending	43 (43)	27 (40)	16 (50)	0.33
Left circumflex	16 (16)	10 (15)	6 (19)	0.61
Right Coronary	41 (41)	31 (45)	10 (31)	0.17
TIMI coronary flow grade pre-PCI:				
<3	9 (99)	67 (99)	32 (100)	0.68
3	1 (1)	1 (1)	0 (0)	0.49
TIMI coronary flow grade post-PCI:				
<3	3 (3)	0 (0)	3 (9)	0.01
3	97 (97)	68 (100)	29 (91)	0.06
Pharmacological therapy post-MI				
Aspirin	100(100)	68 (100)	32 (100)	1.00
Adenosine diphosphate receptor antagonist	100 (100)	68 (100)	32 (100)	1.00
Ace inhibitor/Angiotensin II receptor blocker	100 (100)	68 (100)	32 (100)	1.00
Beta blocker	97 (97)	66 (97)	31 (97)	0.96

Table 6.1: Baseline Demographics

CMR Findings	Acute Scan			P Value
	All patients (n=100)	No remodelling at 12 months (n=68)	Adverse remodelling at 12 months (n=32)	
LVEF (%)	43±9	46±8	37±9	<0.001
LVEDVi (ml/m^2)	79±15	78±13	82±19	0.950**
Infarct Size (% of LV)	22±14	12±10	27±18	<0.001
Infarct transmurality (%)	76±28	68±29	93±13	<0.001
MVO size (g)	1.4±2.8	0.5±1.6	3.1±4.1	<0.001**
Remote regions:				
Native T1 (ms)	1196±60	1186±62	1217±50	0.015
ECV (%)	27±5	27±5	27±3	0.681
T2 (ms)	48±6	47±6	49±4	0.142
MD (x10^{-3}mm^2/s)	1.47±0.08	1.45±0.08	1.52±0.09	<0.001
FA	0.36±0.04	0.36±0.04	0.35±0.03	0.362**
Absolute E2A (°)	52±9	52±9	52±10	0.975
RHM (%)	24±11	23±12	26±11	0.264**
CM (%)	64±14	65±13	60±15	0.181**
LHM (%)	13±7	12±6	14±8	0.719**
Adjacent regions:				
Native T1 (ms)	1295±71	1285±78	1315±48	0.056
ECV (%)	31±6	32±6	29±4	0.079
T2 (ms)	54±7	53±7	54±8	0.466
MD (x10^{-3}mm^2/s)	1.60±0.10	1.58±10	1.63±0.09	0.088
FA	0.33±0.04	0.33±0.04	0.32±0.03	0.836
Absolute E2A (°)	50±8	51±8	48±6	0.078
RHM (%)	15±7	15±7	14±6	0.447
CM (%)	71±11	72±11	71±10	0.674
LHM (%)	14±6	13±7	15±6	0.234
Infarct regions:				
Native T1 (ms)	1488±111	1471±113	1522±102	0.052
ECV (%)	54±11	53±11	57±10	0.081
T2 (ms)	69±13	67±14	71±11	0.216
Presence of IMH (n,%)	34 (34)	16 (24)	18 (56)	<0.001
MD (x10^{-3}mm^2/s)	1.73±0.12	1.71±0.12	1.78±0.13	0.053
FA	0.26±0.04	0.27±0.04	0.23±0.03	<0.001
Absolute E2A (°)	46±9	51±7	37±6	<0.001
RHM (%)	14±8	17±9	8±5	<0.001**
CM (%)	68±8	67±13	67±12	0.722
LHM (%)	18±10	16±9	20±9	0.168

Table 6.2: CMR results from acute scans

CMR Findings	12-month Follow Up Scan			
	All patients (n=100)	No remodelling at 12 months (n=68)	Adverse remodelling at 12 months (n=32)	P Value
LVEF (%)	49±9	53±7	41±9	<0.001
LVEDVi (ml/m^2)	85±22	78±16	103±24	<0.001
Infarct Size (% of LV)	13±10	9±7	27±22	<0.001
Infarct transmurality (%)	52±32	10±5	65±20	<0.001
MVO size (g)	-	-	-	-
Remote regions:				
Native T1 (ms)	1214±67	1189±55	1270±57	<0.001
ECV (%)	28±4	27±4	31±5	<0.001
T2 (ms)	45±9	44±10	49±6	0.060
MD (x10^{-3}mm^2/s)	1.48±0.06	1.46±0.06	1.51±0.06	0.004
FA	0.34±0.03	0.35±0.04	0.34±0.04	0.318
Absolute E2A (°)	48±7	49±6	46±7	0.022
RHM (%)	21±8	20±8	23±9	0.268
CM (%)	68±11	69±12	65±12	0.166
LHM (%)	11±8	11±9	12±7	0.464
Adjacent regions:				
Native T1 (ms)	1230±52	1214±47	1264±46	<0.001
ECV (%)	28±3	27±3	29±3	<0.001
T2 (ms)	49±5	48±4	50±5	0.111
MD (x10^{-3}mm^2/s)	1.50±0.06	1.49±0.06	1.54±0.05	<0.001
FA	0.34±0.03	0.34±0.03	0.33±0.03	0.054
Absolute E2A (°)	46±8	48±8	45±7	0.192
RHM (%)	17±8	18±9	16±9	0.420
CM (%)	67±13	76±13	74±14	0.348
LHM (%)	6±9	6±14	10±10	0.272
Infarct regions:				
Native T1 (ms)	1380±124	1340±95	1472±117	<0.001
ECV (%)	52±17	48±15	60±12	<0.001
T2 (ms)	50±13	51±7	54±7	0.029
Presence of IMH (n,%)	-	-	-	-
MD (x10^{-3}mm^2/s)	1.70±0.14	1.63±0.11	1.82±0.10	<0.001
FA	0.26±0.04	0.28±0.04	0.23±0.02	<0.001
Absolute E2A (°)	44±10	48±9	36±5	<0.001
RHM (%)	14±8	17±6	6±3	<0.001
CM (%)	68±10	68±10	67±12	0.830
LHM (%)	18±9	14±8	27±11	<0.001

Table 6.3: CMR results from 12-month follow-up scans
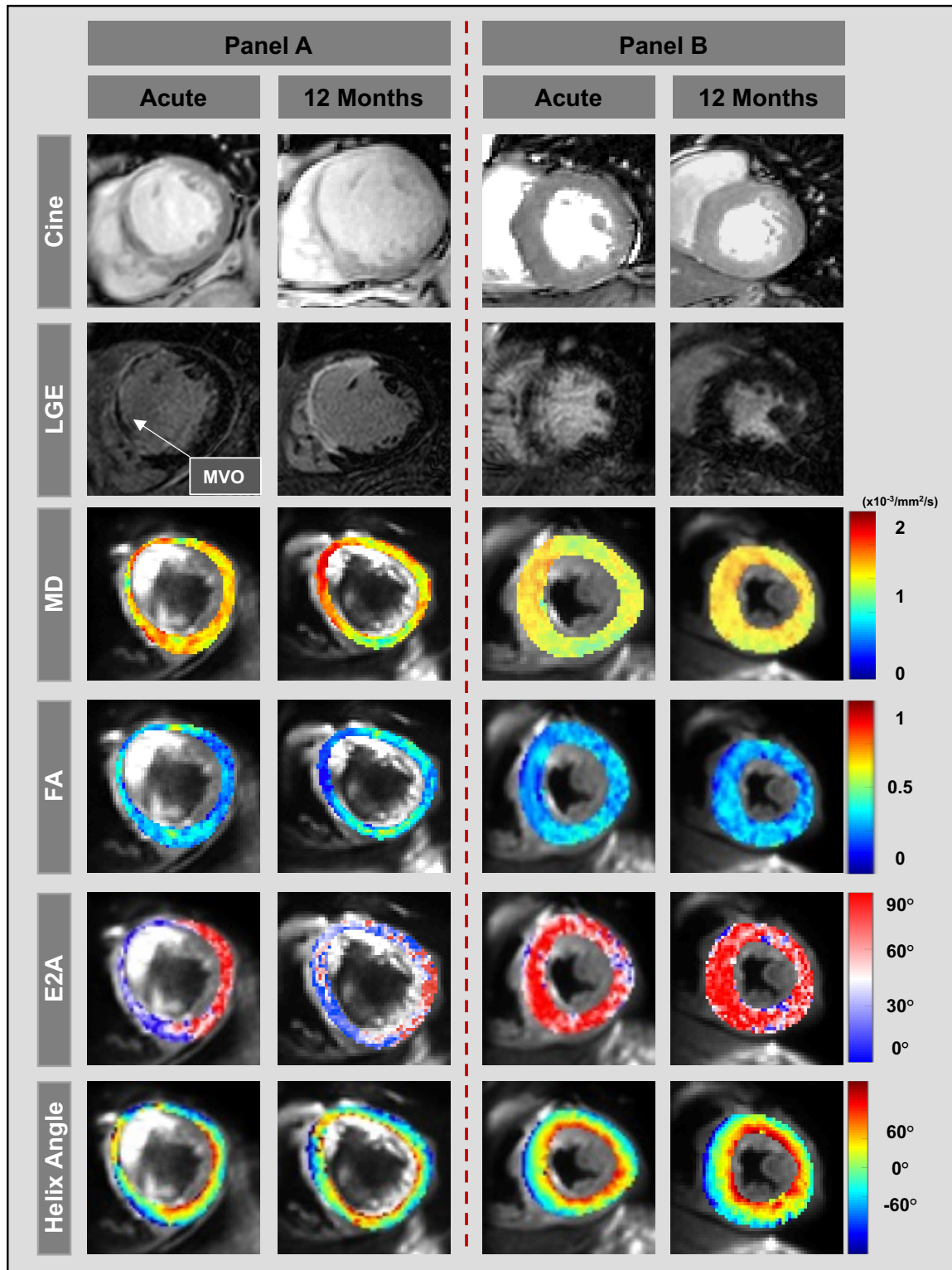
Figure 6.2: Representative CMR images of 2 separate patients

Panel A displays short-axis images obtained from the acute and 12-month scans of a 70-year-old male, who initially presented with anterior ST-elevation and underwent PPCI to the LAD. His acute LVEF remained fixed at 30% at 12 months, but his LVEDV increased from 172mls

to 228mls, fulfilling the criteria for adverse remodelling. In the acute scan, LGE image demonstrates transmural infarction of the basal anterior and septal walls. The corresponding area on diffusion tensor maps show high MD, low FA, low E2A and a reduction of RHM (proportion of red and orange pixels). By 12 months, the anterior and septal walls have thinned and remain transmurally infarcted. MD has increased in areas corresponding to scar, which in the absence of oedema is suggestive of expansion in ECV. FA remains low, indicating underlying collagen deposition and cardiomyocyte disarray. E2A remains low, suggesting the myocardial sheetlets are unable to adopt their usual systolic configuration, and the relative absence of RHM suggests a loss of organisation among subendocardial myocytes.

Meanwhile panel B displays short-axis images of 65-year-old male who also presented with anterior ST-elevation and underwent PPCI to his LAD. By 12 months, his LVEF improved from 44% to 56%, while his LVEDV remained fixed at 115mls. In the acute scan, the LGE image demonstrates subendocardial infarction of the septal walls. MD is raised acutely in infarcted areas, but are not as high as patient A. FA, E2A and proportions of RHM in infarct areas appear relatively preserved (higher) compared to patient A, and remain fixed at 12 months, demonstrating that the preservation of sheetlet angularity (higher E2A) and organisation among subendocardial myocytes (higher RHM) were detectable in the acute scan.

6.3.2 Acute changes in DT-CMT parameters

In the acute scan, MD was higher in infarct regions than remote (1.73±0.12 vs 1.47±0.08x10^{-3}mm^2/s, p<0.001). Meanwhile FA, absolute E2A and the proportion of RHM were all lower in infarct myocardium than remote (FA: 0.26±0.04 vs 0.36±0.04, p<0.001; E2A: 46±9° vs 52±9°, p<0.001; RHM: 14±8% vs 24±11%, p<0.001).

6.3.3 Longitudinal changes over 3 scans

For the 100 patients who completed all 3 scans, longitudinal changes in DT-CMR parameters, specifically in remote and infarct regions are shown in Figure 6.3.
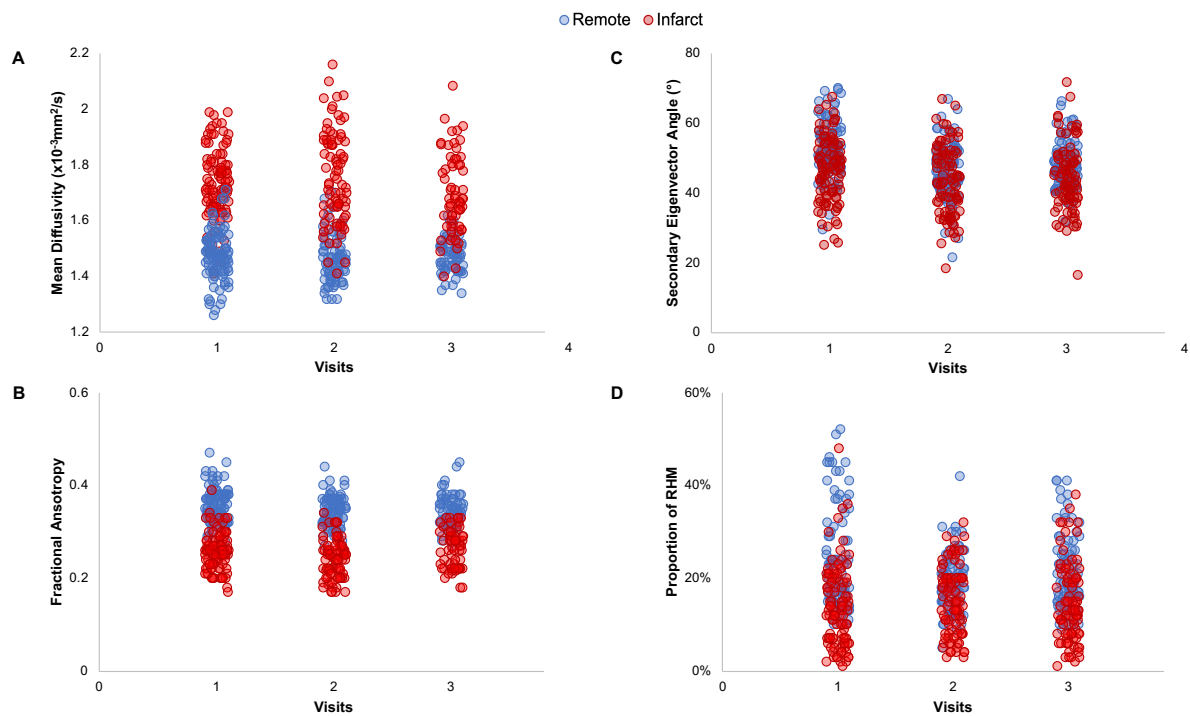
Figure 6.3: Longitudinal changes in DT-CMR parameters across 3 scans

At all 3 scans, MD remains higher (panel A), and FA remains lower (panel B) in infarct regions than remote regions. However, there is considerable overlap in E2A (panel C) and RHM (panel D) of infarct and remote regions.

This data was further subdivided into patients with and without adverse remodelling at 12 months and is displayed in Table 6.4 and Table 6.5 respectively. Patients who

adversely remodelled at 12 months had a significant incremental increase in remote T1 (ANOVA p=0.003), ECV (p = 0.008) and MD (p=0.025) across the 3 cans, as shown in Figure 6.4.   In their infarct regions, MD remained higher; FA, E2A and RHM remained lower through all 3 scans than in the infarct regions of patients who did not remodel. (Figure 6.5) Meanwhile the infarct MD serially decreased across the 3 scans in patients who did not remodel (ANOVA p=0.003).

Parameters	No Adverse Remodelling (n=68)			
	Visit 1	Visit 2	Visit 3	ANOVA
LVEF (%)	46±8	51±8	53±7	<0.001
LVEDVi (ml/m^2)	78±13	77±14	78±16	0.976
Infarct Size (% of LV)	12±10	12±10	9±7	<0.001
Infarct transmurality (%)	68±29	40±29	10±5	<0.001
MVO size (g)	0.5±1.6	0±0	0±0	<0.001
Remote regions:				
Native T1 (ms)	1186±62	1185±72	1189±55	0.783
ECV (%)	27±5	27±5	27±4	0.495
T2 (ms)	47±6	48±5	44±10	0.334
MD (x10^{-3}mm^2/s)	1.45±0.08	1.45±0.06	1.46±0.06	0.698
FA	0.36±0.04	0.35±0.03	0.35±0.04	0.216
Absolute E2A (°)	52±9	47±7	49±6	<0.001
RHM (%)	23±12	19±6	20±8	0.262
CM (%)	65±13	70±8	69±12	0.190
LHM (%)	12±6	11±7	11±9	0.144
Adjacent regions:				
Native T1 (ms)	1285±78	1234±57	1214±47	<0.001
ECV (%)	32±6	32±7	27±3	<0.001
T2 (ms)	53±7	50±5	48±4	<0.001
MD (x10^{-3}mm^2/s)	1.58±10	1.52±0.07	1.49±0.06	<0.001
FA	0.33±0.04	0.32±0.03	0.34±0.03	0.512
Absolute E2A (°)	51±8	47±7	48±8	0.012
RHM (%)	15±7	23±7	18±9	0.254
CM (%)	72±11	71±10	76±13	0.174
LHM (%)	13±7	7±12	6±14	0.636
Infarct regions:				
Native T1 (ms)	1471±113	1382±119	1340±95	<0.001
ECV (%)	53±11	55±15	48±15	0.058
T2 (ms)	67±14	56±8	51±7	<0.001
Presence of IMH (n,%)	16 (24)	16 (24)	16 (24)	1.000
MD (x10^{-3}mm^2/s)	1.71±0.12	1.71±0.15	1.63±0.11	0.003
FA	0.27±0.04	0.25±0.04	0.28±0.04	0.001
Absolute E2A (°)	51±7	47±9	48±9	0.026
RHM (%)	17±9	18±6	17±6	0.929
CM (%)	67±13	71±10	68±10	0.104
LHM (%)	16±9	11±8	14±8	0.001

Table 6.4: Longitudinal changes in patients who did not undergo adverse remodelling

Parameters	Adverse Remodelling (n=32)			
	Visit 1	Visit 2	Visit 3	ANOVA
LVEF (%)	37±9	43±10	41±9	0.053
LVEDVi (ml/m^2)	82±19	96±26	103±24	0.002
Infarct Size (% of LV)	27±18	25±11	27±22	0.326
Infarct transmurality (%)	93±13	78±22	65±20	<0.001
MVO size (g)	3.1±4.1	0±0	0±0	<0.001
Remote regions:				
Native T1 (ms)	1217±50	1255±68	1270±57	0.003
ECV (%)	27±3	28±7	31±5	0.008
T2 (ms)	49±4	48±5	49±6	0.553
MD (x10^{-3}mm^2/s)	1.52±0.09	1.50±0.06	1.51±0.06	0.025
FA	0.35±0.03	0.33±0.04	0.34±0.04	0.157
Absolute E2A (°)	52±10	46±9	46±7	0.012
RHM (%)	26±11	24±7	23±9	0.082
CM (%)	60±15	69±9	65±12	0.072
LHM (%)	14±8	10±7	12±7	0.169
Adjacent regions:				
Native T1 (ms)	1315±48	1255±63	1264±46	<0.001
ECV (%)	29±4	30±6	29±3	0.449
T2 (ms)	54±8	50±3	50±5	0.010
MD (x10^{-3}mm^2/s)	1.63±0.09	1.57±0.12	1.54±0.05	0.004
FA	0.32±0.03	0.32±0.03	0.33±0.03	0.367
Absolute E2A (°)	48±6	45±7	45±7	0.046
RHM (%)	14±6	23±5	16±9	0.115
CM (%)	71±10	69±12	74±14	0.316
LHM (%)	15±6	8±8	10±10	0.333
Infarct regions:				
Native T1 (ms)	1522±102	1453±83	1472±117	0.021
ECV (%)	57±10	67±16	60±12	0.020
T2 (ms)	71±11	65±7	54±7	<0.001
Presence of IMH (n,%)	18 (56)	18 (56)	18 (56)	1.000
MD (x10^{-3}mm^2/s)	1.78±0.13	1.84±0.15	1.82±0.10	0.107
FA	0.23±0.03	0.22±0.03	0.23±0.02	0.465
Absolute E2A (°)	37±6	37±8	36±5	0.862
RHM (%)	8±5	8±6	6±3	0.087
CM (%)	67±12	71±9	67±12	0.240
LHM (%)	20±9	21±10	27±11	0.026

Table 6.5: Longitudinal changes in patients who underwent adverse remodelling
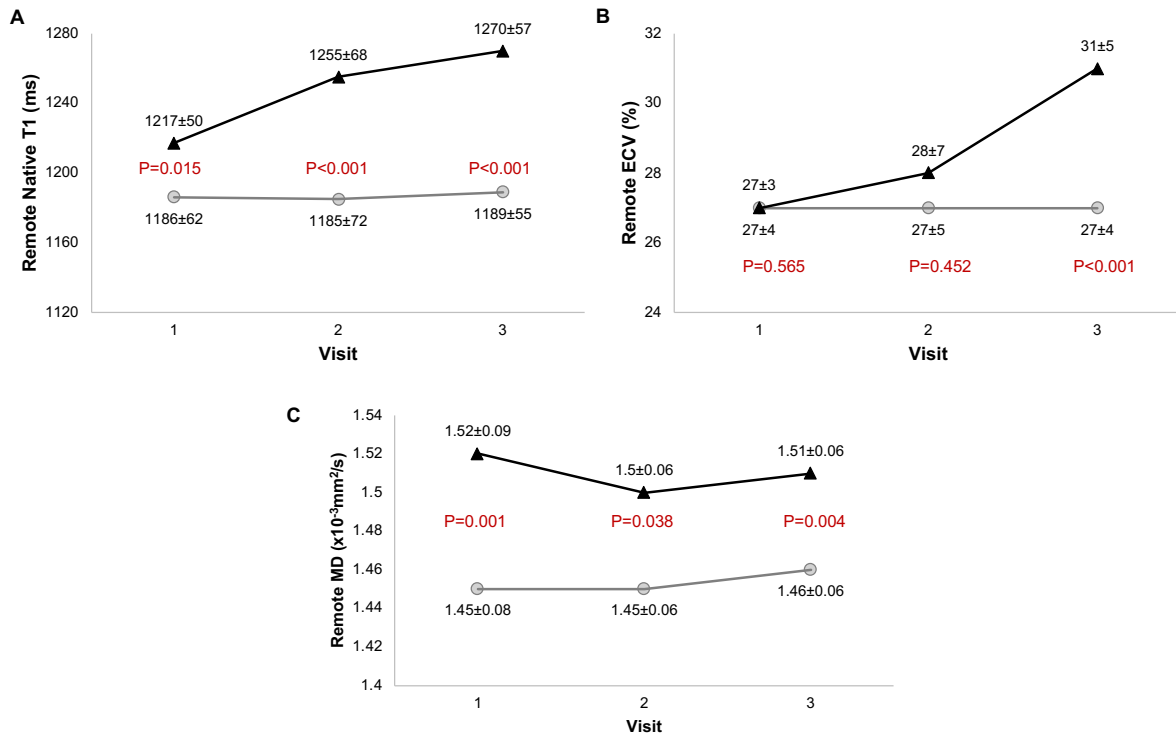
Figure 6.4: Longitudinal changes in remote regions

Patients who underwent adverse remodelling had incremental increase in native T1 (panel A), ECV (panel B) and mean diffusivity (MD – panel C) in their remote regions over the 3 scans.
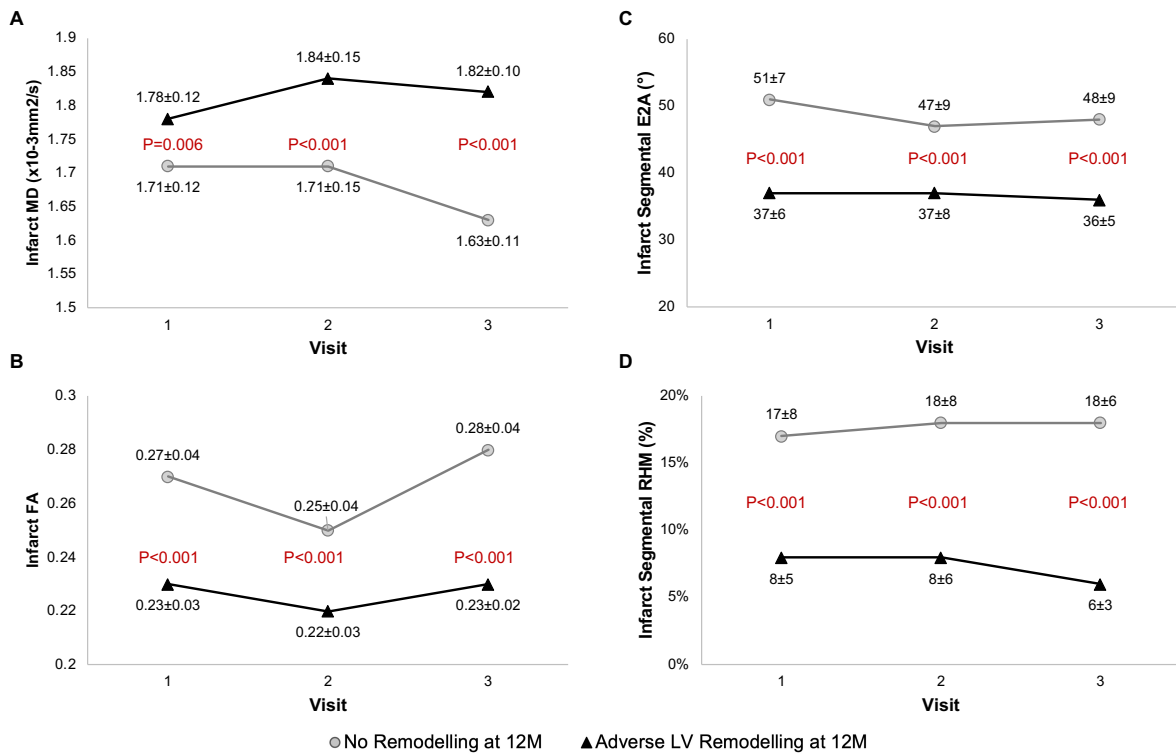
Figure 6.5: Longitudinal changes in DT-CMR parameters in infarct regions

In patients who underwent adverse remodelling by 12 months, MD remained high, while FA, E2A and RHM remained low and did not change significantly between the 3 scans.

6.3.4 Tissue characteristics derived from the 12-month scans

At the 12-month follow up scan, there were significant differences in tissue characteristics of infarct, adjacent and remote myocardium between patients with and without adverse remodelling, derived using parametric mapping and DT-CMR. Infarct regions of remodelled LV had higher MD (1.82 ± 0.10 vs $1.63\pm0.11\times10^{-3}mm^2/s$, p<0.001), lower FA ($0.23\pm0.02$ vs 0.28 ± 0.04, p<0.001), lower E2A ($36\pm5°$ vs $48\pm9°$, p<0.001), lower RHM ($6\pm3\%$ vs $17\pm6\%$) and higher LHM ($27\pm11\%$ vs $18\pm9\%$, p<0.001) than infarct regions of LV that did not adversely remodel.

Between the acute and 12-month scan, MD of infarct regions in adversely remodelled LV longitudinally increased from 1.78 ± 0.13 to $1.82\pm0.10\times10^{-3}mm^2/s$ (p<0.001), while MD in infarct regions of LV which did not remodel decreased from 1.71 ± 0.12 to $1.63\pm0.11\times10^{-3}mm^2/s$ (p<0.001). There was a positive correlation between the serial changes in LVEDVi and MD (Figure 6.6A), native T1 (Figure 6.6B) and ECV (Figure 6.6C) of infarct regions over 12 months.

At 12 months, the adjacent regions of adversely remodelled LV had significantly higher MD (1.54 ± 0.05 vs $1.49\pm0.06\times10^{-3}mm^2/s$, p<0.001), higher ECV ($29\pm3\%$ vs $27\pm3\%$, p<0.001) and higher native T1 ($1264\pm46ms$ vs $1214\pm47ms$, p<0.001) in comparison with adjacent regions of LV that did not remodel (Table 6.2). A similar pattern was noted in remote segments, with adversely remodelled LV having higher MD (1.51 ± 0.06 vs $1.46\pm0.06\times10^{-3}mm^2/s$, p=0.004), higher ECV ($31\pm5\%$ vs $27\pm4\%$, p<0.001) and higher native T1 ($1270\pm57ms$ vs $1189\pm55ms$, p<0.001) in their remote regions than patients that did not undergo LV remodelling (Table 6.2). Correlations between native T1, ECV and MD of adjacent and remote regions and LVEDVi are shown in Figure 6.6 (panels D to I).
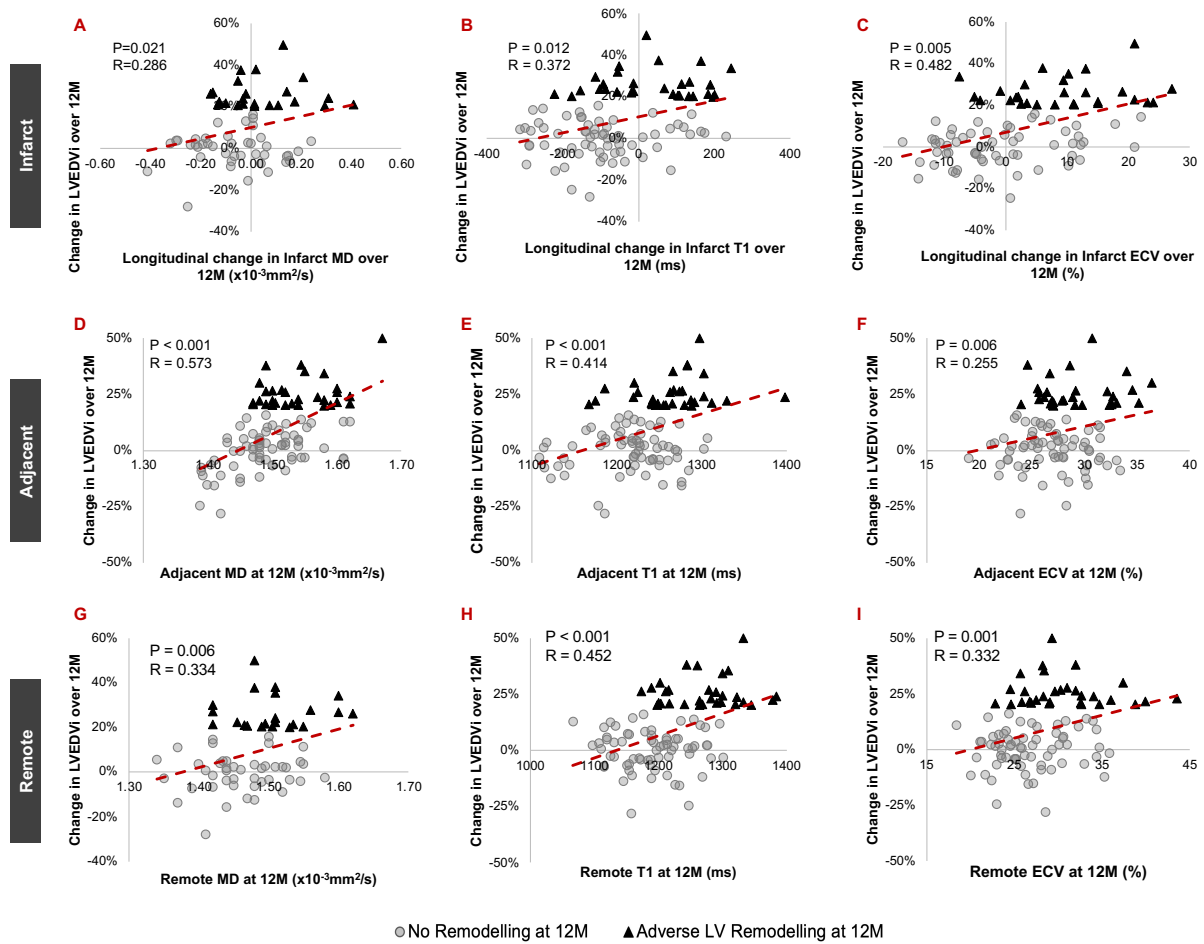
Figure 6.6: Relationship between tissue characteristics of chronic infarct, adjacent and remote regions with serial change in LV size

Serial changes in MD (panel A), native T1 (panel B) and ECV (panel C) of infarct regions correlated with serial change in BSA-indexed LVEDV. The MD, native T1 and ECV of adjacent (panels D,E,F) and remote (panels G,H,I) regions also correlate with change in LVEDVi over 12 months.

6.3.5 Predictive value of acute DT-CMR post ischemic injury

Adverse Remodelling

Out of the 100 patients, 32 developed adverse remodelling by their 12-month scan. These patients had lower FA (0.23±0.03 vs 0.27±0.04, p<0.001), absolute E2A (37±6° vs 51±7°, p<0.001) and proportion of RHM (8±5% vs 17±9%, p<0.001) in their acutely infarcted myocardium than patients who did not develop LV remodelling (Table 6.2). Univariate linear regression analysis identified several CMR-based characteristics from the acute scan to be significantly associated with LVEDVi at 12 months (Table 6.6). Among DT-CMR parameters, acute infarct FA (r=-0.552), E2A (r=-0.594) and RHM (r=-0.447) all correlated with change in LVEDVi over 12 months (Figure 6.7), as did acute remote MD (r=0.331) and FA (r=-0.249). Following multivariate regression analysis adjusting for factors including baseline LVEF, LVEDVi, infarct size/transmurality, extent of MVO and infarct ECV, only infarct FA (standardised β 0.342, p=0.007) and infarct E2A (standardised β 0.323, p=0.008) were independently associated with LVEDVi at 12 months. Following multivariable logistic regression analysis, FA (odds ratio [OR] <0.01, p=0.007) and absolute E2A (OR 0.61, p<0.001) of infarcted myocardium were the only significant factors independently associated with adverse LV remodelling at 12 months after adjusting for LVEF and infarct size, as shown in Table 6.7. An ROC diagram with comparison of AUC of various infarct characteristics are shown in Figure 6.8. Infarct E2A (0.936), RHM (0.810) and FA (0.796) had higher AUC than acute LVEF (0.760) and infarct size derived using LGE (0.759).

Baseline CMR findings	Correlation with change in LVEDVi at 12 months			
	Univariate Analysis		Multivariate Analysis	
	OR (95%CI)	P value	β	P value
LVEF (%)	-0.497	<0.001	0.024	0.850
LVEDVi (ml/m^2)	0.276	0.005	0.133	0.201
Infarct Size (% of LV)	0.410	<0.001	0.036	0.802
Infarct transmurality (%)	0.384	<0.001	-0.098	0.505
MVO size (g)	0.404	<0.001	0.111	0.297
Remote regions:				
Native T1 (ms)	0.404	<0.001	0.129	0.186
ECV (%)	-0.210	0.045	-0.091	0.367
T2 (ms)	0.118	0.300	-	-
MD (x10^{-3}mm^2/s)	0.331	0.001	0.095	0.320
FA	-0.249	0.013	-0.078	0.393
Absolute E2A (°)	-0.031	0.768	-	-
RHM (%)	0.074	0.475	-	-
CM (%)	-0.119	0.254	-	-
LHM (%)	0.106	0.307	-	-
Adjacent regions:				
Native T1 (ms)	0.104	0.306	-	-
ECV (%)	-0.226	0.127	-	-
T2 (ms)	-0.020	0.861	-	-
MD (x10^{-3}mm^2/s)	0.096	0.341	-	-
FA	-0.174	0.284	-	-
Absolute E2A (°)	-0.233	0.147	-	-
RHM (%)	-0.134	0.253	-	-
CM (%)	0.050	0.673	-	-
LHM (%)	0.026	0.825	-	-
Infarct regions:				
Native T1 (ms)	0.165	0.106	-	-
ECV (%)	0.270	0.008	0.027	0.806
T2 (ms)	0.095	0.408	-	-
MD (x10^{-3}mm^2/s)	0.183	0.001	-0.076	0.467
FA	-0.552	<0.001	-0.342	0.007
Absolute E2A (°)	-0.594	<0.001	-0.323	0.008
RHM (%)	-0.447	<0.001	-0.129	0.224
CM (%)	0.051	0.615	-	-
LHM (%)	0.237	0.057	-	-

Table 6.6: Regression analysis of acute predictors of change in LVEDVi over 12 months
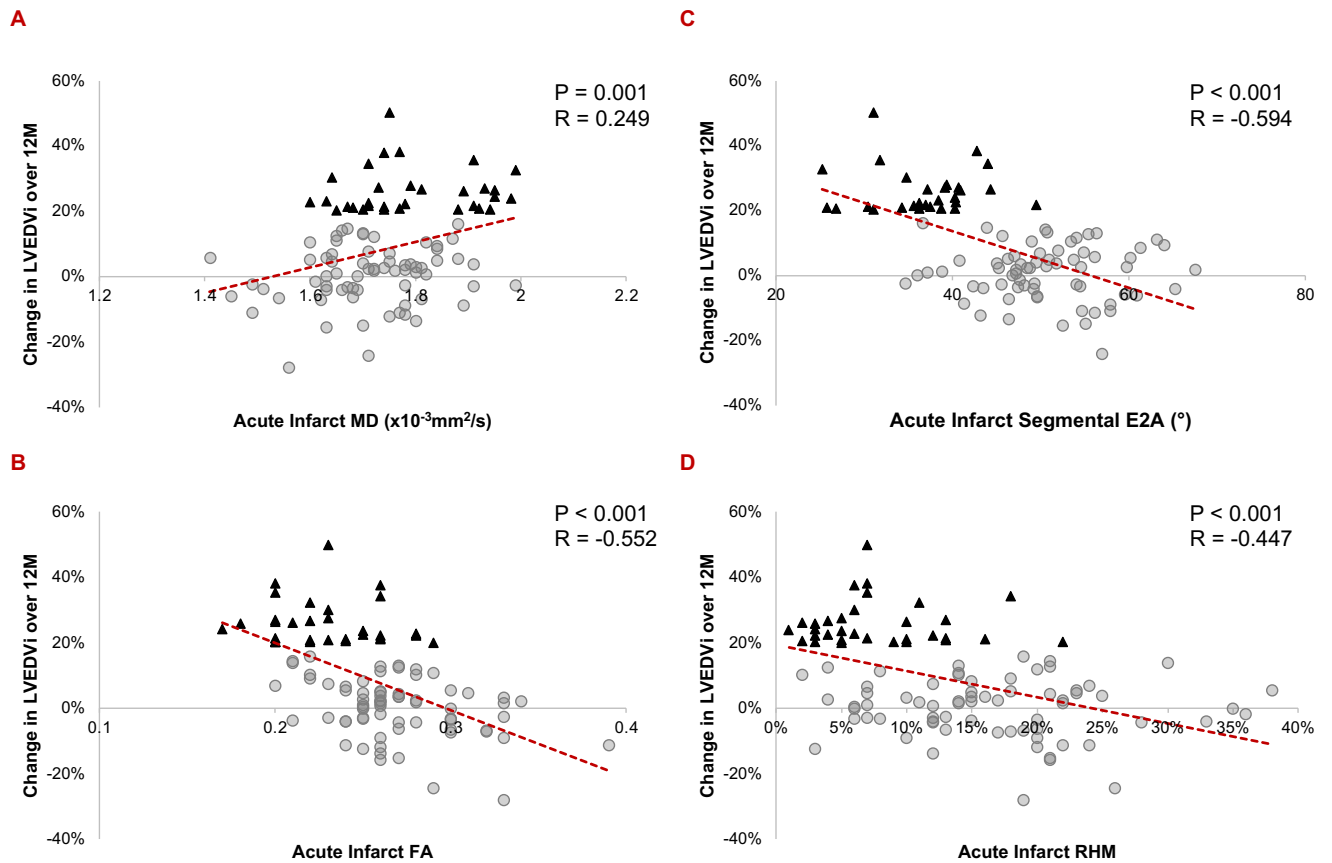
Figure 6.7: Correlation between acute DT-CMR parameters and change in LV size over 12 months

Increased MD (panel A), decreased FA (panel B), decreased absolute E2A (panel C) and decreased proportions of myocytes with RHM (panel D) in acutely infarcted myocardium were all associated with the serial change in LVEDVi over 12 months following STEMI.
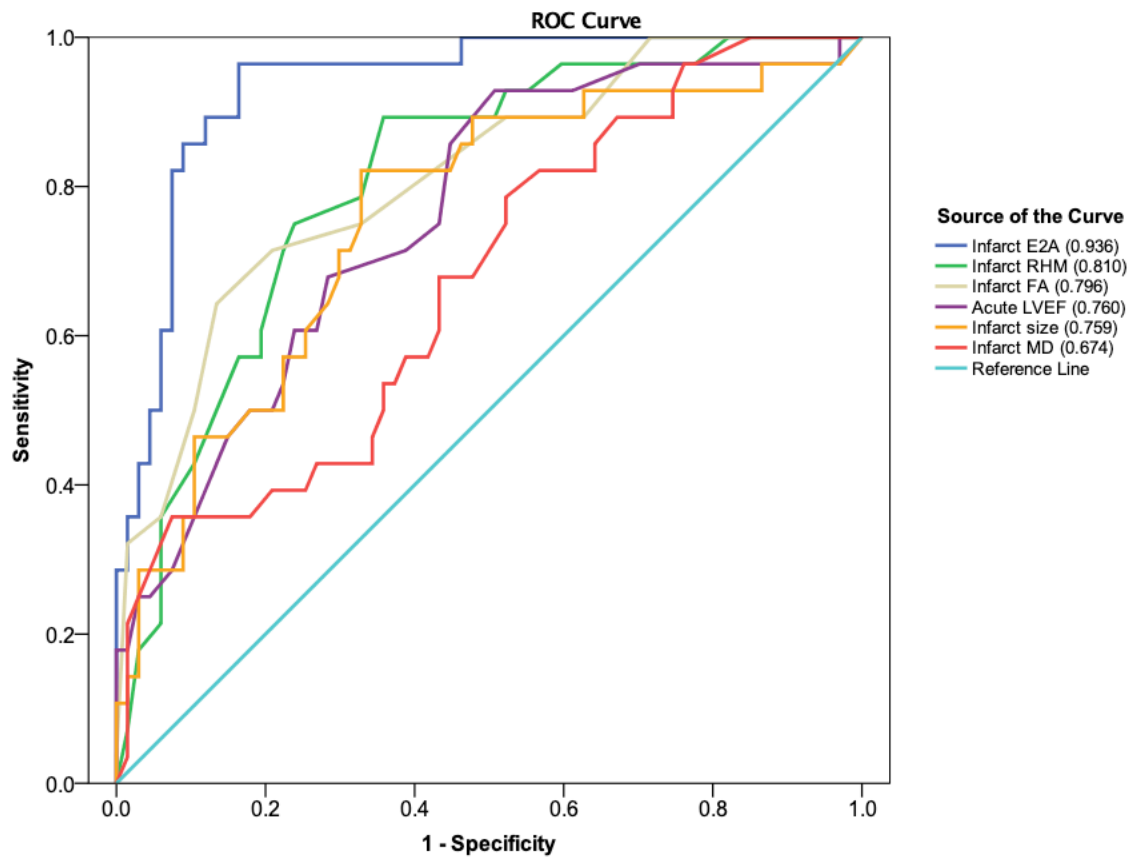
Figure 6.8: Receiver operator characteristics for prediction of adverse remodelling

Comparison of receiver operator characteristics curves between DT-CMR parameters, acute LVEF and acute infarct size derived using LGE. The absolute E2A had the highest AUC.

Table 6.7: Multivariate logistic regression analysis of acute predictors of adverse LV remodelling

Characteristics	Odds Ratio	95% Confidence Interval		P Value
		Lower	Upper	
LVEF (%)	0.95	0.85	1.05	0.945
Infarct size (% of LV)	1.04	0.96	1.30	0.335
Infarct MD ($x10^{-3}mm^2/s$)	0.01	0.01	10.8	0.384
Infarct FA	<0.01	<0.01	0.01	0.007
Infarct E2A (°)	0.73	0.61	0.87	<0.001
Infarct RHM (%)	<0.01	<0.01	3.09	0.070

LVEF at 12 months:

As well as looking at adverse remodelling, univariate linear regression analysis was also carried out to identify acute predictors of long-term LVEF. Several CMR-based characteristics of the acute scan were found to be significantly associated with LVEF at 12-months (Table 6.8); among DT-CMR parameters these included remote MD (r=-0.316), remote E2A (r=0.276), infarct MD (r=-0.302), infarct FA (r=0.494), infarct E2A (r=0.388) and infarct RHM (r=0.483), as shown in Figure 6.9. Following multivariate linear regression analysis adjusting for infarct size/transmurality, baseline LVEF (β 0.396, p<0.001), baseline LVEDVi (β -0.174, p=0.046) and infarct FA (β 0.305, p=0.002) were independent predictors of LVEF at 12 months.

Baseline CMR findings	Correlation with LVEF at 12 months			
	Univariate Analysis		Multivariate Analysis	
	OR (95%CI)	P value	β	P value
LVEF (%)	0.697	<0.001	0.396	<0.001
LVEDVi (ml/m^2)	-0.474	<0.001	-0.174	0.046
Infarct Size (% of LV)	-0.475	<0.001	-0.182	0.116
Infarct transmurality (%)	-0.374	<0.001	0.256	0.028
MVO size (g)	-0.415	<0.001	-0.006	0.944
Remote regions:				
Native T1 (ms)	-0.188	0.069	-	-
ECV (%)	0.179	0.092	-	-
T2 (ms)	-0.100	0.385	-	-
MD (x10^{-3}mm^2/s)	-0.316	0.002	-0.046	0.545
FA	0.148	0.148	-	-
Absolute E2A (°)	0.276	0.008	0.125	0.083
RHM (%)	0.055	0.603	-	-
CM (%)	-0.044	0.675	-	-
LHM (%)	0.016	0.875	-	-
Adjacent regions:				
Native T1 (ms)	-0.020	0.845	-	-
ECV (%)	0.156	0.136	-	-
T2 (ms)	-0.078	0.499	-	-
MD (x10^{-3}mm^2/s)	-0.065	0.523	-	-
FA	0.078	0.444	-	-
Absolute E2A (°)	0.292	0.214	-	-
RHM (%)	0.114	0.342	-	-
CM (%)	-0.146	0.221	-	-
LHM (%)	0.135	0.257	-	-
Infarct regions:				
Native T1 (ms)	-0.099	0.110	-	-
ECV (%)	-0.425	<0.001	-0.042	0.616
T2 (ms)	-0.198	0.250	-	-
MD (x10^{-3}mm^2/s)	-0.302	0.003	0.024	0.769
FA	0.494	<0.001	0.305	0.002
Absolute E2A (°)	0.388	<0.001	-0.021	0.813
RHM (%)	0.483	<0.001	0.185	0.045
CM (%)	-0.122	0.231	-	-
LHM (%)	-0.179	0.069	-	-

Table 6.8:Regression analysis of acute predictors of 12-month LVEF
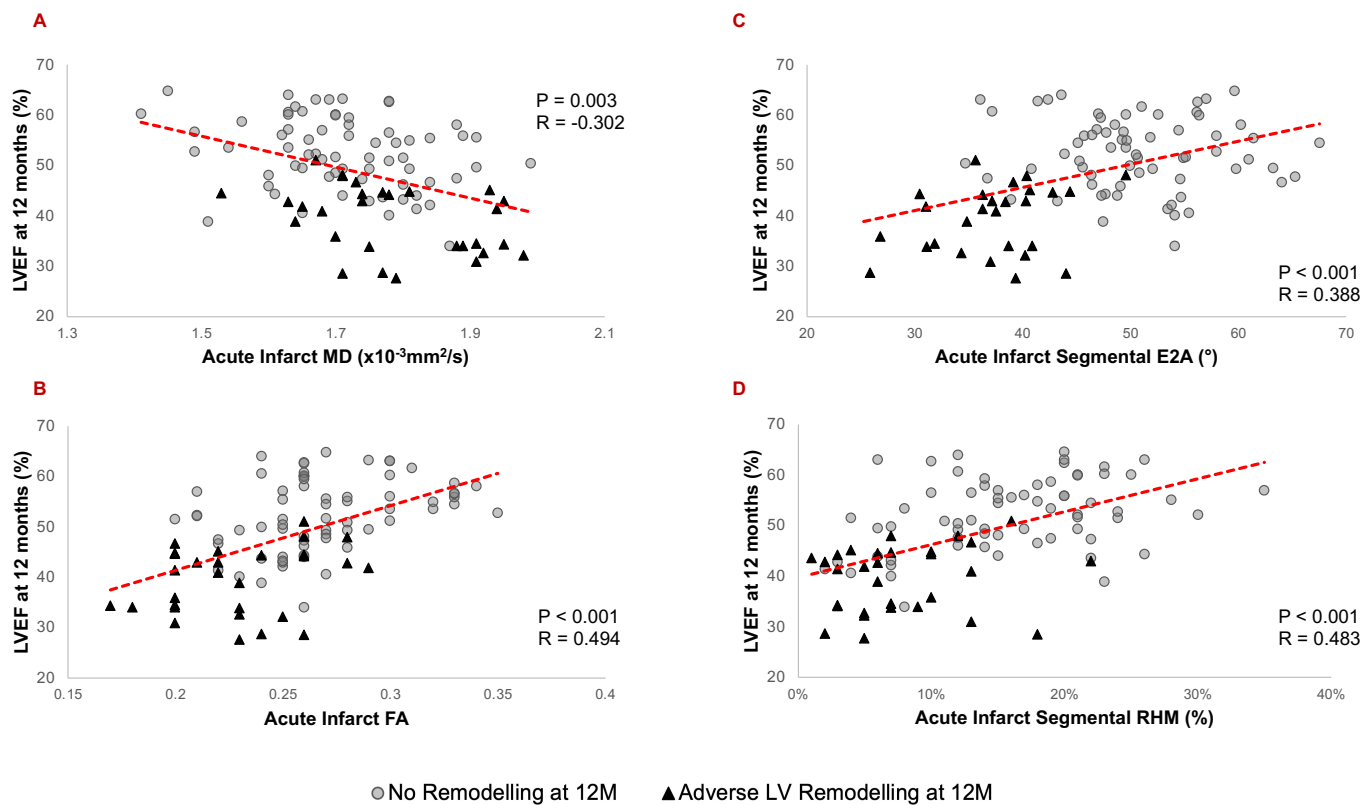
Figure 6.9: Correlations between acute DT-CMR parameters and LVEF % at 12 months

Increased MD (panel A), decreased FA (panel B), decreased absolute E2A (panel C) and decreased proportions of RHM (panel D) in acutely infarcted myocardium were all associated with lower LVEF at 12 months following STEMI.

6.4 Discussion

To the best of our knowledge, this is the first study to report on the ability of DT-CMR to predict long-term adverse LV remodelling in patients with acute STEMI and to compare it with previously established CMR parameters. Our results also provide novel mechanistic insight into the acute and long-term pathophysiological sequelae of STEMI. Our main findings are:

1. In the acute stages following STEMI, the diffusion of water molecules in infarcted myocardium of patients who undergo adverse remodelling by 12 months is more isotropic. The myocardial sheetlets in the infarct region are unable to adopt their usual orientation in systole as suggested by low absolute

E2A values and have less RHM, highlighting the early loss of organisation amongst subendocardial myocytes.

2. In the 12 months after acute STEMI, not just the infarcted and but also the adjacent and remote myocardium of adversely remodelled hearts shows evidence of interstitial changes, as demonstrated by an increase in MD over time, indicating increasingly unrestricted global diffusion.

3. DT-CMR markers of wall strain with reduced sheetlet angularity (E2A) and cardiomyocyte disarray (FA) in acutely infarcted myocardium are independent predictors of adverse remodelling at 12 months. Acute infarct FA is also independently associated with LVEF at 12 months.

These findings can help elucidate some of the pathophysiological mechanisms that drive adverse remodelling following STEMI and provide novel biomarkers for risk stratification.

6.4.1 Acute irreversible changes in myocardial architecture

Owing to transmural variance in vascular compliance, subendocardial myocytes are more vulnerable to ischaemic injury. (129) Meanwhile foci of myocytes can remain preserved within areas of infarction, depending on the extent of local reperfusion, raising the potential for functional recovery. (12,130) In our results, we observe that preservation of sheetlet angularity during systole (higher E2A) and organisation of subendocardial myocytes (higher proportion of RHM) in the acute scan reduces the likelihood of long-term adverse remodelling. Meanwhile significant cardiomyocyte disarray (evidenced by low FA) is predictive of adverse remodelling and poor long-term functional recovery, matching findings from a recent DT-CMR study. (128)

6.4.2 Longitudinal changes over 12 months

Following infarction, the degradation of inter-myocyte collagen struts leads to slippage between muscle bundles, resulting in a wall thinning and impaired contractility. (5) In the convalescent phase, in an attempt to improve the integrity of the scar tissue, connective tissue infiltrates the myocyte compartment to unite the disrupted myocytes. In order to resist LV dilatation, the replacement scar tissue requires sufficient tensile strength to overcome the stretching forces from increased pre-load. (4) The impact of

adverse remodelling is known to extend beyond infarct regions; in an adaptive response to the acute rise in pre-load following MI, the increased wall stress detected by mechanoreceptors stimulates cellular hypertrophy and upregulation of contractile assembly units in non-infarcted myocardium. (4) In a recent study, Carrick et al (124) observed that LVs which went on to remodel following STEMI had significantly higher native T1 in their remote myocardium during their acute scans, and attributed this to a combination of oedema and hypercellularity.

In this current study, we observed a serial reduction in MD, T1 and ECV in the infarct myocardium of patients who did not undergo remodelling; this reduction is likely attributable to the resolution of oedema and adaptive infiltration of connective tissue. However, in the adverse remodelling group, MD, T1 and ECV serially increased in not only infarcted, but also adjacent and remote myocardium over 12 months. Given that much of the acute myocardial oedema is expected to have settled by this stage, this longitudinal increase is likely reflective of an expansion in extracellular volume. In the infarcted myocardium, if this equates to a decline in tensile strength, it may explain the association between the LV cavity dilatation and the serial increase in MD, T1 and ECV of scar tissue. Separate histological studies have also observed an up to 70% increase in cell volume of remote myocardium following MI (131) – and the increased remote and adjacent MD may also be reflective of this.

6.4.3 Predictive value of DT-CMR

Infarct size and MVO detected using LGE are already recognised as excellent prognostic biomarkers following MI. LGE provides accurate measurement of chronic infarct size but with the exception of MVO detection, does not provide quantitative estimation of the severity of injury to underlying structures. This is especially relevant in the acute stages following MI, where factors such as oedema adds complexity to LGE interpretation. (12) By using DT-CMR, the changes in the axes of microstructural components appear to be detectable within a week and are shown to remain fixed over time. This likely explains why parameters such as FA and E2A were independently predictive of adverse remodelling even after accounting for clinical and angiographic factors. Our results demonstrate how acute DT-CMR imaging can complement current clinical and imaging risk factors in early prognostic risk-

stratification following MI, prompting earlier initiation of aggressive heart failure and device therapy to those at highest risk of adverse outcomes.

6.4.4 Limitations

Conclusions drawn from this study are based on correlations with published evidence and other cardiac MRI markers, whereas validation with histological specimens would be preferable. By allowing for non-contrast and free-breathing acquisitions, DT-CMR SE offers some practical benefits in the context of acute imaging post-STEMI; however, acquisition was limited to only 3 slices and technical developments are needed to allow full LV coverage in shorter scan times. Post-processing can be labour-intensive and clinical implementation requires further optimisation, particularly with tractography postprocessing for accurate definition of HA variation across the myocardium and scar borders. (79)

6.5 Conclusion

Following myocardial infarction, extensive cardiomyocyte disarray as evidenced by low FA, acute loss of sheetlet angularity as evidenced by low E2A, and a greater loss of organisation among cardiomyocytes with right-handed orientation, corresponding to subendocardium, are all associated with long-term adverse remodelling and functional impairment. Longitudinal changes in MD suggests diffusion becomes more unrestricted globally in adversely remodelled hearts, highlighting diffuse interstitial changes in infarct, adjacent and remote myocardium. These findings now warrant further validation in larger multicentre DT-CMR studies.

Chapter 7: Insights Into myocardial microstructure of Athletes and Hypertrophic Cardiomyopathy Patients using diffusion tensor cardiac magnetic resonance imaging

Short title: DT-CMR study of controls, athletes and HCM

7.1 Introduction

As discussed in chapter 1.2.2.4, it remains challenging yet important to differentiate between physiologically adaptive left ventricular (LV) hypertrophy observed in athletes' hearts from pathological LV hypertrophy seen in HCM patients. While transthoracic echocardiography remains the first line imaging modality for imaging HCM patients, CMR has gradually established itself as a potent complementary tool thanks to its distinctive advantage of tomographic imaging allowing for tissue characterization and accurate measurement of wall thickness.(132) However given its ability to characterise in-vivo changes in myocardial architecture, DT-CMR is well suited for exploring the different mechanisms underpinning physiological versus pathological hypertrophy. Swoboda et al demonstrated HCM patients to have higher ECV than athletes(47), but thus far DT-CMR has not been performed on athletes.

7.1.1 Hypothesis and aims

The purpose of our study was to perform DT-CMR on healthy volunteers, athletes and HCM patients in order to explore the differences in the myocardial microstructure between these groups. I hypothesised there would be significant differences in DT-CMR parameters between the 3 cohorts.

7.2 Methods

20 healthy controls, 20 athletes and 20 HCM patients were recruited for this study. See chapter 3 for full details regarding subject recruitment (chapter 3.2), image acquisition (chapter 3.3.1), image analysis (chapter 3.4) and basic statistical analysis methods (3.5).

Detailed statistics

ANOVA with Bonferroni post-hoc comparisons were used to compare CMR measurements between controls, athletes and HCM patients. Pearson correlation analysis was used to calculate the correlation coefficients between different CMR biomarkers including wall thickness, percentage of LGE, DT-CMR and parametric biomarkers.

7.3 Results

The study flowchart is shown in Figure 7.1.
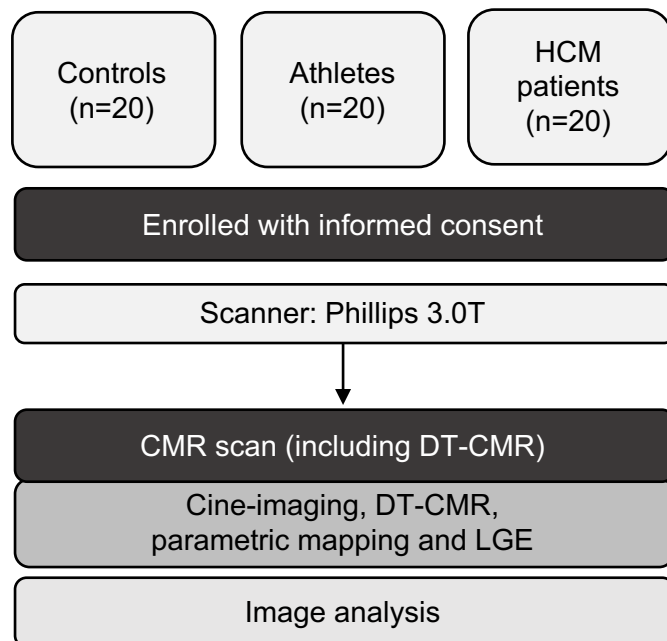
Figure 7.1: Flow chart for study enrolment

The baseline demographics are displayed in Table 7.1. Athletes on average performed 9.4±3 hours of exercise per week, for an average of 7.7±5 years and had significantly lower mean body mass than HCM patients (p<0.05). Seventeen athletes completed the exercise test with a mean VO_{2peak} of 58 ± 6 ml/kg/min. There was no significant difference in systolic or diastolic blood pressure between the two cohorts.

The global MRI characteristics are shown in Table 7.2. Athletes had significantly higher mean BSA-indexed LV-end-diastolic-volume and stroke volume than HCM patients and volunteers (p<0.05). Three athletes had evidence of LGE. Nineteen of the HCM patients were LGE positive and overall had significantly higher global LGE (p<0.05), native T1 (p<0.05) and ECV (p<0.05) values than athletes.

	HCM (n=20)	Athletes (n=20)	Volunteers (n=20)	ANOVA/ K-W test	HCM vs athletes	HCM vs volunteers	Athletes vs volunteers
Age (years)	55 ± 9	41 ± 8	27 ± 8	<0.05	<0.05	<0.05	<0.05
Sex (Male %)	70%	95%	45%	-	-	-	-
SBP (mmHg)	128±16	126±10	-	-	0.2	-	-
DBP (mmHg)	74±5	73±8	-	-	0.5	-	-
BMI (kg/m^2)	28±4	24±3	25±6	<0.05	<0.05	0.14	0.4

Table 7.1: Baseline demographics

K-W = Kruskal-Wallis, SBP = Systolic Blood Pressure, DBP = Diastolic Blood Pressure, BMI = Body Mass Index

	HCM (n=20)	Athletes (n=20)	Volunteers (n=20)	ANOVA/ K-W test	HCM vs athletes (p value)	HCM vs volunteers (p value)	Athletes vs volunteers (p value)
LVEDV (ml)	152 ± 30	225 ± 27	165 ± 41	<0.05*	<0.05	0.3	<0.05
LVEDVi (ml/m^2)	76 ± 13	115 ± 12	90 ± 21	<0.05	<0.05	0.8	<0.05
LVSV (ml	93 ± 16	127 ± 15	104 ± 23	<0.05	<0.05	0.8	0.05
LVSVi (ml/m^2)	29 ± 7	50 ± 6	33 ± 12	<0.05	<0.05	0.42	<0.05
LVEF (%)	61 ± 7	56 ± 4	64 ± 6	<0.05	<0.05	0.4	0.05
LV Mass (g)	123 ± 27	110 ± 21	96 ± 31	0.03	0.09	<0.05	0.2
LV Mass index (g/m^2)	65 ± 18	56 ± 11	52.6 ± 17	0.09	0.10	0.42	0.95
LGE (% of LV)	6.5 ±4	0.75 ± 0.1	-	-	<0.001	-	-
Native T1 (ms)	1277 ±77	1221 ±38	-	-	<0.01	-	-
ECV (%)	27.8±4	25.6±3	-	-	0.05	-	-
Global DT-CMR							
MD (x10^{-3}mm^2 /s)	1.52±0.06	1.49±0.03	1.47±0.02	<0.001	<0.05	<0.05	0.16
FA	0.30±0.02	0.35±0.02	0.36±0.03	<0.001	<0.05	<0.05	0.5
E2A (°)	58.8±4	47.0±5	38.5±7	<0.001	<0.05	<0.05	<0.05
HA gradient °/mm	-5.4±0.86	-6.81±1.17	-8.26±1.48	<0.001	<0.05	<0.05	<0.05
HA gradient °/%	-0.54±0.10	-0.50±0.10	-0.51±0.08		0.22	0.28	0.78
Thickest segments							
Mean thickness (mm)	18.5	10.4	7.5	<0.001	<0.05	<0.05	<0.05
LGE (% of LV)	15.0±4	0.6±0.3	-	-	<0.05	-	-
Native T1 (ms)	1296±85	1251±48	-	-	<0.05	-	-
ECV (%)	29.4±5	26.0±3	-	-	0.05	-	-
MD (x10^{-3}mm^2 /s)	1.54±0.09	1.49±0.09	1.47±0.08	0.02*	<0.05	<0.05	0.12
FA	0.26±0.04	0.35±0.04	0.38±0.03	<0.001*	<0.05	<0.05	0.1
E2A (°)	66.8±7	49.1±12	38.9±12	<0.001	<0.05	<0.05	<0.05
HA gradient °/mm	-4.8±1.30	-6.75±1.20	-8.10±1.48	0.02	<0.05	<0.05	<0.05
HA gradient °/%	-0.57±0.19	-0.57±0.16	-0.56±0.14		0.85	0.83	0.91
Remote segments							
Mean thickness (mm)	6.6±2†	7.5±1.8†	-	-	0.15	-	-
LGE (% of LV)	3.8±7.1†	0.9±1.3	-	-	0.07	-	-
Native T1 (ms)	1244±75	1251±48	-	-	0.15	-	-
ECV (%)	26.2±2.3†	25.2±2	-	-	0.22	-	-
MD (x10^{-3}mm^2 /s)	1.50±0.1	1.50±0.10	-	-	0.99	-	-
FA	0.32±0.05†	0.36±0.03	-	-	<0.05	-	-
E2A (°)	51.2±9†	48.7±11	-	-	0.14	-	-
HA gradient °/mm	-5.62±2.81	-7.05±2.98	-	-	0.14	-	-
HA gradient °/%	-0.46±0.21	-0.50±0.21	-	-	0.49	-	-

Table 7.2: CMR Results

Values are displayed as mean ± standard deviation for continuous variables. LVSVi = left ventricular stroke volume indexed for body surface area, *indicates the use of K-W test †indicates significant difference (p<0.05) in comparison to thickest segment

7.3.1 DT-CMR Acquisition

DT-CMR acquisition was successful in all subjects. Figure 7.2 shows representative LGE and DT-CMR maps for a healthy volunteer, athlete and HCM patient. Global DT-CMR measurements are reported in Table 7.2. There was no significant difference in global MD between athletes and volunteers ($MD_{Volunteers}=1.47\pm0.02\times10^{-3}mm^2/s$, $MD_{Athletes}=1.49\pm0.03\times10^{-3}mm^2/s$, p=0.16, however HCM patients had significantly higher global MD than athletes ($MD_{HCM}=1.52\pm0.06\times10^{-3}mm^2/s$, p<0.05). There was no significant difference in global FA between athletes and volunteers ($FA_{Volunteers}=0.36\pm0.03$, $FA_{Athletes}=0.35\pm0.02$, p=0.5), however HCM patients had significantly lower global FA than athletes ($FA_{HCM}=0.30\pm0.02$, p<0.05). Healthy volunteers had steeper HA gradient progression from endocardium to epicardium per millimetre of LV wall thickness compared to athletes, who had steeper progressions than HCM patients (HA gradient $_{Volunteers}$ = -8.26±1.48 °/mm, HA gradient $_{Athletes}$ = -6.81±1.17 °/mm, HA gradient $_{HCM}$ = -5.4±0.86 °/mm, ANOVA p<0.05). No significant differences were found when looking at the HA gradient progression per percentage of LV wall. Athletes had significantly higher global absolute E2A than volunteers ($E2A_{volunteers}=38.5\pm7°$, $E2A_{athletes}=47\pm5°$, p<0.05), and HCM patients had significantly higher absolute E2A than athletes ($E2A_{HCM}=58.8\pm4°$, p<0.05), reflecting the increased contractile configuration in mid-systole.
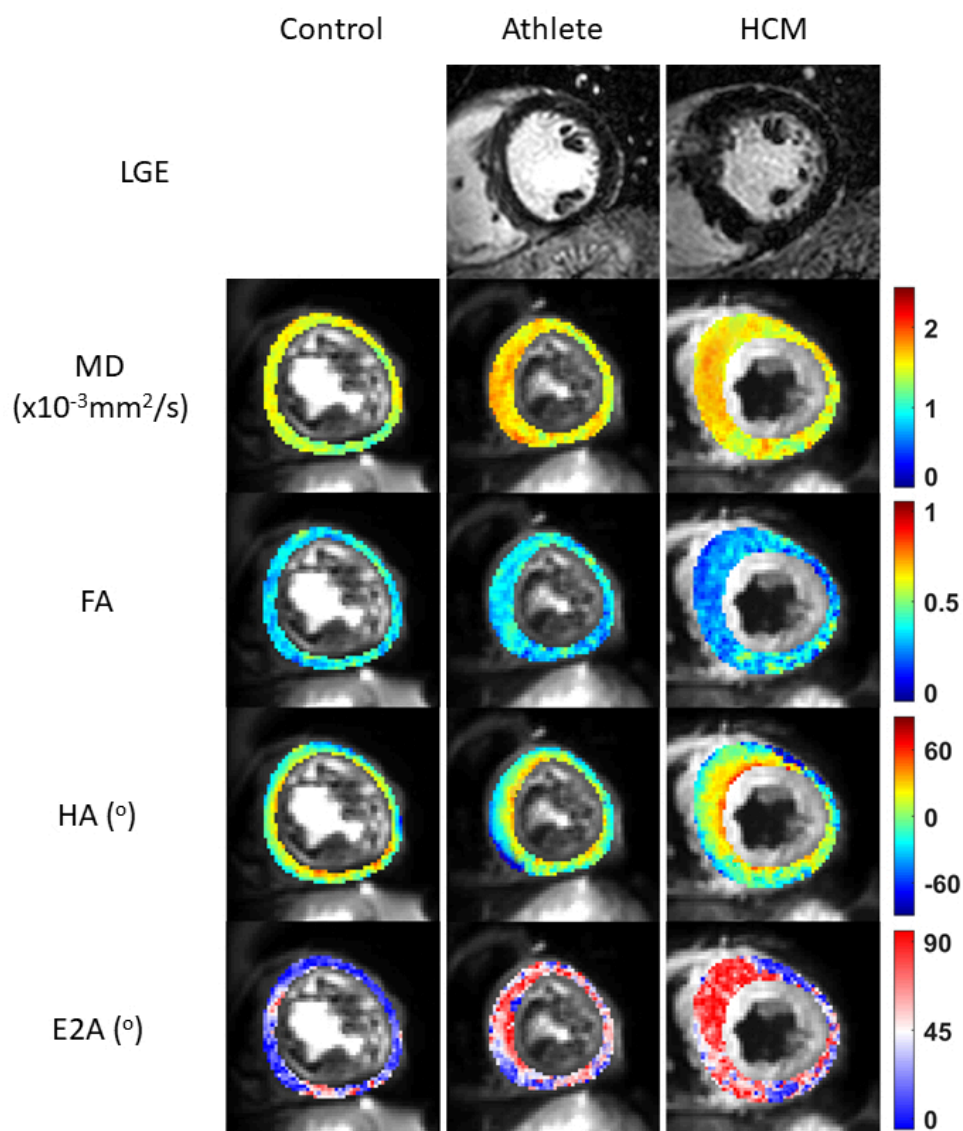
Figure 7.2: Representative maps of a healthy control, athlete and HCM patient

Column A displays a typical basal LV slice obtained in a healthy volunteer showing a normal MD, FA, E2A and HA maps. Column B demonstrates a basal LV slice in an athlete with diffuse fibrosis in the septal segments, with an eccentric increase in MD and a concentric increase in E2A throughout the myocardium. Column C demonstrates a basal LV slice in a HCM patient with an eccentric increase in MD and E2A, and reduction in FA in the hypertrophied segment.

7.3.2 Analysis of thickest segments

Given the eccentric nature of hypertrophy and pathology usually seen in HCM patients, additional focussed analysis of the thickest myocardial segments was undertaken for each cohort. The thickest segments of HCM patients had significantly higher mean thickness ($p<0.05$), more LGE ($p<0.05$), higher native T1 ($p<0.05$) and ECV ($p<0.05$) values than the thickest segments of athletes. DT-CMR analysis of thickest segments reflected similar patterns to those shown in global analysis, with HCM patients having significantly higher MD ($p<0.05$), lower FA ($p<0.05$, Figure 7.3a) and higher absolute E2A ($p<0.05$, Figure 7.3b) than athletes. In line with previously published data, MD values of thickest segments correlated with the LGE% in the corresponding segment ($p<0.05$, Figure 7.3c). Athletes with LGE in their thickest segments (n=3) had significantly higher MD values than athletes without LGE ($p<0.05$, Figure 7.3d).
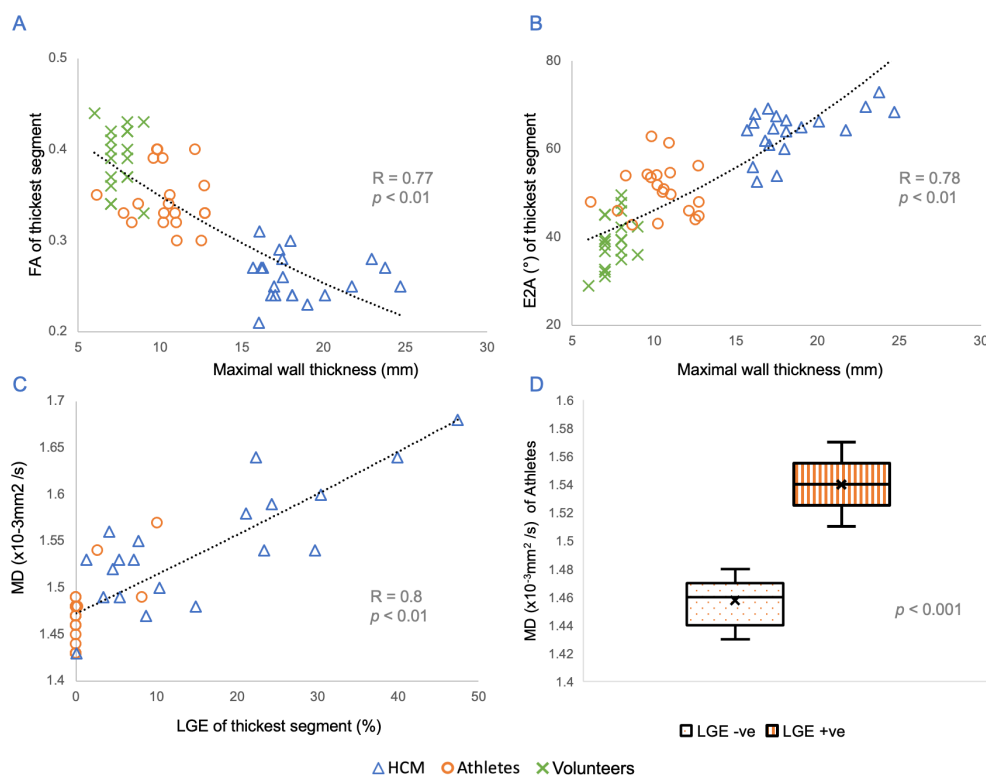
Figure 7.3: Analysis of thickest segments

Wall thickness of the thickest segments across all cohorts correlated with their segmental FA (panel A) and E2A (panel A) values. Amongst athletes, LGE% correlated with segmental MD

values (panel A), and athletes with LGE had significantly higher MD than athletes without LGE in their thickest segments (panel A).

Figure 7.4a demonstrates the relationship between the wall thickness and corresponding segmental ECV in thickest segments of athletes and HCM patients. In the thickest segments of HCM patients, higher ECV values correlated with lower FA (p<0.05, Figure 7.4b) and higher MD (p<0.05, Figure 7.4c). Lower FA also correlated with higher absolute E2A values in the thickest segments of HCM patients (p<0.05, Figure 7.4d). HCM patients had significantly higher absolute E2A values in their thickest segments in comparison to the remote segments (p<0.05, Table 7.2), while in athletes, there was no significant difference in absolute E2A between thickest and remote segments (p=0.70).
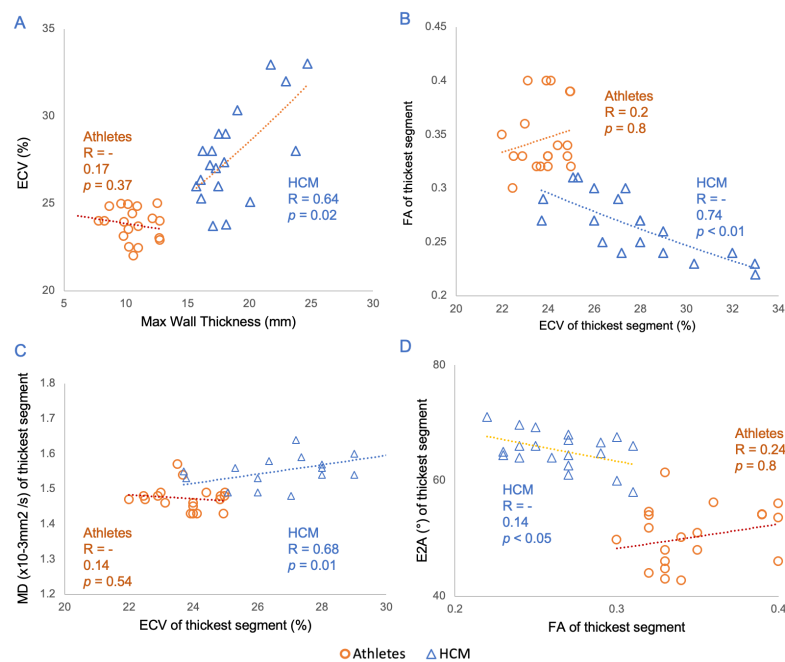
Figure 7.4: Correlations between wall thickness, ECV and DT-CMR

In the thickest segments of HCM patients, wall thickness correlated with ECV in the corresponding segment (panel A). ECV also correlated with FA (panel B) and MD (panel C). Lower FA correlated with higher E2A (panel D). Athletes meanwhile did not show any significant correlations between ECV and DT-CMR parameters in their thickest segments.

7.4 Discussion

This study directly compared DT-CMR parameters between normal volunteers, athletes and HCM patients. Our results demonstrate:

1) In mid systole, the myocardial sheetlets of HCM patients and athletes adopt steeper configurations than volunteers as reflected by the significantly higher global absolute E2A values. In HCM patients, this pattern is of an eccentric nature with highest values in their thickest segments, while athletes demonstrate a concentric rise in absolute E2A across the whole myocardium.

2) Diffusion is more unrestricted and anisotropic in the myocardium of HCM patients compared to athletes and volunteers as reflected by increased MD and decreased FA.

These results provide valuable insights into the underlying myocardial microstructural differences between volunteers, athletes and HCM patients.

7.4.1 Contractile configurations based on DT-CMR

In agreement with previously published studies, we demonstrated HCM patients to have significantly higher absolute E2A values than volunteers. (70,108) This is attributable to the pathologically hypercontracted myocardial sheetlet configurations in HCM patients. Our results demonstrate athletes have significantly higher absolute E2A values than volunteers, suggesting their laminar sheetlets are in a more 'hyper-angulated' state, possibly as a result of athletic remodelling, however not to the same extent as that seen in HCM patients. In the thickest segments of HCM patients, higher ECV correlated with lower FA and higher absolute E2A, suggesting that the expansion of extracellular space coupled with cardiomyocyte disarray results in the concomitant segment of myocardium adopting a more 'hyper-contracted' state in systole. Interestingly, in athletes, there was no significant difference in absolute E2A between their thickest and remote segments, indicating that the hyperangulation appears to be uniformly spread in concentric fashion across the entire myocardium as opposed to being exaggerated in the thickest segment as seen in HCM patients.

The cardiomyocytes in the myocardial mid-wall are made up of circumferentially oriented cardiomyocytes.(133) The mid-walls of HCM patients undergo disarray and fibrosis, particularly at the interventricular junctions and hypertrophied segments,(134) however given that the pattern of infiltration is diffuse, the distribution of circumferential mid-wall cardiomyocytes remains relatively unchanged overall. Hence the mean HA gradient progression in HCM and athletes is not expected to differ significantly from volunteers. The more gentle HA gradient progression per millimetre of LV wall observed in HCM patients and athletes compared to volunteers may be a reflection of the relatively increased wall thickness rather than a marker of pathology, as no significant differences were found in the HA progression per percentage of LV wall between the three cohorts. These findings warrant further investigations.

7.4.2 Fibrosis and cardiomyocyte disarray

MD is a measure of how freely water molecules can diffuse, and as biophysiological barriers such as cell membranes break down, MD is expected to increase. In keeping with previous DT-CMR studies on HCM patients (135), our results show a direct correlation between segmental MD and LGE values in HCM patients, who had significantly higher MD and LGE than athletes and volunteers. Histological analysis of healthy athlete hearts is lacking, however Swoboda *et al* (47) demonstrated athletes to have significantly lower ECV than HCM patients and postulated that the increase in LV mass in athletes is mediated by cellular hypertrophy, whereas in HCM it is driven by cellular disarray and extracellular matrix expansion. Cell membranes remain intact during cellular hypertrophy; hence changes in MD are likely to be less pronounced than in fibrosis. This likely explains how, despite having significantly thicker walls, athletes in our studies had comparable MD values to volunteers, but significantly lower than HCM patients. Meanwhile athletes with evidence of LGE, i.e., fibrosis, had significantly higher MD levels in their corresponding segments.

Histological analysis of myocardium resected from HCM patients undergoing surgical myectomy has demonstrated specimens to have disorganised matrix connective tissue and increased collagen content in comparison to volunteers.(136) In such areas of cardiomyocyte disarray, the diffusion of water molecules is expected to be more

isotropic, hence FA is expected to be low. Previous DT-CMR studies of ex-vivo human hearts have also demonstrated FA correlates negatively with histological measurements of collagen.(87) Therefore, the significantly lower FA values in HCM patients in this study compared with both volunteers and athletes is in agreement with findings from previous similar studies (68) and likely reflects a composite measure of both cardiomyocyte disarray and fibrosis. As discussed previously, athletes in our study had significantly thicker LV walls than volunteers, likely in response to athletic remodelling, but despite having significantly higher absolute E2A values than volunteers, FA values did not differ significantly between the two cohorts. This suggests athletic remodelling may result in the myocardial sheetlets adopting steeper configurations in systole; but does not lead to the disarray of cardiomyocytes as seen in HCM patients.

7.4.3 Limitations:

This is an exploratory study including only a limited number of subjects who were not age and sex matched. However, it is yet to be established whether DT-CMR parameters change with age or gender. The ECV of healthy volunteers was not obtained as it was not felt ethically justifiable to administer contrast in this cohort. Our study also lacked athletes and HCM patients with 'borderline' wall thickness between the 12-15mm range, however the intention for this study was to observe the microstructural differences between the different cohorts rather than assess the diagnostic capabilities of DT-CMR.

7.5 Conclusion

Athletic training is associated with a spectrum of morphological and functional changes in the myocardium. Through the use of DT-CMR, our study has derived possible preliminary insights into some of these changes in myocardial architecture in-vivo. Future DT-CMR studies should target larger cohorts of athletes with greater LV mass and wall thickness, in order to validate the clinical applicability and accuracy of these DT-CMR parameters in differentiating athlete's heart from HCM.

Chapter 8: Phenotyping hypertrophic cardiomyopathy using cardiac diffusion MRI: the relationship between microvascular dysfunction and microstructural changes

Short title: Phenotyping HCM using DT-CMR

8.1 Introduction

Microvascular dysfunction (MVD) is a common feature of HCM, (137) and is thought to be responsible for ischaemia-mediated myocyte death in HCM, which ultimately leads to replacement fibrosis and LV remodelling. (43) Prospective studies have identified the degree of MVD as an independent predictor of clinical decline and death in HCM patients; meanwhile patients can remain asymptomatic with severe MVD for several years prior to deterioration. (58) Hence MVD has been recognised as a potential target for prevention of disease progression and heart failure in HCM; but effective disease-modifying therapies have proved elusive. This may in-part be because of the incomplete understanding of the pathophysiological process. Abnormal muscle, abnormal physiology and abnormal architecture form the basis of various proposed mechanisms to explain the typical subendocardial pattern of hyperaemic ischaemia. While the cause is thought to be multifactorial, histological studies to date have failed to demonstrate any relationship between fiber disarray, fibrosis and small vessel disease. (138) Results from the previous chapter demonstrated how DT-CMR parameters vary between HCM and controls globally, and in morphologically abnormal (i.e hypertrophied and scarred) segments. In order to understand the relationship between myocardial microstructure and local vascular function, a more regional approach is required focussing specifically on areas with perfusion defects, such as the subendocardium. Focussed analysis of myocardial segments which lack typical morphological features such as wall hypertrophy and scar may also elucidate early microstructural changes that precede clinical expression of the disease.

8.1.1 Hypothesis and aims

The purpose of this study was to examine the associations between perfusion and DT-CMR parameters in HCM patients in order to understand the sequence of pathophysiology and the interrelation between vascular function and underlying myocardial microstructure. I hypothesised that there would be significant differences in DT-CMR parameters between healthy controls and even the 'normal' segments of HCM patients, where there is no evidence of perfusion defect, wall hypertrophy or scarring.

8.2 Methods

10 healthy controls and 20 HCM patients were recruited for this study. See chapter 3 for full details regarding subject recruitment (chapter 3.2), image acquisition (chapter 3.3.2), image analysis (chapter 3.4) and basic statistical analysis methods (3.5).

Detailed statistics

Pearson correlation analysis was used to calculate the correlation coefficients between different CMR biomarkers including wall thickness, DT-CMR, parametric and perfusion biomarkers. ANOVA with Bonferroni post-hoc comparisons were used to compare subgroups of myocardial segments in HCM patients (classified by wall thickness, myocardial perfusion reserve and the presence of LGE).

Subgroup Analysis

Subgroup analysis was carried out in order to investigate the DT-CMR characteristic of HCM segments with different morphological features (i.e wall hypertrophy, abnormal perfusion and presence of scar). The normal range for myocardial blood flow at stress, rest and the perfusion reserve were derived from age and sex-matched volunteers who underwent perfusion imaging as previously reported, (139) and were as follows: Stress MBF 1.3-3.7 ml/g/min, Rest MBF 0.4-1.8 ml/g/min and MPR 2.2 – 5.8. Hence 2.2 was used as a cut-off to define segments with abnormal perfusion. All myocardial segments of HCM patients were subsequently classified into the following 4 sub-

groups: **Group 1** (titled 'normal') included segments with normal wall thickness (≤11mm), normal perfusion reserve (≥2.2) and no visual LGE; **Group 2** (titled 'normal thickness, abnormal perfusion') included segments with normal wall thickness (≤11mm), abnormal perfusion reserve (<2.2) and no visual LGE; **Group 3** (titled 'wall hypertrophy, abnormal perfusion') included segments with abnormal wall thickness (>11mm), abnormal perfusion reserve (<2.2) and no visual LGE; and **Group 4** (titled 'scar') included all segments with visual evidence of LGE.

8.3 Results

The study flowchart is shown in Figure 8.1. Twenty HCM patients (M:F = 8:12, aged 48 ± 18 years) were included in the study; baseline characteristics are shown in Table 8.1. Two patients were unable to tolerate the side-effects of adenosine, hence the stress perfusion sequence was omitted. HCM patients had a mean ejection fraction of 67 ± 6%, mean myocardial mass of 149 ± 80 g and mean LGE of 5.9 ± 10.1%. Ten healthy controls (M:F = 4:6, aged 27 ± 9 years) underwent DT-CMR. Of all basal and mid slice segments, 24/240 segments (10%) were rejected due to imaging artefacts that remained post data rejection; these image artefacts resulted from unsuppressed fat, localised signal loss or low signal-noise ratio.
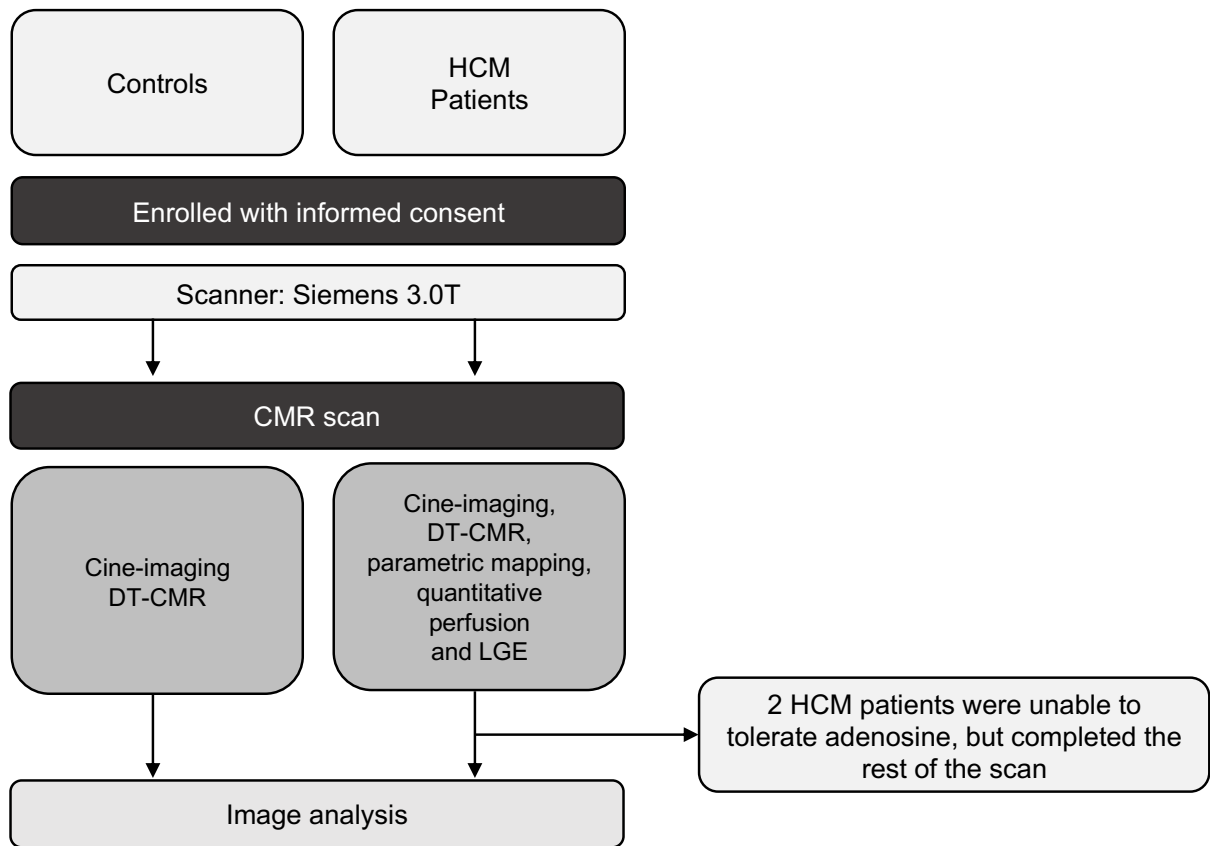
Figure 8.1: Flowchart of study enrolment

	HCM (n=20)	Controls (n=10)	P value
Age (years)	48 ± 18	27 ± 9	<0.01
Male (n)	8/20	4/10	1.00
BSA (m^2)	1.9 ± 0.2	2.2 ± 0.4	0.19
LV end-diastolic volume index (ml/m^2)	78 ± 14	80 ± 10	0.65
LV ejection fraction (%)	67 ± 6	64 ± 4	0.76
LV Mass index (g/m^2)	81 ± 41	61 ± 16	0.31
Maximal LV wall thickness (mmm)	19 ± 5	11 ± 1	<0.001
Left atrial diameter (mm)	43 ± 6	35 ± 2	<0.001
Global T1 (ms)	1323 ± 75	-	-
Global ECV (%)	27 ± 4	-	-
LGE present (n)	17 (85%)	-	-
LGE (% of LV mass)	5.9 ± 10.1	-	-

Table 8.1: Baseline characteristics of HCM patients and control subjects

Representative LGE, perfusion and DT-CMR maps are shown in Figure 8.2. HCM patients had significantly increased global MD (MD $_{HCM}$ 1.62±0.10 x10^{-3} mm^2/s vs MD $_{Controls}$ 1.47±0.1x10^{-3} mm^2/s, p<0.001), absolute E2A (E2A $_{HCM}$ 64±10° vs E2A $_{Controls}$ 36±12°, p<0.001) and significantly lower FA (FA $_{HCM}$ 0.29±0.04 vs FA $_{Controls}$ 0.34±0.04, p<0.001) than controls. HCM patients had significantly lower myocardial blood flow at both stress and at rest, and significantly lower mean myocardial perfusion reserve than controls (Stress MBF $_{HCM}$ = 1.4 ± 0.5 ml/g/min, Stress MBF $_{Controls}$ = 2.5 ± 0.6 ml/g/min, p<0.001, MPR $_{HCM}$ = 2.1 ± 0.8, MPR $_{controls}$ = 4.0 ± 0.9, p<0.001). Segmental MD correlated moderately with ECV (p<0.001, Figure 8.3a), LGE (p<0.001) and MPR in the corresponding segment (p<0.001, Figure 8.3b) while segmental absolute E2A correlated moderately with wall thickness (p<0.001, Figure 8.3c).
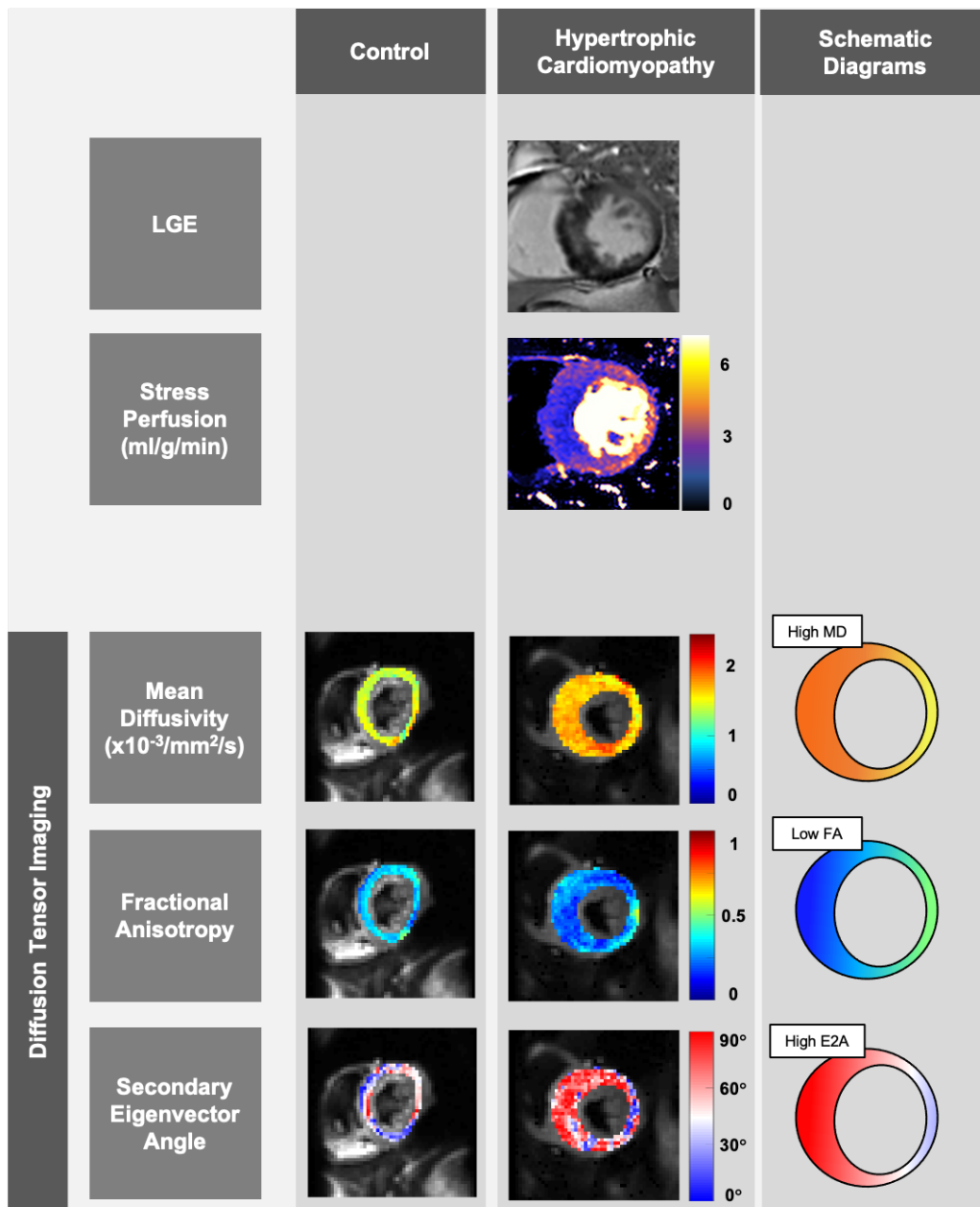
Figure 8.2: Representative maps for a healthy control subject and HCM patient

Representative mid left ventricular slices obtained in a healthy control subject (first column) and a patient with HCM (second column), with schematic diagrams (third column). On the LGE image, there is evidence of midwall fibrosis in the hypertrophied septal segments, which corresponds with reduced myocardial blood flow on the stress perfusion maps. On the diffusion tensor imaging maps, in comparison to the control subject, the HCM patient has increased MD, reduced FA and increased absolute E2A values globally, even in segments with normal wall thickness and no scar.

Panel A
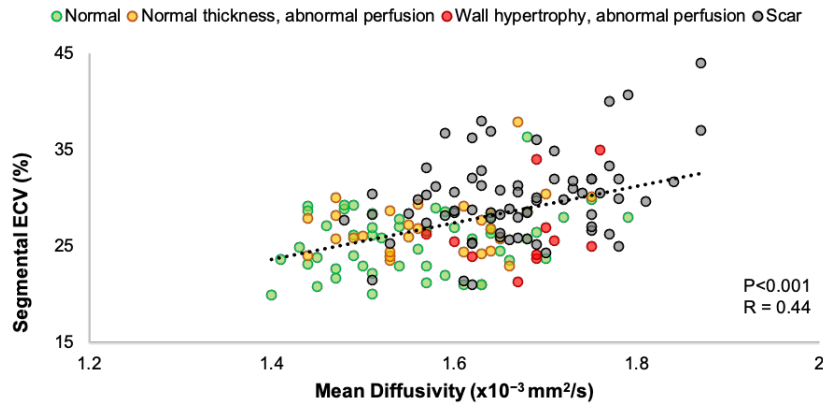
Panel B
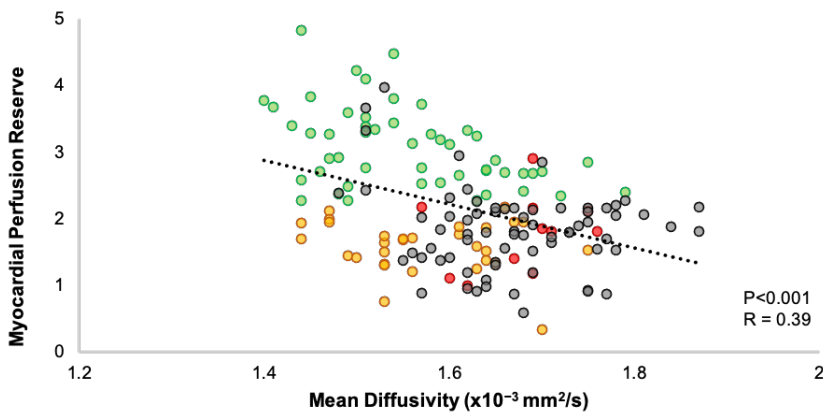
Panel C
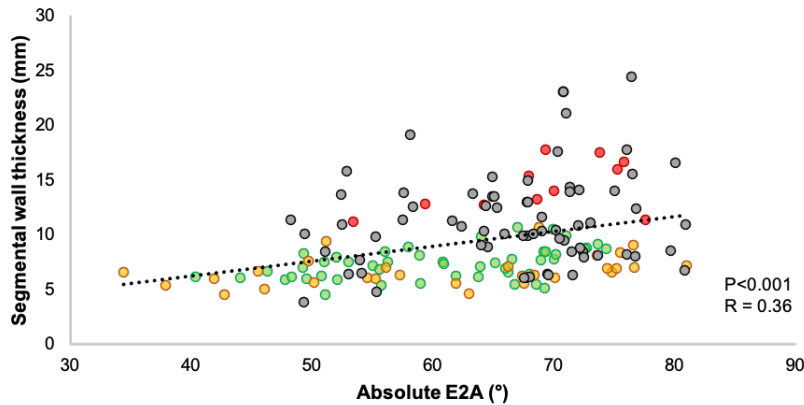
Figure 8.3: Correlations between ECV and wall thickness with perfusion and DT-CMR parameters

A positive correlation was noted between MD and ECV in the segments of HCM patients (Panel A). Segmental MD also correlated with myocardial perfusion reserve in corresponding segments (Panel B) and segmental absolute E2A in systole correlated with the wall thickness of corresponding segments in end diastole.

8.3.1 Subgroup analyses

The results of subgroup analysis are displayed in Table 8.2 and Figure 8.4. Of the 216 analysed segments, 63 (29%) were classified as 'normal' (group 1), 45 (21%) had 'normal thickness, abnormal perfusion' (group 2), 22 (10%) had 'wall hypertrophy, abnormal perfusion' (group 3) and 86 (40%) had 'scar' (group 4). Of note, there were no hypertrophied segments with normal perfusion. Compared to controls, 'normal' (Group 1) HCM segments had significantly increased MD (MD $_{\text{HCM Group1: Normal}}$ $1.56\pm0.09\text{x}10^{-3}$ mm^2/s vs MD $_{\text{Controls}}$ $1.47\pm0.08\text{x}10^{-3}$ mm^2/s, $p<0.001$), increased absolute E2A (E2A $_{\text{HCM Group 1: Normal}}$ $60\pm9°$ vs E2A $_{\text{Controls}}$ $38\pm12°$, $p<0.001$) and decreased FA (FA $_{\text{Group 1: Normal}}$ = 0.30 ± 0.04 vs FA $_{\text{Controls}}$ = 0.34 ± 0.03, $p<0.001$). Compared to segments with 'normal wall thickness, abnormal perfusion' (group 2), segments with 'wall hypertrophy, abnormal perfusion' (group 3) had significantly higher MD (MD $_{\text{Group 2: Normal thickness, abnormal perfusion}}$ $1.57\pm0.08\text{x}10^{-3}$ mm^2/s vs MD $_{\text{Group 3: Wall hypertrophy, abnormal perfusion}}$ $1.68\pm0.06\text{x}10^{-3}$ mm^2/s, $p<0.001$). Compared to the other groups, segments with LGE (group 4) had significantly higher MD (MD $_{\text{HCM Scar}}$ $1.67\pm0.09\text{x}10^{-3}$ mm^2/s vs MD $_{\text{HCM Groups 1-3: No Scar}}$ $1.58\pm0.09\text{x}10^{-3}$ mm^2/s, $p<0.001$) and significantly lower FA (FA $_{\text{HCM Group 4: Scar}}$ 0.26 ± 0.04 vs FA $_{\text{HCM Groups 1-3: No Scar}}$ 0.30 ± 0.03 $p<0.001$). Of note, there was no significant difference in absolute E2A between hypertrophied segments with and without scar.

Sub-groups of segments	Controls	Group 1 'Normal'	Group 2 'Normal wall thickness, abnormal perfusion'	Group 3 'Abnormal wall thickness, abnormal perfusion'	Group 4 'Scar'	ANOVA
Variable cut-offs:	-	Thickness ≤11mm MPR ≥ 2.2 No LGE	Thickness ≤11mm MPR <2.2 No LGE	Thickness > 11mm MPR <2.2 No LGE	LGE present	
Number of segments (%)	120 (100) *	63 (29)	45 (21)	22 (10)	86 (40)	-
Wall Thickness (mm)	7.6 ± 2.1 *	7.6 ± 1.5	6.9 ± 1.5	14.4 ± 2.7	11.3 ± 4.3	<0.001
LGE (%)	-	-	-	-	12.0 ± 13.2	-
Native T1 (ms)	-	1275 ± 48	1295 ± 62	1375 ± 55	1379 ± 76	<0.001
ECV (%)	-	24.9 ± 3.3	26.8 ± 2.8	25.4 ± 4.0	30.2 ± 3.8	<0.001
Stress MBF (ml/g/min)	2.5 ± 0.6 **	1.83 ± 0.37	1.41 ± 0.37	1.12 ± 0.38	1.11 ± 0.40	<0.001
Rest MBF (ml/g/min)	0.6 ± 0.1 **	0.63 ± 0.17	0.89 ± 0.19	0.60 ± 0.16	0.63 ± 0.18	<0.001
MPR	4.0 ± 0.9 **	2.99 ± 0.59	1.60 ± 0.35	1.82 ± 0.44	1.79 ± 0.61	<0.001
MD ($\times 10^{-3}$ mm^2/s)	1.47 ± 0.08 *	1.56 ± 0.09	1.57 ± 0.08	1.68 ± 0.06	1.67 ± 0.09	<0.001
FA	0.34 ± 0.03 *	0.30 ± 0.04	0.29 ± 0.03	0.29 ± 0.02	0.26 ± 0.04	<0.001
Absolute E2A (°)	38 ± 12 *	60 ± 9	61 ± 13	69 ± 7	68 ± 8	<0.001

Table 8.2: CMR results from sub-group analysis of HCM patients and healthy controls
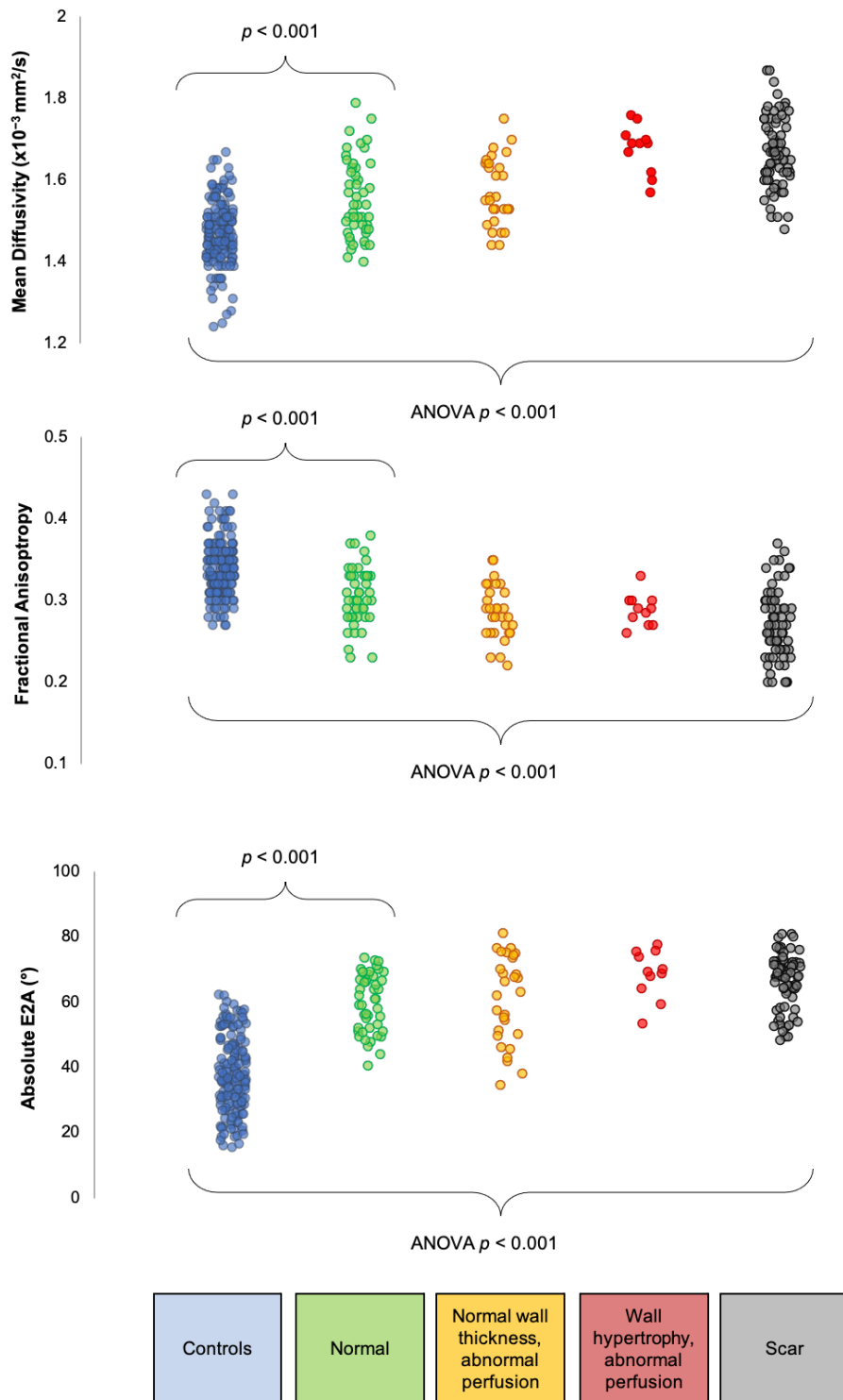
Figure 8.4: Subgroup analysis of DT-CMR parameters between different HCM segments

Segmental MD, FA and absolute E2A values are plotted according to the classification of the segments. 'Normal' HCM segments had significantly increased MD, absolute E2A and decreased FA than controls.

8.3.2 Regional variance in perfusion and DT-CMR

In HCM patients, subendocardial MBF during stress was significantly lower than subepicardial MBF during stress (1.28 ± 0.65 ml/g/min vs 1.47 ± 0.56 ml/g/min, p<0.001) and subendocardial MPR was significantly lower than subepicardial MPR (1.85± 0.83 vs 2.28 ± 0.87, p<0.001). Among controls, there was no difference between subendocardial and subepicardial MD, however HCM patients had significantly higher subendocardial MD than subepicardial MD (MD $_{Endo}$ 1.64±0.10x10^{-3} mm^2/s vs MD $_{Epi}$ 1.54±0.16x10^{-3} mm^2/s, p<0.001) as shown in Figure 8.5. All HCM segments were then subdivided into segments with normal perfusion reserve (MPR$\geq$2.2) and abnormal perfusion reserve (MPR<2.2). Even segments with normal perfusion reserve had significantly higher subendocardial MD than subepicardial MD (MD $_{Endo}$ 1.63±0.10x10^{-3} mm^2/s vs MD $_{Epi}$ 1.57±0.11x10^{-3} mm^2/s, p <0.01). This pattern was also seen in segments with abnormal perfusion reserve (MD $_{Endo}$ 1.62±0.14x10^{-3} mm^2/s vs MD $_{Epi}$ 1.56±0.12x10^{-3} mm^2/s, p <0.001). Subendocardial FA and subepicardial FA did not vary significantly in controls (FA $_{Endo}$ 0.34±0.05 vs FA $_{Epi}$ 0.34±0.05, p=0.82) or HCM patients (FA $_{Endo}$ 0.28±0.06 vs FA $_{Epi}$ 0.29±0.06, p=0.58).
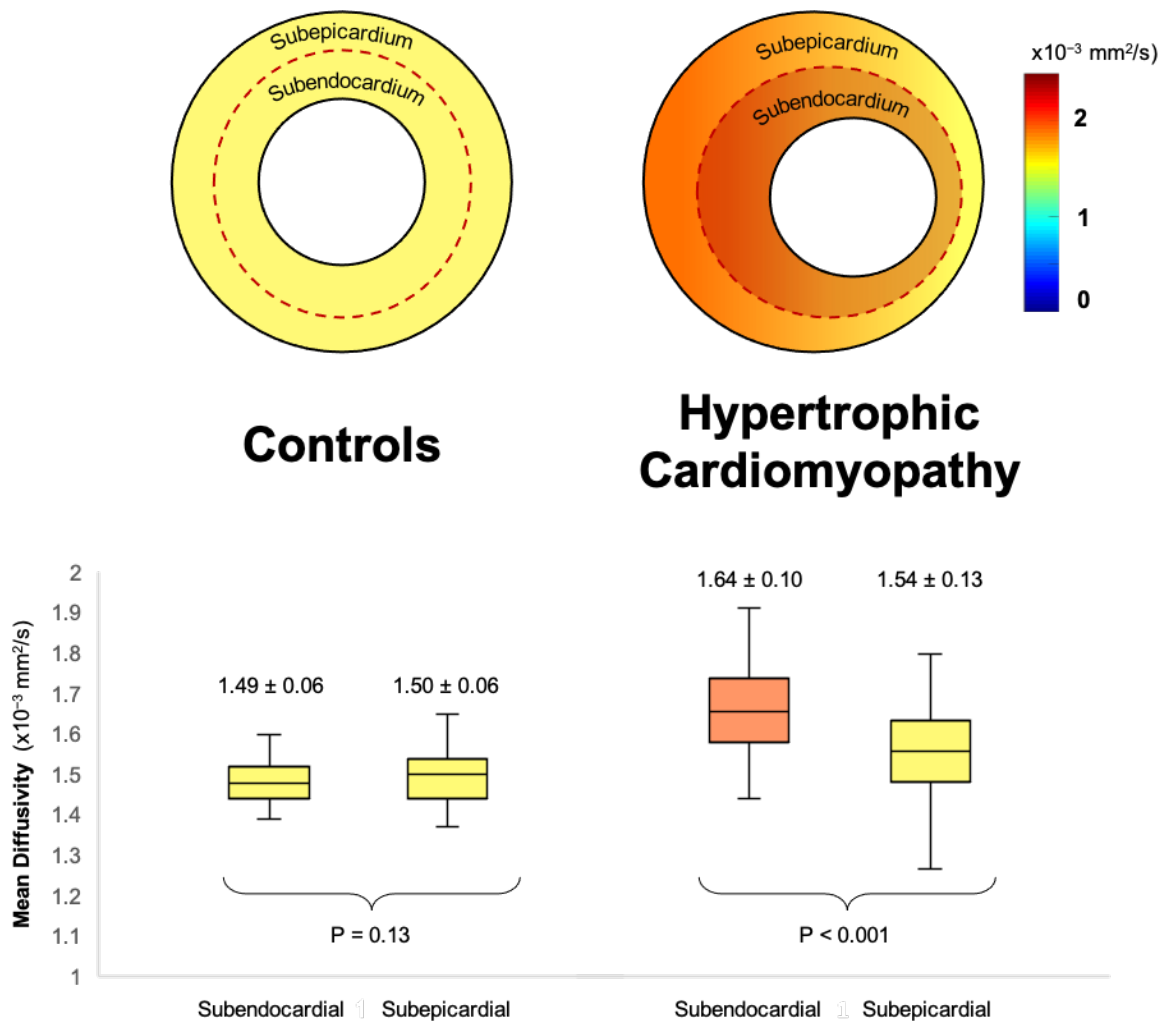
Figure 8.5: Regional variance in MD in healthy controls and HCM patients

In controls, there were no significant differences in subendocardial and subepicardial MD, however in HCM patients, subendocardial MD was significantly higher than subepicardial MD.

8.4 Discussion

In clinical practice, recognising the phenotypic expression of HCM is largely limited to the detection of wall hypertrophy and scar formation. This approach fails to acknowledge several of the underlying pathophysiological changes, such as MVD that is thought to precede macroscopic change and yet affect long-term clinical outcome. (57,58) In this prospective study we compare 20 HCM patients with controls, use quantitative perfusion to differentiate segments with normal and abnormal perfusion reserve; and use DT-CMR to gain insights into underlying microstructural differences.

The main findings from our study include: 1) HCM patients had increased MD, increased absolute E2A and reduced FA compared to controls, even in segments with normal thickness and normal perfusion reserve; 2) subendocardial MD was significantly higher than subepicardial MD, matching the pattern seen with perfusion imaging. The results from this study could help elucidate some early pathophysiological changes that occur in patients with HCM.

In agreement with the largest quantitative perfusion study of HCM patients to date, (57) our results demonstrate stress MBF and MPR to be reduced, particularly at the subendocardium; this occurs not only in hypertrophied and scarred segments, but also in segments that morphologically appear 'normal'. In fact, 42% of the segments with wall thickness <11mm had abnormally low MPR (>2.5 standard deviations lower than control cohort range), while all 108 segments with wall thickness >11mm had abnormally low MPR, supporting the hypothesis that microvascular dysfunction precedes the development of macroscopic abnormalities. (55,57)

Using DT-CMR, we compared the myocardium of controls with the myocardial segments of HCM patients that had normal wall thickness, normal perfusion reserve and no scar, and still noted several distinct microstructural differences, suggesting such changes may also precede the development of macroscopic abnormalities. Firstly, in these 'normal' HCM segments, MD was significantly higher than controls, suggesting water molecules are able to diffuse more freely. In healthy specimens, cell membranes provide a bio-physiological barrier for diffusion; and previous authors have observed how areas with high MD correlate with areas of scarring, fibrosis and increased ECV, where cellular apoptosis has resulted in the breakdown of cell membranes. (83,135) However in the 'normal' HCM segments in our study, ECV values were comparable with normal published values, (140) and there was no evidence of scar with LGE, warranting the exploration of alternative explanations. On a cellular level, a physical increase in myocyte size is a hallmark of HCM.(141) As previously shown in brain studies using diffusion-weighted imaging, (142,143) an increase in intracellular volume creates a greater distance between restrictive cell membranes, which results in increase in MD. Hence the increased subendocardial MD could be representative of regional myocyte hypertrophy. Various histological studies

have demonstrated subendocardial arterioles in HCM patients to have smaller cross-sectional lumen area (29) and greater coronary flow resistance (144) than controls, and authors have speculated whether this could be due to compressive effects of regional hypertrophy. (145,146)This hypothesis is supported by our finding of an inverse correlation between subendocardial MD and MPR, however histological corroboration of this is still lacking. The incremental increase in MD in segments with hypertrophy and scarring in our cohort correlates with an increase in ECV and LGE; and would seem to be more attributable to a gradual interstitial fibrotic process that ensues in these segments, as other authors have observed. (83,135)

In a recent pre-clinical DT-CMR study in which rat hearts underwent pressure-overload LV hypertrophy, the authors noted regional structural remodelling in the form of increased dispersion of the helix angle, most notably at the subendocardium of the specimens. (147) They did not report a subendocardial rise in MD, however it is worth noting that the pathophysiology of LVH in HCM is driven by sarcomeric mutations rather than pressure-overload.

Previous studies have observed absolute E2A to be globally increased in HCM patients compared to controls suggesting that the myocardial sheetlets adopt hypercontracted configurations during systole, (69,70,91) however in this study we demonstrate this to be the case even in segments with normal thickness and normal perfusion. Previous authors have speculated whether the compressive deformation of intramyocardial blood vessels during systole can explain the increased coronary flow resistance in these patients; (148) however results from our study are unable to corroborate this, as absolute E2A did not vary significantly between segments with normal and abnormal perfusion reserve. What we did note was a correlation between segmental absolute E2A and wall thickness. It is the dynamic rearrangement of the myocardial sheetlets that drives radial thickening during systole; however in HCM patients, sheetlet mobility is impaired so they remain hypercontracted and fail to relax in diastole. (70) This could explain why segments with higher absolute E2A in systole had greater LV wall thickness in end-diastole.

FA reflects the anisotropy of diffusion; studies have shown FA to correlate inversely with histological measurements of collagen, a major component of fibrotic tissue. (87)

This explains the significant reduction in FA in segments with scar in our study. Histological analysis of HCM patients undergoing surgical myomectomy has found that, in addition to collagen deposition, the specimens also had disorganised matrix connective tissue. (149) The diffusion of water molecules in enlarged cardiomyocytes within disorganised matrixes is more random and isotropic, leading to lower FA values. (68) Hence low FA in the absence of scar is suggestive of underlying cardiomyocyte disarray, which could explain why FA values were lower in HCM patients than controls even in segments with no scar. Preclinical studies on mice have noted cardiomyocyte disarray to be an early response to sarcomeric mutations, while hypertrophy and fibrosis occur later and are more secondary responses. (138) It remains to be seen if low FA values in the absence of scar in HCM patients can identify patients who are genotype-positive but phenotype-negative. A recent study by Ariga et al demonstrated an association between low FA and ventricular arrhythmia in HCM patients. (68) The authors used an alternative stimulated echo DT-CMR sequence which involves longer diffusion times, hence direct comparison of values cannot be made with our results, however the study still highlights the clinical relevance of low FA in the absence of scar in this population.

8.4.1 Limitations

The study sample is relatively small, but in keeping with similar studies. (91) DT-CMR volunteers were not age matched to the HCM subjects, however it is yet to be established whether DT-CMR parameters change with age. The ECV of healthy volunteers was not obtained, as it was not felt ethically justifiable to administer contrast in this cohort. Conclusions drawn from this study are based on correlations with published evidence and other cardiac MRI markers, whereas validation with histological specimens would be preferable. DT-CMR in a novel technique still under validation: as such the accuracy of DT-CMR measurements in relation to the impact of partial volume effects requires further investigations on a large multicentre scale.

8.5 Conclusion

By using a combination of quantitative perfusion and DT-CMR, our results demonstrate a complex relationship between abnormal anatomy, abnormal physiology and abnormal microstructure in HCM patients, the concomitant effects of which can help explain the underlying mechanisms behind MVD. Even in segments which lack phenotypic features of HCM, diffusion is more isotropic than controls, the myocardial sheetlets adopt hypercontracted configurations in mid-systole, and the mean diffusivity is higher particularly in the subendocardium, indicating regional remodelling which may impact on myocardial perfusion reserve. These findings highlight some of the microstructural changes that may precede macroscopic abnormalities and could prove useful for early detection of the disease, family screening and early phenotyping. Further larger studies will be needed to validate these findings.

Chapter 9: Conclusions and future directions

Recent advancements in CMR imaging have permitted the development of various sequences which are capable of depicting and quantifying myocardial oedema, scarring and contractility with great reproducibility and accuracy. While DT-CMR is a relatively novel sequence which requires further validation, it remains unique in its ability to characterise the organisation and integrity of underlying myocardial microstructure in-vivo – something previously only possible in post-mortem examinations. Thus, it is well suited for early detection of pathological and irreversible changes in the myocardium, which can assist clinicians in identifying patients with worse prognosis. This thesis primarily focusses on the clinical utility of DT-CMR in MI and HCM patients.

9.1 DT-CMR for MI patients

This work is currently the largest in-vivo DT-CMR study of STEMI patients. Previous studies to date, mainly based on animal specimens, demonstrated infarcted myocardium to have increased MD and reduced FA, reflecting how diffusion becomes more unrestricted and isotropic following the loss of organisation of cardiomyocytes. While the work in this thesis demonstrates this on a large cohort of patients, it also demonstrates for the first time regional impact of ischaemic injury to microstructural components, such as the loss of angularity of myocardial sheetlets in systole (through reduced E2A) and the loss of organisation among subendocardial myocytes (through reduced proportions of RHM in helix angle maps). The axes of microstructural components are shown to change from as early as a week following MI, and remain fixed over the following 12 months, highlighting how DT-CMR can allow for detection of early irreversible damage. Markers of severe injury in the acute scan, which includes reduced FA, reduced E2A and reduced RHM were all associated with lower LVEF and larger LV cavity size at 12 months, underpinning the predictive value of DT-CMR. These findings now warrant further validation in larger multicentre DT-CMR studies.

9.2 DT-CMR for HCM patients

Previous authors have already used DT-CMR to detect differences between healthy controls and HCM patients. In this thesis, we use DT-CMR to detect changes in the microstructure of HCM patients, even in segments with no macroscopic abnormalities. As well as elucidating the sequence of pathophysiology, our findings highlight how DT-CMR can be used for early detection of the disease, for instance in the screening of family members who are genotype positive but phenotype negative. We also for the first time detect increased MD at the subendocardium, which could signify regional remodelling and explain perfusion abnormalities seen in the HCM population. These findings also warrant further validation in larger multicentre DT-CMR studies with prospective follow up.

9.3 Future Directions

This thesis only explores the clinical utility in the MI and HCM population but opens the door for clinical applications in a wider range of conditions. Future studies may focus on the accuracy of DT-CMR in differentiating HCM from phenocopies such as hypertension and aortic stenosis, where LVH is mediated by increased afterload rather than genetic mutations. DT-CMR could also be used to detect irreversible damage to myocardium following inflammatory/autoimmune injury such as myocarditis. This would help identify the patients who will retain permanent scarring, reduced LVEF and ultimately carry a worse prognosis. Even within the MI population, DT-CMR may improve the detection of patients at higher risk of ventricular arrhythmia and sudden death, thus helping clinicians decide on who needs ICD therapy.

Spin-echo DT-CMR is a significant refinement of the STEAM technique as it is less susceptible to the effects of strain and does not require long breath-holding from the subjects. However, there are still numerous obstacles to overcome. DT-CMR acquisition times are still significantly longer than other sequences, making it less favourable in busy real-world practice. Tractography imaging can allow for more accurate definition of HA variation across the myocardium and scar borders, however this ideally requires full LV coverage, which markedly increases scan time, hence is

not feasible in patients shortly following MI, or with advanced heart failure. R-R variability significantly impacts on the signal-to-noise ratio (SNR) and image quality; hence it remains highly challenging to perform DT-CMR on patients with arrhythmia. Future work is needed to shorten scan duration times by using novel acceleration techniques such as compressed sensing and multiband imaging.

Through the validation work in this thesis, we demonstrate the stability of our DT-CMR sequence. However, DT-CMR sequences vary substantially from centre to centre. In order to pave the way for larger multi-centre studies, collaboration is required between the different centres on deciding upon the reference sequence parameters. The post-processing pathway also varies between centres, and is time-consuming, currently requiring visual inspection of all acquired images for quality control. Future approaches should look to take advantage of recent developments in artificial intelligence technology, with a view of using machine-based-learning driven algorithms to speed up and streamline this process. Ultimately, a unified post-processing pipeline needs to be established and adopted by all the different DT-CMR centres. This will need to be followed by inter-centre reproducibility studies, firstly in phantoms, followed by healthy controls and patients, which will enable us to confidently define a reference range for 'healthy myocardium' and help derive the thresholds for defining diseased myocardium in patients. Such validation work will be essential for merging DT-CMR into the clinical arena.

References

1. Aljizeeri A, Sulaiman A, Alhulaimi N, Alsaileek A, Al-Mallah MH. Cardiac magnetic resonance imaging in heart failure: where the alphabet begins! Heart Failure Reviews. 2017.

2. Saleh M, Ambrose JA. Understanding myocardial infarction. F1000Research. 2018;7.

3. Pasotti M, Prati F, Arbustini E. The pathology of myocardial infarction in the pre- and post-interventional era. Heart. 2006 Nov;92(11):1552–6.

4. St John Sutton M, Lee D, Rouleau JL, Goldman S, Plappert T, Braunwald E, et al. Left ventricular remodeling and ventricular arrhythmias after myocardial infarction. Circulation. 2003;107(20):2577–82.

5. Pfeffer MA, Braunwald E. Ventricular remodeling after myocardial infarction. Experimental observations and clinical implications. Circulation. 1990 Apr;81(4):1161–72.

6. Velagaleti RS, Pencina MJ, Murabito JM, Wang TJ, Parikh NI, D'Agostino RB, et al. Long-term trends in the incidence of heart failure after myocardial infarction. Circulation. 2008;118(20):2057–62.

7. Ibanez B, Aletras AH, Arai AE, Arheden H, Bax J, Berry C, et al. Cardiac MRI Endpoints in Myocardial Infarction Experimental and Clinical Trials: JACC Scientific Expert Panel. J Am Coll Cardiol. 2019;74(2):238–56.

8. De Waha S, Desch S, Eitel I, Fuernau G, Zachrau J, Leuschner A, et al. Impact of early vs. late microvascular obstruction assessed by magnetic resonance imaging on long-term outcome after ST-elevation myocardial infarction: A comparison with traditional prognostic markers. Eur Heart J. 2010;31(21):2660–8.

9. Stone GW, Selker HP, Thiele H, Patel MR, Udelson JE, Ohman EM, et al. Relationship between Infarct Size and Outcomes Following Primary PCI Patient-

Level Analysis from 10 Randomized Trials. J Am Coll Cardiol. 2016;67(14):1674–83.

10. de Waha S, Patel MR, Granger CB, Ohman EM, Maehara A, Eitel I, et al. Relationship between microvascular obstruction and adverse events following primary primary percutaneous coronary intervention for ST-segment elevation myocardial infarction: an individual patient data pooled analysis from seven randomized trials. Eur Heart J. 2017;

11. Bulluck H, Hammond-Haley M, Weinmann S, Martinez-Macias R, Hausenloy DJ. Myocardial Infarct Size by CMR in Clinical Cardioprotection Studies: Insights From Randomized Controlled Trials. JACC Cardiovasc Imaging. 2017;10(3):230–40.

12. Kidambi A, Motwani M, Uddin A, Ripley DP, McDiarmid AK, Swoboda PP, et al. Myocardial Extracellular Volume Estimation by CMR Predicts Functional Recovery Following Acute MI. JACC Cardiovasc Imaging. 2017 Sep 1;10(9):989–99.

13. Ferreira VM, Piechnik SK. CMR Parametric Mapping as a Tool for Myocardial Tissue Characterization. Korean Circ J. 2020 Aug;50(8):658–76.

14. Salerno M, Kramer CM. Advances in parametric mapping with CMR imaging. JACC Cardiovasc Imaging. 2013 Jul;6(7):806–22.

15. Piechnik SK, Ferreira VM, Lewandowski AJ, Ntusi NA, Banerjee R, Holloway C, et al. Normal variation of magnetic resonance T1 relaxation times in the human population at 1.5 T using ShMOLLI. J Cardiovasc Magn Reson. 2013 Dec 20;15(1):13.

16. Khan JN, McCann GP. Cardiovascular magnetic resonance imaging assessment of outcomes in acute myocardial infarction. World J Cardiol. 2017;9(2):109.

17. Carberry J, Carrick D, Haig C, Ahmed N, Mordi I, McEntegart M, et al. Persistent Iron Within the Infarct Core After ST-Segment Elevation Myocardial Infarction.

Implications for Left Ventricular Remodeling and Health Outcomes. JACC: Cardiovascular Imaging. 2017;

18. Dall'Armellina E, Piechnik SK, Ferreira VM, Si Q Le, Robson MD, Francis JM, et al. Cardiovascular magnetic resonance by non contrast T1-mapping allows assessment of severity of injury in acute myocardial infarction. J Cardiovasc Magn Reson. 2012;

19. Liu D, Borlotti A, Viliani D, Jerosch-Herold M, Alkhalil M, De Maria GL, et al. CMR Native T1 Mapping Allows Differentiation of Reversible Versus Irreversible Myocardial Damage in ST-Segment-Elevation Myocardial Infarction: An OxAMI Study (Oxford Acute Myocardial Infarction). Circ Cardiovasc Imaging. 2017;10(8).

20. Carrick D, Haig C, Rauhalammi S, Ahmed N, Mordi I, McEntegart M, et al. Prognostic significance of infarct core pathology revealed by quantitative non-contrast in comparison with contrast cardiac magnetic resonance imaging in reperfused ST-elevation myocardial infarction survivors. Eur Heart J. 2016;37(13):1044–59.

21. Kidambi A, Motwani M, Uddin A, Ripley DP, McDiarmid AK, Swoboda PP, et al. Myocardial Extracellular Volume Estimation by CMR Predicts Functional Recovery Following Acute MI. JACC Cardiovasc Imaging. 2016;1–11.

22. Carberry J, Carrick D, Haig C, Rauhalammi SM, Ahmed N, Mordi I, et al. Remote Zone Extracellular Volume and Left Ventricular Remodeling in Survivors of ST-Elevation Myocardial Infarction. Hypertension. 2016;68(2):385–91.

23. Reinstadler SJ, Stiermaier T, Liebetrau J, Fuernau G, Eitel C, de Waha S, et al. Prognostic Significance of Remote Myocardium Alterations Assessed by Quantitative Noncontrast T1 Mapping in ST-Segment Elevation Myocardial Infarction. JACC Cardiovasc Imaging. 2018;11(3):373–82.

24. Eitel I, Stiermaier T, Lange T, Rommel K-P, Koschalka A, Kowallick JT, et al. Cardiac Magnetic Resonance Myocardial Feature Tracking for Optimized

Prediction of Cardiovascular Events Following Myocardial Infarction. JACC Cardiovasc Imaging. 2018;

25. Bolognese L, Neskovic AN, Parodi G, Cerisano G, Buonamici P, Santoro GM, et al. Left ventricular remodeling after primary coronary angioplasty: Patterns of left ventricular dilation and long-term prognostic implications. Circulation. 2002;106(18):2351–7.

26. Pedrizzetti G, Claus P, Kilner PJ, Nagel E. Principles of cardiovascular magnetic resonance feature tracking and echocardiographic speckle tracking for informed clinical use. J Cardiovasc Magn Reson. 2016 Dec 26;18(1):51.

27. Cecchi F, Charron P, Alain Hagege A, Lafont A, Limongelli G, Mahrholdt H, et al. ESC GUIDELINES 2014 ESC Guidelines on diagnosis and management of hypertrophic cardiomyopathy The Task Force for the Diagnosis and Management of Hypertrophic Cardiomyopathy of the European Society of Cardiology (ESC).

28. Noorden S V., Olsen EGJ, Pearse AGE. Hypertrophic obstructive cardiomyopathy, a histological, histochemical, and ultrastructural study of biopsy material. Cardiovasc Res. 1971 Jan 1;5(1):118–31.

29. Schwartzkopff B, Mundhenke M, Strauer BE. Alterations of the Architecture of Subendocardial Arterioles in Patients With Hypertrophic Cardiomyopathy and Impaired Coronary Vasodilator Reserve: A Possible Cause for Myocardial Ischemia. J Am Coll Cardiol. 1998 Apr 1;31(5):1089–96.

30. Anderson KR, Sutton MGSJ, Lie JT. Histopathological types of cardiac fibrosis in myocardial disease. J Pathol. 1979 Jun 1;128(2):79–85.

31. Hughes SE. The pathology of hypertrophic cardiomyopathy. Histopathology. 2004 May 1;44(5):412–27.

32. Maron MS. Clinical utility of cardiovascular magnetic resonance in hypertrophic cardiomyopathy. Journal of Cardiovascular Magnetic Resonance. 2012.

33. Semsarian C, Ingles J, Maron MS, Maron BJ. New Perspectives on the Prevalence of Hypertrophic Cardiomyopathy. J Am Coll Cardiol. 2015 Mar 31;65(12):1249–54.

34. Maron BJ, Maron MS. Hypertrophic cardiomyopathy. Lancet (London, England). 2013 Jan 19;381(9862):242–55.

35. Maron BJ, Niimura H, Casey SA, Soper MK, Wright GB, Seidman J., et al. Development of left ventricular hypertrophy in adults with hypertrophic cardiomyopathy caused by cardiac myosin-binding protein C gene mutations. J Am Coll Cardiol. 2001 Aug 1;38(2):315–21.

36. Pennell DJ. Cardiovascular magnetic resonance. Circulation. 2010 Feb 9;121(5):692–705.

37. Maron BJ, Yeates L, Semsarian C. Clinical challenges of genotype positive (+)-phenotype negative (-) family members in hypertrophic cardiomyopathy. Am J Cardiol. 2011 Feb 15;107(4):604–8.

38. Maron MS, Maron BJ, Harrigan C, Buros J, Gibson CM, Olivotto I, et al. Hypertrophic Cardiomyopathy Phenotype Revisited After 50 Years With Cardiovascular Magnetic Resonance. J Am Coll Cardiol. 2009 Jul 14;54(3):220–8.

39. Maron MS, Finley JJ, Bos JM, Hauser TH, Manning WJ, Haas TS, et al. Prevalence, clinical significance, and natural history of left ventricular apical aneurysms in hypertrophic cardiomyopathy. Circulation. 2008 Oct 7;118(15):1541–9.

40. Maron MS, Olivotto I, Harrigan C, Appelbaum E, Gibson CM, Lesser JR, et al. Mitral valve abnormalities identified by cardiovascular magnetic resonance represent a primary phenotypic expression of hypertrophic cardiomyopathy. Circulation. 2011 Jul 5;124(1):40–7.

41. Harrigan CJ, Appelbaum E, Maron BJ, Buros JL, Gibson CM, Lesser JR, et al. Significance of papillary muscle abnormalities identified by cardiovascular

magnetic resonance in hypertrophic cardiomyopathy. Am J Cardiol. 2008 Mar 1;101(5):668–73.

42.   Varma P, Neema P. Hypertrophic cardiomyopathy: Part 1 - Introduction, pathology and pathophysiology. Ann Card Anaesth. 2014;17(2):118.

43.   Maron MS, Olivotto I, Maron BJ, Prasad SK, Cecchi F, Udelson JE, et al. The Case for Myocardial Ischemia in Hypertrophic Cardiomyopathy. J Am Coll Cardiol. 2009 Aug 25;54(9):866–75.

44.   Galati G, Leone O, Pasquale F, Olivotto I, Biagini E, Grigioni F, et al. Histological and Histometric Characterization of Myocardial Fibrosis in End-Stage Hypertrophic Cardiomyopathy: A Clinical-Pathological Study of 30 Explanted Hearts. Circ Heart Fail. 2016 Sep;9(9).

45.   Maron BJ. Distinguishing hypertrophic cardiomyopathy from athlete's heart physiological remodelling: clinical significance, diagnostic strategies and implications for preparticipation screening. Br J Sports Med. 2009 Sep 1;43(9):649–56.

46.   Małek ŁA, Bucciarelli-Ducci C, Łukasz Małek CA. Myocardial fibrosis in athletes- Current perspective. 2020;

47.   Swoboda PP, McDiarmid AK, Erhayiem B, Broadbent DA, Dobson LE, Garg P, et al. Assessing Myocardial Extracellular Volume by T1 Mapping to Distinguish Hypertrophic Cardiomyopathy from Athlete's Heart. Journal of the American College of Cardiology. 2016.

48.   Deva DP, Hanneman K, Li Q, Ng MY, Wasim S, Morel C, et al. Cardiovascular magnetic resonance demonstration of the spectrum of morphological phenotypes and patterns of myocardial scarring in Anderson-Fabry disease. J Cardiovasc Magn Reson. 2016 Dec 31;18(1):14.

49.   Moon JCC, McKenna WJ, McCrohon JA, Elliott PM, Smith GC, Pennell DJ. Toward clinical risk assessment in hypertrophic cardiomyopathy with gadolinium cardiovascular magnetic resonance. J Am Coll Cardiol. 2003 May 7;41(9):1561–

7.

50. Choudhury L, Mahrholdt H, Wagner A, Choi KM, Elliott MD, Klocke FJ, et al. Myocardial scarring in asymptomatic or mildly symptomatic patients with hypertrophic cardiomyopathy. J Am Coll Cardiol. 2002 Dec 18;40(12):2156–64.

51. Xu J, Zhuang B, Sirajuddin A, Li S, Huang J, Yin G, et al. MRI T1 Mapping in Hypertrophic Cardiomyopathy: Evaluation in Patients Without Late Gadolinium Enhancement and Hemodynamic Obstruction. Radiology. 2020;294(2):275–86.

52. Huang L, Ran L, Zhao P, Tang D, Han R, Ai T, et al. MRI native T1 and T2 mapping of myocardial segments in hypertrophic cardiomyopathy: tissue remodeling manifested prior to structure changes. Br J Radiol. 2019 Dec;92(1104):20190634.

53. Ruberg FL. T1 mapping in cardiac amyloidosis: Can we get there from here? JACC: Cardiovascular Imaging. 2013.

54. Camici P, Chiriatti G, Lorenzoni R, Bellina RC, Gistri R, Italiani G, et al. Coronary vasodilation is impaired in both hypertrophied and nonhypertrophied myocardium of patients with hypertrophic cardiomyopathy: a study with nitrogen-13 ammonia and positron emission tomography. J Am Coll Cardiol. 1991 Mar 15;17(4):879–86.

55. Petersen SE, Jerosch-Herold M, Hudsmith LE, Robson MD, Francis JM, Doll HA, et al. Evidence for Microvascular Dysfunction in Hypertrophic Cardiomyopathy. Circulation. 2007 May 8;115(18):2418–25.

56. Chiribiri A, Leuzzi S, Conte MR, Bongioanni S, Bratis K, Olivotti L, et al. Rest perfusion abnormalities in hypertrophic cardiomyopathy: correlation with myocardial fibrosis and risk factors for sudden cardiac death. Clin Radiol. 2015;70:495–501.

57. Camaioni C, Knott KD, Augusto JB, Seraphim A, Rosmini S, Ricci F, et al. Inline perfusion mapping provides insights into the disease mechanism in hypertrophic cardiomyopathy. Heart. 2019;

58. Cecchi F, Olivotto I, Gistri R, Lorenzoni R, Chiriatti G, Camici PG. Coronary Microvascular Dysfunction and Prognosis in Hypertrophic Cardiomyopathy. Vol. 11, n engl j med. 2003.

59. Robinson AA, Salerno M, Kramer CM. Contemporary Issues in Quantitative Myocardial Perfusion CMR Imaging. Curr Cardiovasc Imaging Rep. 2019 Mar 14;12(3):9.

60. Einstein A. Über die von der molekularkinetischen Theorie der Wärme geforderte Bewegung von in ruhenden Flüssigkeiten suspendierten Teilchen. Ann Phys. 1905 Jan 1;322(8):549–60.

61. Huisman TAGM. Diffusion-weighted and diffusion tensor imaging of the brain, made easy. Cancer Imaging. 2010 Oct 4;10 Spec no(SPEC. ISS. A):S163-71.

62. Le Bihan D, Breton E, Lallemand D, Grenier P, Cabanis E, Laval-Jeantet M. MR imaging of intravoxel incoherent motions: application to diffusion and perfusion in neurologic disorders. Radiology. 1986 Nov;161(2):401–7.

63. Stejskal EO, Tanner JE. Spin Diffusion Measurements: Spin Echoes in the Presence of a Time-Dependent Field Gradient. J Chem Phys. 1965 Jan 2;42(1):288–92.

64. Reese TG, Weisskoff RM, Smith RN, Rosen BR, Dinsmore RE, Wedeen VJ. Imaging myocardial fiber architecture in vivo with magnetic resonance. Magn Reson Med. 1995 Dec;34(6):786–91.

65. Wu MT, Su MYM, Huang YL, Chiou KR, Yang P, Pan HB, et al. Sequential Changes of Myocardial Microstructure in Patients Postmyocardial Infarction by Diffusion-Tensor Cardiac MRCLINICAL PERSPECTIVE. Circ Cardiovasc Imaging. 2009;2(1):32.

66. Tseng WY, Reese TG, Weisskoff RM, Wedeen VJ. Cardiac diffusion tensor MRI in vivo without strain correction. Magn Reson Med. 1999 Aug;42(2):393–403.

67. Wu M-T, Wen-Yih ;, Tseng I, Mao-Yuan ;, Su M, Liu C-P, et al. Diffusion Tensor

Magnetic Resonance Imaging Mapping the Fiber Architecture Remodeling in Human Myocardium After Infarction Correlation With Viability and Wall Motion. 2006;

68. Ariga R, Tunnicliffe EM, Manohar SG, Mahmod M, Raman B, Piechnik SK, et al. Identification of Myocardial Disarray in Patients With Hypertrophic Cardiomyopathy and Ventricular Arrhythmias. J Am Coll Cardiol. 2019;73:2493–502.

69. Nielles-Vallespin S, Khalique Z, Ferreira PF, de Silva R, Scott AD, Kilner P, et al. Assessment of Myocardial Microstructural Dynamics by In Vivo Diffusion Tensor Cardiac Magnetic Resonance. J Am Coll Cardiol. 2017;69(6):66.

70. Ferreira PF, Kilner PJ, Mcgill LA, Nielles-Vallespin S, Scott AD, Ho SY, et al. In vivo cardiovascular magnetic resonance diffusion tensor imaging shows evidence of abnormal myocardial laminar orientations and mobility in hypertrophic cardiomyopathy. J Cardiovasc Magn Reson. 2014;

71. Jones DK, Horsfield MA, Simmons A. Optimal strategies for measuring diffusion in anisotropic systems by magnetic resonance imaging. Magn Reson Med. 1999 Sep 1;42(3):515–25.

72. Basser PJ, Mattiello J, LeBihan D. MR diffusion tensor spectroscopy and imaging. Biophys J. 1994;

73. Ahn S, Lee S-K. Diffusion Tensor Imaging: Exploring the Motor Networks and Clinical Applications. Korean J Radiol. 2011;12(6):651.

74. Holmes AA, Scollan DF, Winslow RL. Direct histological validation of diffusion tensor MRI in formaldehyde- fixed myocardium. Magn Reson Med. 2000;44(1):157–61.

75. Teh I, McClymont D, Burton RAB, Maguire ML, Whittington HJ, Lygate CA, et al. Resolving fine cardiac structures in rats with high-resolution diffusion tensor imaging. Sci Rep. 2016;

76. Scollan DF, Holmes A, Winslow R, Forder J, Histological JF. Histological validation of myocardial microstructure obtained from diffusion tensor magnetic resonance imaging. 2020.

77. Hsu EW, Muzikant AL, Matulevicius SA, Penland RC, Henriquez CS. Magnetic resonance myocardial fiber-orientation mapping with direct histological correlation. Am J Physiol. 1998;

78. Pettigrew JB. On the Arrangement of the Muscular Fibres in the Ventricles of the Vertebrate Heart; with Physiological Remarks. Am J Med Sci. 1866;51(102):497–502.

79. Mekkaoui C, Jackowski MP, Kostis WJ, Stoeck CT, Thiagalingam A, Reese TG, et al. Myocardial scar delineation using diffusion tensor magnetic resonance tractography. J Am Heart Assoc. 2018;7(3).

80. Von Deuster C, Stoeck CT, Genet M, Atkinson D, Kozerke S. Spin Echo Versus Stimulated Echo Diffusion Tensor Imaging of the In Vivo Human Heart. Magn Reson Med. 2016;76(3):862–72.

81. Christian S, Deuster C von, Martin G, David A, Sebastian K. Second-order motion-compensated spin echo diffusion tensor imaging of the human heart. Magn Reson Med. 2015 May;75(4):1669–76.

82. Scollan DF, Holmes A, Winslow R, Forder J. Histological validation of myocardial microstructure obtained from diffusion tensor magnetic resonance imaging. Am J Physiol - Hear Circ Physiol. 1998;

83. Chen J, Song S-K, Liu W, McLean M, Allen JS, Tan J, et al. Remodeling of cardiac fiber structure after infarction in rats quantified with diffusion tensor MRI. Am J Physiol - Hear Circ Physiol. 2003;285(3):946–54.

84. Nguyen C, Fan Z, Xie Y, Dawkins J, Tseliou E, Bi X, et al. In vivo contrast free chronic myocardial infarction characterization using diffusion-weighted cardiovascular magnetic resonance. 2014.

85.   Wang Y, Cai W, Wang L, Xia R, Chen W, Zheng J, et al. Evaluation of the differences of myocardial fibers between acute and chronic myocardial infarction: Application of diffusion tensor magnetic resonance imaging in a rhesus monkey model. Korean J Radiol. 2016;17(5):725–33.

86.   Moulin K, Viallon M, Romero W, Chazot A, Mewton N, Isaaz K, et al. MRI of reperfused acute myocardial infarction edema: ADC quantification versus T1 and T2 mapping. Radiology. 2020;295(3):542–9.

87.   Abdullah OM, Drakos SG, Diakos NA, Wever-Pinzon O, Kfoury AG, Stehlik J, et al. Characterization of Diffuse Fibrosis in the Failing Human Heart via Diffusion Tensor Imaging and Quantitative Histological Validation NIH Public Access. NMR Biomed. 2014;3100(1):1378–86.

88.   Nguyen C, Fan Z, Sharif B, He Y, Dharmakumar R, Berman DS, et al. In vivo three-dimensional high resolution cardiac diffusion-weighted MRI: A motion compensated diffusion-prepared balanced steady-state free precession approach. Magn Reson Med. 2014 Nov 1;72(5):1257–67.

89.   Teh I, Romero W, Dall'Armellina E, Ennis D, Ferreira PF, Kalra P, Kolipaka A, Kozerke S, Lohr D, Moulin K, Nguyen C, Nielles-Vallespin S, Pontre B, Schreiber LM, Scott A, Sosnovik D, Stoeck CT, Tous C, Tunnicliffe E, Wang V, Weng AM, Young A, Croisille P, SJ. Multi-centre evaluation of diffusion tensor imaging (DTI) in an isotropic phantom: Towards validation of cardiac DTI sequences. In: SCMR. 2020.

90.   Mills R. Self-diffusion in normal and heavy water in the range 1-45.deg. J Phys Chem. 1973 Mar 1;77(5):685–8.

91.   Das A, Chowdhary A, Kelly C, Teh I, Stoeck CT, Kozerke S, et al. Insight Into Myocardial Microstructure of Athletes and Hypertrophic Cardiomyopathy Patients Using Diffusion Tensor Imaging. J Magn Reson Imaging. 2020;

92.   Elliott PM. 2014 ESC guidelines on diagnosis and management of hypertrophic cardiomyopathy. Russ J Cardiol. 2015;

93. Stoeck CT, Von Deuster C, GeneT M, Atkinson D, Kozerke S. Second-order motion-compensated spin echo diffusion tensor imaging of the human heart. Magn Reson Med. 2016;75(4):1669–76.

94. Simonetti OP, Finn JP, White RD, Laub G, Henry DA. Black blood T2-weighted inversion-recovery MR imaging of the heart. Radiology. 1996 Apr 1;199(1):49–57.

95. Andersson T, Romu T, Karlsson A, Norén B, Forsgren MF, Smedby Ö, et al. Consistent intensity inhomogeneity correction in water-fat MRI. J Magn Reson Imaging. 2015 Aug 1;42(2):468–76.

96. Zaman A, Higgins DM, Motwani M, Kidambi A, Kouwenhoven M, Kozerke S, et al. Robust myocardial T_2 and T_2* mapping at 3T using image-based shimming. J Magn Reson Imaging. 2015 Apr 1;41(4):1013–20.

97. Brown LAE, Saunderson CED, Das A, Craven T, Levelt E, Knott KD, et al. A comparison of standard and high dose adenosine protocols in routine vasodilator stress cardiovascular magnetic resonance: dosage affects hyperaemic myocardial blood flow in patients with severe left ventricular systolic impairment. J Cardiovasc Magn Reson. 2021 Dec 18;23(1):37.

98. Nguyen CT, Christodoulou AG, Coll-Font J, Ma S, Xie Y, Reese TG, et al. Free-breathing diffusion tensor MRI of the whole left ventricle using second-order motion compensation and multitasking respiratory motion correction. Magn Reson Med. 2021 May 30;85(5):2634–48.

99. Kellman P, Hansen MS, Nielles-Vallespin S, Nickander J, Themudo R, Ugander M, et al. Myocardial perfusion cardiovascular magnetic resonance: optimized dual sequence and reconstruction for quantification. J Cardiovasc Magn Reson. 2017;

100. Kramer CM, Barkhausen J, Flamm SD, Kim RJ, Nagel E. Standardized cardiovascular magnetic resonance (CMR) protocols 2013 update. Journal of Cardiovascular Magnetic Resonance. 2013.

101. Augusto JB, Davies RH, Bhuva AN, Knott KD, Seraphim A, Alfarih M, et al. Articles Diagnosis and risk stratification in hypertrophic cardiomyopathy using machine learning wall thickness measurement: a comparison with human test−retest performance. 2020;

102. Freitas P, Ferreira AM, Arteaga-Fernández E, De Oliveira Antunes M, Mesquita J, Abecasis J, et al. The amount of late gadolinium enhancement outperforms current guideline-recommended criteria in the identification of patients with hypertrophic cardiomyopathy at risk of sudden cardiac death.

103. Cerqueira MD, Weissman NJ, Dilsizian V, Jacobs AK, Kaul S, Laskey WK, et al. Standardized myocardial segmentation and nomenclature for tomographic imaging of the heart: A statement for healthcare professionals from the Cardiac Imaging Committee of the Council on Clinical Cardiology of the American Heart Association. J Nucl Cardiol. 2002;

104. Messroghli DR, Moon JC, Ferreira VM, Grosse-Wortmann L, He T, Kellman P, et al. Clinical recommendations for cardiovascular magnetic resonance mapping of T1, T2, T2 and extracellular volume: A consensus statement by the Society for Cardiovascular Magnetic Resonance (SCMR) endorsed by the European Association for Cardiovascular Imagin. Vol. 19, Journal of Cardiovascular Magnetic Resonance. 2017.

105. Anderson LJ, Holden S, Davis B, Prescott E, Charrier CC, Bunce NH, et al. Cardiovascular T2-star (T2*) magnetic resonance for the early diagnosis of myocardial iron overload. Eur Heart J. 2001;22:2171–9.

106. DeLong ER, DeLong DM, Clarke-Pearson DL. Comparing the Areas under Two or More Correlated Receiver Operating Characteristic Curves: A Nonparametric Approach. Biometrics. 1988 Sep;44(3):837.

107. Gerdes AM, Capasso JM. Structural remodeling and mechanical dysfunction of cardiac myocytes in heart failure. J Mol Cell Cardiol. 1995 Mar 1;27(3):849–56.

108. Nielles-Vallespin S, Scott A, Ferreira P, Khalique Z, Pennell D, Firmin D. Cardiac

Diffusion: Technique and Practical Applications. J Magn Reson Imaging. 2020;52(2):348–68.

109. Lee SE, Nguyen C, Yoon J, Chang HJ, Kim S, Kim CH, et al. Three-dimensional Cardiomyocytes Structure Revealed by Diffusion Tensor Imaging and Its Validation Using a Tissue-Clearing Technique. Sci Rep. 2018;8(1).

110. Holmes JW, Nunez JA, Covell JW. Functional implications of myocardial scar structure. Am J Physiol - Hear Circ Physiol. 1997;5(2):2123–30.

111. Reimer KA, Jennings RB. The "wavefront phenomenon" of myocardial ischemic cell death. II. Transmural progression of necrosis within the framework of ischemic bed size (myocardium at risk) and collateral flow. Lab Investig. 1979;

112. Mojsejenko D, Mcgarvey JR, Dorsey SM, Gorman Iii JH, Burdick JA, Pilla JJ, et al. Estimating passive mechanical properties in a myocardial infarction using MRI and finite element simulations. Biomech Model Mechanobiol. 2015;14:633–47.

113. Van Kranenburg M, Magro M, Thiele H, DeWaha S, Eitel I, Cochet A, et al. Prognostic value of microvascular obstruction and infarct size, as measured by CMR in STEMI patients. JACC: Cardiovascular Imaging. 2014.

114. Mather AN, Fairbairn TA, Ball SG, Greenwood JP, Plein S. Reperfusion haemorrhage as determined by cardiovascular MRI is a predictor of adverse left ventricular remodelling and markers of late arrhythmic risk. Heart. 2011;97(6):453–9.

115. Basso C, Corbetti F, Silva C, Abudureheman A, Lacognata C, Cacciavillani L, et al. Morphologic Validation of Reperfused Hemorrhagic Myocardial Infarction by Cardiovascular Magnetic Resonance. Am J Cardiol. 2007;100(8):1322–7.

116. Bulluck H, Rosmini S, Abdel-Gadir A, White SK, Bhuva AN, Treibel TA, et al. Residual Myocardial Iron Following Intramyocardial Hemorrhage During the Convalescent Phase of Reperfused ST-Segment–Elevation Myocardial Infarction and Adverse Left Ventricular Remodeling. Circ Cardiovasc Imaging.

2016 Oct;9(10).

117. Xu X, Wang Q, Zhong J, Zhang M. Iron deposition influences the measurement of water diffusion tensor in the human brain: a combined analysis of diffusion and iron-induced phase changes.

118. Jones DK, Basser PJ. "Squashing peanuts and smashing pumpkins": How noise distorts diffusion-weighted MR data. Magn Reson Med. 2004 Nov;52(5):979–93.

119. Bastin ME, Armitage PA, Marshall I. A theoretical study of the effect of experimental noise on the measurement of anisotropy in diffusion imaging. Magn Reson Imaging. 1998 Sep;16(7):773–85.

120. Pierpaoli C, Basser PJ. Toward a quantitative assessment of diffusion anisotropy. Magn Reson Med. 1996 Dec;36(6):893–906.

121. Wang G, Yang H-J, Kali A, Cokic I, Tang R, Xie G, et al. Influence of Myocardial Hemorrhage on Staging of Reperfused Myocardial Infarctions With T 2 Cardiac Magnetic Resonance Imaging: Insights Into the Dependence on Infarction Type With Ex Vivo Validation.

122. Romano S, Judd RM, Kim RJ, Kim HW, Klem I, Heitner JF, et al. Feature-Tracking Global Longitudinal Strain Predicts Death in a Multicenter Population of Patients with Ischemic and Nonischemic Dilated Cardiomyopathy Incremental to Ejection Fraction and Late Gadolinium Enhancement. JACC: Cardiovascular Imaging. 2018;

123. Kali A, Cokic I, Tang R, Dohnalkova A, Kovarik L, Yang HJ, et al. Persistent Microvascular Obstruction after Myocardial Infarction Culminates in the Confluence of Ferric Iron Oxide Crystals, Proinflammatory Burden, and Adverse Remodeling. Circ Cardiovasc Imaging. 2016;9(11).

124. Carrick D, Haig C, Rauhalammi S, Ahmed N, Mordi I, McEntegart M, et al. Pathophysiology of LV Remodeling in Survivors of STEMI: Inflammation, Remote Myocardium, and Prognosis. 2015.

125. Thulborn KR, Waterton JC, Matthews PM, Radda GK. Oxygenation dependence of the transverse relaxation time of water protons in whole blood at high field. Vol. 714, Biochimica et Biophysica Acta. 1982.

126. Zhong J, Kennan RP, Gore JC. Effects of susceptibility variations on NMR measurements of diffusion. J Magn Reson. 1991;

127. McClymont D, Teh I, Schneider JE. The impact of signal-to-noise ratio, diffusion-weighted directions and image resolution in cardiac diffusion tensor imaging – insights from the ex-vivo rat heart. J Cardiovasc Magn Reson. 2017 Dec 20;19(1):90.

128. Das A, Kelly C, Teh I, Stoeck CT, Kozerke S, Chowdhary A, et al. Acute Microstructural Changes after ST-Segment Elevation Myocardial Infarction Assessed with Diffusion Tensor Imaging. Radiology. 2021 Feb 9;203208.

129. Algranati D, Kassab GS, Lanir Y. Why is the subendocardium more vulnerable to ischemia? A new paradigm. Am J Physiol Heart Circ Physiol. 2011 Mar;300(3):H1090-100.

130. Fishbein, MC, Maclean D, Maroko PR. The Histopathologic Evolution of Myocardial Infarction. Chest. 1978 Jun 1;73(6):843–9.

131. Anversa P, Beghi C, Kikkawa Y, Olivetti G. Myocardial response to infarction in the rat. Morphometric measurement of infarct size and myocyte cellular hypertrophy. Am J Pathol. 1985;118(3):484.

132. Parisi R. Multimodality imaging in apical hypertrophic cardiomyopathy. World J Cardiol. 2014;

133. Streeter DD, Spotnitz HM, Patel DP, Ross J, Sonnenblick EH. Fiber orientation in the canine left ventricle during diastole and systole. Circ Res. 1969;

134. Kuribayashi T, Roberts WC. Myocardial disarray at junction of ventricular septum and left and right ventricular free walls in hypertrophic cardiomyopathy. Am J Cardiol. 1992;

135. Wu R, An DA, Shi RY, Chen B hua, Jiang M, Bacyinski A, et al. Myocardial fibrosis evaluated by diffusion-weighted imaging and its relationship to 3D contractile function in patients with hypertrophic cardiomyopathy. J Magn Reson Imaging. 2018;

136. Factor SM, Butany J, Sole MJ, Wigle ED, Williams WC, Rojkind M. Pathologic fibrosis and matrix connective tissue in the subaortic myocardium of patients with hypertrophic cardiomyopathy. J Am Coll Cardiol. 1991 May;17(6):1343–51.

137. Bravo PE. Is there a role for cardiac positron emission tomography in hypertrophic cardiomyopathy? J Nucl Cardiol. 2019 Aug 14;26(4):1125–34.

138. Varnava AM, Elliott PM, Sharma S, Mckenna J, Davies MJ. Hypertrophic cardiomyopathy: the interrelation of disarray, fibrosis, and small vessel disease. Heart. 2000;84:476–82.

139. Brown LAE, Onciul SC, Broadbent DA, Johnson K, Fent GJ, Foley JRJ, et al. Fully automated, inline quantification of myocardial blood flow with cardiovascular magnetic resonance: repeatability of measurements in healthy subjects. J Cardiovasc Magn Reson. 2018 Dec 9;20(1):48.

140. Gottbrecht M, Kramer CM, Salerno M. Native T1 and extracellular volume measurements by cardiac MRI in healthy adults: A meta-analysis. Radiology. 2019;

141. Harvey PA, Leinwand LA. The cell biology of disease: Cellular mechanisms of cardiomyopathy. J Cell Biol. 2011;194(3):355.

142. Baird AE, Warach S. Magnetic Resonance Imaging of Acute Stroke. J Cereb Blood Flow Metab. 1998 Jun;18(6):583–609.

143. Liu K-F, Li F, Tatlisumak T, Garcia JH, Sotak CH, Fisher M, et al. Regional Variations in the Apparent Diffusion Coefficient and the Intracellular Distribution of Water in Rat Brain During Acute Focal Ischemia. Stroke. 2001 Aug 1;32(8):1897–905.

144. Krams R, Kofflard MJM, Duncker DJ, Von Birgelen C, Carlier S, Kliffen M, et al. Decreased Coronary Flow Reserve in Hypertrophic Cardiomyopathy Is Related to Remodeling of the Coronary Microcirculation. Circulation. 1998 Jan 27;97(3):230–3.

145. Marszalek RJ, Solaro RJ, Wolska BM. Coronary arterial vasculature in the pathophysiology of hypertrophic cardiomyopathy. Pflügers Arch Eur J Physiol. 2019;471(5):769–80.

146. De Oliveira Antunes M, Luis Scudeler T. Hypertrophic cardiomyopathy. IJC Hear Vasc. 2020;27:100503.

147. Carruth ED, Teh I, Schneider JE, McCulloch AD, Omens JH, Frank LR. Regional variations in ex-vivo diffusion tensor anisotropy are associated with cardiomyocyte remodeling in rats after left ventricular pressure overload. J Cardiovasc Magn Reson. 2020 Apr 2;22(1).

148. Raphael CE, Cooper R, Parker KH, Collinson J, Vassiliou V, Pennell DJ, et al. Mechanisms of Myocardial Ischemia in Hypertrophic Cardiomyopathy Insights From Wave Intensity Analysis and Magnetic Resonance. Vol. 68, Journal of the American College of Cardiology. 2016.

149. Wigle ED, Sole MJ, Williams WC. Pathologic fibrosis and matrix connective tissue in the subaortic myocardium of patients with hypertrophic cardiomyopathy. J Am Coll Cardiol. 1991;

Appendix

9.4 Ethical approval, patient information sheets and consent forms for chapters 4-6

NHS

Health Research Authority

Email: hra.approval@nhs.net

Dr Erica Dall'Armellina
University Academic Fellow
University of Leeds
Leeds Institute of Cardiovascular and Metabolic Medicine,
Division of Biomedical Imaging
University of Leeds, LIGHT building, Clarendon way
Leeds
LS2 9JT

24 April 2017

Dear Dr Dall'Armellina

Letter of HRA Approval

Study title:	Quantitative cardiovascular magnetic resonance imagingtechniques for prediction of complications after acute myocardial infarction
IRAS project ID:	220657
REC reference:	17/YH/0062
Sponsor	University of Leeds

I am pleased to confirm that HRA Approval has been given for the above referenced study, on the basis described in the application form, protocol, supporting documentation and any clarifications noted in this letter.

Participation of NHS Organisations in England

The sponsor should now provide a copy of this letter to all participating NHS organisations in England.

Appendix B provides important information for sponsors and participating NHS organisations in England for arranging and confirming capacity and capability. **Please read Appendix B carefully**, in particular the following sections:
- *Participating NHS organisations in England* – this clarifies the types of participating organisations in the study and whether or not all organisations will be undertaking the same activities
- *Confirmation of capacity and capability* - this confirms whether or not each type of participating NHS organisation in England is expected to give formal confirmation of capacity and capability. Where formal confirmation is not expected, the section also provides details on the time limit given to participating organisations to opt out of the study, or request additional time, before their participation is assumed.
- *Allocation of responsibilities and rights are agreed and documented (4.1 of HRA assessment criteria)* - this provides detail on the form of agreement to be used in the study to confirm capacity and capability, where applicable.

Further information on funding, HR processes, and compliance with HRA criteria and standards is also provided.

It is critical that you involve both the research management function (e.g. R&D office) supporting each organisation and the local research team (where there is one) in setting up your study. Contact details and further information about working with the research management function for each organisation can be accessed from www.hra.nhs.uk/hra-approval.

Appendices
The HRA Approval letter contains the following appendices:
• A – List of documents reviewed during HRA assessment
• B – Summary of HRA assessment

After HRA Approval
The document *"After Ethical Review – guidance for sponsors and investigators"*, issued with your REC favourable opinion, gives detailed guidance on reporting expectations for studies, including:

• Registration of research
• Notifying amendments
• Notifying the end of the study

The HRA website also provides guidance on these topics, and is updated in the light of changes in reporting expectations or procedures.

In addition to the guidance in the above, please note the following:
• HRA Approval applies for the duration of your REC favourable opinion, unless otherwise notified in writing by the HRA.
• Substantial amendments should be submitted directly to the Research Ethics Committee, as detailed in the After Ethical Review document. Non-substantial amendments should be submitted for review by the HRA using the form provided on the HRA website, and emailed to hra.amendments@nhs.net.
• The HRA will categorise amendments (substantial and non-substantial) and issue confirmation of continued HRA Approval. Further details can be found on the HRA website.

Scope

HRA Approval provides an approval for research involving patients or staff in NHS organisations in England.

If your study involves NHS organisations in other countries in the UK, please contact the relevant national coordinating functions for support and advice . Further information can be found at http://www.hra.nhs.uk/resources/applying-for-reviews/nhs-hsc-rd-review/.

If there are participating non-NHS organisations, local agreement should be obtained in accordance with the procedures of the local participating non-NHS organisation.

User Feedback
The Health Research Authority is continually striving to provide a high quality service to all applicants and sponsors. You are invited to give your view of the service you have received and the application procedure. If you wish to make your views known please use the

feedback form available on the HRA website: http://www.hra.nhs.uk/about-the-hra/governance/quality-assurance/.

HRA Training
We are pleased to welcome researchers and research management staff at our training days – see details at http://www.hra.nhs.uk/hra-training/

Your IRAS project ID is **220657**. Please quote this on all correspondence.

Yours sincerely

Miss Lauren Allen
Assessor
Email: hra.approval@nhs.net

Appendix A - List of Documents

The final document set assessed and approved by HRA Approval is listed below.

Document	Version	Date
Evidence of Sponsor insurance or indemnity (non NHS Sponsorsonly) [liability insurance]		
GP/consultant information sheets or letters [GP letter DT in MI]	1.0	13 February 2017
IRAS Application Form [IRAS_Form_14022017]		14 February 2017
Letter from funder [award letter]		01 December 2016
Other [Schedule of Events]	1	28 February 2017
Other [Statement of Activities]	1	28 February 2017
Other [Response to REC]		03 April 2017
Other [Telephone follow-up script]	1.0	31 March 2017
Other [PIS and consent clean]	1.1	31 March 2017
Other [PIS and consent tracked changes]	1.1	31 March 2017
Research protocol or project proposal [study protocol DT-CMR in MI]	1.0	13 February 2017
Summary CV for Chief Investigator (CI) [EDA CV]		14 February 2017

Appendix B - Summary of HRA Assessment

This appendix provides assurance to you, the sponsor and the NHS in England that the study, as reviewed for HRA Approval, is compliant with relevant standards. It also provides information and clarification, where appropriate, to participating NHS organisations in England to assist in assessingand arranging capacity and capability.

For information on how the sponsor should be working with participating NHS organisations inEngland, please refer to the, *participating NHS organisations*, *capacity and capability* and *Allocation of responsibilities and rights are agreed and documented (4.1 of HRA assessment criteria)* sections in this appendix.

The following is the sponsor contact for the purpose of addressing participating organisation questionsrelating to the study: Tel: 01133437587 Email: governance-ethics@leeds.ac.uk

HRA assessment criteria

Section	HRA Assessment Criteria	Compliant with Standards?	Comments
1.1	IRAS application completedcorrectly	Yes	No comments
2.1	Participant information/consent documents and consentprocess	Yes	No comments
3.1	Protocol assessment	Yes	No comments
4.1	Allocation of responsibilitiesand rights are agreed and documented	Yes	The Statement of Activities and Schedule of Events will act as the agreement between the site and sponsor.

4.2	Insurance/indemnity arrangements assessed	Yes	Where applicable, independent contractors (e.g. General Practitioners)should ensure that the professional indemnity provided by their medical defence organisation covers the activities expected of them for this research study
4.3	Financial arrangements assessed	Yes	No funding will be provided to the site.
5.1	Compliance with the DataProtection Act and data security issues assessed	Yes	No comments
5.2	CTIMPS – Arrangements for compliance with the Clinical Trials Regulations assessed	Not Applicable	No comments
5.3	Compliance with any applicable laws or regulations	Yes	No comments
6.1	NHS Research Ethics Committee favourable opinion received for applicable studies	Yes	No comments
6.2	CTIMPS – Clinical Trials Authorisation (CTA) letterreceived	Not Applicable	No comments

6.3	Devices – MHRA notice of no objection received	Not Applicable	No comments
6.4	Other regulatory approvals and authorisations received	Not Applicable	No comments

Participating NHS Organisations in England

This provides detail on the types of participating NHS organisations in the study and a statement as to whether the activities at all organisations are the same or different.
There is one site type. The study activity will be conducted at the site as detailed in the Protocol andsupporting documents.

The Chief Investigator or sponsor should share relevant study documents with participating NHS organisations in England in order to put arrangements in place to deliver the study. The documents should be sent to both the local study team, where applicable, and the office providing the research management function at the participating organisation. For NIHR CRN Portfolio studies, the Local LCRN contact should also be copied into this correspondence. For further guidance on working withparticipating NHS organisations please see the HRA website.

If Chief Investigators, sponsors or Principal Investigators are asked to complete site level forms forparticipating NHS organisations in England which are not provided in IRAS or on the HRA website, the Chief Investigator, sponsor or Principal Investigator should notify the HRA immediately at hra.approval@nhs.net. The HRA will work with these organisations to achieve a consistent approachto information provision. |

Confirmation of Capacity and Capability

This describes whether formal confirmation of capacity and capability is expected from participating NHS organisations in England.
Participating NHS organisations in England will be expected to formally confirm their capacityand capability to host this research.
- The sponsor should ensure that participating NHS organisations are provided with a copy ofthis letter and all relevant study documentation, and work jointly with NHS organisations to arrange capacity and capability whilst the HRA assessment is ongoing.
- Further detail on how capacity and capability will be confirmed by participating NHS organisations, following issue of the Letter of HRA Approval, is provided in the *Participating NHS Organisations* and *Allocation of responsibilities and rights are agreed and documented(4.1 of HRA assessment criteria)* sections of this appendix.
The Assessing, Arranging, and Confirming document on the HRA website provides further information for the sponsor and NHS organisations on assessing, arranging and confirming capacityand capability.

Principal Investigator Suitability

This confirms whether the sponsor position on whether a PI, LC or neither should be in place is correct for each
type of participating NHS organisation in England and the minimum expectations for education, training and experience that PIs should meet (where applicable).

A Principal Investigator will need to be in place at the site. The sponsor has confirmed that the
Principal Investigator will be required to have completed NIHR GCP training.

GCP training is not a generic training expectation, in line with the HRA statement on training expectations.

HR Good Practice Resource Pack Expectations

This confirms the HR Good Practice Resource Pack expectations for the study and the pre-engagement checks that should and should not be undertaken

No access arrangements will be needed for study activity conducted by staff employed by the site. External staff (e.g. University) will be expected to have Honorary Research Contracts to conduct the study activities listed at IRAS A18 and A19, other than collection of demographic, clinical and follow-up data where Letters of Access would be appropriate. Disclosure and Barring Service and Occupational Health checks will be expected where Honorary Research Contracts or Letters of Access are in place.

Other Information to Aid Study Set-up

This details any other information that may be helpful to sponsors and participating NHS organisations in England to aid study set-up.

- The applicant has indicated that they intend to apply for inclusion on the NIHR CRN Portfolio.

The Leeds Teaching Hospitals **NHS**
NHS Trust

UNIVERSITY OF LEEDS

Study code DT-CMR in MI

Quantitative cardiovascular magnetic resonance imaging techniques for prediction of complications after acute myocardial infarction

PARTICIPANT INFORMATION SHEET

Version 1.2; 23 February 2018

Chief Investigator: Dr E. Dall'Armallina

Dear Participant,

You are being invited to take part in a research study. Before you decide it is important for you to understand why the research is being done and what it will involve. Please take time to read the following information carefully and discuss it with friends, relatives and your GP if you wish. Ask us if there is anything that is not clear or if you would like more information. Take time to decide whether or not you wish to take part.

Purpose of the study

Magnetic Resonance Imaging (MRI) is a test, which produces detailed pictures of your internal organs by putting you within a strong magnetic field. With Cardiac MRI we are able to detect several important abnormalities that are caused by heart disease, for example the scarring of the heart from heart attacks and the restrictions of blood flow to the heart muscle that lead to angina. Also, MRI produces pictures of the heart with much greater detail than with other types of heart scans. Importantly, MRI is also a safer test than most other heart scans, because it does not expose participants to any harmful radiation and pictures of the heart can be taken "from the outside". Because of all of these qualities, MRI may become one of the most important tests in patients who suffer with different types of heart disease. We have been doing MRI scans of the heart in Leeds since 1995. We are continuously carrying out research into improving the images and thereby improving patient care.

During a heart attack the heart muscle cells are damaged. Some heart muscle will not return to normal and will be replaced by a scar. Other parts of the heart muscle are less severely affected by the heart attack and can recover to normal over time. Such changes in the muscle of your heart can cause your heart to function poorly over time and cause difficulty in breathing or palpitations. With MRI the consequences of a heart attack can be shown in much greater detail than with other tests. In this research we aim to find out how heart attacks affect the heart from the early hours up to 18 months. We would therefore like to scan participants like you three times over an 18 month period

Why have I been chosen?

This study is looking at people like you, who have recently had a heart attack and had the blocked blood vessel reopened. We are hoping to recruit 160 participants like you into this study.

Do I have to take part?

It is up to you to decide whether or not to take part. If you do decide to take part you will be given this information sheet to keep and be asked to sign a consent form. If you decide to take part you are still free to withdraw at any time and without giving a reason. This will not affect the standard of care that you receive from the NHS. If there is a possibility that you might be pregnant, you should not take part in the study. Our research team will be happy to discuss any other questions that you may have concerning your suitability for the study, before you decide whether to take part.

What will happen to me if I take part?

You will be asked to attend the hospital for three visits over 12 to 18 months. A small number of patients (15 to 20) will be invited for a fourth visit. The details of the visits are described below. At each visit you will have the opportunity to ask further questions.

During the study visit we would undertake the following procedures:

1. We will ask you some questions about your general health and medications. (approximately 5 minutes)
2. MRI scans. We would aim to scan you within 5 to 7 days after your heart attack to assess the condition of your heart, followed by a scan at 3 months to find out how

changes in the heart evolve, and a final scan between 12 and18 months. A small number of patients will be invited to have an additional scan within 24 hours of admission. We will only ask you if you are feeling well, and, like study participation, this additional scan remains entirely voluntary.

The MRI scans will be performed at the Leeds General Infirmary and will each take approximately 90 minutes to complete (this would usually be continuous, but could include breaks if needed). MRI scans are painless but involve the use of a strong magnetic field, so if you have any of the following, you would not be suitable for a scan, and would not be able to take part in this trial:

- a permanent pacemaker

- metal clips in blood vessels of the brain

- an injury to the eye involving fragments of metal (unless excluded by previous Xray)

- you are pregnant

- shrapnel injuries

- other metal or electronic implants affected by the magnetic field

The MRI scanner is shaped like a short tunnel, a picture of a scanner is shown above. You will be asked to lie still on your back while your heart is scanned. The scanner can be noisy, so to protect your ears we provide headphones that also allow you to listen to music of your choice during the scan. The scanner is a slightly confined space and a small minority of people can find this distressing. You will be asked to breathe in and out and hold your breath for several seconds for some of the scans. We will remain in communication with you throughout the scan. During the scan, we will inject an MRI contrast dye (gadolinium) into a vein in your arm (this will be discussed with you before the scan). With your permission, we will insert a small tube (cannula) in a vein in your arm. If you come down from the ward with a cannula (whilst you are staying in hospital) we would use the one that is already there. If there have

been no blood samples to check your kidney function in the past 6 months we will take a small blood sample to test this. The cannula would then be used to administer gadolinium during the scan. Usually people are not aware of the actual contrast dye injection. The contrast medication (gadolinium) is safe with very few reported side effects.

3. ECG recording – this is a simple tracing of the electrical activity of your heart. It takes around 5 minutes to record.
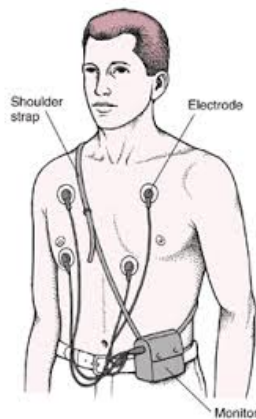
4. ECG Holter monitoring. This test is non-invasive and allows us to record the electrical activity of your heart which can be affected during a heart attack. This involves carrying a belt with a small external "box" (as big as a small wallet, see figure above). 10 leads will be attached to you using adhesive pads. These are then attached to the small box that records the electrical activity of your heart whilst you go about your daily business. We aim to monitor your heart up to a maximum of 48 hours during your hospital stay, at 3 months (± 4 weeks) and at 12 to18 months.

5. Whilst you are an in-patient on the ward you will have a blood sample taken every day. This would happen regardless of whether you are in the study or not. We will use some of the results for the research study. We will also take a blood sample (at most 15 mls = 3 teaspoons) from you at every scan visit. We will take this from the cannula we have to insert to inject the contrast dye so there are no extra needles involved. With your permission we will store these samples and analyze them at the end of the study for markers of heart function. Any use of your samples after this study could only happen if an ethics committee approved it.

As part of the study we would like to make a follow-up telephone call to you at 18 months, at 3 and at 5 years to ask you some simple questions about your health. With your permission we may also look at your hospital records, request access to your GP records, central NHS records and/or use information from NHS Digital.

After you leave hospital it is very helpful if we can continue to track your health condition over a long term period. NHS Digital allows us to access health information about you with your permission. In order to do this we are seeking your permission to provide NHS Digital with some of your personal details (including your name, date of birth, address and NHS number) and with this information NHS Digital will be able to provide us with simple health information about you in the 5 year follow up period of this study. It is very important to understand the long term health conditions of participants after a heart attack to find out if the treatments we are giving are effective. Information will be provided to NHS Digital in strict confidence and will be kept securely by them and will not be released to a third party. With your permission, during follow up we may also contact you to invite you to participate in new research studies.

Risks and discomforts

Magnetic Resonance Imaging (MRI) (both at 1.5T at 3T) is safe and no x-rays or radiation are used for this scan. There are no known risks from this technique. Some people may experience claustrophobia. Our MRI staff will do all that they can to make you feel comfortable during the scan, and will be monitoring you via a video camera and an audio link. If we are unable to make you feel comfortable in the scanner, we will not go ahead with scanning. The contrast medication we use during the scan is very safe but, as with any injection, reactions may occur. These include a warm sensation at the injection site, nausea or vomiting and transient skin rash. These effects usually only last for a few minutes. People with a history of allergy are more likely to suffer a more severe reaction, but this is rare (less than 1 in 3000). The department is equipped to cope with allergic reactions if they happen.

ECG Holter monitoring devices are external and safe. Should the Holter too burdensome to wear for the 48 hours, you are free to remove it and indicate the reason for stopping recording earlier. You will still be able to continue taking part in the study.

Benefits to you

This study does not form part of your normal clinical care and is done solely for research purposes.

Expenses

We will provide reasonable travel expenses should this be necessary for you to attend the MRI scan. We are also happy to arrange transport to the hospital and return you home if needs be.

Will my taking part be kept confidential?

All information collected about you during the course of the study will be kept strictly confidential. This information will be securely stored, electronically on the Leeds General Infirmary secure server, and on paper, under the provisions of the 1998 Data Protection Act. The data collected will be coded and your personal details will be kept separately. You will not be identified in any publication that may result from this research.

With your permission we will inform your GP of your participation in the study. If any unexpected abnormality or condition were found we would inform your GP and your cardiologist.

With your permission, your data may also provide a resource for future studies. If any information from this study is used to develop new research, data protection regulations will be observed and strict confidentiality maintained. Any information about you which leaves the hospital will have your name and address removed so that you cannot be identified. Your data and or images may be sent to institutions in the UK, the European Economic Area or outside the EEA. Ethical approval will be obtained for any future studies involving your data.

If you withdraw consent from further study follow-up, or if you were to become incapacitated, any data collected about you up to that point will remain on file and will be included in the final study analysis.

What will happen to the results of the research study?

When the study is complete the results will be published in a medical journal, but no individual participants will be identified. If you would like a copy of the published results, please ask your doctor.

Indemnity/Compensation

If you are harmed as a direct result of taking part in this study, there are no special compensation arrangements. If you are harmed due to someone's negligence, then you may

have grounds to a legal action. Regardless of this, if you have any cause to complain about any aspect of the way you have been approached or treated during the course of this study, the normal National Health Service complaints mechanisms are available to you.

The research organisation

This is a research project of the Cardiac MRI department of the Leeds General Infirmary and the University of Leeds.

Who has reviewed the study?

The study has been reviewed and approved both by Yorkshire and Humber – Leeds West Research Ethics Committee and your hospital Research and Development Office. More details can be provided, on request, by your study doctor.

For further information please contact:

Dr Erica Dall'Armellina

Honorary Consultant Cardiology

University Academic Fellow

BHF Intermediate Clinical Research Fellow

Leeds Institute of Cardiovascular and Metabolic Medicine, Division of Biomedical Imaging, University of Leeds,

LIGHT building,

LS2 9JT

email: E.DallArmellina@leeds.ac.uk

tel: 0113 3438306

UNIVERSITY OF LEEDS

CONSENT FORM v 1.2 23 February 2018

Quantitative cardiovascular magnetic resonance imaging techniques for prediction of complications after acute myocardial infarction

CI: Dr E. Dall'Armellina

Patient Study Number: ……………..   Date of Birth: …………………

Please initial boxes

1. I have read the Patient Information Sheet dated 23 February 2018 (Version 1.2) for the above study and I have had the opportunity to ask questions and discuss the research study and I am satisfied with the answers to my questions.

2. I understand that my participation is voluntary and that I am free to withdraw from the study at any time without giving a reason.

3. I give my consent for my General Practitioner to be informed, and I understand that my cardiologist will be informed only if we find any abnormality over and above which is already known.

4. I understand that data and images collected will be stored on a computer system, and, after my personal details have been removed, may be available to researchers at other institutions in the UK, the EEA, and countries outside the EEA.

5. I understand that some of the blood samples taken from me will be stored and may be analyzed at the end of this study for markers of a heart attack.

6. I give permission for my stored blood samples to be used in future, ethically approved research.

7. I understand that relevant sections of my medical notes and data collected during the study may be looked at by individuals from the University of Leeds, from regulatory authorities, or from the Leeds Teaching Hospitals NHS Trust, where it is relevant to my taking part in this research. I give permission for these individuals to have access to my records.

8. I understand that information held by the NHS and records maintained by NHS Digital and by my General Practitioner may be used to contact me and provide information about my health status. I give permission for this information to be obtained from NHS Digital and/or my GP if necessary.

9. If I were to lose capacity or withdraw consent for further follow-up I understand that data already collected will be kept and used for the purposes of the study.

10. I agree to take part in this research study and that the general results of the study will be made available to the medical community most likely through publication in a reputable medical journal.

11. I am happy to be contacted regarding my possible participation in future related studies.

Signature..

Name (block capitals).. Date...............

Signature of researcher   ....

Name (block capitals)..Date……………

1 copy to be given to the patient

1 copy to be filed in notes

1 copy to be retained researcher

9.5 Ethical approval, patient information sheets and consent forms for chapter 7

Ymchwil Iechyd
a Gofal Cymru

Health and Care
Research Wales

NHS
Health Research
Authority

Professor Sven Plein
BHF Professor of Cardiology and Honorary Consultant
Cardiologist
University of Leeds
LICAMM
LIGHT building
University of Leeds
LS2 9JT

Email: hra.approval@nhs.net
Research-permissions@wales.nhs.uk

15 June 2018

Dear Professor Plein

**HRA and Health and Care
Research Wales (HCRW)
Approval Letter**

Study title:	Advanced Magnetic Resonance Imaging: Optimization of Image Acquisition and Analysis Methods (AMaRI)
IRAS project ID:	245109
REC reference:	18/YH/0168
Sponsor	University of Leeds

I am pleased to confirm that HRA and Health and Care Research Wales (HCRW) Approval has been given for the above referenced study, on the basis described in the application form, protocol, supporting documentation and any clarifications received. You should not expect to receive anything further relating to this application.

How should I continue to work with participating NHS organisations in England and Wales?
You should now provide a copy of this letter to all participating NHS organisations in England and Wales, as well as any documentation that has been updated as a result of the assessment.

Following the arranging of capacity and capability, participating NHS organisations should **formally confirm** their capacity and capability to undertake the study. How this will be confirmed is detailed in the "*summary of assessment*" section towards the end of this letter.

You should provide, if you have not already done so, detailed instructions to each organisation as to how you will notify them that research activities may commence at site following their confirmation of capacity and capability (e.g. provision by you of a 'green light' email, formal notification following a site initiation visit, activities may commence immediately following confirmation by participating organisation, etc.).

IRAS project ID	245109

It is important that you involve both the research management function (e.g. R&D office) supporting each organisation and the local research team (where there is one) in setting up your study. Contact details of the research management function for each organisation can be accessed here.

How should I work with participating NHS/HSC organisations in Northern Ireland and Scotland?
HRA and HCRW Approval does not apply to NHS/HSC organisations within the devolved administrations of Northern Ireland and Scotland.

If you indicated in your IRAS form that you do have participating organisations in either of these devolved administrations, the final document set and the study wide governance report (including this letter) has been sent to the coordinating centre of each participating nation. You should work with the relevant national coordinating functions to ensure any nation specific checks are complete, and with each site so that they are able to give management permission for the study to begin.

Please see IRAS Help for information on working with NHS/HSC organisations in Northern Ireland and Scotland.

How should I work with participating non-NHS organisations?
HRA and HCRW Approval does not apply to non-NHS organisations. You should work with your non-NHS organisations to obtain local agreement in accordance with their procedures.

What are my notification responsibilities during the study?
The document "*After Ethical Review – guidance for sponsors and investigators*", issued with your REC favourable opinion, gives detailed guidance on reporting expectations for studies, including:
- Registration of research
- Notifying amendments
- Notifying the end of the study

The HRA website also provides guidance on these topics, and is updated in the light of changes in reporting expectations or procedures.

I am a participating NHS organisation in England or Wales. What should I do once I receive this letter?
You should work with the applicant and sponsor to complete any outstanding arrangements so you are able to confirm capacity and capability in line with the information provided in this letter.

The sponsor contact for this application is as follows:

Name: NHS Research Ethics Officer
Email: governance-ethics@leeds.ac.uk

Who should I contact for further information?
Please do not hesitate to contact me for assistance with this application. My contact details are below.

Your IRAS project ID is **245109**. Please quote this on all correspondence.

IRAS project ID	245109

Yours sincerely

Thomas Fairman
HRA Assessor

Email: hra.approval@nhs.net

Copy to: *NHS Research Ethics Office, Leeds University, (Sponsor Contact)*
             Ms Anne Gowing, Leeds Teaching Hospitals NHS Trust, (Lead NHS R&D Contact)

IRAS project ID	245109

List of Documents

The final document set assessed and approved by HRA and HCRW Approval is listed below.

Document	Version	Date
Copies of advertisement materials for research participants [AMaRI recruitment email]	1.0	27 March 2018
Evidence of Sponsor insurance or indemnity (non NHS Sponsors only) [Confirmation of Liability]		21 September 2017
HRA Schedule of Events	1.0	11 April 2018
HRA Statement of Activities	1.0	11 April 2018
IRAS Application Form [IRAS_Form_06042018]		06 April 2018
Laboratory Manual [Laboratory manual]	1.0	01 March 2018
Letter from funder [BHF Programme Grant]		24 May 2016
Letter from sponsor [confirmation of sponsorship]		27 March 2018
Letters of invitation to participant [AMaRI invitation letter]	1.0	27 March 2018
Participant consent form [AMaRI PIS Consent Patients (tracked changes)]	1.1	12 June 2018
Participant consent form [AMaRI PIS Consent Volunteers]	1.1	12 June 2018
Research protocol or project proposal [AMaRI Protocol]	1.1	12 June 2018
Response to Additional Conditions Met		
Summary CV for Chief Investigator (CI) [CV]		01 November 2017

IRAS project ID	245109

Summary of assessment

The following information provides assurance to you, the sponsor and the NHS in England and Wales that the study, as assessed for HRA and HCRW Approval, is compliant with relevant standards. It also provides information and clarification, where appropriate, to participating NHS organisations in England and Wales to assist in assessing, arranging and confirming capacity and capability.

Assessment criteria

Section	Assessment Criteria	Compliant with Standards	Comments
1.1	IRAS application completed correctly	Yes	No comments
2.1	Participant information/consent documents and consent process	Yes	No comment
3.1	Protocol assessment	Yes	No comment
4.1	Allocation of responsibilities and rights are agreed and documented	Yes	The sponsor has submitted the HRA Statement of Activities and intends for this to form the agreement between the sponsor and study sites.

The sponsor is not requesting, and does not require any additional contracts with study sites. |
4.2	Insurance/indemnity arrangements assessed	Yes	Where applicable, independent contractors (e.g. General Practitioners) should ensure that the professional indemnity provided by their medical defence organisation covers the activities expected of them for this research study
4.3	Financial arrangements assessed	Yes	External study funding has been secured from the British Heart Foundation. Study funding will be provided to sites, as detailed at Schedule 1 of the Statement of Activities.

IRAS project ID	245109

Section	Assessment Criteria	Compliant with Standards	Comments
5.1	Compliance with the Data Protection Act and data security issues assessed	Yes	No comment
5.2	CTIMPS – Arrangements for compliance with the Clinical Trials Regulations assessed	Not Applicable	No comments
5.3	Compliance with any applicable laws or regulations	Yes	No comments
6.1	NHS Research Ethics Committee favourable opinion received for applicable studies	Yes	No comments
6.2	CTIMPS – Clinical Trials Authorisation (CTA) letter received	Not Applicable	No comments
6.3	Devices – MHRA notice of no objection received	Not Applicable	No comments
6.4	Other regulatory approvals and authorisations received	Not Applicable	No comments

Participating NHS Organisations in England and Wales

This provides detail on the types of participating NHS organisations in the study and a statement as to whether the activities at all organisations are the same or different.

All participating NHS organisations will undertake the same study activities. There is therefore only one study site 'type' involved in the research.

The Chief Investigator or sponsor should share relevant study documents with participating NHS organisations in England and Wales in order to put arrangements in place to deliver the study. The documents should be sent to both the local study team, where applicable, and the office providing the research management function at the participating organisation. Where applicable, the local LCRN contact should also be copied into this correspondence.

If chief investigators, sponsors or principal investigators are asked to complete site level forms for participating NHS organisations in England and Wales which are not provided in IRAS, the HRA or HCRW websites, the chief investigator, sponsor or principal investigator should notify the HRA immediately at hra.approval@nhs.net or HCRW at Research-permissions@wales.nhs.uk. We will work with these organisations to achieve a consistent approach to information provision.

IRAS project ID	245109

Principal Investigator Suitability

This confirms whether the sponsor position on whether a PI, LC or neither should be in place is correct for each type of participating NHS organisation in England and Wales, and the minimum expectations for education, training and experience that PIs should meet (where applicable).

A Principal Investigator should be appointed at study sites.

GCP training is <u>not</u> a generic training expectation, in line with the <u>HRA/HCRW/MHRA statement on training expectations</u>.

HR Good Practice Resource Pack Expectations

This confirms the HR Good Practice Resource Pack expectations for the study and the pre-engagement checks that should and should not be undertaken

As a non-commercial study undertaken by local staff, it is unlikely that letters of access or honorary research contracts will be applicable, except where local network staff employed by another Trust (or University) are involved (and then it is likely that arrangements are already in place).

Where arrangements are not already in place, network staff (or similar) undertaking any of the research activities listed in A18 or A19 of the IRAS form (except for administration of questionnaires or surveys), would be expected to obtain an honorary research contract from one NHS organisation (if university employed), followed by Letters of Access for subsequent organisations. This would be on the basis of a Research Passport (if university employed) or an NHS to NHS confirmation of pre-engagement checks letter (if NHS employed). These should confirm enhanced DBS checks, including appropriate barred list checks, and occupational health clearance.

For research team members only administering questionnaires or surveys, a Letter of Access based on standard DBS checks and occupational health clearance would be appropriate.

Other Information to Aid Study Set-up

This details any other information that may be helpful to sponsors and participating NHS organisations in England to aid study set-up.

The applicant has indicated that they <u>do intend</u> to apply for inclusion on the NIHR CRN Portfolio.

UNIVERSITY OF LEEDS

PARTICIPANT INFORMATION SHEET - PATIENTS

Version 1.2 –October 04 2018

AMaRI

<u>A</u>dvanced <u>M</u>agnetic <u>R</u>esonance <u>I</u>maging: Optimization of Image Acquisition and Analysis Methods

Chief Investigator: Professor Sven Plein

Dear Patient,

You are being invited to take part in a research study. Before you decide it is important for you to understand why the research is being done and what it will involve. Please take time to read the following information carefully and discuss it with friends, relatives and your GP if you wish. Ask us if there is anything that is not clear or if you would like more information. Take time to decide whether or not you wish to take part.

Purpose of the study

Magnetic Resonance Imaging (MRI) is a test which produces detailed pictures of your internal organs by putting you within a strong magnetic field. MRI allows us to detect abnormalities in many organs in the human body with a very high sensitivity. Importantly, MRI is a safe test and does not use any harmful radiation. It is therefore an increasingly used test in many areas of medicine with over 100,000 MRI scans performed in the NHS every year.

In Leeds, we have an ongoing research programme that aims to continuously improve the

way we acquire MRI pictures. This is mostly achieved by making scans shorter, increasing the detail in the image or finding out new information from within the acquired images. These developments are first tested in phantoms (bottles filled with a special liquid) and later need confirmation in volunteers and then in patients.

Why have I been chosen*?*

This study is looking at up to 300 people like you, who may have a range of conditions that are of interest to our research into improving imaging. We are also asking 400 healthy volunteers to participate in the study.

Do I have to take part?

No. It is up to you to decide whether or not to take part. If you do decide to take part you will be given this information sheet to keep and be asked to sign a consent form. If you decide to take part you are still free to withdraw at any time and without giving a reason. This will not affect the standard of care that you receive from the NHS. If there is a possibility that you might be pregnant, you should not take part in the study. Our research team will be happy to discuss any other questions that you may have concerning your suitability for the study, before you decide whether to take part.

What will happen to me if I take part?

Most patients will have a single MRI scan. A small group of participants in this study will be asked to undergo up to four MRI scans to allow comparisons between different ways of obtaining MRI pictures. It is entirely up to you how many scans you wish to volunteer for, and you will remain free to withdraw from the study at any time. All scans will be performed at the Leeds General Infirmary, and will be performed on separate days. The MRI scan will take approximately 60 to 90 minutes to complete. You lie in a short 'tunnel', which holds a large magnet. Short bursts of radio waves from the MRI scanner allow images to be created. You will hear periodical loud "banging" noises while we are acquiring the images, so we protect your ears with headphones through which you can listen to the radio or one of your own CDs. We will remain in communication with you throughout the scan.

For most scans we will insert one or two cannulae (small plastic tubes) into veins in your arm. It is likely that we will inject a contrast dye during the scan. Usually people are not aware of the contrast dye injection. At one point we may also inject a medication (Adenosine, or

occasionally Dobutamine) into a vein in your arm, which is a drug to increase the blood flow to your heart. This can cause a brief feeling of warmth, breathlessness or chest discomfort. However all of these feelings, if they occur, usually settle within one or two minutes of the medication being stopped. A doctor will stay in the room with you whilst you are having the medication. In some cases instead of using adenosine we may immerse your hands or feet in cold water for up to 2 minutes to achieve the same increased blood flow to the heart muscle, or we may ask you to use a cycle ergometer, a bicycle which can be used whilst lying down in the scanner.

If we wish to obtain specific images of your heart arteries we will wrap a belt around your abdomen to help improve the quality of the pictures. This is not painful and is a recognized method of doing this type of scan. You may be given a nitrate (GTN) spray under the tongue which helps us to obtaining good images. If your heart beat is quite fast we would give you a beta blocker tablet to reduce your heart rate. Again, these methods are widely used in other centres worldwide and are used in normal clinical work too.

As this study is about improving our scan protocols on an ongoing basis for a period of four years the information we give you has to describe all the different techniques we wish to use in the study overall, but not all the techniques described above will be used during your scan(s). Before you sign the consent form we will discuss with you the specific scanning protocol that we are going to use.

We may ask you for a blood sample (5 to 10 mls. or 1 to 2 teaspoons), which would be taken whilst we insert the cannula in your arm for the contrast, so there are no extra needles involved. Knowing your haematocrit (the volume percentage of red blood cells in the blood) helps us to create specific images which are applicable to clinical practice. We may also test your blood glucose and lipid levels. With your permission we may store serum samples and analyse them at the end of the study for markers of heart function.
We may ask you to come for the scan in a fasted state, or offer to scan you following a meal which we will provide you with, so that we can assess the influence of fed or fasted state on the heart scan assessments. We may ask you to have an ECG, this is a heart tracing to measure the electrical impulses within the heart. It involves having 10 stickers applied to your chest for 5 minutes.

In the unlikely event of any abnormality we will, with your permission, inform your GP.

Risks and discomforts

Magnetic Resonance Imaging (MRI) is safe and no x-rays or radiation are used for this scan. There are no known risks from this technique. Some people may experience claustrophobia. Our MRI staff will do all that they can to make you feel comfortable during the scan, and will be monitoring you via a video camera and an audio link. If we are unable to make you feel comfortable in the scanner, we will not go ahead with scanning. You may experience minor bruising or irritation at the site where we place the cannula in your arm.The contrast medication which we use is very safe but, as with any injection, reactions may occur. These include a warm sensation at the injection site, nausea or vomiting and transient skin rash. These effects usually only last for a few minutes. People with a history of allergy are more likely to suffer a more severe reaction, but this is rare (less than 1 in 3000). The department is equipped to cope with allergic reactions if they happen. Adenosine, the medication we use to increase the blood flow to the heart, can cause flushing, breathlessness and chest discomfort. However, all of these feelings usually subside within one or two minutes or even more quickly if the medication is stopped. Immersing your hands or feet in cold water is unpleasant, but the effects wear off very quickly. Nitrates and a beta blocker can cause temporary light headedness. For this reason if these drugs are used you will be kept under observation until the effects have worn off.

Benefits to you

This study does not form part of your normal clinical care and is done solely for research purposes. Your participation may however benefit future patients.

Expenses

We will provide reasonable travel expenses should this be necessary for you to attend the MRI scan. We are also happy to arrange transport to the hospital and return you home if needs be.

Will my taking part be kept confidential?

All information, which is collected about you during the course of the research will be kept strictly confidential. This information will be securely stored at the Cardiac MRI Unit at Leeds

General Infirmary on paper and electronically, under the provisions of the 2018 Data Protection Act. The data collected will be coded and your personal details will be kept separately. If we keep any of your serum samples these will be stored in -80°C freezers in a secure environment, in University of Leeds or Leeds Teaching Hospitals NHS Trust Research laboratories. Stored serum samples will be anonymized and identified only by sample IDs. You will not be identified in any publication that may result from this research. We will inform your General Practitioner (GP) in the event of an unexpected abnormality being found.

With your permission, your data may also provide a resource for future studies. If any information from this study is used to develop new research, data protection regulations will be observed and strict confidentiality maintained. Your anonymized data and or images may be sent to institutions in the UK, the European Economic Area or outside the EEA. Ethical approval will be obtained for any future studies involving your data. You will not be identified in the results of any future studies.

The University of Leeds is the sponsor for this study based in the United Kingdom. We will be using information from you and/or your medical records in order to undertake this study and will act as the data controller for this study. This means that we are responsible for looking after your information and using it properly. The University of Leeds and the Leeds Teaching Hospitals NHS Trust (on behalf of the University of Leeds), will keep identifiable information about you for the purpose of the study for a maximum of 15 years after the study has finished. Your rights to access, change or move your information are limited, as we need to manage your information in specific ways in order for the research to be reliable and accurate. If you withdraw from the study, we will keep the information about

What will happen to the results of the research study?

When the study is complete the results will be published in a medical journal, but no individual participants will be identified. If you would like a copy of the published results, please ask your doctor.

Indemnity/Compensation

If you are harmed as a direct result of taking part in this study, there are no special compensation arrangements. If you are harmed due to someone's negligence, then you may have grounds to a legal action. Regardless of this, if you have any cause to complain about any aspect of the way

you have been approached or treated during the course of this study, the normal National Health Service complaints mechanisms are available to you.

The research organisation

This is a research project of the Department of Biomedical Imaging Science at the Leeds Institute of Cardiovascular and Metabolic Medicine (LICAMM).

For further information please contact:
Research Nurses
CMR Clinical Research Group
X47, Sunshine Corridor
Leeds General Infirmary
Leeds
LS1 3EX
T 0113 392 5481 or 392 5504
cmrresearch@leeds.ac.uk

UNIVERSITY OF LEEDS

CONSENT FORM v 1.2 October 04 2018

AMaRI

Advanced Magnetic Resonance Imaging: Optimization of Image Acquisition and Analysis Methods

Chief Investigator: Professor Sven Plein

Patient Number: ……………..   Date of Birth: ………………

Patient initials ………………………………

Please initial boxes

1. I have read the Patient Information Sheet dated October 042018 (Version 1.2) for the above study and I have had the opportunity to ask questions and discuss the research study and I am satisfied with the answers to my questions.

2. I have received enough information about this study.

3. I understand that my participation is voluntary and that I am free to withdraw from the study at any time without giving a reason.

4. I give my consent for my General Practitioner to be informed in the event of any abnormality being discovered and that the cardiologist will be informed only if we find any abnormality over and above which is already known.

5. I understand that images collected will be stored on an NHS computer system, and, after my personal details have been removed, may be available to researchers at other institutions in the UK, the EEA, and countries outside the EEA.

6. I understand that some of the blood samples taken from me may be stored and may be analyzed in the future for markers related to heart disease

7. I understand that relevant sections of my medical notes and data collected during the study, may be looked at by individuals from the University of Leeds, from regulatory authorities, or from the Leeds Teaching Hospitals NHS Trust, where it is relevant to my taking part in this research. I give permission for these individuals to have access to my records.

8. If I were to lose capacity, I understand that data already collected will be kept and used for the purposes of the study.

9. I agree to take part in this research study and that the general results of the study will be made available to the medical community most likely through publication in a reputable medical journal.

	Yes	No

10.   I am willing to be contacted again in the future to receive information about the publication of this study.

	Yes	No

11.   I am willing to be contacted again in the future with regard to potentially taking part (without any obligation) in further related research studies or attending for further MRI scans.

12.   I would like to receive a summary of the final results when they are available

Signature...

Name (block capitals)...   Date................

Signature of researcher...

Name (block capitals)..   Date…………..

9.6 Ethical approval, patient information sheets and consent forms for chapters 8

Dr. Erica Dall'Armellina

University Academic Fellow   Email: hra.approval@nhs.net

University of Leeds   Research-permissions@wales.nhs.uk

Leeds Institute of Cardiovascular and Metabolic Medicine,

Division of Biomedical Imaging, University of Leeds

LIGHT building, Clarendon way , Leeds,

LS2 9JT

11 December 2018

Dear Dr. Dall'Armellina

HRA and Health and Care

   Research Wales (HCRW) Approval Letter

Study title: Developing novel cardiac diffusion MRI techniques to risk
                                    stratify patients with hypertrophic cardiomyopathy

IRAS project ID: 249941

REC reference: 18/YH/0372

Sponsor   University of Leeds

I am pleased to confirm that **HRA and Health and Care Research Wales (HCRW) Approval** has been given for the above referenced study, on the basis described in the application form, protocol, supporting documentation and any clarifications received. You should not expect to receive anything further relating to this application.

How should I continue to work with participating NHS organisations in England and Wales? You should now provide a copy of this letter to all participating NHS organisations in England and Wales, as well as any documentation that has been updated as a result of the assessment.

Following the arranging of capacity and capability, participating NHS organisations should **formally confirm** their capacity and capability to undertake the study. How this

will be confirmed is detailed in the "*summary of assessment*" section towards the end of this letter.

You should provide, if you have not already done so, detailed instructions to each organisation as to how you will notify them that research activities may commence at site following their confirmation of capacity and capability (e.g. provision by you of a 'green light' email, formal notification following a site initiation visit, activities may commence immediately following confirmation by participating organisation, etc.).

Page **1** of **7**

It is important that you involve both the research management function (e.g. R&D office) supporting each organisation and the local research team (where there is one) in setting up your study. Contact details of the research management function for each organisation can be accessed [here](#).

How should I work with participating NHS/HSC organisations in Northern Ireland and Scotland?

HRA and HCRW Approval does not apply to NHS/HSC organisations within the devolved administrations of Northern Ireland and Scotland.

If you indicated in your IRAS form that you do have participating organisations in either of these devolved administrations, the final document set and the study wide governance report (including this letter) has been sent to the coordinating centre of each participating nation. You should work with the relevant national coordinating functions to ensure any nation specific checks are complete, and with each site so that they are able to give management permission for the study to begin.

Please see IRAS Help for information on working with NHS/HSC organisations in Northern Ireland and Scotland.

How should I work with participating non-NHS organisations?

HRA and HCRW Approval does not apply to non-NHS organisations. You should work with your nonNHS organisations to obtain local agreement in accordance with their procedures.

What are my notification responsibilities during the study?

The document "*After Ethical Review – guidance for sponsors and investigators*", issued with your REC favourable opinion, gives detailed guidance on reporting expectations for studies, including: Registration of research

- Notifying amendments
- Notifying the end of the study

The HRA website also provides guidance on these topics, and is updated in the light of changes in reporting expectations or procedures.

I am a participating NHS organisation in England or Wales. What should I do once I receive this letter?

You should work with the applicant and sponsor to complete any outstanding arrangements so you are able to confirm capacity and capability in line with the information provided in this letter.

The sponsor contact for this application is as follows:

Tel: 01133437587

Email: governance-ethics@leeds.ac.uk

Who should I contact for further information?

Please do not hesitate to contact me for assistance with this application. My contact details are below.

Your IRAS project ID is **249941**. Please quote this on all correspondence.

Yours sincerely

Laura Greenfield

Assessor

Email: hra.approval@nhs.net

Copy to: Faculty Research Ethics and Governance Administrator at University of Leeds

[Sponsor Contact on behalf of University of Leeds]

Ms Anne Gowing [Lead NHS R&D Office Contact on behalf of Leeds Teaching Hospitals NHS Trust]

List of Documents

The final document set assessed and approved by HRA and HCRW Approval is listed below.

Document	Version	Date
Evidence of Sponsor insurance or indemnity (non NHS Sponsors only) [Insurance letter]		21 September 2017
Evidence of Sponsor insurance or indemnity (non NHS Sponsors only) [Insurance letter]		17 September 2018
GP/consultant information sheets or letters [GP letter]	1.1	25 October 2018
HRA Schedule of Events	1	11 December 2018
HRA Statement of Activities	1	02 October 2018
IRAS Application Form [IRAS_Form_23082018]		23 August 2018
IRAS Checklist XML [Checklist_26102018]		26 October 2018
IRAS Checklist XML [Checklist_22112018]		22 November 2018
Laboratory Manual [Laboratory manual]	1.0	01 March 2018

Letters of invitation to participant [Letter of invitation and reply slip]	1.0	27 June 2018
Other [Grant award HRUK]		30 May 2018
Other [Email to confirm no adverts / posters used]		13 September 2018
Other [volunteer recruitment email]	1.0	25 October 2018
Other [research volunteer checklist]	1.0	01 September 2018
Other [study protocol]	1.1	20 November 2018
Other [Participant consent form Volunteers]	1.2	20 November 2018
Other [Participant consent form Patients]	1.2	20 November 2018
Other [Participant Information sheet Volunteers]	1.2	20 November 2018
Other [Participant Information Sheet Patients]	1.2	20 November 2018

Referee's report or other scientific critique report [External Peer Review Form]		
Summary CV for Chief Investigator (CI) [Chief Investigator CV]		14 February 2018

Summary of assessment

The following information provides assurance to you, the sponsor and the NHS in England and Wales that the study, as assessed for HRA and HCRW Approval, is compliant with relevant standards. It also provides information and clarification, where appropriate, to participating NHS organisations in England and Wales to assist in assessing, arranging and confirming capacity and capability.

Assessment criteria

Section	Assessment Criteria	Compliant with Standards	Comments
1.1	IRAS application completed correctly	Yes	No comments
2.1	Participant information/consent	Yes	No comments

	documents and consent process		
3.1	Protocol assessment	Yes	No comments
4.1	Allocation of responsibilities and rights are agreed and documented	Yes	A statement of activities has been submitted and the sponsor is not requesting and does not expect any other site agreement to be used.
4.2	Insurance/indemnity arrangements assessed	Yes	No comments
4.3	Financial arrangements assessed	Yes	Funding will be provided as described within the Statement of Activities.
5.1	Compliance with the Data Protection Act and data security issues assessed	Yes	No comments

Section	Assessment Criteria	Compliant with Standards	Comments
5.2	CTIMPS – Arrangements for compliance with the Clinical Trials Regulations assessed	Not Applicable	No comments
5.3	Compliance with any applicable laws or regulations	Yes	No comments
6.1	NHS Research Ethics Committee favourable opinion received for applicable studies	Yes	No comments
Section	Assessment Criteria	Compliant with Standards	Comments
6.2	CTIMPS – Clinical Trials Authorisation (CTA) letter received	Not Applicable	No comments
6.3	Devices – MHRA notice of no objection received	Not Applicable	No comments

6.4	Other regulatory approvals and authorisations received	Not Applicable	No comments

Participating NHS Organisations in England and Wales

This provides detail on the types of participating NHS organisations in the study and a statement as to whether the activities at all organisations are the same or different.

There is one type of participating NHS organisation; activities will be the same at all organisations.

The Chief Investigator or sponsor should share relevant study documents with participating NHS organisations in England and Wales in order to put arrangements in place to deliver the study. The documents should be sent to both the local study team, where applicable, and the office providing the research management function at the participating organisation. Where applicable, the local LCRN contact should also be copied into this correspondence.

If chief investigators, sponsors or principal investigators are asked to complete site level forms for participating NHS organisations in England and Wales which are not provided in IRAS, the HRA or HCRW websites, the chief investigator, sponsor or principal investigator should notify the HRA immediately at hra.approval@nhs.net or HCRW at Research-permissions@wales.nhs.uk. We will work with these organisations to achieve a consistent approach to information provision.

Principal Investigator Suitability

This confirms whether the sponsor position on whether a PI, LC or neither should be in place is correct for each type of participating NHS organisation in England and Wales, and the minimum expectations for education, training and experience that PIs should meet (where applicable).

A Principal Investigator is expected to be in place at the participating NHS site

GCP training is <u>not</u> a generic training expectation, in line with the <u>HRA/HCRW/MHRA statement on</u> <u>training expectations</u>.

HR Good Practice Resource Pack Expectations

This confirms the HR Good Practice Resource Pack expectations for the study and the pre-engagement checks that should and should not be undertaken

The activities at the participating NHS organization will be undertaken by local clinical staff therefore it is expected that adequate contractual relationship with the host organization are already in place. Where prior arrangements are not in place, network staff (or similar) undertaking any of the research activities listed in IRAS form A18 and A19, would be expected to obtain honorary research contracts on the basis of Research Passports (if University employed), or Letters of Access on the basis of NHS to NHS confirmation of pre-engagement checks letters (if NHS employed).

These should confirm enhanced DBS checks, including appropriate barred list checks, and occupational health clearance. For research team members administering questionnaires only, a Letter of Access based on standard DBS checks and occupational health clearance would be appropriate.

Other Information to Aid Study Set-up

This details any other information that may be helpful to sponsors and participating NHS organisations in England and Wales to aid study set-up.

- The applicant has indicated that they <u>intend</u> to apply for inclusion on the NIHR CRN Portfolio.
- Please note that the remit of HRA Approval is limited to the NHS involvement in the study. Research activity undertaken at non-NHS sites is therefore not covered and the research team should make appropriate alternative arrangements with relevant management at these organisations to conduct the research there.

The Leeds Teaching Hospitals **NHS**
NHS Trust

UNIVERSITY OF LEEDS

Developing novel cardiac diffusion MRI techniques to risk stratify patients with hypertrophic cardiomyopathy

IVIM in HCM

PARTICIPANT INFORMATION SHEET - Patients

Version 1.2

Date 20 November 2018

Dear Patient,

You are being invited to take part in a research study. Before you decide whether or not to take part, it is important for you to understand why the research is being done and what it will involve. Please take time to read the following information carefully, and discuss it with others if you wish. Ask us if there is anything that is not clear, or if you would like more information. Take time to decide whether or not you wish to take part.

Purpose of the study?

Hypertrophic cardiomyopathy (HCM) can affect 1 in 200 individuals. It is also the most common cause of sudden death in young adults. Most of the time individuals with HCM are completely asymptomatic. The cells of the muscles of HCM hearts are enlarged and in disarray causing the walls to thicken. Doctors use standard clinical tests to determine whether individuals with HCM are at risk of sudden death; however it is known that these tools are not as good as we would like. More sophisticated and accurate diagnostic investigations are needed.

In this study we aim to test and validate a new cardiac magnetic resonance (CMR) technique to compare changes that occur in the heart muscle of individuals with HCM compared to normal hearts. This technique is called IVIM-DT-CMR (Intravoxel Coherent Motion Diffusion Tensor Imaging) and could potentially allow us to assess the severity of cell disarray and changes in structure. If successful we could be the first CMR centre to provide a novel way to assess the heart of HCM patients for risk of sudden death.

Why have I been chosen?

This study is looking at 30 individuals like you, who have been diagnosed with HCM. We are also asking 10 healthy volunteers to participate in the study. This is a pilot study which may form the basis for a future larger study.

Do I have to take part?

No. It is up to you to decide whether or not to take part. If you do decide to take part you will be given this information sheet to keep and be asked to sign a consent form. If you decide to

take part you are still free to withdraw at any time and without giving a reason. If there is a possibility that you might be pregnant, you should not take part in the study. Our research team will be happy to discuss any other questions that you may have concerning your suitability for the study, before you decide whether to take part.

What will happen to me if I take part?

If you want to take part you will come to the Leeds General Infirmary up to two times. On each visit you will have a cardiac MRI scan, blood sample taken, and an ECG performed.

CMR scan: This will last approximately 60 to 90m minutes. During the MRI you will lie flat in the scanner (i.e. a short 'tunnel') and be asked to hold your breath intermittently. During the scan, you will hear periodical loud "banging" noises while we are acquiring the images, so we protect your ears with headphones through which you can listen to the radio or one of your own CDs. We will remain in communication with you throughout the scan. We will insert two cannulae (small plastic tubes) into veins in your arm. We will inject a contrast dye during the scan. Usually people are not aware of the contrast dye injection. At one point we will inject a medication (Adenosine) into a vein in your arm, which is a drug to increase the blood flow to your heart. This can cause a brief feeling of warmth, breathlessness or chest discomfort. However all of these feelings, if they occur, usually settle within one or two minutes of the medication being stopped.

Blood sampling: We will ask you for a blood sample to calculate your full blood count (5 to 10 mls. or 1 to 2 teaspoons), which would be taken whilst we insert the cannula in your arm for the contrast, so there are no extra needles involved. Your blood sample will be analysed at the Leeds General Infirmary and will not be stored afterwards.

ECG: Using an ECG we can measure the electrical impulses within the heart. This provides important information about the heart's 'wiring' and how muscular the heart is.

You might be asked to come back for another CMR in the next 6 months: by performing another cardiac MRI examination we would like to assess changes in your heart over time.

In the unlikely event of any abnormality being found we will, with your permission, inform your GP.

Risks and discomforts

Magnetic Resonance Imaging (MRI) is safe and no radiation is used for this scan. There are no known risks from the technique. Some people may experience claustrophobia (fear of confined spaces). Our MRI staff will do all that they can to make you feel comfortable during the scan, and will be monitoring you via a video camera and an audio link. If we are unable to make you feel comfortable in the scanner, we will not go ahead with scanning.

We will need to insert a small tube (cannula) into your arm for the contrast dye. The contrast medication we use during the scan is very safe but, as with any injection, reactions may occur. These include a warm sensation at the injection site, nausea or vomiting and transient skin rash.

People with a history of allergy are more likely to suffer a more severe reaction to the medication used, but this is rare (less than 1 in 3000). The department is equipped to cope with allergic reactions if they happen. With some older MRI contrast agents, accumulation of contrast in the organs (mostly skin and brain) potentially leading to long lasting chronic changes of the tissues has been reported in a very small number of patients with abnormal kidney function. These risks are known to be negligible in patients with normal kidney function and with newer contrast agents. Hence we will always check your kidney function before the

scan; we will not scan you if your kidney function is not normal; and we always use the lowest dose needed of the safest types of contrast agents available. Adenosine, the medication we use to increase the blood flow to the heart, can cause flushing, breathlessness and chest discomfort. However, all of these feelings usually subside within one or two minutes or even more quickly if the medication is stopped. Other side effects may include: abdominal discomfort; transient changes in the heart rhythm ('heart block'), transient drop in blood pressure, transient speeding up of the heart rate, tightening of the airways (bronchospasm); chest pain; dizziness; dry mouth; headache; throat discomfort.

To prevent side effects from happening, we will screen you in advance and make sure you have no contraindication to the medication; we will also acquire an ECG. The adenosine will be given to you for 3-6 minutes max during which we will monitor your heart rate and blood pressure and we will constantly talk to you and ask how you feel. Should any of the side effects happen and make you uncomfortable, we will stop the medication; any uncomfortable feeling you will experience will subside within one or two minutes or even more quickly once the medication is stopped.

Benefits to you

This study does not form part of your normal clinical care and is done solely for research purposes. Your participation may however benefit future patients.

Expenses

We are able to reimburse you £20 per visit as a contribution towards your time and travelling expenses.

Will my part in this study be kept confidential?

All information collected about you during the course of the study will be kept strictly confidential. This information will be securely stored, electronically on the Leeds Teaching Hospitals NHS Trust secure server, and on paper, under the provisions of the 2018 Data Protection Act. The data collected will be coded and your personal details will be kept separately. You will not be identified in any publication that may result from this research. With your permission, we will inform your GP of your participation in the study. If any unexpected abnormality or condition were found we would inform your GP. If you withdraw consent from further study follow-up, or if you were to become incapacitated, any data collected about you up to that point will remain on file and will be included in the final study analysis.

The University of Leeds is the sponsor for this study based in the United Kingdom. We will be using information from you and/or your medical records in order to undertake this study and will act as the data controller for this study. This means that we are responsible for looking after your information and using it properly. Leeds Teaching Hospitals NHS Trust and the University of Leeds will keep identifiable information about you for the purpose of the study for 20 years after the study has finished. Your rights to access, change or move your information are limited, as we need to manage your information in specific ways in order for the research to be reliable and accurate. If you withdraw from the study, we will keep the information about you that we have already obtained. To safeguard your rights, we will use the minimum personally-identifiable information possible. You can find out more about how we use your information at http://www.leeds.ac.uk/secretariat/data_protection.html

Leeds Teaching Hospitals NHS Trust and the University of Leeds will use your name, NHS number, and contact details to contact you about the research study, and make sure that relevant information about the study is recorded for your care, and to oversee the quality of the study. Individuals from the University of Leeds and regulatory organizations may look at your

medical and research records to check the accuracy of the research study. The Leeds Teaching Hospitals NHS Trust will pass these details to the University of Leeds along with the information collected from you and/or your medical records. The only people in the University of Leeds who will have access to information that identifies you will be people who need to contact you to or audit the data collection process. The people who analyse the information will not be able to identify you and will not be able to find out your name, NHS number or contact details

When you agree to take part in a research study, the information about your health and care may be provided to researchers running other research studies in this organisation and in other organisations. These organisations may be universities, NHS organisations or companies involved in health and care research in this country or abroad. Your information will only be used by organisations and researchers to conduct research in accordance with the UK Policy Framework for Health and Social Care Research.

This information will not identify you and will not be combined with other information in a way that could identify you. The information will only be used for the purpose of health and care research, and cannot be used to contact you or to affect your care. It will not be used to make decisions about future services available to you, such as insurance.

What will happen to any samples I give?

Samples will analysed and then destroyed. Your samples will not be stored.

What will happen to the results of the research study?

When the study is complete the results will be published in a medical journal, but no individual participants will be identified. If you would like a copy of the published results, please ask your doctor.

Indemnity/Compensation

If you are harmed as a direct result of taking part in this study, there are no special compensation arrangements. If you are harmed due to someone's negligence, then you may have grounds to a legal action. Regardless of this, if you have any cause to complain about any aspect of the way you have been approached or treated during the course of this study, the normal National Health Service complaints mechanisms are available to you.

The research organisation

This study is being organised by the Leeds Institute of Cardiovascular and Metabolic Medicine (LICAMM) within the University of Leeds.

Who has reviewed the study?

This study was given favourable ethical opinion for conduct in the NHS by Sheffield Research Ethics Committee.

Contact for further information

You are encouraged to ask any questions you wish, before, during or after your research investigations. If you have any questions about the study, please speak to your study nurse or doctor, who will be able to provide you with up to date information about the drug(s)/procedure(s) involved. If you wish to read the research on which this study is based, please ask your study nurse or doctor. If you require any further information or have any concerns while taking part in the study please contact one of the following people:

Dr Erica Dall'Armellina

Cardiac MRI department,

Clarendon wing, Leeds General Infirmary

email: E.DallArmellina@leeds.ac.uk

tel: 01133438306

Research Nurses

Cardiovascular Research

Sunshine Corridor, Leeds General Infirmary

Tel: 0113 392 5481 or 392 5504

cmrresearch@leeds.ac.uk

If you decide you would like to take part then please read and sign the consent form. You will be given a copy of this information sheet and the consent form to keep. A copy of the consent form will filed with the study records. You can have more time to think this over if you are at all unsure. Thank you for taking the time to read this information sheet and to consider this study.

UNIVERSITY OF LEEDS

CONSENT FORM - Patients v 1.2 20 Nov 2018

Developing novel cardiac diffusion MRI techniques to risk stratify patients with hypertrophic cardiomyopathy

CI: Dr. E.Dall'Armellina

Subject Study Number: ……………..   Subject Initials...................

Please initial boxes

1.   I have read the Participant Information Sheet (Patient) dated (version 1.2 20 Nov 2018) for the above study and I have had the opportunity to ask questions and discuss the research study and I am satisfied with the answers to my questions.

2.   I understand that my participation is voluntary and that I am free to withdraw from the study at any time without giving a reason.

3   I give my consent for my General Practitioner to be informed, and I understand that my cardiologist will be informed only if we find any abnormality over and above what is already known.

4.   I understand that data and images collected will be stored on a computer system, and, after my personal details have been removed, may be sent to an independent laboratory, and may be available to researchers at other institutions in the UK, the EEA, and countries outside the EEA.

5.   I understand that relevant sections of my medical notes and data collected during the study (including personal data) may be looked at by individuals from the University of Leeds, from regulatory authorities, or from the Leeds Teaching Hospitals NHS Trust, where it is relevant to my taking part

in this research. I give permission for these individuals to have access to my records.

6.   If I were to lose capacity or withdraw consent for further follow-up I understand that data already collected will be kept and used for the purposes of the study.

7.   I wish to receive a summary of the results of this study at its conclusion.

8.   I agree to take part in this research study and that the general results of the study will be made available to the medical community most likely through publication in a reputable medical journal.

9.   I am willing to be contacted again in the future with regard to potentially taking part (without any obligation) in further related research studies.

Signature...

Name (block capitals)... Date...............

Signature of researcher...

Name (block capitals)...Date…………….

1 copy for patient

1 copy for medical records

1 copy for Investigator Site File